



HAL
open science

Supported metal disulfide (TMS) catalysts for ultra-deep HDS : coupling of IR spectroscopy and microscopy for a deeper insight into active sites

Luz Adela Zavala Sanchez

► To cite this version:

Luz Adela Zavala Sanchez. Supported metal disulfide (TMS) catalysts for ultra-deep HDS : coupling of IR spectroscopy and microscopy for a deeper insight into active sites. Catalysis. Normandie Université, 2019. English. NNT : 2019NORMC258 . tel-02872878

HAL Id: tel-02872878

<https://theses.hal.science/tel-02872878>

Submitted on 18 Jun 2020

HAL is a multi-disciplinary open access archive for the deposit and dissemination of scientific research documents, whether they are published or not. The documents may come from teaching and research institutions in France or abroad, or from public or private research centers.

L'archive ouverte pluridisciplinaire **HAL**, est destinée au dépôt et à la diffusion de documents scientifiques de niveau recherche, publiés ou non, émanant des établissements d'enseignement et de recherche français ou étrangers, des laboratoires publics ou privés.



Normandie Université

THÈSE

Pour obtenir le diplôme de doctorat

Spécialité CHIMIE

Préparée au sein de l'Université de Caen Normandie

**Supported metal disulfide (TMS) catalysts for ultra-deep HDS:
Coupling of IR spectroscopy and microscopy for a deeper insight
into active sites.**

**Présentée et soutenue par
Luz Adela ZAVALA SANCHEZ**

**Thèse soutenue publiquement le 17/12/2019
devant le jury composé de**

Mme VALÉRIE BRIOIS	Directeur de recherche, Synchrotron SOLEIL	Rapporteur du jury
M. CHRISTOPHE GEANTET	Directeur de recherche au CNRS, Université Lyon 1 Claude Bernard	Rapporteur du jury
M. THIBAUT ALPHAZAN	Ingénieur de recherche, EURECAT France Sas	Membre du jury
Mme ELODIE DEVERS	Ingénieur de recherche, IFP énergies nouvelles	Membre du jury
M. XAVIER PORTIER	Professeur des universités, Université Caen Normandie	Président du jury
M. EELCO VOGT	Conseiller scientifique, Albemarle Catalysts company BV	Membre du jury

Thèse dirigée par FRANCOISE MAUGE et LAETITIA OLIVIERO, Laboratoire catalyse et spectrochimie (Caen)



UNIVERSITÉ
CAEN
NORMANDIE



Normande de Chimie



Laboratoire
Catalyse & Spectrochimie

*Dedicado con todo mi amor, admiración y gratitud a mi Mamá Lulú, mi papá Genaro,
mi hermanita Lulú, mi hermano José y a mis abuelitos Lucha y Amadeo*

“Creativity is intelligence having fun”

A. Einstein

Acknowledgments

Firstly, I want to thank both Dr. Françoise Maugé and Dr. Laetitia Oliviero for these three years of being my supervisors. But not only for being my bosses, but also for being people I could always rely for advice and for all the help they always gave me from day one, for including me in great moments and for their constant motivation to do things and live life in the best way. I will always be grateful to you for all that you offered to me in these three years. I admire you both very much and I will never forget all your support. You are the definition of strong and independent women!

I want to thank to the members of the jury Dr. Christophe Geantet, Dr. Valérie Briois, Dr. Elodie Devers, Dr. Eelco Vogt and Dr. Thibault Alphazan for agreeing to be revisors and participants of this moment. A special thanks to Dr. Xavier Portier for his great disposition to collaborate with this project and the knowledge shared during the microscopy sessions and to Dr. Jean Francois Paul for the disposition he has always showed at the moment of giving the orientation and training necessary for carrying out the theoretical part of this thesis.

Next, to my daily motivation to get out of my bed and face the world, my FAMILY. These three years being so far away from you have been very difficult but knowing that you will always be there, supporting me and loving me allows me to continue. Thank you for all your help, for your daily caring messages, for always listening to me and supporting me when I could not take it anymore. Simply, for making me never give up and believe in myself. The best gift of the world is to have you all in my life. I am so blessed for having you as family. My beloved Mom, Profe Genaro, Lulú, José, my grandma and my little nephew, Thai. Also, I know that from heaven you take care of me, Grandpa.

I have to thank of course, to the wonderful friends I made during this PhD time. Those friends who made the difficulties somewhat lighter and for whom I never felt alone. To Eli (guapi), thank you for being such an outstanding person with me since day one, for everything you taught me, for all the time you accompanied me and for everything we laughed and cry together. To Sandra, for all her advice and for always receiving me in the best way at her home with Clemonsín. To my Kamilita for being so kind and nice to me and taking care of

me so many times (perreooo!). To Dusan and Nastya, for all the shared moments and conversations. To my friend, office and gym partner, Maxime. To Kristoffer for his excellent friendship and help during the time he spent at the LCS. To Rafa and his adventures, to Radek, Farah, Cesare, Honza, Ibrahim, Bruno, Ghinwa, Edwin, Stas, Alberto and Vilny. To Jérémié for his excellent company and great moments shared. Thankfully, the list of amazing people that have crossed in my life is extensive, but to all the amazing people that I have had the opportunity to meet during these years in France: Thank you all for always been there when I could not afford a therapist! I know that in many times we spent together for too short, but the shared moments were always pleasant and memorable and I treasure them so much.

I would also like to thank to all the people that work at LCS for their help and disposition, especially to Sophie, Blandine, Adrien, Benjamin, Valérie and Alexandre. To Dr. Gabriel Alonso and his wife Lourdes Serrato for being there when I needed in Ensenada and in Lyon. Lastly, to Dr. Sergio Fuentes, for his help during the time I was in his lab in Mexico, without your help this dream would not have come true.

Agradecimientos

En primer lugar, quiero agradecer a la Dra. Francoise Maugé y a la Dra. Laetitia Oliviero por estos tres años como supervisoras. Pero no solo por ser mis jefas, sino también por ser personas en las que siempre pude confiar para recibir consejos y por toda la ayuda que siempre me brindaron desde el primer día, por incluirme en grandes momentos y por su constante motivación para hacer las cosas y vivir la vida de la mejor manera. Siempre les agradeceré todo lo que me ofrecieron en estos tres años. Los admiro mucho a ambos y nunca olvidaré todo su apoyo. ¡Son la definición de mujer fuerte e independiente!

También muchas gracias a los miembros del jurado Dr. Christophe Geantet, Dr. Valérie Briois, Dr. Elodie Devers, Dr. Eelco Vogt y Dr. Thibault Alphazan por aceptar ser revisores y participantes de este momento. Un agradecimiento especial al Dr. Xavier Portier por su gran disposición para colaborar con este proyecto y el conocimiento compartido sobre microscopía y al Dr. Jean Francois Paul por la disposición que siempre ha mostrado al momento de brindar la orientación y capacitación necesarias para llevar a cabo parte teórica de esta tesis.

Enseguida, a mi motivación diaria para salir de mi cama y enfrentar el mundo, mi FAMILIA. Han sido muy difíciles estos tres años lejos de ustedes, me he perdido de momentos muy felices y muy tristes también, pero saber que siempre me apoyarán y amarán, me permite continuar. Gracias por toda su ayuda, por sus mensajes de cariño diarios, por escucharme siempre y apoyarme cuando no podía soportarlo más y por hacer que nunca me rindiera y creyera en mi mamá. El mejor regalo del mundo es tenerlos a todos en mi vida, mi amada mamá, Profe Genaro, Lulú, José, mi abuelita y mi pequeño Thai. También, sé que desde el cielo me cuidas y me orientas, abuelito.

Tengo que agradecer, por supuesto, a los maravillosos amigos que hice durante este tiempo de doctorado. Esos amigos que hicieron las dificultades algo más ligeras y por quienes nunca me sentí sola. A Eli (guapi), gracias por ser una persona tan sobresaliente conmigo desde el primer día, por todo lo que me enseñaste, por todo el tiempo que me hiciste compañía y por todo lo que reímos y lloramos juntas. A Sandra por todos sus consejos y por recibirme

siempre de la mejor manera en su casa con Clemonsín, a mi Kamilita por ser tan amable y buena conmigo y por cuidarme tantas veces (¡perreooo!). A Dusan y Nastya, por todos los momentos y conversaciones compartidas, a mi amigo, compañero de oficina y gimnasio, Maxime, a Kristoffer por su excelente amistad y ayuda durante el tiempo que pasó en el LCS. A Rafa y sus aventuras, a Radek, Farah, Cesare, Honza, Ibrahim, Bruno, Peng, Ghinwa, Edwin, Stas, Alberto y Vilny. A Jérémié por su excelente compañía y grandes momentos compartidos. Afortunadamente, la lista de personas es larga, pero gracias a todas las personas increíbles que he tenido la oportunidad de conocer durante estos años en Francia, que en muchas ocasiones pasamos juntos poco tiempo pero que los momentos compartidos siempre fueron agradables y memorables. Gracias a todos por haber estado siempre allí cuando no podía pagar o encontrar un terapeuta.

También me gustaría agradecer a todas las personas que trabajan en el LCS por su ayuda y disposición, especialmente a Sophie, Blandine, Adrien, Benjamin, Valérie y Alexandre. Al Dr. Gabriel Alonso y su esposa Lourdes Serrato por estar allí cuando lo necesitaba en Ensenada y en Lyon. Por último, al Dr. Sergio Fuentes, por su ayuda durante el tiempo que estuve en su laboratorio en México, sin su ayuda este sueño no se habría hecho realidad.

Table of contents

General Introduction	13
Chapter I: Bibliographic study	19
Chapter II: Experimental Section	69
Chapter III: Deep insight into structure and quantification of edge sites of WS ₂ /Al ₂ O ₃ catalysts coupling IR/CO and DFT calculations.....	99
Chapter IV: High Resolution STEM-HAADF microscopy on γ -Al ₂ O ₃ supported MoS ₂ catalyst – Proof by image of the changes in dispersion and morphology of the slabs with addition of citric acid.....	139
Chapter V: Promoter location in NiW/Al ₂ O ₃ catalysts by parallel between IR/CO spectroscopy and High Resolution STEM-HAADF microscopy	169
Chapter VI: Evidence of modifications in growth of CoMoS particles by the addition of Citric Acid as chelating agent: A High resolution HAADF-STEM microscopy study.....	209
Chapter VII: General Conclusion and Perspectives.....	235
Résumé en français	249

General introduction

In order to face the more severe environmental legislations as well as the decrease of light oil resources, heavy crude oils have to be refined into ultra-low sulfur content transportation fuel. The use of such a large amount of oil results in crucial environmental problems due to the presence of considerable amounts of sulfur, nitrogen and metal impurities in it. The negative impact on the environment caused by the combustion of fossil fuels is a major global concern. In addition to global temperature increase due to the emission of CO₂, the emissions of toxic particles and gases such as NO_x and SO_x also have drastic consequences on air quality, human health and the preservation of the environment. Therefore, in most countries, governments implement or make more drastic regulations such as regulations for the amount of sulfur in land transportation fuel. Regulations on the amount of sulfur in maritime transport fuel are also being implemented. To meet the very restrictive regulation demands, a challenge is to develop catalysts with improved activity and controlled selectivity to desired products and stronger resistance to poisons.

Hydrotreatment processes (HDT) as hydrodesulfurization (HDS), hydrodenitrogenation (HDN), hydrodeoxygenation (HDO), and hydrodemetallization (HDM), are the main process for removal of sulfur, nitrogen, oxygen and metals. In these catalytic processes, are used catalysts whose active phase is a mixed transition metal sulfide (TMS) phase prepared from molybdenum (Mo) or tungsten (W), promoted by cobalt (Co) or nickel (Ni). Among these catalysts, it is recognized that the mixed NiWS phases are more active than the NiMoS and CoMoS phases in the hydrogenation of aromatic

compounds. They are as active as the NiMoS phases in hydrodenitrogenation, and more efficient than the CoMoS phases. Nevertheless, the limited sulfurization of W compared to Mo leads manufacturers to prefer catalysts based on Mo. However, considering that crude oil tends to get heavier and heavier, meaning that the heteroatom containing molecules are bigger and bigger and thus more refractory, there is an increased interest in NiW catalysts. Indeed, their high hydrogenation potential is a desired feature for performing deep HDS of diesel fuels. Thus, a better understanding of the nature of the active phases and of the role of the promoter in NiW-based catalysts is of prime importance. However, the distinct chemical and morphological properties of tungsten-based catalysts are poorly understood when compared to the current level of information available for molybdenum-based catalysts.

Based on the rich understanding about the relation between structure and activity, now designing HDS catalysts with controlled structure and functionalities is becoming a trend [1]. To improve the performance of HDS catalysts, several methods are considered, worth mentioning are the use of chelating agents during the preparation stage, the optimization of pressure and temperature of sulfidation and of the metal loading. The positive effect of chelating agent addition on the catalytic performance is well documented. Nevertheless, the origin of such positive effect is still a matter of debate. Hence, there is a strong concern in the implementation of characterization methods able to account for the local structures of the active sites of industrial catalysts as well as their role in the HDS reaction. The characterization of the concentration of these sites and the distinction of the sites promoted on the two different edges exposed by the MoS₂ sheets is essential to explain in fine their

activity and their selectivity as well as the role of the parameters of preparation of these catalysts (effect of support, conditions for the preparation of the initial oxide phase, sulfurization conditions). However, there are few methods to obtain this information. By X-ray photoelectron spectroscopy (XPS), it is possible to reach the overall concentration in CoMoS sites but without distinction of their position on one or the other edge of the sheet. By scanning tunneling microscopy (STM), Lauritsen *et al.* [2–4] group was able to observe the morphology of the slabs and to distinguish the two edges as well as their promotion, but the catalysts studied are model catalysts distant in their composition and the conditions of preparation of those used industrially. The characterization of sulfide and metallic catalysts by low temperature CO adsorption followed by infrared spectroscopy (IR/CO) allows quantifying the concentration of active sites, and thus gives access to the site dispersion and then to their intrinsic activity [5]. Thus, IR/CO has been intensively used to probe the edges sites of MoS₂ slabs on MoS₂/Al₂O₃ catalysts. It has been observed that there are two different CO adsorption bands when CO interacts with MoS₂ edges. Combining experimental infrared spectra and DFT calculations, it has been established that these bands correspond to CO adsorption on M-edge and S-edge sites of MoS₂ slabs. In addition, a quantitative evaluation of the M-edge and S-edge site concentrations on MoS₂/Al₂O₃ catalysts can be obtained after determination of the integrated molar extinction coefficient of CO adsorbed on each edge [6]. This quantitative approach via the S-edge/M-edge ratio has provided experimental demonstration of the morphology modification of industrial like catalysts i.e. prepared by the conventional method of impregnation and supported on oxides.

This characterization method opens a promising pathway in streamlining the design of more active and selective HDT catalysts. However, it remains an indirect technique and should be compared to direct observation of nanosheets. This one can be obtained thanks to the high resolution electron microscopy in dark field (HR STEM-HAADF) based on chemical contrast. For elements with a higher atomic number (Z), more electrons are scattered at higher angles due to greater electrostatic interactions between the nucleus and electron beam. Because of this, the STEM HAADF detector senses a greater signal from atoms with a higher Z , causing them to appear brighter in the resulting image. This high dependence on Z (with contrast proportional to $Z^{1.7}$) makes STEM HAADF a useful way to easily identify small areas of an element with a high Z in a matrix of material with a lower Z . With this in mind, a common application for STEM HAADF is in heterogeneous catalysis research, as determination of the size of metal particles and their distribution is extremely important.

The present PhD thesis deals with a deep molecular insight into sulfide phase of HDT catalysts. In this work, a special effort was made to understand the factors that affect the sulfide phase morphology and the consequence of the morphological changes on the catalytic activity. Thus, we investigate the nature of active phase, especially the slab morphology in the promoted and non-promoted Mo, CoMo, W, NiW supported on alumina systems. To this aim, we study in parallel IR spectroscopy with cutting edge characterization techniques as DFT calculations and HR STEM HAADF, the morphology of Al_2O_3 supported sulfide catalysts prepared at exactly the same conditions of synthesis and sulfidation than the ones for the catalytic application.

The detailed study in this manuscript is divided into six main parts: In the first part, we present a bibliographic study focused on sulfide catalysts, and the state of the art of the characterization of their active phase. The second part is devoted to the description of the modes of preparation of all the catalytic materials and also presents the analytical techniques. Third chapter is devoted to the coupling between IR/CO and DFT calculation for determining the active sites in W/Al₂O₃ catalysts focusing on distinction of the M-edge and S-edge for such catalysts. In the fourth chapter we present a study of the parallel between IR/CO and HAADF-STEM as a proof of morphology variations due to the addition of citric acid on Mo/Al₂O₃ catalyst. In the fifth chapter citric acid effect on NiW/Al₂O₃ catalysts is described. In particular, coupling of HAADF-STEM and IR/CO studies allowed the discrimination of promoted edges. Finally in the sixth chapter HAADF-STEM results on sulfided CoMo/Al₂O₃ catalysts before and after thiophene HDS reaction are presented. We end this manuscript with a general conclusion and the perspectives envisaged for the continuation of this work.

Chapter I: Bibliographic study

Content Chapter I: Bibliographic Study

I.1. Hydrotreating generalities	21
I.2. Hydrodesulfurization (HDS)	24
1.3. Catalysts used in HDS processes	27
1.3.1. Sulfide Phase: structure model.	30
1.3.2. Microscopy for observation of TMS morphology	34
I.3.3. Mo based catalyst morphology.....	35
1.3.4. W based hydrotreating catalyst morphology	42
1.4. Catalyst preparation with chelating agents.....	44
1.4.1. Role of chelating agents.....	45
1.4.2. Citric acid as chelating agent	48
1.5 Low temperature CO adsorption followed by IR spectroscopy (IR/CO) contribution to characterize promoted and non-promoted catalysts.....	49
1.5.1. Characterization of non-promoted catalysts by IR spectroscopy.....	49
1.5.2. Characterization of promoted catalysts by IR spectroscopy.....	52
I.6. Conclusion and scope of the thesis.....	55
I.7. REFERENCES.....	57

I.1. Hydrotreating generalities

Hydrotreating or Hydrotreatment (HDT) refers to a variety of catalytic hydrogenation processes that saturate unsaturated hydrocarbons and remove S, N, O, metals from different petroleum streams in a refinery and enhances cetane number, density and smoke point [7]. These processes represent some of the most important catalytic processes and annual sales of HDT catalysts represent a considerable part of the global catalyst market. HDT usually involves small changes in the overall molecular structure. Nowadays, HDT is widely used for the conversion of heavy feedstock and for improving the quality of the final products. HDT also plays an essential role in the pretreatment of streams for other refining processes, such as catalytic reforming (HCR) and fluid catalytic cracking (FCC) [7]. Fluid catalytic cracking (FCC) is one of the major conversion technologies in the oil refinery industry. To 2015, it was estimated that ~2300 metric tons of FCC catalyst are produced per day, or ~840 000 metric tons per year. [8]

Historically, HDT processes have developed from the cracking and hydrogenation processes introduced in the 1930s [9,10]. For a long time, the most important HDT reaction has been the removal of sulfur from various fuel fractions. Accordingly, HDT catalysts are also commonly referred as hydrodesulfurization (HDS) catalysts. Among numerous atmospheric pollution sources, sulfur contained in gasoline is well known for its particularly disastrous effects. Indeed, its presence in the exhaust gas as SO₂ is not only responsible for allergies and respiratory disorders such as asthma, but it is also a poison for the catalytic exhaust converters, decreasing progressively their efficiency. Facing this health and environmental problem, laws limiting the sulfur emissions

were early established and, they have to be regularly revised in order to meet more and more exigent environmental protection standards. Environmental regulations in many countries require the sulfur content in transport fuels down to about 10 ppm with the aim of reducing engines harmful emissions and improving air quality [Figure 1]. It has been observed the continued worldwide movement toward lower sulfur content in diesel and many countries have positioned themselves through policy initiatives to make advances in this area in the near future [11]. However, current petroleum resources have higher sulfur and heavy molecular weight impurities concentration. With little competition from alternative fuels today, oil is expected to continue to be the main source of energy for transportation around the world.

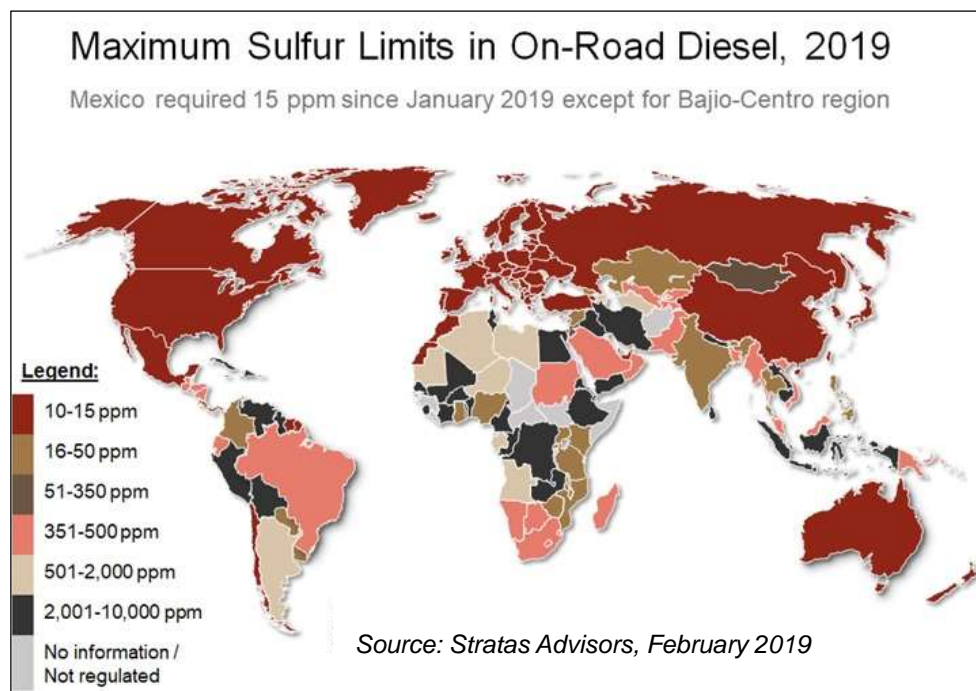


Figure 1. Maximum sulfur limits in transportation fuels in 2019. The map below shows current maximum on-road diesel sulfur limits worldwide [11].

Crude oil is processed to produce those transportation fuels in refineries that have a total world capacity of more than 80 million barrels per day at present [12]. In recent years, the refining industry efforts to meet the global trend for more rigorous clean fuels specifications, the growing demand for transportation fuels [Figure 2] and the shift toward diesel have made of HDT an important matter of research and study. If in most industrialized countries, the number of vehicles per person or motorization level is already high the transportation energy demand is projected to increase dramatically coincident with the continuous rising in population and economic output per capita assumed in the emerging countries [13]. Though great effort has been put in the research of alternative sources of energy, they are not enough to fulfill the demand worldwide.

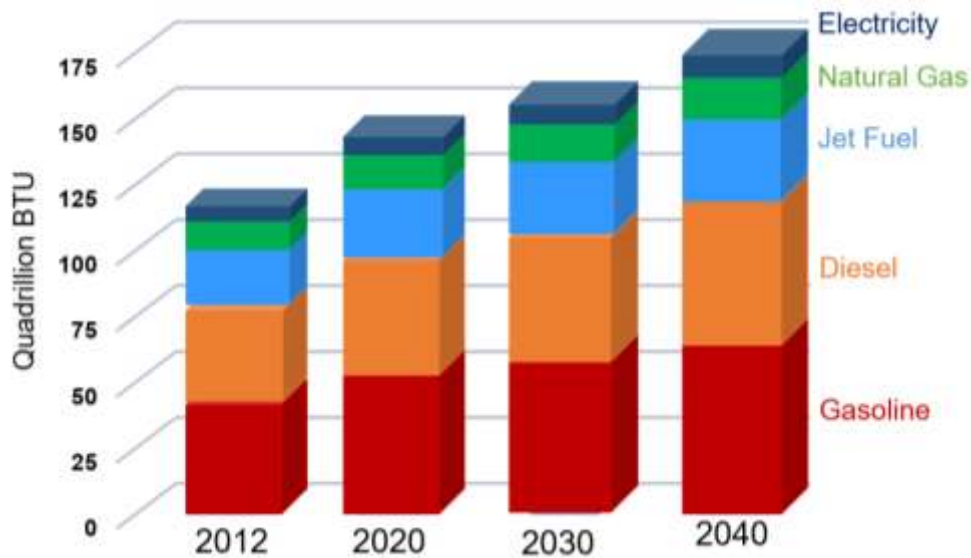


Figure 2. World transportation sector : delivered energy consumption by energy source, 2012-2040 [13].

Due to its importance in the overall oil refining process, HDS will be described with more detail in further sections. Up to now it is generally believed that

current HDS processes and catalysts will be unsuitable for the large scale production of ultra-low sulfur diesel (ULSD), sulfur content as low as 10 ppm or less. Meanwhile this production requires hydrogenation of aromatic molecules in order to increase the cetane number. Thus, the improvement of the hydrogenation selectivity will play a critical role in future HDT processing.

1.2. Hydrodesulfurization (HDS)

Hydrodesulfurization (HDS), belonging to a group of processes called hydrotreating, is a catalytic chemical process widely used to remove sulfur (S) from natural gas and from refined petroleum products, such as gasoline, jet fuel, kerosene, diesel fuel, and fuel oils [14]. HDS has for a long time been one of the most important processes in oil refineries. The reaction has therefore been studied extensively over a period of years. Sulfur is the most abundant heteroatom impurity in crude oil, its content varies with its origin territory. Crude oil can be classified into light or heavy oil following some important properties such as (i) API gravity (inverse of density) which is thus directly linked with the density of the crudes and (ii) sulfur percentage, since a greater amount of heterocompound is found in heavy oils (see **Table I**).

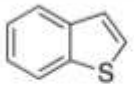
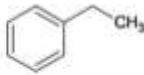
Table I. Properties of crude oils (API sulfur amount).

Crude oil class	Property Range	
	Gravity (°API)	Sulfur (wt. %)
Light	35-60	> 0.5
Medium	26-35	> 1.1
Heavy	13-26	> 1.1

Due to its organic origin, crude oil contains several percent of –S and –N containing molecules that have a detrimental effect on catalysts used for cracking and reforming. The purpose of removing the sulfur, and creating products such as ultra-low-sulfur diesel, is to reduce the sulfur dioxide (SO₂) emissions that result from using those fuels in automotive vehicles, aircraft, railroad locomotives, ships, gas or oil burning power plants, residential and industrial furnaces, and other forms of fuel combustion. Another important reason for removing sulfur from the naphtha streams within a petroleum refinery is that sulfur, even in extremely low concentrations, poisons the noble metal catalysts (Pt and Re) in the catalytic reforming units that are subsequently used to upgrade the octane rate of the naphtha streams. The industrial HDS processes include facilities for the capture and removal of the resulting hydrogen sulfide (H₂S) gas. In petroleum refineries, the hydrogen sulfide gas is then subsequently converted into byproduct elemental sulfur or sulfuric acid (H₂SO₄). In fact, the vast majority of sulfur produced worldwide is byproduct sulfur from refineries and other hydrocarbon processing plants [15]. HDS involves reactions leading to removal of organic sulfur compounds by their conversion into H₂S and hydrocarbon products. This process consists in the cleavage of C-S bonds, which is generally accompanied by the saturation or the partial hydrogenation of some unsaturated compounds [16]. Some typical HDS reactions are listed in **Table II**. Only the global transformation is presented since the pathway schemes of these reactions are often more complicated and may depend on the nature of the organic molecule under consideration. Besides the HDS reaction, hydrocracking (HCK), hydrodenitrogenation (HDN) and

hydrogenation of unsaturated compounds simultaneously occur under HDS reaction conditions.

Table II. Typical Hydrodesulfurization (HDS) reactions.

Thiol	$R-SH + H_2 \rightarrow RH + H_2S$
Disulfide	$R-SS-R' + 3H_2 \rightarrow RH + R'H + H_2S$
Sulfide	$R-S-R' + 2H_2 \rightarrow RH + R'H + H_2S$
Thiophene	 + $XH_2 \rightarrow C_4 \text{ mixture} + H_2S$
Benzothiophene	 + $3H_2 \rightarrow$  + H_2S
Dibenzothiophene	 + $2H_2 \rightarrow$  + H_2S

The transformation of S-containing molecules happens through two parallel reactions: direct desulfurization (DDS) and hydrogenation (HYD) (**Figure 3**). Thiophene HDS occurs via parallel pathways involving direct desulfurization (DDS) to form butadiene and butenes and hydrogenation (HYD) to form tetrahydrothiophene. The secondary reactions hydrogenate butadiene and butene and remove the S atoms of tetrahydrothiophene as H_2S [17]. In thiophene reaction, sulfur anion vacancies have for a long time been considered to be the active sites for HDS. In view of this, it seems logical to suggest that the adsorption of thiophene occurs on these coordinatively unsaturated sites (CUS), and that the bonding is through the S atom.

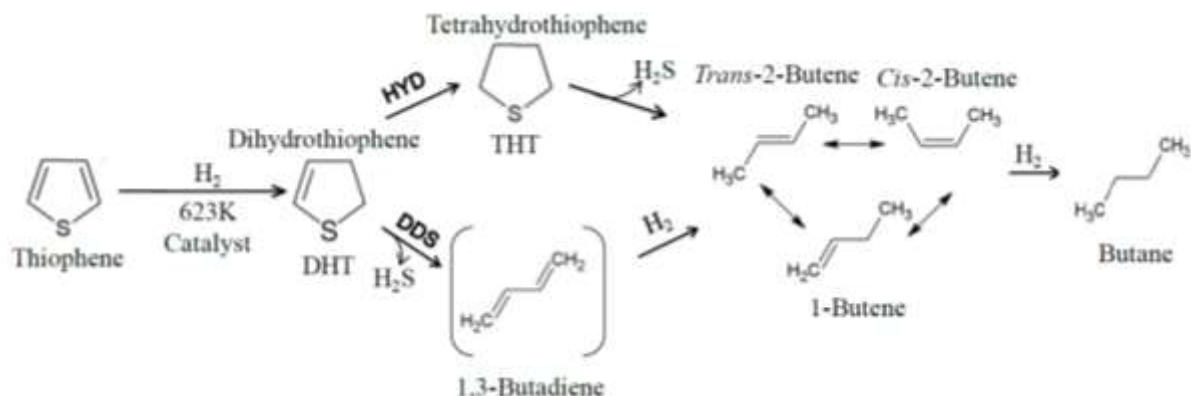


Figure 3. Scheme of HDS reaction and pathway for thiophene [18].

I.3. Catalysts used in HDS processes

HDS catalysts are mainly based on supported transition-metal sulfides (TMS) [19]. The TMS active phase is usually composed of tungsten (W) or molybdenum (Mo), promoted by metals of the group VIII as nickel (Ni) or cobalt (Co). Mo-based sulfide catalysts are widely used in hydrotreatment processes that aim at reducing the heteroatom content (sulfur, nitrogen, and metals) of petroleum feedstocks. CoMoS active phase [20,21] are known to be not only active but also selective in the HDS of thiophenic molecules, with respect to the hydrogenation (HYD) of olefinic ones [22]. Meanwhile Ni-promoted WS₂ catalysts lead to activity improvement in aromatic hydrogenation [23,24]. The catalytic activity of these catalysts in hydrotreating reactions such as HDS is usually related to anionic vacancies (coordinatively unsaturated sites, CUS) located on these edges.

The precursors of these metals are deposited on oxide supports with a large specific surface area such as silica, alumina, or silica-alumina. The more classical preparations proceed by pore volume impregnation with a solution of

metal salts (Figure 4). The conventional preparation procedure for TMS supported catalysts may be divided in two different stages. The metal deposition on the support surface is typically carried away by incipient wetness impregnation method [25]. The impregnation solution is formed by metal precursors dissolved in water with a volume equal to the pore volume of the support. The metallic species diffuse inside the support pores and between these species and the support surface sites several interactions occur. Finally, the sulfide species are created by the transformation of the metal oxides under $\text{H}_2\text{S}/\text{H}_2$ flow. This activation is a key step of the catalyst formation.

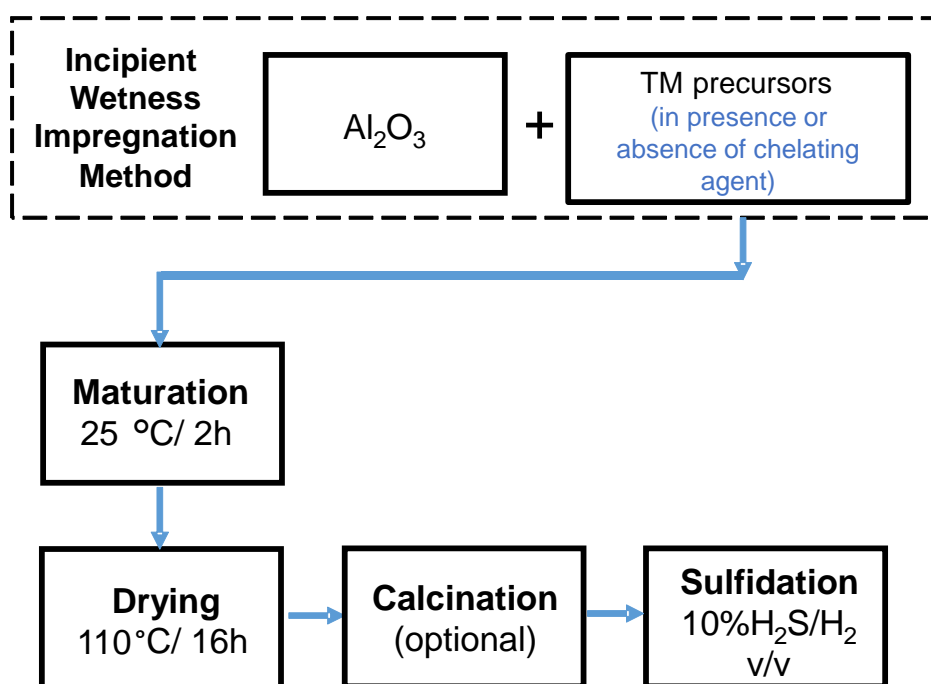


Figure 4. Scheme of preparation of sulfide conventional catalysts for HDS.

In academic laboratories, the sulfidation process is generally performed under $\text{H}_2\text{S}/\text{H}_2$ atmosphere. In industrial units, sulfidation is performed under liquid phase using directly the sulfur compounds that are contained in the petroleum cut and under high pressure of hydrogen. However, this process requires a slow

temperature increase due to the difficulties to decompose the sulfur compounds into H_2S and for limiting the reduction by H_2 of the metal precursor [26]. To mend this problem, organic molecules containing several sulfur atoms are added to the feed as H_2S source since their decompositions occurs at lower temperatures. The most used compounds are TNPS (TertioNonyPentaSulfide), DMS (DiMethylsulfide), DMDS (DiMethylDisulfide), DMSO (DimethylSulfoxyde), butyl mercaptan, which are added in the feed during the sulfidation period. The sulfidation induces a deep modification of the isopolyanion (**Figure 5**): the oxygen ligands are replaced by sulfur atoms and the metal passes from a degree of oxidation + VI to + IV. This transformation causes a reorganization of the surface species, as well as a change in the crystallographic environment of the metal, from octahedral structure to trigonal prismatic structure.

In addition, the range of temperatures used industrially is between 300 °C and 400 °C. However, these transformation phenomena are not so simple, and there are several influences during the different steps as:

- a. Physicochemical phenomena during the impregnation: metal diffusion into pores, acid-base reaction (controlled by acid constant of the species in solution and support surface), adsorption, complexation or precipitation, etc.

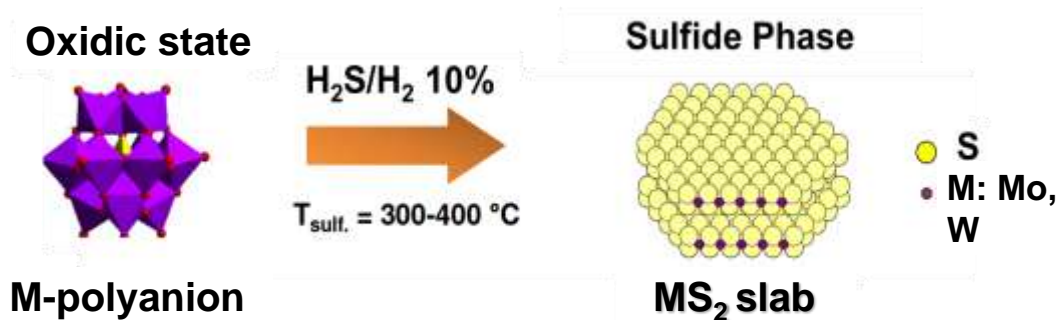


Figure 5. Schematic diagram of the transformation of an oxidic phase into a sulfide phase [27].

- b. Formation of different oxidic species during drying and calcination process from the species presents in the initial solution.
- c. The temperature and the ratio between H_2S and H_2 in sulfidation procedure, which can modify the sulfide species nature.

For that reason, the studies of HDS catalysts in “so-called” oxidic form, as well as, the transition products during sulfidation procedure are fundamental to understand sulfide species formation.

I.3.1. Sulfide Phase: structure model.

An intensive effort has been made to understand the structure and nature of the catalytic sites of the sulfide catalysts $(\text{Co},\text{Ni})\text{Mo}(\text{W})/\text{Al}_2\text{O}_3$. Several models, such as the monolayer model, the intercalation model, the contact synergy model and the rim-edge model, have been proposed to provide an interpretation of the surface structure of the HDS catalysts [28–31]. However, most of the models have been left behind or held by a minority for further investigation. The discussions hereinafter are based in the CoMoS edge model proposed by *Topsøe et al.* [20,21,32] that is widely accepted up to now (**Figure 6**). After

sulfidation process, a bimetallic sulfide phase is formed, typically called the NiWS, NiMoS, or CoMoS phase, whose structure corresponds to a two-dimensional (2D) nanolayer of Mo(W)S₂ decorated by the promoter at its (100) edges [3,7,32].

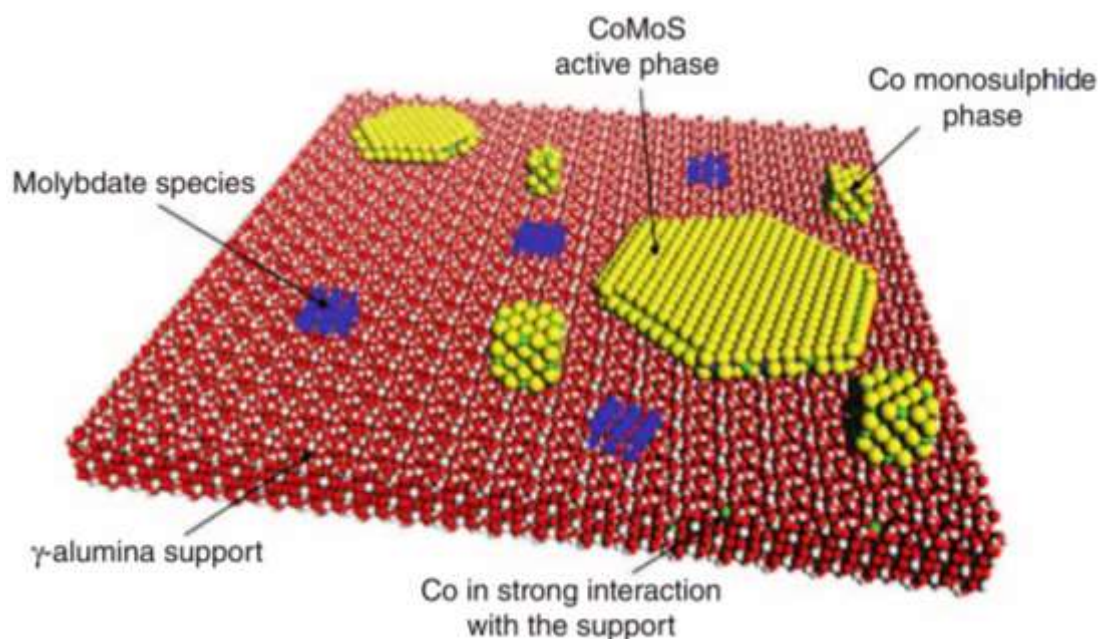


Figure 6. Schematic representation of the γ -alumina supported CoMoS catalyst. Color key: Al: red balls, O: red balls, H: white balls, S: yellow balls, Mo: violet and blue balls, Co: green balls. Scheme extracted from reference [33].

Along with this formation, some side phases are formed during the preparation and sulfidation stages. The sulfide phase presents a lamellar structure, formed by layers of MS₂ (M = W, Mo). The S-M-S layers are held together by van der Waals interactions (**Figure 7**). Each layer is composed of two hexagonal planes of S atoms and an intermediate hexagonal plane of M atoms, which are trigonal prismatic coordinated to S atoms. The 2D morphology of these layers, their average stacking (~1 to 4) and their average size (~2 to 6 nm) depend on the preparation and sulfidation conditions.

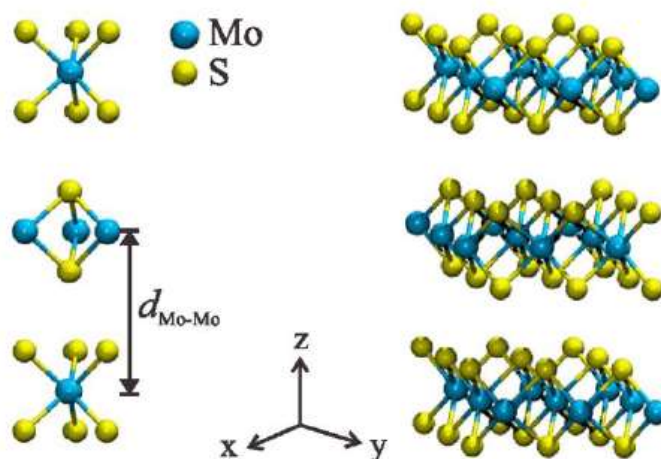


Figure 7. Crystalline structure of MS_2 clusters. Schematic representation of the stacking of a lamellar MS_2 structure formed by a layer of metallic atoms intercalated between two layers of sulfur atoms.

It should be noticed that the CoMoS, NiMoS and NiWS structures are not a single, bulk phase with a fixed overall Co(Ni):Mo(W):S stoichiometry. Rather, it should be seen as a family of structures with a wide range of promoter (Co, Ni) concentrations, ranging from pure MS_2 (M=Mo or W) up to full coverage of the MS_2 edges by Co or Ni. The promoter atoms in the CoMoS, NiMoS and NiWS may not have identical properties due to such effects as different edge-sites geometries, Co-Co and Ni-Ni interactions, and changes in sulfur coordination. On **Figure 8**, the top view of a MS_2 slab is presented. The most stable edges are formed by direct cleavage of the basal plane without considering further rearrangement. The structure of the MS_2 slabs makes it possible to distinguish the M located in different regions: basal plane (type I), edge sites (type II and II), corner sites (type IV) and brim sites (type V).

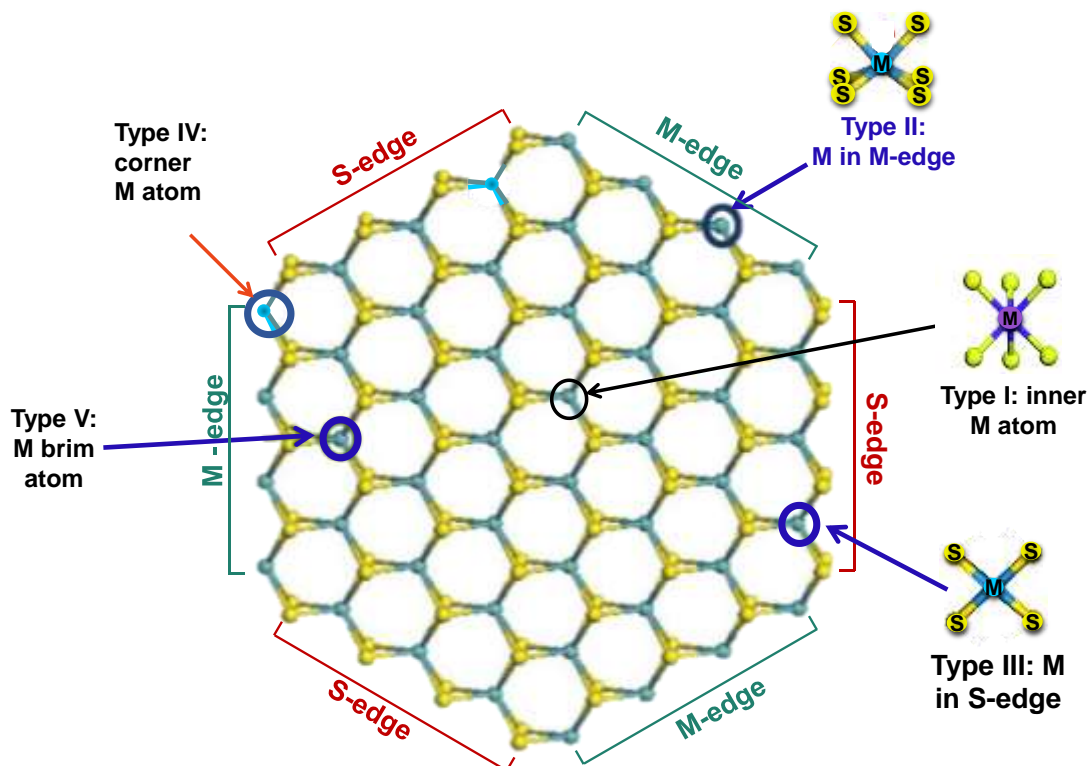


Figure 8. Representation of MoS₂ slab with hexagonal shape. Sulfur atoms are represented by yellow balls and molybdenum atoms by blue balls.

In a general agreement, the basal plane (Type I) is formed by M⁴⁺ hexacoordinated with sulfur atoms, i.e. these atoms are perfectly stable, and therefore inactive from a catalytic insight. However, edge part is formed by M⁴⁺ penta- or tetra-coordinated (Types II to IV) with sulfur atoms depending on the sulfur coverage [34]. The M atoms in the corner are characterized by being formed by a smaller coordination number than the Mo at the edges (Type V). And finally, the edge sites are splitted between M-edge and S-edge. In this way, M atoms located at the edge or corner participates in the catalytic activity due to the creation of some CUS sites [28,32,35]. Is important to keep in mind that the involvement of brim sites in catalytic activity is a recent hypothesis proposed by Topsøe et al. and co-workers [2]. They determine that the sites next to the border (so called, brim sites) have a more metallic state [36]. The STM

combined with DFT studies showed that these sites can play a role in the adsorption, hydrogenation and cleavage of C-S even if they are completely saturated with S.

I.3.2. Microscopy for observation of TMS morphology

The lack of detailed structural information at the atomic scale in real-world TMS catalysts under working conditions remains one of the major obstacles for a rational design of bimetallic catalysts for industrial applications. Transmission electron microscopy (TEM) has become an indispensable technique to obtain detailed structural information on materials [37]. This technique is very powerful to elucidate the catalyst nanostructure and thus to obtain correlation with their catalytic activity. Traditionally, for characterization of transition metal sulfide (TMS) slabs deposited on an industrial support such as γ -alumina, TEM mode is used for classical analysis [38–41]. It provides a first insight and information on some general parameters such as the length and stacking of the slabs. Several authors have pointed out that the distinction of the basal plane of MoS_2 on $\gamma\text{-Al}_2\text{O}_3$ is hardly possible from conventional TEM images. One approach has been the electron tomography, which combines multiple images taken at different tilt angles to reconstruct the object's 3D morphology. This approach has been shown to be a versatile method to characterize the 3D structure of catalysts [37,42]. Thanks to the improvement of the electron microscopic techniques and the arrival of the Transmission Electron Aberration-Corrected Microscopy (TEAM) as well as theoretical methodologies, the atomic structure of catalysts are better understood than by traditional TEM [43]. In case of aberration corrected electron microscopes, high-angle annular dark field scanning transmission electron microscopy (HAADF-STEM) offers extreme

resolution limits and thus, single atom imaging based on the Z-contrast is now routinely achieved. A HAADF-STEM image is characterized by a Z-contrast (atomic number of atoms in the sample) dependence, and this mode is very appropriate for the study of small nanoparticles made of heavy elements, especially if they are deposited on a lighter support [44]. By HAADF-STEM, additional information on the morphology of TMS based nanostructures have also been obtained [19,23,45–48]. Furthermore, with the combination of these new technologies, it is now possible to elucidate the detailed structure, such as the layer edges, the sulfur coverage (tailored particles) and the sulfur vacancies or defects which are considered to be the responsible for the catalytic properties. The principle of operation and the parameters used for this project are described in detail in Chapter II.

I.3.3. Mo based catalyst morphology

As previously seen in **Figure 8**, it is well established that the TMS slab presents in its perfect crystallographic (100) plane, two types of edges: the metal terminated edge (M-edge) and the sulfur terminated edge (S-edge). Both the M-edge and the S-edge can show different configurations with different sulfur coverage. The morphology of the MoS₂ slabs is of significant importance to the catalytic performance because it has been demonstrated that activity is linked to this parameter. For mentioning some examples, Chen et al. demonstrated that the edges in MoS₂/Al₂O₃ catalysts have different intrinsic activities [49], and it has been suggested that promoter atoms have different affinities towards M-edge and S-edge [50,51].

Almost twenty years ago, Helveg *et al.* published the first scanning tunneling microscopy (STM) images showing non-promoted MoS₂ catalysis slabs, deposited on a gold surface whose crystallographic phase exposed the (111) plane, had a triangular structure [52]. Later, Schweiger *et al.* used density functional theory (DFT) to predict the morphology of non-promoted MoS₂ slabs versus the temperature and H₂S partial pressure in the surrounding atmosphere. The variation of chemical potential was studied for different sulfidation conditions (**Figure 9**). Thus, for typical sulfidation condition (673 K and $P(\text{H}_2\text{S})/P(\text{H}_2) \sim 0.05$), the chemical potential calculated is between -1 and -0.8 eV [53,54]. The edge energies for M- and S-edge were also calculated depending on the chemical potential of sulfur, indicating that the energy on M-edge is lower than the energy of S-edge in the wide chemical potential range, which reveals that M-edge is the most stable edge. Thus, triangular-shaped MoS₂ terminated by M-edge are observed to be the equilibrium structure under pure sulfiding condition (H₂S pure) while the single-layer nanoparticles can become truncated with both M-edge and S-edge under sulfo-reductive conditions ($P(\text{H}_2\text{S})/P(\text{H}_2) \sim 0.05$) [54].

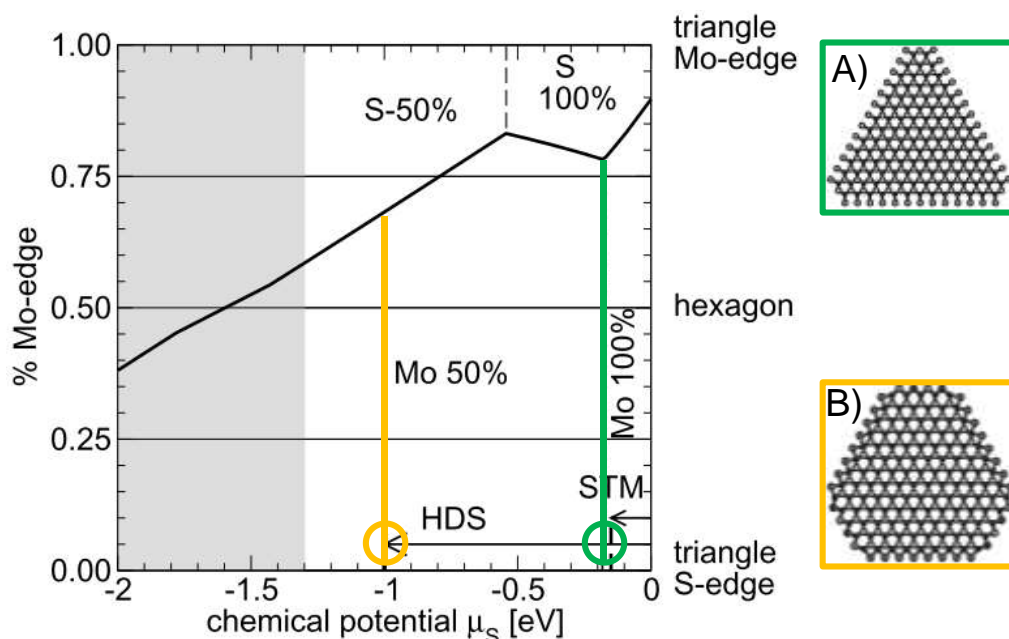


Figure 9. Morphology of the MoS₂ nanosize particles as a function of chemical potential of sulfur. The ordinate represents the percentage of Mo-edge. The thick line indicates the equilibrium morphology. (A) Strong sulfiding conditions and (B) HDS working conditions. Scheme extracted from reference [54].

This theoretical calculations were then confirmed by the STM analyzes performed by Lauritsen *et al.* [55]. Here, the MoS₂ nanoparticles supported on Au substrate prepared by a special procedure under ultra-high vacuum (UHV) condition. The pure metal Mo was deposited on the Au (111) surface by an e-beam evaporator in the H₂S atmosphere of 1x10⁻⁶ mbar at 400 K. Subsequently, the obtained crystal is annealed at 673 K for 15 min in the same H₂S atmosphere and single-layered MoS₂nanoparticles were formed with the basal (001) plane parallel to the Au (111) surface. Therefore, it can be stated that the morphology of MoS₂ nanoparticles can vary from a triangle to a hexagon with sulfo-reductive conditions as it is shown on **Figure 10**.

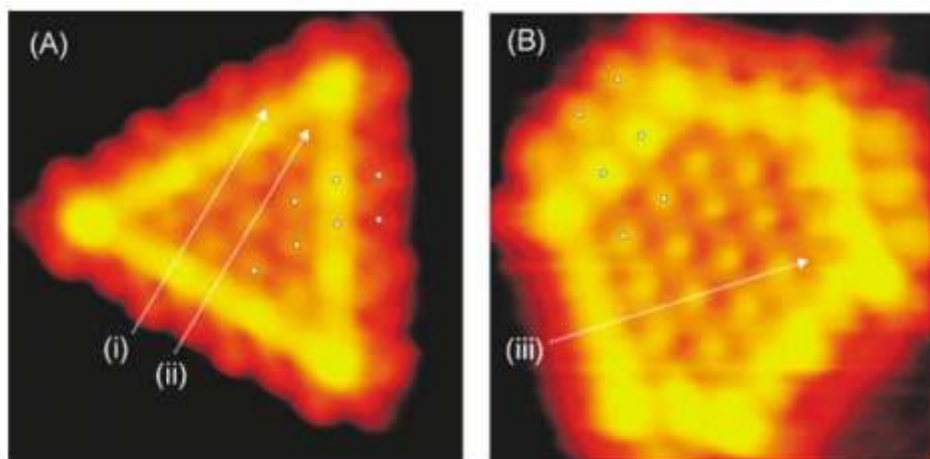


Figure 10. Atom-resolved STM image of a triangular single-layer MoS₂ nanocluster synthesized under the sulfiding conditions (A) and (B) Atom-resolved STM image of a hexagonal single-layer MoS₂ nanocluster synthesized under sulfo-reductive conditions [56].

Nevertheless, majority of these results are not quite scalable to the commercial catalysts because the preparation and characterization conditions are significantly different from the standard ones used in operation conditions.

Advances in electron microscopy have opened new routes to address the atomic-scale structure of catalytic materials [57–59]. For instance, in the early beginnings of the field, transmission electron microscopy (TEM) allows the observation of metallic particles of subnanometric dimensions [60]. When it comes to the morphological study, one of the obstacles is that TEM images undergo contrast perturbation due to the support, particularly when this one is such a strong insulator like alumina. To solve this problem High Resolution Scanning Transmission Electron Microscopy in High-Angle Annular Dark Field mode (HR STEM-HAADF) or Z-contrast image mode offers a significant advantage compared to classical image modes, bright-field (BF) and dark-field (DF). Few years ago, Brorson *et al.* showed for the first time HAADF-STEM to reveal the morphology of MoS₂, WS₂, Co–Mo–S, Ni–Mo–S and Ni–W–S

nanoclusters supported on graphitic carbon (non-industrial support). They found that Unpromoted MoS₂ and WS₂ are predominantly present as slightly truncated triangular clusters. The addition of promoter atoms results in more heavy truncations [61]. Recently, Beaubet *et al.* studied the effect of temperature and H₂/H₂S ratio on Co-promoted and non-promoted MoS₂ nanoslabs supported on alumina by a systematic analysis of HR HAADF-STEM images (**Figure 13**).

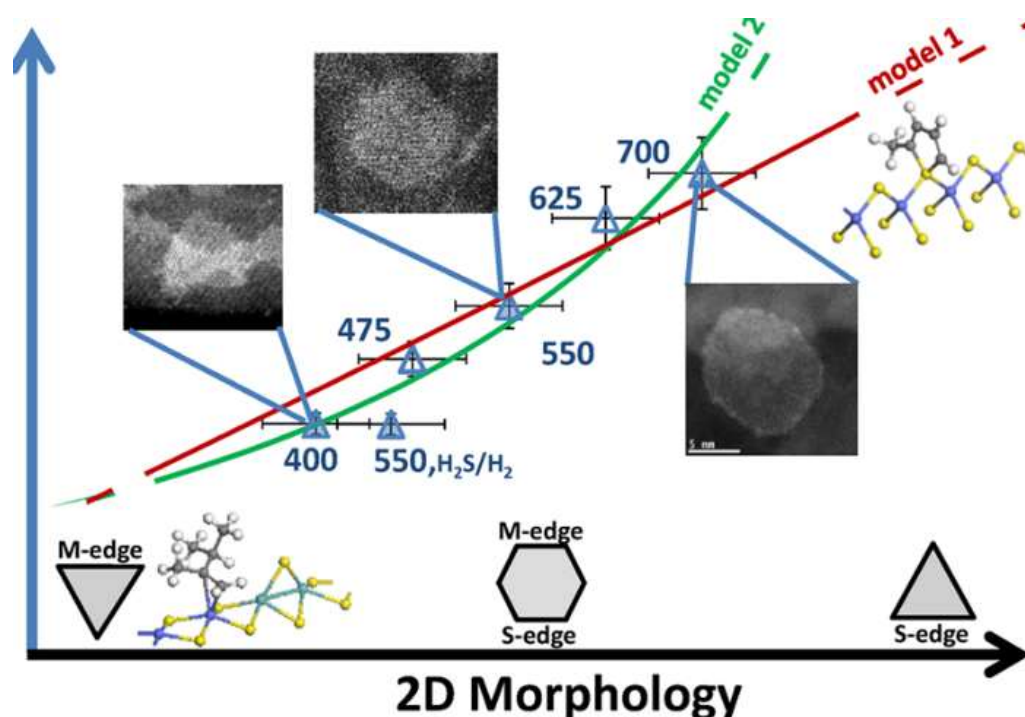


Figure 11. Evolution of the shape of the MoS₂ and CoMoS slabs according to the sulfidation conditions. Scheme reproduced from reference [62].

It was shown that this shape is directly linked to the nature of active M- and S-edges exposed by the CoMoS nanolayers, as proposed by DFT calculations [62]. From this work it is worth noting that in addition to the good atomic resolution, the samples analyzed are similar to those usually used in the industry.

Another outstanding approach of detailed 3D representation of heterogeneous industrial catalyst was recently presented by Eijsbouts *et al.*,

where it was presented the results of a 3D (STEM-HAADF) study of a high metal loading Ni–Mo catalyst [42]. The three-dimensional (3D) reconstruction showed that the active phase is mainly present as MoS₂ single slabs of various shapes aligned with the support. This is of great interest, because electronic microscopy is the most unambiguous method for the determination of the dispersion of the active phase in these catalysts.

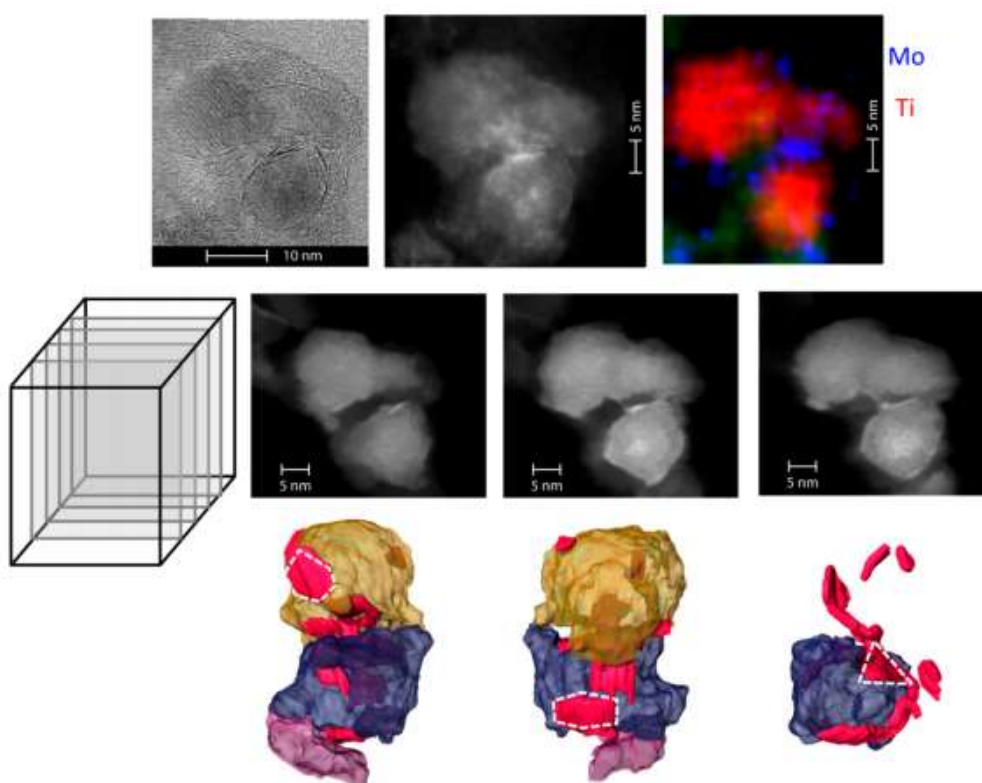


Figure 12. Particles imaged via 2D TEM, STEM-HAADF and STEM-EDX, via cross sections of the 3D image generated by 3D STEM-HAADF (middle) and after generation of a 3D reconstruction as viewed from different angles (bottom). Scheme extracted from reference [42].

As a proven technique, the adsorption of CO at low temperature followed by infrared spectroscopy (IR/CO) has been used intensively to probe the edges of MoS₂ slabs in HDS catalysts for several decades. Chen et al. reported on an advance towards industrial catalysts by showing IR/CO can discriminate

between M-edge and S-edge sites of alumina- supported MoS₂ phase. These results were based on a parallel study between Density Functional Theory (DFT) calculations and variations in position and intensity of IR bands of CO adsorbed on MoS₂/Al₂O₃ sulfided at various temperatures [6].

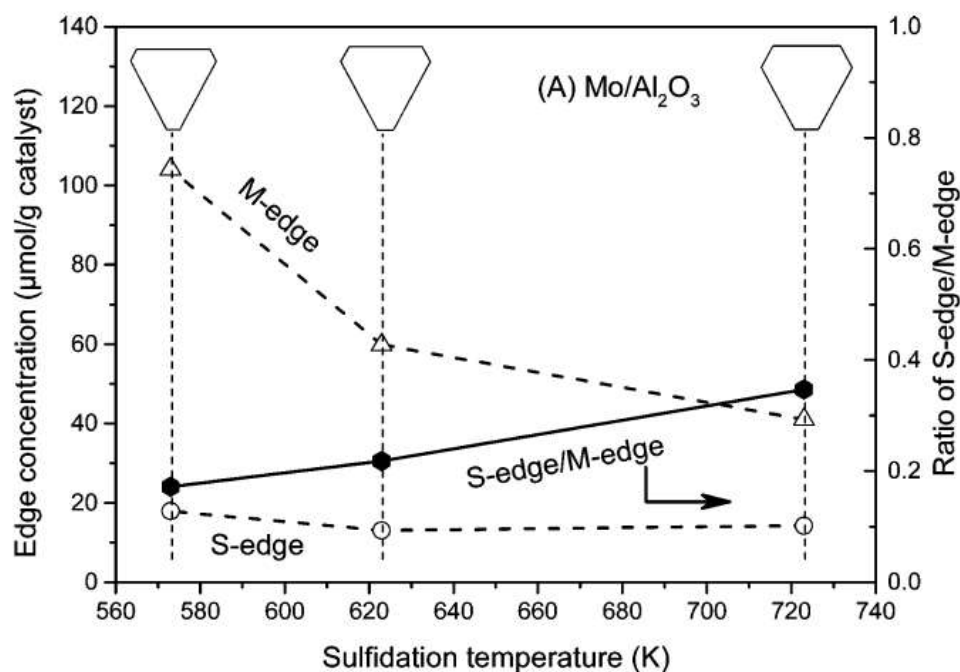


Figure 13. M-edge and S-edge site concentration detected by low-temperature CO adsorption (dash line) and the ratio of S-edge/M-edge (solid line) on (A) Mo/Al₂O₃ [6].

Since the molar extinction coefficients for each contribution were determined, the IR/CO technique allowed to inform on the amount on Mo sites on M- and S-edges of sulfided Mo/Al₂O₃, and thus, accounted for the shape of the MoS₂ nanoslabs [5,63]. This way, IR demonstrated to be a reliable technique to recognize the morphology of the particles as well as the quantification of active sites exposed by the slab giving access to the site dispersion and then to intrinsic activity. It has been also shown that TMS slab morphology is strongly influenced by the sulfide phase - support interactions [41]. For instance, Dominguez *et al.* demonstrated that the slab morphology is

strongly modified by the support nature, finding that the stronger the MoS₂-support interaction the higher the S-/M- edge ratio [64]. On TMS/Al₂O₃ too, it has been widely documented that the addition of an organic additive or a chelating agent during the impregnation stage can alter these interactions [49,65]. The role of chelating agent in HDS catalysts is described in deeper in the section 1.4.

I.3.4. W based hydrotreating catalyst morphology

W-based catalysts differ from Mo-based catalysts in many aspects. For example, W catalysts in oxidic form are much more difficult to convert to sulfidic form than molybdenum catalysts, and there is still no general agreement to what are the optimal sulfidation conditions for proper activation of these catalysts.

It was found that HAADF-STEM, in contrast to high-resolution transmission electron microscopy (HRTEM), enables ready observation of all the WS₂ nanoclusters and gives direct insight into their morphology. Conversely, when using characterization techniques as STEM-HAADF (atomic number sensitive technique) W-based catalysts are preferred for the observation, since this metal provides better contrast with Al₂O₃ compared to Mo due to the difference in atomic number. The first observations date from more than a decade ago, Carlsson *et al.* reported tungsten disulfide (WS₂) nanoclusters supported on high surface area graphite [48]. For these type of observations, the semiconductive qualities of graphite as support, allows a clear view of the well-ordered and regular structures, though the atomic resolution is not reached [66].

A study that stays closer to the observation of industrial catalysts, this is, using an industrial support, is the one recently presented by Alphazan et al. [27,67,68]. In here, they reported highly active W-based catalysts prepared through controlled surface chemistry supported on Amorphous Silica Alumina (ASA), whose enhanced activities are explained by the 2D hexagonal-like morphology of WS₂ particles (**Figure 14**). In that work, it was found that the morphology differences induce a change in the distribution of M-edge and S-edge sites around the crystallites, affecting the catalytic activity of WS₂.

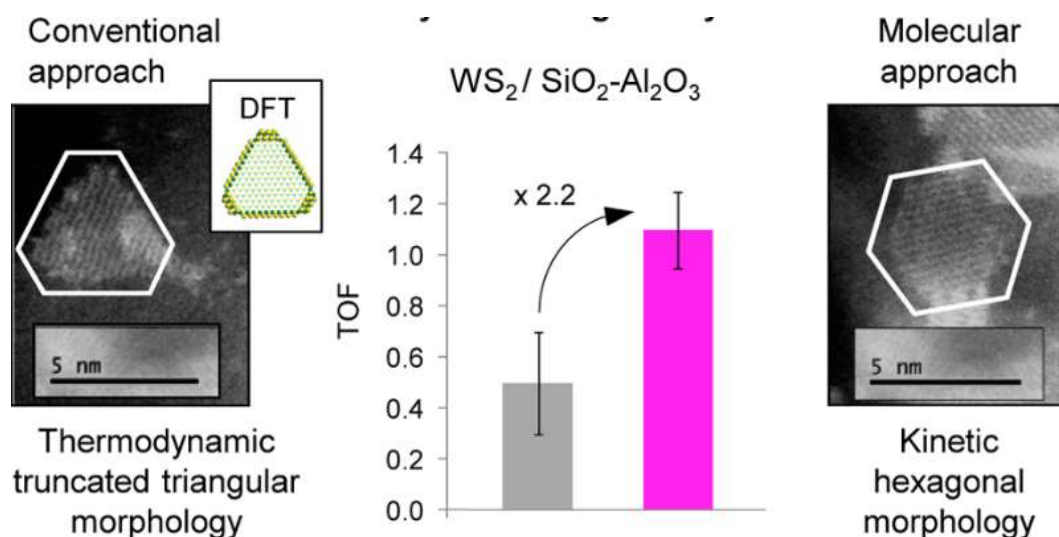


Figure 14. HAADF-STEM image evidence of the change of morphology and increase of catalytic activity. Scheme reproduced from reference [67].

Regarding spectroscopic techniques as IR, so far no reports have been established on the quantification of the W-based active sites or the assignment of their specific in situ FT-IR bands. The available spectra representing these samples are rather limited, and their interpretation based mainly on supposed analogies with chromium- and molybdenum-containing systems.

Thus, a better understanding of the nature of the active phases and of the role of the promoter in NiW-based catalysts is of prime importance. However,

the distinct chemical and morphological properties of tungsten-based catalysts are poorly understood when compared to the current level of information available for Mo-based catalysts. Despite intense research in this area, a strong challenge resides in the continuous improvement of the intrinsic catalytic performance of these active phases, and more particularly for WS₂ based catalysts. One of the major problems is the difficulty in improving the level of sulfidation of the active phase due to the formation of WO_xS_y and amorphous WO₃ inactive phases, probably as a result of the overly strong metal-support interactions[69,70]. The second challenge lies in the control of the morphology (shape) and size of the WS₂ or nanocrystallites [19].

I.4. Catalyst preparation with chelating agents

Chelating agents are organic molecules, which are added during the catalysts preparation in order to modify the formation and the properties of the sulfide phase.

Generally the chelating agents are organic compounds with carboxylic acid functions or amine ones. Since the patent from Shell in 1986, where it was shown the positive effect of the addition of diamino tetracetic acid (EDTA) on HDS CoMo catalysts supported on SiO₂ [71], the use of chelating agents have been extensively reported [72,73]. Recently, several studies have been published that affirm the outstanding effect of chelating agents on the activity of hydrotreatment catalysts [74–77]. They are able to form complex species either with the promoter metal like Co or Ni or the main metal (Mo or W). The main chelating agents under consideration are summarized in **Figure 15**.

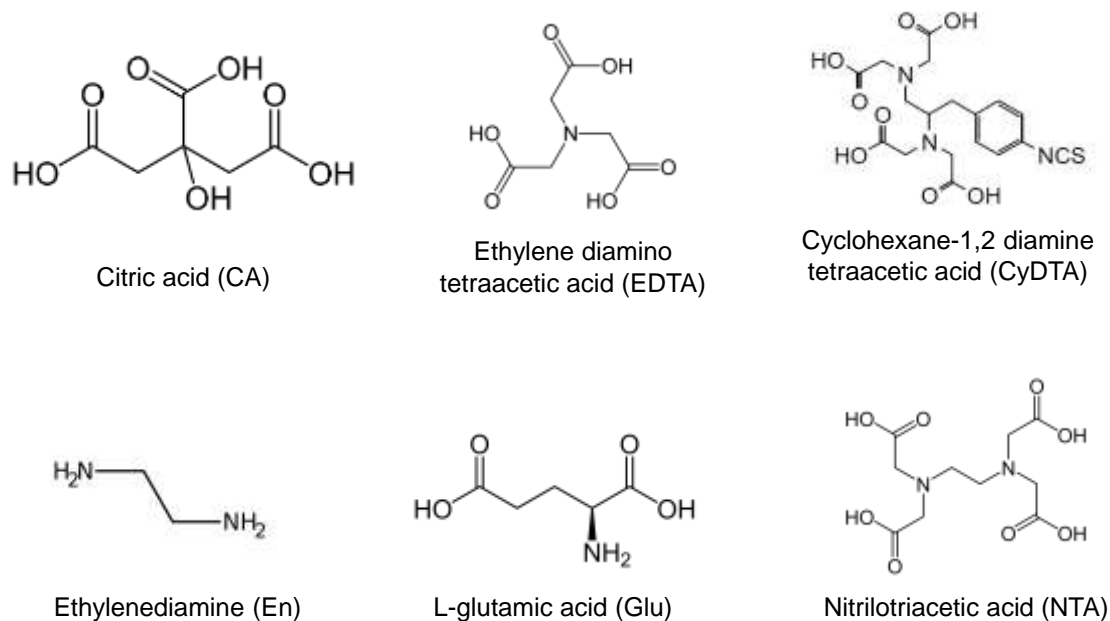


Figure 15. Chelating agents used for hydrotreatment catalyst preparations.

The preparation of catalysts containing organic compounds is carried out by several methods. Some of these organic compounds can be added during the incipient wetness impregnation of the active metals [78,79], or impregnated directly into the oxidic form of the catalyst in a second step [76,80]. Subsequently, the catalyst is dried to keep the different complexes intact and then, the catalyst is directly sulfided [81]. It seems that the beneficial effect is maximum if the interaction between the metal complexes and the chelating agent is preserved during the start of the sulfidation process [82].

I.4.1. Role of chelating agents

The addition of chelating agents is generally beneficial for the catalytic activity of hydrodesulfurization and hydrotreatment catalysts [74]. The origin of the effect is still under debate, although many proposals are reported in the literature [5,6,83,84]. The support plays a role on several aspects of the structure of the MoS₂ active phase (size, morphology, orientation, sulfidation

ratio, etc.) with important industrial implications for the design of improved catalytic formulations [85]. It has been also shown that MoS₂ morphology is strongly influenced by the sulfide phase - support interactions [41]. On MoS₂/Al₂O₃, the addition of an organic additive or a chelating agent during the impregnation stage can alter these interactions [38,86]. Thereby, chelating agent addition can change MoS₂ slab morphology of Mo catalyst deposited on industrially used support such as γ -Al₂O₃. However, direct information regarding the morphology of the MoS₂ prepared in presence of citric acid remains scarce. Another proposal is that the chelating agent will interact directly with the promoter and form a metallic complex.

The formation of this complex will have a direct effect on the sulfidation rate of the promoter (Co, Ni). Thus, the sulfidation of the Co or Ni would occur after the complete sulfidation of Mo (or W) [87]. Another proposal is that the chelation limits the loss of promoter by diffusion in the support. By the formation of a complex, the presence of chelating agent could limit the interaction between the metal and the carrier surface. Suárez-Toriello et al. proposed on NiW/Al₂O₃ catalysts that the citric acid presence and the impregnation pH influenced the NiWS phase formation. Citric acid provided isolation to supported metal species avoiding strong metal-support interactions, delaying nickel reduction at higher temperatures and decreasing WS₂ sintering when compared with a free-citric acid catalyst [80].

.An increase of activity is generally observed when a catalyst is prepared with a chelating agent [73,81,88]. Nevertheless, very different levels of increase are reported. This could be explained by nonconformities in the preparation modes as the presence or not of a calcination step before sulfidation, the nature or

amount of metallic precursors and/or of chelating agent molecule, the temperature program during the sulfidation stage as well as the HDS reactions conditions.

Several hypothesis have been proposed in the literature to explain, when observed, the positive effect of chelating agent addition on the activity of hydrotreatment catalysts.

1. Increase of Co in decoration position instead of Co inserted in alumina or the CoMoO_4 spinel.
2. Increase of the viscosity of the impregnation solution. This modification would lead to sol-gel formation, homogeneous dispersion of the active components and decrease of their interaction with the support.
3. Delay of the sulfidation and modification of the nature of the sites: one important effect of complexing agents is the delay of the separated Co or Ni sulfidation observed [89]. Studies have shown that, in CoMo catalysts prepared without complexing agents, the sulfidation of Co starts at 50°C and is completed at 150°C , whereas Mo is fully sulfided above 175°C . Thus, the sulfidation of the promoter metals (Co or Ni) is completed before the Mo one. On the other hand, in the catalysts prepared with chelating agents as EDTA and NTA, the sulfidation of the promoter starts around 150°C and is completed at 225°C . The chelating agent decreased the early sulfidation of the promoter.
4. Decrease of the interaction between the active phase and the support.

I.4.2. Citric acid as chelating agent

The incorporation of citric acid (CA) in the impregnation solutions during the catalysts synthesis is associated to a noticeable increase in the formation of the active phase (CoMoS, NiMoS and/or NiWS) and, to an increase in the HDS catalytic activity [73,90–93]. In general, it has been agreed that the catalytic improvements are related to combined effects involving the weakening of metal-support interaction and promoter sulfidation delay. Citric acid is highly soluble and it is environmentally harmless. In addition, it has economics advantages over other chelating agents used to improve TMS catalysts [80]. In previous works, Chen *et al.* [5,49,83,94] reported that the MoS₂ morphology can be gradually changed from a slightly truncated triangle exposing mainly M-edge to a hexagon exposing both M-edge and S-edge by means of adding citric acid. Here, the effect of citric acid on the morphology change of MoS₂ slabs is tentatively interpreted as lessening the amount of OH- groups available to interact with Mo atoms during the formation of MoS₂ phase [95] and thus reducing the MoS₂-Al₂O₃ interaction. The reduction of MoS₂-Al₂O₃ interaction likely changes the M-edge and S-edge relative free energy and, therefore, changes the MoS₂ morphology [4]. In this way, the MoS₂-Al₂O₃ interaction can be gradually reduced by varying the addition of citric acid because the amount of OH groups consumed must be correlated with the amount of citric acid used [49].

I.5 Low temperature CO adsorption followed by IR spectroscopy (IR/CO) contribution to characterize promoted and non-promoted catalysts.

I.5.1. Characterization of non-promoted catalysts by IR spectroscopy

The interactions of the probe molecule with the surface of sulfide MoS/Al₂O₃ type catalyst are of two types: the interactions of CO with the sulfide species and the interactions of CO with the support. On the IR spectra, several vibration bands between 2120 and 2000 cm⁻¹ have been reported. Various authors have proposed that there are due to the interaction of the probe molecule CO with the coordinatively unsaturated sites (CUS) M^{δ+}. The bands observed then result from the interaction of CO with atoms Mo⁰ or Mo⁴⁺ [96,97]. The interactions of CO with the support are characterized on the IR spectra by the presence of vibration bands at 2156 cm⁻¹ (interaction of CO by hydrogen bond with the Brønsted acid sites of the support) and between 2230 cm⁻¹ and 2180 cm⁻¹ (CO coordination with Lewis acid sites) [98]. The frequency position of vibration bands is directly related to the acidic strength of the probed sites.

Recently, a combination of experimental and theoretical studies carried out for non-promoted catalysts could distinguish stretching vibration of CO/Mo located on M-edge or S-edge of MoS₂ nanoparticles. It has been seen that CO interacts with Mo atoms located in M- and S-edge leading to two contributions at different wavenumbers, 2110 cm⁻¹ and 2070 cm⁻¹ due to their different environments [99,100]. The parallel between experimental and calculated results on MoS₂ allowed to attribute the main ν(CO) bands [100]. From DFT calculations, it was stated that the band characteristic of CO adsorbed on S-edge sites should be observed at lower wavenumber than the one for CO

adsorption on M-edge. Calculations indicate that various configurations of adsorption are possible on this kind of edges that could explain the broadness of the low wavenumber features (**Figure 16**).

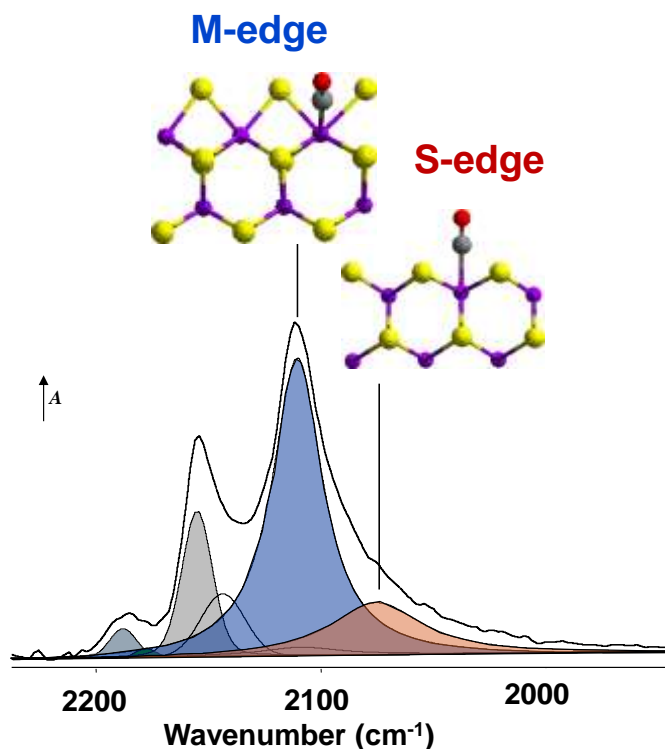


Figure 16. Assigned bands for MoS₂ according to DFT calculations [100].

Further researches proposed the decomposition of non-promoted catalysts spectra consists of seven components attributed to sulfided species and they can be assigned from lower wavenumber to higher wavenumber following: 1995 cm⁻¹ band is ascribed to metallic Mo [101], 2020, 2040 and 2068 cm⁻¹ bands are ascribed to Mo located on S-edge, 2099 and 2110 cm⁻¹ bands are ascribed to Mo located on M-edge, and finally 2126 cm⁻¹ band is ascribed to partially sulfided species.

On the other hand, the research studies on W/Al₂O₃ catalyst are less documented than their Mo counterpart. In some of the most relevant studies

carried out by Crepau et al. and Duchet et al. four main bands at 2191, 2154, 2117 and 2066 cm^{-1} are observed [97,102].

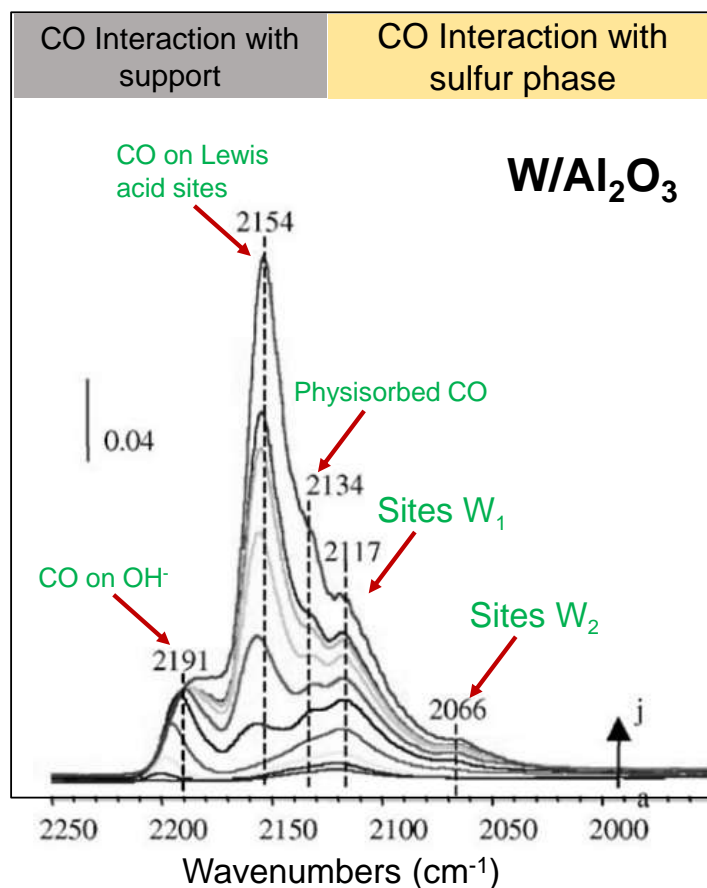


Figure 17. IR spectra of CO adsorbed at 100K on sulfided W catalysts with increasing doses. Spectra taken from reference [78].

These bands can be attributed, respectively, to coordination of CO on Lewis acid sites of the alumina support, CO in hydrogen bonding with the support hydroxyl groups and to CO in interaction with the edges of the WS_2 crystallites. In the work of Crepéau [102], these two bands at 2117 and 2066 cm^{-1} are denoted as W_1 and W_2 , respectively. At high CO uptake, the CO/OH band at 2154 cm^{-1} is observed to be dominant, and a shoulder at 2134 cm^{-1} , corresponding to physisorbed CO, appears. Later Zuo et al. studied the non-promoted W catalysts in order to follow the formation of the active phase in

sulfided NiW/Al₂O₃, nevertheless, major information about the W active sites is absent and still no assignation of the bands is showed [78].

The lack of information that allows to assign and quantify the IR results for sulfide W catalysts provoke that the results obtained from W based systems fall short in terms of the information they can provide. Since the assignment of the bands and decomposition of W catalysts is less documented than the MoS₂, in this work we will get into deeper understanding on chapters 1 and 3.

I.5.2. Characterization of promoted catalysts by IR spectroscopy

The characterization by CO/IR spectroscopy of the supported CoMo type catalysts is more complex than that of MoS₂ sheets. The IR spectrum does not result directly from the combination of the spectra obtained from the interaction of the probe molecule with the surface of the monometallic catalysts [98]. New bands appear and a change in intensities is observed, as it is observed in **Figure 18**. These changes in the IR spectra are directly related to the appearance of CoMo promoted sites as contrary to non-promoted sites. In **Figure 18**, is shown an example of IR spectra obtained for the CO adsorption on sulfided CoMo/Al₂O₃ and a Mo/ Al₂O₃ catalyst, carried out at 100 K. Two types of contributions are detected, the interactions of CO with the support and interactions of CO with the sulfide phase.

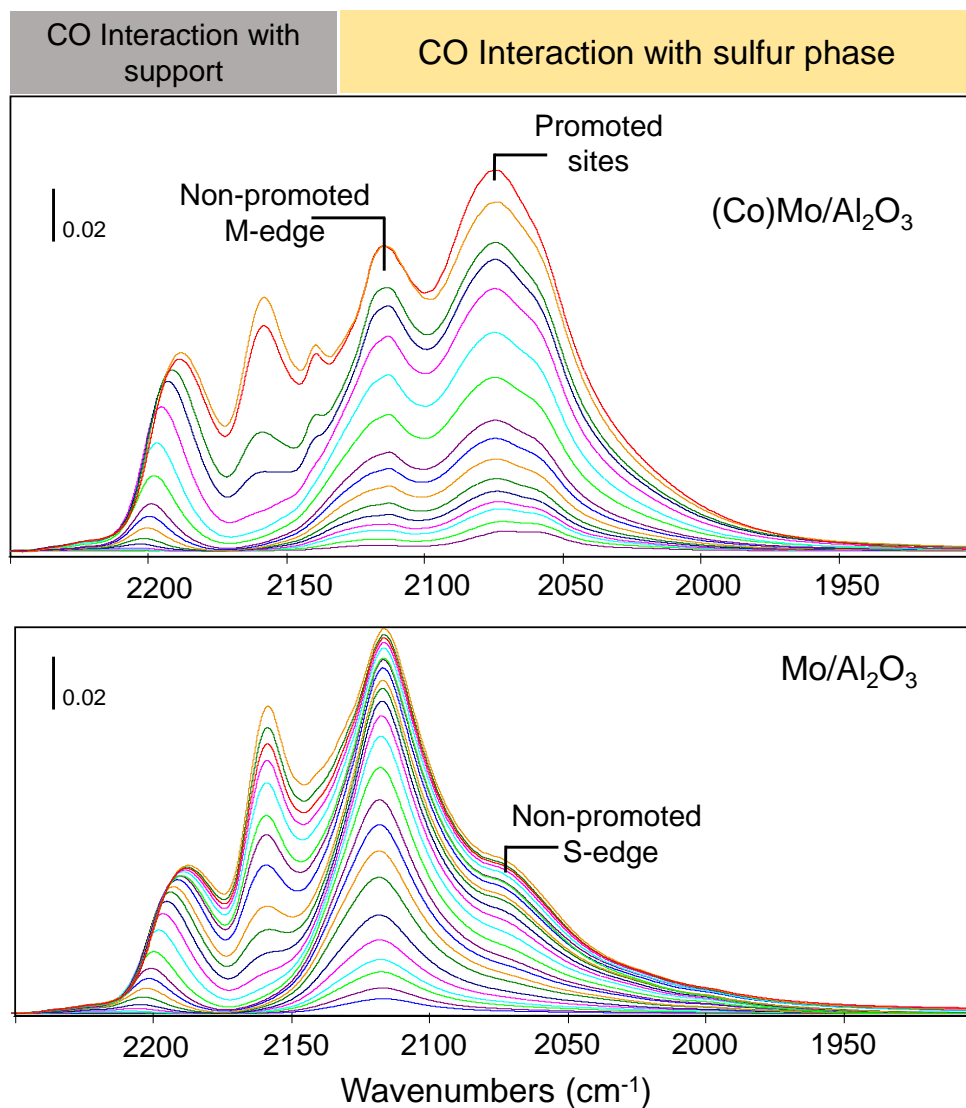


Figure 18. Obtained spectra for promoted and non-promoted catalysts sulfided at 623 K during 2h under 10% H₂S/H₂ mixture.

Thus, the assignment of CO stretching vibrations for promoted catalysts is still not completely established. The studies could only assign the $\nu(\text{CO})$ bands to CO interacting with non-promoted and promoted sites at 2110 cm⁻¹ and 2050-2090 cm⁻¹, respectively [63,65,103,104].

For the case of promoted W catalysts, Zuo et al. observed that the addition of Ni to W/Al₂O₃ brings three new bands at 2128, 2096 and 2068 cm⁻¹ (**Figure 19**).

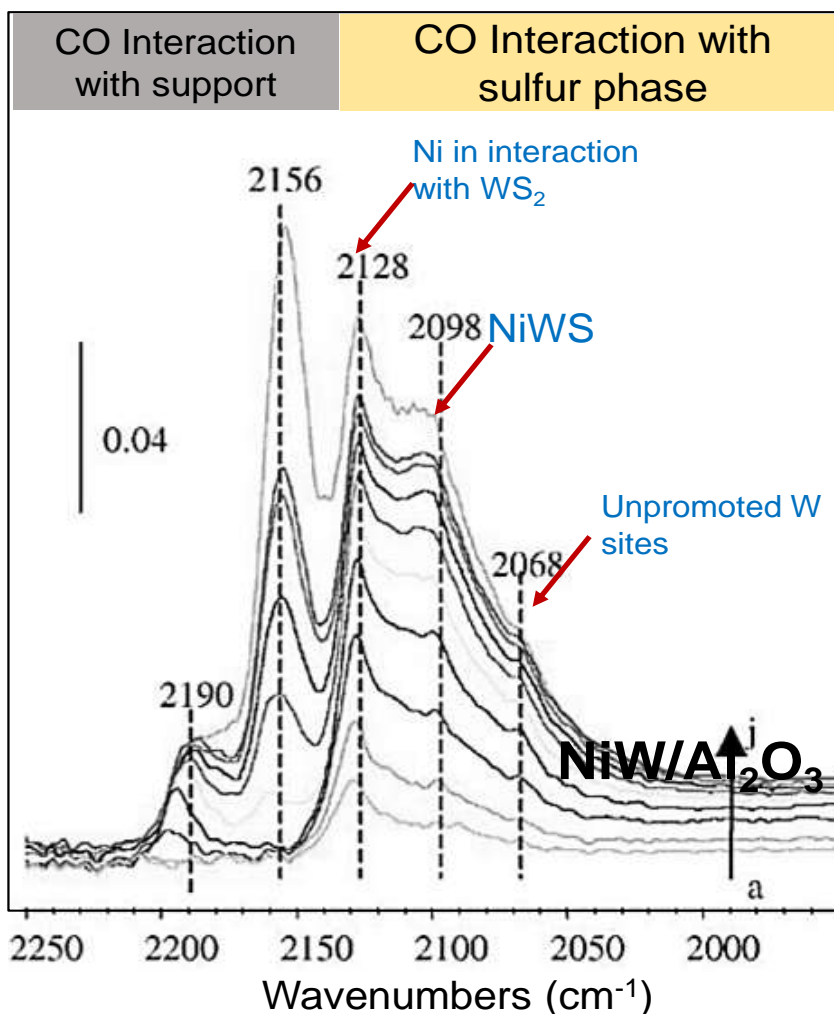


Figure 19. IR spectra of CO adsorbed at 100K on sulfided NiW catalysts with increasing doses. Figure taken from reference [78].

In the study of Duchet *et al.* [97], the 2090 cm^{-1} band (observed by Zuo *et al.* at 2096 cm^{-1}) was ascribed to the promoted NiWS phase while the two other bands at 2127 and 2073 cm^{-1} were attributed to a WS_2 phase perturbed by Ni. It was noticeable that these two later bands (2127 and 2073 cm^{-1}) are shifted to higher wavenumber with respect to unpromoted $\text{W}/\text{Al}_2\text{O}_3$ (2110 and 2060 cm^{-1}). Moreover, Maugé *et al.* [105] have also reported that the CO bands interacting with the NiMoS phase are shifted to higher wavenumbers as compared to the unpromoted Mo sites. In the above mentioned works, IR/CO spectroscopy

resulted to be reliable characterization to confirm the formation of the NiWS phase upon the addition of Ni.

I.6. Conclusion and scope of the thesis

The detailed characterization of the structure of TMS edge sites by infrared spectroscopy has been the subject of recent research. This has successfully provided the first experimental demonstration of industrial catalyst morphology by discriminating the two types of exposed edges (S edge and M edge). This IR/CO characterization method opens a promising path in streamlining the design of more active and selective hydrotreatment catalysts. However, it remains an indirect technique and it would benefit from being compared to direct observation of nano-sheets. This can be achieved using high-resolution dark field electron microscopy (HR STEM HAADF) based on a chemical contrast. Hence, one of the aim of the present work is to obtain a direct characterization of the slab morphology of MoS₂ supported on Al₂O₃ catalysts, prepared with exactly the same conditions of synthesis and sulfidation as those of the catalytic application. With this objective, a parallel study by means of HR STEM-HAADF (direct approach) and IR/CO spectroscopy method (indirect approach) is carried out on Mo catalysts prepared without or with citric acid.

Despite the considerable amount of research that has been made on Mo based systems, an accurate description of W based catalysts sites is still lacking. The aim is to use molecular modelling techniques to assign the stretching frequencies of CO adsorbed on an unpromoted WS₂ catalyst. For this, a parallel between IR/CO and DFT calculations will provide an insight into the assignation of exposed sites, matter that to this point has never been

reported before. We will compare both the methods of investigation and discuss the attribution of the IR bands in relation with our model.

This project is therefore a scientifically motivating challenge but also a concrete perspective to improve the performance of these catalysts whose large-scale use (30 000 ton/year) has a significant economic impact. This project is particularly innovative since the method of characterizing the morphology of MoS₂ slabs by CO adsorption followed by IR spectroscopy has been developed during the last few years.

I.7. REFERENCES

- [1] S. Eijsbouts, On the flexibility of the active phase in hydrotreating catalysts, *Appl. Catal. A Gen.* 158 (1997) 53–92.
- [2] F. Lauritsen, J. V., Nyberg, M., Vang, R. T., Bollinger, M. V., Clausen, B. S., Topsøe, H., ... & Besenbacher, Chemistry of one-dimensional metallic edge states in MoS₂ nanoclusters., *Nanotechnology.* 14 (2003) 385.
- [3] J. V. Lauritsen, S. Helveg, E. Lægsgaard, I. Stensgaard, B.S. Clausen, H. Topsøe, F. Besenbacher, Atomic-scale structure of Co-Mo-S nanoclusters in hydrotreating catalysts, *J. Catal.* 197 (2001) 1–5. doi:10.1006/jcat.2000.3088.
- [4] J. V Lauritsen, J. Kibsgaard, G.H. Olesen, P.G. Moses, B. Hinnemann, S. Helveg, J.K. Nørskov, B.S. Clausen, H. Topsøe, E. Laegsgaard, F. Besenbacher, Location and coordination of promoter atoms in Co-and Ni-promoted MoS₂-based hydrotreating catalysts, *J. Catal.* 249 (2007) 220–233. doi:10.1016/j.jcat.2007.04.013.
- [5] J. Chen, E. Dominguez Garcia, L. Oliviero, F. Maugé, How the CO molar extinction coefficient influences the quantification of active sites from CO adsorption followed by IR spectroscopy? A case study on MoS₂/Al₂O₃ catalysts prepared with citric acid, *J. Catal.* 332 (2015) 77–82. doi:10.1016/j.jcat.2015.09.005.
- [6] J. Chen, V. Labruyere, F. Maugé, A.A. Quoineaud, A. Hugon, L. Oliviero, IR Spectroscopic Evidence for MoS₂ Morphology Change with Sulfidation Temperature on MoS₂/Al₂O₃ Catalyst, *J. Phys. Chem. C.* 118 (2014) 30039–30044. doi:10.1021/jp510470g.
- [7] F.E. Topsøe, H., Clausen, B. S., & Massoth, *Catalysis Science and Technology*, Springer, Berlin, 1996. doi:doi.org/10.1007/978-3-642-61040-0_1.
- [8] E.T.C. Vogt, B.M. Weckhuysen, Fluid catalytic cracking: recent developments on the grand old lady of zeolite catalysis, *Chem. Soc. Rev.* 44 (2015) 7342. doi:10.1039/c5cs00376h.
- [9] A.C. Byrns, W.E. Bradley, M.W. Lee, Catalytic Desulfurization of Gasolines by Cobalt Molybdate Process, *Ind. Eng. Chem.* 35 (1943) 1160–1167. doi:10.1021/ie50407a007.
- [10] J.A. Rob Van Veen, What's new? On the development of sulphidic HT catalysts before the molecular aspects, *Catal. Today.* 292 (2017) 2–25. doi:10.1016/j.cattod.2016.09.027.
- [11] S. Advisors, Stratas Advisors, Sulfur Limits in On-Road Diesel. (2019). stratasadvisors.com/-sulfur-ranking2019.

- [12] Volume 1 World Oil Review 2018, (2018).
- [13] I.E. Agency, Oil Market Report, (2019). <https://www.iea.org/oilmarketreport/>.
- [14] G.E. Gary, J.H.; Handwerk, Petroleum refining processes, 2nd Editio, Marcel Dekker, Inc, 1984.
- [15] Mineral Commodity Summaries, (2019) Sulfur production report by the United States Geol.
- [16] M.E. Dry, Handbook of heterogeneous catalysis., 2008.
- [17] H. Wang, E. Iglesia, Thiophene hydrodesulfurization catalysis on supported Ru clusters: Mechanism and site requirements for hydrogenation and desulfurization pathways, *J. Catal.* 273 (2010) 245–256. doi:10.1016/J.JCAT.2010.05.019.
- [18] Delmon, B., Grange, P., & Froment, G. F. (Eds.), Hydrotreatment and hydrocracking of oil fractions, Elsevier, Antwerpen, 1999.
- [19] T. Alphazan, A. Bonduelle-Skrzypczak, C. Legens, A.S. Gay, Z. Boudene, M. Girleanu, O. Ersen, C. Copéret, P. Raybaud, Highly active nonpromoted hydrotreating catalysts through the controlled growth of a supported hexagonal WS₂ phase, *ACS Catal.* 4 (2014) 4320–4331. doi:10.1021/cs501311m.
- [20] C. Wivel, R. Candia, B.S. Clausen, S. Mørup, H. Topsøe, On the catalytic significance of a CoMoS phase in CoMo Al₂O₃ hydrodesulfurization catalysts: Combined in situ Mössbauer emission spectroscopy and activity studies, *J. Catal.* 68 (1981) 453–463. doi:10.1016/0021-9517(81)90115-9.
- [21] C. Wivel, B.S. Clausen, R. Candia, S. Mørup, H. Topsøe, Mössbauer emission studies of calcined CoMo Al₂O₃ catalysts: Catalytic significance of Co precursors, *J. Catal.* 87 (1984) 497–513. doi:10.1016/0021-9517(84)90210-0.
- [22] S. Brunet, D. Mey, G. Pérot, C. Bouchy, F. Diehl, On the hydrodesulfurization of FCC gasoline: a review, (2004). doi:10.1016/j.apcata.2004.10.012.
- [23] M. Girleanu, T. Alphazan, Z. Boudene, A. Bonduelle-Skrzypczak, C. Legens, A.S. Gay, C. Copéret, O. Ersen, P. Raybaud, Magnifying the morphology change induced by a nickel promoter in tungsten(IV) sulfide industrial hydrocracking catalyst: A HAADF-STEM and DFT study, *ChemCatChem.* 6 (2014) 1594–1598. doi:10.1002/cctc.201402115.
- [24] A. Stanislaus, B.H. Cooper, Aromatic Hydrogenation Catalysis: A Review, *Catal. Rev.* 36 (1994) 75–123. doi:10.1080/01614949408013921.
- [25] C. Bara, E. Devers, M. Digne, A.F. Lamic-Humblot, G.D. Pirngruber, X. Carrier, Surface Science Approaches for the Preparation of Alumina-Supported Hydrotreating Catalysts, *ChemCatChem.* 7 (2015) 3422–3440. doi:10.1002/cctc.201500436.

- [26] A. Absi-Halabi, M., Beshara, J., Qabazard, H., & Stanislaus, Catalysts in Petroleum Refining and Petrochemical Industries, 1995.
- [27] T. Alphazan, Towards the molecular design of hydrotreating catalysts prepared with metallo-organic precursors, 'École Normale Supérieure de Lyon Université de Lyon, 2013. <https://tel.archives-ouvertes.fr/tel-00998376>.
- [28] C. Dujardin, M.A. Lélías, J. Van Gestel, A. Travert, J.C. Duchet, F. Maugé, Towards the characterization of active phase of (Co)Mo sulfide catalysts under reaction conditions—Parallel between IR spectroscopy, HDS and HDN tests, *Appl. Catal. A Gen.* 322 (2007) 46–57. doi:10.1016/j.apcata.2007.01.010.
- [29] F.E. Massoth, Studies of molybdena-alumina catalysts. II. Kinetics and stoichiometry of reduction, *J. Catal.* 30 (1973) 204–217. doi:10.1016/0021-9517(73)90067-5.
- [30] J.M.J.G. Lipsch, G.C.A. Schuit, The CoO MoO₃ Al₂O₃ catalyst. III. Catalytic properties, *J. Catal.* 15 (1969) 179–189. doi:10.1016/0021-9517(69)90022-0.
- [31] R.J.H. Voorhoeve, Electron spin resonance study of active centers in nickel-tungsten sulfide hydrogenation catalysts, *J. Catal.* 23 (1971) 236–242. doi:10.1016/0021-9517(71)90045-5.
- [32] S. Topsøe, H., Clausen, B. S., Candia, R., Wivel, C., & Mørup, In Situ Mössbauer Emission Spectroscopy Studies of Unsupported and Supported Sulfided Co-Mo Hydrodesulfurization Catalysts: Evidence for and Nature of a Co-Mo-S Phase, *J. Catal.* 68 (1981) 433–452. doi:10.1016/0021-9517(81)90114-7.
- [33] P. Raybaud, H. Toulhoat, Catalysis by Transition Metal Sulfides: from molecular theory to industrial application, Technip, Paris, France, 2013, ISBN: 9782710809913.
- [34] L.S. Byskov, J.K. Nørskov, B.S. Clausen, H. Topsøe, Edge termination of MoS₂ and CoMoS catalyst particles, *Catal. Letters.* 64 (2000) 95–99. doi:10.1023/A:1019063709813.
- [35] E.J.M. Hensen, Y. Van Der Meer, J.A.R. Van Veen, J.W. Niemantsverdriet, Insight into the formation of the active phases in supported NiW hydrotreating catalysts, *Appl. Catal. A Gen.* 322 (2007) 16–32. doi:10.1016/j.apcata.2007.01.003.
- [36] M. V. Bollinger, J. V. Lauritsen, K.W. Jacobsen, J.K. Nørskov, S. Helveg, F. Besenbacher, One-Dimensional Metallic Edge States in MoS₂, *Phys. Rev. Lett.* 87 (2001) 196803. doi:10.1103/PhysRevLett.87.196803.
- [37] K.P. De Jong, Leon, C.A. Van Den Oetelaar, E.T.C. Vogt, S. Eijsbouts, A.J.

- Koster, H. Friedrich, P.E. De Jongh, High-Resolution Electron Tomography Study of an Industrial Ni-Mo/ γ -Al₂O₃ Hydrotreating Catalyst, (2006). doi:10.1021/jp061584f.
- [38] L. Dimitrov, R. Palcheva, A. Spojakina, K. Jiratova, Synthesis and characterization of W-SBA-15 and W-HMS as supports for HDS, *J. Porous Mater.* 18 (2011) 425–434. doi:10.1007/s10934-010-9394-0.
- [39] L. Vradman, M. V Landau, M. Herskowitz, V. Ezersky, M. Talianker, S. Nikitenko, Y. Kolytyn, A. Gedanken, High loading of short WS₂ slabs inside SBA-15: promotion with nickel and performance in hydrodesulfurization and hydrogenation, *J. Catal.* 213 (2003) 163–175. doi:S0021-9517(02)00012 -X.
- [40] Z.D. Huang, W. Bensch, L. Kienle, S. Fuentes, G. Alonso, C. Ornelas, SBA-15 as support for Ni-MoS₂HDS catalysts derived from sulfur-containing molybdenum and nickel complexes in the reaction of HDS of DBT: An all sulfide route, *Catal. Letters.* 127 (2009) 132–142. doi:10.1007/s10562-008-9656-5.
- [41] R. Nava, R.A. Ortega, G. Alonso, C. Ornelas, B. Pawelec, J.L.G. Fierro, CoMo/Ti-SBA-15 catalysts for dibenzothiophene desulfurization, *Catal. Today.* 127 (2007) 70–84. doi:10.1016/J.CATTOD.2007.02.034.
- [42] S. Eijsbouts, X. Li, J. Juan-Alcaniz, L.C.A. Van Den Oetelaar, J.A. Bergwerff, J. Loos, A. Carlsson, E.T.C. Vogt, Electron Tomography Reveals the Active Phase–Support Interaction in Sulfidic Hydroprocessing Catalysts, (2017). doi:10.1021/acscatal.7b01201.
- [43] W.D. Pyrz, D.J. Buttrey, Particle size determination using TEM: A discussion of image acquisition and analysis for the novice microscopist, *Langmuir.* 24 (2008) 11350–11360. doi:10.1021/la801367j.
- [44] S. Yamashita, J. Kikkawa, K. Yanagisawa, T. Nagai, K. Ishizuka, K. Kimoto, Atomic number dependence of Z contrast in scanning transmission electron microscopy, *Sci. Rep.* 8 (2018) 1–7. doi:10.1038/s41598-018-30941-5.
- [45] F. Besenbacher, M. Brorson, B.S. Clausen, S. Helveg, B. Hinnemann, J. Kibsgaard, J. V Lauritsen, P.G. Moses, J.K. Nørskov, H. Topsøe, Recent STM, DFT and HAADF-STEM studies of sulfide-based hydrotreating catalysts: Insight into mechanistic, structural and particle size effects, *Catal. Today.* 130 (2007) 86–96. doi:10.1016/j.cattod.2007.08.009.
- [46] L. Zavala-sanchez, X. Portier, F. Maugé, L. Oliviero, High Resolution STEM-HAADF microscopy on γ - Al₂O₃ supported MoS₂ catalyst – Proof by image of the changes in dispersion and morphology of the slabs with addition of citric acid, *Nanotechnology.* (2019) 1–10.

- [47] F. Besenbacher, M. Brorson, B.S. Clausen, S. Helveg, B. Hinnemann, J. Kibsgaard, J. V. Lauritsen, P.G. Moses, J.K. Nørskov, H. Topsøe, Recent STM, DFT and HAADF-STEM studies of sulfide-based hydrotreating catalysts: Insight into mechanistic, structural and particle size effects, *Catal. Today*. 130 (2008) 86–96. doi:10.1016/j.cattod.2007.08.009.
- [48] A. Carlsson, M. Brorson, H. Topsøe, Morphology of WS₂ nanoclusters in WS₂/C hydrodesulfurization catalysts revealed by high-angle annular dark-field scanning transmission electron microscopy (HAADF-STEM) imaging, *J. Catal.* 227 (2004) 530–536. doi:10.1016/j.jcat.2004.08.031.
- [49] J. Chen, F. Maugé, J. El Fallah, L. Oliviero, IR spectroscopy evidence of MoS₂ morphology change by citric acid addition on MoS₂/Al₂O₃ catalysts – A step forward to differentiate the reactivity of M-edge and S-edge, *J. Catal.* 320 (2014) 170–179. doi:10.1016/j.jcat.2014.10.005.
- [50] H. Schweiger, P. Raybaud, H. Toulhoat, Promoter Sensitive Shapes of Co(Ni)MoS Nanocatalysts in Sulfo-Reductive Conditions, *J. Catal.* 212 (2002) 33–38. doi:10.1006/JCAT.2002.3737.
- [51] E. Krebs, B. Silvi, P. Raybaud, Mixed sites and promoter segregation: A DFT study of the manifestation of Le Chatelier's principle for the Co(Ni)MoS active phase in reaction conditions, *Catal. Today*. (2008) 160–169. doi:10.1016/j.cattod.2007.06.081.
- [52] S. Helveg, J. V Lauritsen, E. Laegsgaard, I. Stensgaard, J.K. Nørskov, B.S. Clausen, H. Topsøe, F. Besenbacher, Atomic-Scale Structure of Single-Layer MoS₂ Nanoclusters, 2000.
- [53] P. Raybaud, J. Hafner, G. Kresse, S. Kasztelan, H. Toulhoat, Structure, Energetics, and Electronic Properties of the Surface of a Promoted MoS₂ Catalyst: An ab Initio Local Density Functional Study, *J. Catal.* 190 (2000) 128–143. doi:10.1006/jcat.1999.2743.
- [54] H. Schweiger, P. Raybaud, G. Kresse, H. Hervé, H. Toulhoat, Shape and Edge Sites Modifications of MoS₂ Catalytic Nanoparticles Induced by Working Conditions: A Theoretical Study, *J. Catal.* 207 (2002) 76–87. doi:10.1006/jcat.2002.3508.
- [55] J.V. Lauritsen, M. Nyberg, J.K. Nørskov, B.S. Clausen, H. Topsøe, E. Lægsgaard, F. Besenbacher, Hydrodesulfurization reaction pathways on MoS₂ nanoclusters revealed by scanning tunneling microscopy, *J. Catal.* 224 (2004) 94–106. doi:10.1016/J.JCAT.2004.02.009.
- [56] J. V Lauritsen, M. V Bollinger, E. Laegsgaard, K.W. Jacobsen, J.K. Nørskov,

- B.S. Clausen, H. Topsøe, F. Besenbacher, Atomic-scale insight into structure and morphology changes of MoS₂ nanoclusters in hydrotreating catalysts, *J. Catal.* 221 (2004) 510–522. doi:10.1016/j.jcat.2003.09.015.
- [57] S.J. Nellist, P. D., & Pennycook, Direct Imaging of the Atomic Configuration of Ultradispersed Catalysts, *Science* (80-.). 274 (1996) 413–415. doi: 10.1126/science.274.5286.413%0AArticle.
- [58] S.J. Pennycook, A.R. Lupini, M. Varela, A. Borisevich, Y. Peng, M.P. Oxley, K. Van Benthem, M.F. Chisholm, Scanning transmission electron microscopy for nanostructure characterization, in: *Scanning Microsc. Nanotechnol. Tech. Appl.*, Springer New York, 2007: pp. 152–191. doi:10.1007/978-0-387-39620-0_6.
- [59] S. Hillyard, J. Silcox, in *ADF STEM imaging*, *Ultramicroscopy*. 58 (1995) 6–17.
- [60] M. Vrinat, M. Breyse, C. Geantet, J. Ramirezb, A. Massoth, Effect of MoS₂ morphology on the HDS activity of hydrotreating catalysts, *Catal. Letters*. 26 (1994) 25–35.
- [61] M. Brorson, A. Carlsson, H. Topsøe, The morphology of MoS₂, WS₂, Co–Mo–S, Ni–Mo–S and Ni–W–S nanoclusters in hydrodesulfurization catalysts revealed by HAADF-STEM, (2007). doi:10.1016/j.cattod.2007.01.073.
- [62] B. Baubet, M. Girleanu, A.S. Gay, A.L. Taleb, M. Moreaud, F. Wahl, V. Delattre, E. Devers, A. Hugon, O. Ersen, P. Afanasiev, P. Raybaud, Quantitative Two-Dimensional (2D) Morphology-Selectivity Relationship of CoMoS Nanolayers: A Combined High-Resolution High-Angle Annular Dark Field Scanning Transmission Electron Microscopy (HR HAADF-STEM) and Density Functional Theory (DFT) Study, *ACS Catal.* 6 (2016) 1081–1092. doi:10.1021/acscatal.5b02628.
- [63] F. Maugé, J.C. Lavalley, FT-IR Study of CO Adsorption on Sulfided Mo/Al₂O₃ Unpromoted or Promoted by Metal Carbonyls: Titration of Sites, *J. Catal.* 137 (1992) 69–76. doi:10.1016/0021-9517(92)90139-9.
- [64] E. Dominguez Garcia, J. Chen, E. Oliviero, L. Oliviero, F. Maugé, New insight into the support effect on HDS catalysts: evidence for the role of Mo-support interaction on the MoS₂ slab morphology, (2020). doi:10.1016/j.apcatb.2019.117975.

- [65] M.A. Lé Lias, E. Le Guludec, L. Mariey, J. Van Gestel, A. Travert, L. Oliviero, F. Maugé, Effect of EDTA addition on the structure and activity of the active phase of cobalt-molybdenum sulfide hydrotreatment catalysts, *Catal. Today*. 150 (n.d.) 179–185. doi:10.1016/j.cattod.2009.07.107.
- [66] A. Carlsson, M. Brorson, H. Topsøe, Supported metal sulphide nanoclusters studies by HAADF-STEM., *J. Microsc. (Oxford, United Kingdom)*. 223 (2006) 179–181. doi:10.1111/j.1365-2818.2006.01614.x.
- [67] T. Alphazan, A. Bonduelle-Skrzypczak, L. Legens, A.-S. Gay, Z. Boudene, M. Girleanu, O. Ersen, C. Cope, P. Raybaud, Highly Active Nonpromoted Hydrotreating Catalysts through the Controlled Growth of a Supported Hexagonal WS₂ Phase, *ACS Catal.* 4 (2014) 42. doi:10.1021/cs501311m.
- [68] T. Alphazan, A. Bonduelle-Skrzypczak, C. Legens, Z. Boudene, A.L. Taleb, A.S. Gay, O. Ersen, C. Copéret, P. Raybaud, Improved promoter effect in NiWS catalysts through a molecular approach and an optimized Ni edge decoration, *J. Catal.* 340 (2016) 60–65. doi:10.1016/j.jcat.2016.05.004.
- [69] J.A. Bergwerff, T. Visser, B.R.G. Leliveld, B.D. Rossenaar, A. Krijn P. de Jong, Bert M. Weckhuysen, Envisaging the Physicochemical Processes during the Preparation of Supported Catalysts: Raman Microscopy on the Impregnation of Mo onto Al₂O₃ Extrudates, (2004). doi:10.1021/JA040107C.
- [70] X. Carrier, A. J. F. Lambert, M. Che, Ligand-Promoted Alumina Dissolution in the Preparation of MoOX/γ-Al₂O₃ Catalysts: Evidence for the Formation and Deposition of an Anderson-type Alumino Heteropolymolybdate, (1997). doi:10.1021/JA971981R.
- [71] G. Busca, Acid catalysts in industrial hydrocarbon chemistry, *Chem. Rev.* 107 (2007) 5366–5410. doi:10.1021/cr068042e.
- [72] M.A. Lé Lias, E. Le Guludec, L. Mariey, J. Van Gestel, A. Travert, L. Oliviero, F. Maugé, Effect of EDTA addition on the structure and activity of the active phase of cobalt-molybdenum sulfide hydrotreatment catalysts, *Catal. Today*. 150 (n.d.) 179–185. doi:10.1016/j.cattod.2009.07.107.
- [73] Q. Wei, Y. Zhou, C. Xu, Effects of citric acid used as chelating agent on the performance of heavy oil hydrotreating catalysts, *ACS Natl. Meet. B.*

- Abstr. (2011).
- [74] P. Mazoyer, C. Geantet, F. Diehl, S. Loridant, M. Lacroix, Role of chelating agent on the oxidic state of hydrotreating catalysts, *Catal. Today*. 130 (2007) 75–79. doi:10.1016/j.cattod.2007.07.013.
- [75] V.Y. Pereyma, P.P. Dik, O. V Klimov, S. V Budukva, K.A. Leonova, A.S. Noskov, Hydrocracking of Vacuum Gas Oil in the Presence of Catalysts NiMo/Al₂O₃-Amorphous Aluminosilicates and NiW/Al₂O₃- Amorphous Aluminosilicates, *Russ. J. Appl. Chem.* 88 (2015) 1722–1728. doi:10.1134/S10704272150120113.
- [76] C.E. Santolalla-Vargas, V.A. Suarez Toriello, J.A. De los Reyes, D.K. Cromwell, B. Pawelec, J.L.G. Fierro, Effects of pH and chelating agent on the NiWS phase formation in NiW/ γ -Al₂O₃ HDS catalysts, *Mater. Chem. Phys.* 166 (2015) 105–115. doi:10.1016/j.matchemphys.2015.09.033.
- [77] K. Al-Dalama, A. Stanislaus, A Comparative Study of the Influence of Chelating Agents on the Hydrodesulfurization (HDS) Activity of Alumina and Silica-Alumina-Supported CoMo Catalysts, *Energy and Fuels*. 20 (2006) 1777–1783. doi:10.1021/ef060125a.
- [78] D. Zuo, M. Vrinat, H. Nie, F. Maugé, Y. Shi, M. Lacroix, D. Li, The formation of the active phases in sulfided NiW/Al₂O₃ catalysts and their evolution during post-reduction treatment, *Catal. Today*. 93–95 (2004) 751–760. doi:10.1016/j.cattod.2004.06.078.
- [79] S.K. Fabrice Diehl, Christophe Bouchy, Tivadar Cseri, HYDROTREATING CATALYST THAT CONTAINS ANTROGEN-CONTAINING ORGANIC COMPOUND AND ITS USE, patent US 2007/O 155618 A1, 2007.
- [80] V.A. Suárez-Toriello, C.E. Santolalla-Vargas, J.A. De Los Reyes, A. Vázquez-Zavala, M. Vrinat, C. Geantet, Influence of the solution pH in impregnation with citric acid and activity of NiW/Al₂O₃ catalysts, *Journal Mol. Catal. A, Chem.* 404–405 (2015) 36–46. doi:10.1016/j.molcata.2015.04.005.
- [81] A. Van Veen, J. R., Gerkema, E., Van der Kraan, A. M., & Knoester, A real support effect on the activity of fully sulphided CoMoS for the hydrodesulphurization of thiophene., *J. Chem. Soc., Chem. Comm.* 22 (1987) 1684–1686.
- [82] AkzoNobel, European Patent, 2000.
- [83] J. Chen, J. Mi, K. Li, X. Wang, E. Dominguez Garcia, Y. Cao, L. Jiang, L. Oliviero, F. Oise, Role of Citric Acid in Preparing Highly Active CoMo/Al₂O₃

- Catalyst: From Aqueous Impregnation Solution to Active Site Formation, *Ind. Eng. Chem. Res.* 56 (2017) 14172–14181. doi:10.1021/acs.iecr.7b02877.
- [84] V.Y. Pereyma, O. V Klimov, I.P. Prosvirin, E.Y. Gerasimov, S.A. Yashnik, A.S. Noskov, Effect of thermal treatment on morphology and catalytic performance of NiW/Al₂O₃ catalysts prepared using citric acid as chelating agent, (2018). doi:10.1016/j.cattod.2017.07.019.
- [85] C. Bara, L. Plais, K. Larmier, E. Devers, M. Digne, A.F. Lamic-Humblot, G.D. Pirngruber, X. Carrier, Aqueous-Phase Preparation of Model HDS Catalysts on Planar Alumina Substrates: Support Effect on Mo Adsorption and Sulfidation, *J. Am. Chem. Soc.* 137 (2015) 15915–15928. doi:10.1021/jacs.5b10975.
- [86] Y. Okamoto, K. Hioka, K. Arakawa, T. Fujikawa, T. Ebihara, T. Kubota, Effect of sulfidation atmosphere on the hydrodesulfurization activity of SiO₂-supported Co-Mo sulfide catalysts: Local structure and intrinsic activity of the active sites, *J. Catal.* 268 (2009) 49–59. doi:10.1016/j.jcat.2009.08.017.
- [87] A.M. De Jong, V.H.J. (San,) De Beer, J.A. Rob Van Veen, H. Niemantsverdriet, Surface Science Model of a Working Cobalt-Promoted Molybdenum Sulfide Hydrodesulfurization Catalyst: Characterization and Reactivity, *J. Phys. Chem.* 100 (1996) 17772–17724..
- [88] M. Sun, D. Nicosia, R. Prins, The effects of fluorine, phosphate and chelating agents on hydrotreating catalysts and catalysis, *Catal. Today.* 86 (2003) 173–189. doi:10.1016/S0920-5861(03)00410-3.
- [89] R. Cattaneo, T. Shido, R. Prins, The Relationship between the Structure of NiMo/SiO₂ Catalyst Precursors Prepared in the Presence of Chelating Ligands and the Hydrodesulfurization Activity of the Final Sulfided Catalysts, *J. Catal.* 185 (1999) 199–212. doi:10.1006/JCAT.1999.2492.
- [90] L.I.U. Bin, L.I.U. Lei, C. Yong-ming, Z. Jin-chong, L.I.U. Chen-guang, Essential role of promoter Co on the MoS₂ catalyst in selective hydrodesulfurization of FCC gasoline, *J. Fuel Chem. Technol.* 46 (2018) 441–450. doi:10.1016/S1872-5813(18)30019-7.
- [91] T. Fujikawa, Highly Active HDS Catalyst for Producing Ultra-low Sulfur Diesel Fuels, *Top. Catal.* 52 (2009) 872–879. doi:10.1007/s11244-009-9228-y.
- [92] Y. Fan, H. Xiao, G. Shi, H. Liu, Y. Qian, T. Wang, G. Gong, X. Bao, Citric acid-assisted hydrothermal method for preparing NiW/USY-Al₂O₃ ultradeep hydrodesulfurization catalysts, (2011). doi:10.1016/j.jcat.2010.12.014.
- [93] D. Valencia, T. Klimova, Kinetic study of NiMo/SBA-15 catalysts prepared with citric acid in hydrodesulfurization of dibenzothiophene, *CATCOM.* 21 (2012) 77–

81. doi:10.1016/j.catcom.2012.02.003.
- [94] J. Chen, E. Dominguez Garcia, E. Oliviero, L. Oliviero, F. Maugé, Effect of high pressure sulfidation on the morphology and reactivity of MoS₂ slabs on MoS₂/Al₂O₃ catalyst prepared with citric acid, *J. Catal.* 339 (2016) 153–162. doi:10.1016/j.jcat.2016.04.010.
- [95] P. Blanchard, C. Lamonier, A. Griboval, E. Payen, New insight in the preparation of alumina supported hydrotreatment oxidic precursors: A molecular approach, *Appl. Catal. A Gen.* (2007) 33–45. doi:10.1016/j.apcata.2007.01.018.
- [96] D. Bachelier, J., Tilliette, N. J., Cornac, M., Duchet, J. C., Lavalley, J. C., & Cornet, SULFIDED CoMo/Al₂O₃ CATALYSTS: CARBON MONOXIDE CHEMISORPTION AND SURFACE STRUCTURES, *Bull. Des Sociétés Chim. Belges.* 93 (1984) 743–750.
- [97] D. Duchet, J. C., Lavalley, J. C., Housni, S., Ouafi, D., Bachelier, J., Lakhdar, M., ... & Cornet, Carbon monoxide and oxygen chemisorption and functionalities of sulphided Ni-W/Al₂O₃ hydrotreating catalysts, *Catal. Today.* 4 (1988) 71–96. doi:10.1016/0920-5861(88)87047-0.
- [98] Vincent Labruyère, Structure des sites sulfures des catalyseurs d'hydrotraitement: Approche combinée par spectroscopie IR et modélisation moléculaire, Université de Caen, France., 2014.
- [99] A. Travert, C. Dujardin, F. Maugé, E. Veilly, S. Cristol, J.-F. Paul, E. Payen, CO Adsorption on CoMo and NiMo Sulfide Catalysts: A Combined IR and DFT Study, *Phys. Chem. B.* 110 (2006) 1261–1270. doi:10.1021/jp0536549.
- [100] A. Travert, C. Dujardin, F. Maugé, S. Cristol, J.F. Paul, E. Payen, D. Bougeard, Parallel between infrared characterisation and ab initio calculations of CO adsorption on sulphided Mo catalysts, *Catal. Today.* 70 (2001) 255–269.
- [101] E. DECANIO, D.A. (Texaco I.. B.N. (United S. Storm, Determination of Zero-valent molybdenum after moderate temperature reduction of alumina-supported catalysts, *J. Catal.* 130 (1991) 653–656. doi:10.1016/0021-9517(91)90144-S.
- [102] G. Crepéau, caractérisation de l'acidité de catalyseurs d'hydrocraquage amorphes sulfures., University of Caen, 2002.
- [103] C. Dujardin, M.A. Lélías, J. Van Gestel, A. Travert, J.C. Duchet, F. Maugé, Towards the characterization of active phase of (Co)Mo sulfide catalysts under reaction conditions-Parallel between IR spectroscopy, HDS and HDN tests, (2007). doi:10.1016/j.apcata.2007.01.010.
- [104] M.A. Lélías, P.J. Kooyman, L. Mariey, L. Oliviero, A. Travert, J. Van Gestel, J.A.R. Van Veen, F. Maugé, Effect of NTA addition on the structure and activity

- of the active phase of cobalt-molybdenum sulfide hydrotreating catalysts, (2009). doi:10.1016/j.jcat.2009.07.006.
- [105] F. Maugé, J.C. Duchet, J.C. Lavalley, S. Houssenbay, E. Payen, J. Grimblot, S. Kasztelan, The sulphided state of nickel molybdenum catalysts supported on zirconia and aluminates, *Catal. Today*. 10 (1991) 561–577. doi:10.1016/0920-5861(91)80039-C.

Chapter II: Experimental Section

Content Chapter II. Experimental Section

II.1. Catalyst Preparation.....	71
II.2. Textural properties and composition.	72
II.2.1. Surface properties: Nitrogen adsorption.	72
II.2.2. Elemental analysis by Inductively Coupled Plasma (ICP).	73
II.3. FTIR spectroscopy: Principe of the technique.	73
II.3.1. FTIR and probe molecules.	77
II.3.2. Carbon monoxide as a probe molecule.	78
II.3.3. IR spectroscopy: set up used for this thesis.	81
II.3.4. Spectra decomposition and treatment.	83
II.4. Microscopy aspects.	86
II.4.1. High-resolution Transmission Electron Microscopy (HRTEM).	86
II.4.2. HR-STEM HAADF as a tool for observing MS ₂ morphology at atomic scale.	87
II.4.3. HR STEM-HAADF operation parameters.	89
II.5. Density Functional Theory (DFT) calculations.	90
II.5.1. The Vienna Ab Initio Simulation Package VASP — Basic Methodology.	91
II.5.2. Computational techniques used for this work.	92
II.6. Catalytic activity measurements: Thiophene HDS reaction.	93
II.7. Conclusions of the Experimental part.	94
II.8. References	95

II.1. Catalyst Preparation.

The materials studied consisted in a series of unpromoted and promoted M_1 - $(M_2)/Al_2O_3$ ($M_1=Mo,W$) ($M_2=Co,Ni$) catalyst supported on commercial γ - Al_2O_3 (Sasol extrudates, surface area ($242\text{ m}^2\cdot\text{g}^{-1}$)). In Table III the list of the different precursor salts is listed. The catalysts were prepared by a one-step pore volume impregnation method and, citric acid (CA, $C_6H_8O_7\cdot H_2O$, PROLABO) was used as a chelating agent in some of them. Before impregnation, alumina support was crushed and sieved between 0.2 – 0.5 mm and calcined in an air flow at 723 K for 4 h.

Table III. Summary of reagents used for catalyst preparations.

Precursors salts		
Catalyst	Transition metal	Promoter
Mo/γ-Al_2O_3	AHT, $(NH_4)_6Mo_7O_{24}\cdot 4H_2O$ MERK	
CoMo/γ-Al_2O_3	AHT, $(NH_4)_6Mo_7O_{24}\cdot 4H_2O$ MERK	$Co(NO_3)_2\cdot 6H_2O$, Alfa Aesar, 98%
W/γ-Al_2O_3	$(NH_4)_6H_2W_{12}O_{40}\cdot xH_2O$ Aldrich	
NiW/γ-Al_2O_3	$((NH_4)_6H_2W_{12}O_{40}\cdot xH_2O$ Aldrich	$Ni(NO_3)_2\cdot 6H_2O$, Alfa Aesar, 98 %

For the non-promoted catalysts, alumina was impregnated with an aqueous solutions of appropriate amounts of ammonium heptamolybdate tetrahydrate (AHT, $(NH_4)_6Mo_7O_{24}\cdot 4H_2O$) or ammonium metatungstate hydrate [$(NH_4)_6H_2W_{12}O_{40}\cdot H_2O$]. For the promoted catalysts, $Co(NO_3)_2\cdot 6H_2O$, Alfa Aesar, 98% or $Ni(NO_3)_2\cdot 6H_2O$, Alfa Aesar, 98% in appropriate ratio was added to the impregnation solutions. After impregnation, the materials were left for maturation at room temperature for 2 h and subsequently the catalysts were dried at 383 K for 16 h. This later step was performed inside a rotatory furnace with air flow ($100\text{ ml}\cdot\text{min}^{-1}$). The heating rate was fixed at $3\text{ K}\cdot\text{min}^{-1}$. Note that these catalysts were not calcined in order to keep the chelating agent in its initial form. The scheme of preparation is described in **Figure 20**. Hereinafter,

the catalysts prepared with citric acid are denoted as $M_1(M_2)$ ($CA/(M_1+M_2) = x$)/ Al_2O_3 , x refers to the molar ratio of citric acid (CA) to M_1+M_2 . $x = 0, 0.5, 1.0,$ and 2.0 . For activation, the oxide sample was submitted to a flow mixture H_2S/H_2 10% at 623 K (Mo) or 673 K (W) during 2h.

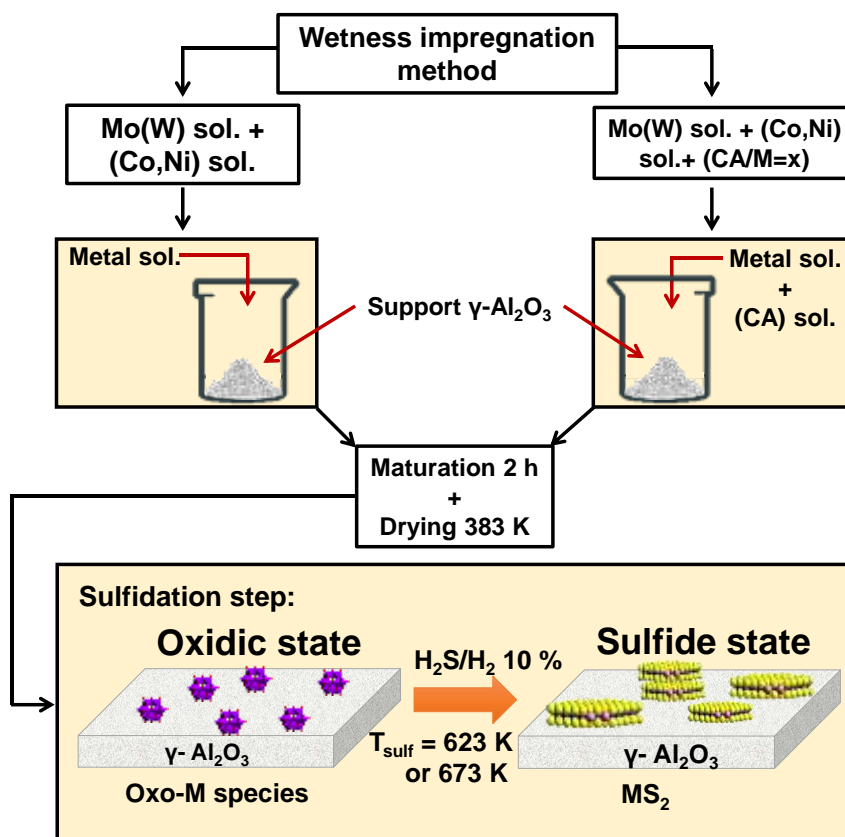


Figure 20. Catalyst preparation scheme used for the materials studied in this thesis.

II.2. Textural properties and composition.

II.2.1. Surface properties: Nitrogen adsorption.

Nitrogen adsorption/desorption isotherms were measured at -196 °C using Micrometrics Model ASAP 2020 volumetric adsorption analyzer. Samples were degassed at 250 °C under vacuum for 12 h prior to analysis. Specific surface areas were determined from the BET equation. The total pore volume was

calculated from the volume adsorbed at $P/P_0 = 0.95$. Pore size distributions of solids were estimated by Barrett-Joyner-Halenda (BJH) method.

II.2.2. Elemental analysis by Inductively Coupled Plasma (ICP).

Oxide catalysts were sulfided ex-situ in a glass reactor connected with 10% H_2S/H_2 flow ($30 \text{ ml}\cdot\text{min}^{-1}$). Catalysts were sulfided at 623 K during 2 h with a heating rate of $3 \text{ K}\cdot\text{min}^{-1}$. After, the temperature was cooled down to 298 K under N_2 flow ($30 \text{ ml}\cdot\text{min}^{-1}$). The catalyst inside the closed reactor was introduced in a dry box under Ar flow, to avoid totally air contact. Then, inside the dry box, 50 mg of sample was dissolved in hydrofluoric acid, aqua regia, boric acid, and water in a specific proportion with a total volume of 100 ml. Mo, W, Co, Ni and S amount present in the catalysts was quantified by an inductively coupled plasma atomic emission spectrometry (ICP-AES) using a PerkinElmer Optima 330DV ICP instrument.

II.3. FTIR spectroscopy: Principe of the technique.

Material surfaces are directly involved in important catalysis processes such as adsorption, desorption, diffusion, etc. Normally, surfaces are formed by the presence of a large number of defects of the crystalline lattice as edges, corners, terraces, steps, in the dispersed material that lead to having different surface properties. The ions on the surface are characterized by less coordination than those in the volume (coordinately unsaturated sites, CUS), and the unfilled coordination of these ions makes them active for adsorption of molecules and then for catalysis. IR spectroscopy is outstandingly valuable for investigation of solid samples as powders. It provides direct information about the chemical nature of surface or adsorbed species as well as about their

structures and strengths of the chemical bonds. Thus, IR is a great technique to study the catalyst surface and understand the role of the active sites in catalytic reaction. Heterogeneous catalysts are complex systems whose properties are given by a combination of multiple factors. A series of important surface characteristics are directly involved in the stages of catalytic processes, consequently, surface science is a cornerstone for modern chemistry and physics [1]. Infrared spectroscopy (IR) relies on the interaction of electromagnetic radiation with a sample. This radiation is characterized by its frequency (ν), or its wavelength (λ). The wavenumber, which corresponds to the inverse of the wavelength ($1/\lambda$) is more widely used in IR spectroscopy. IR spectroscopy gives access to an identification of chemical functions from their vibrational properties. The comparison between incident and transmitted radiation through the sample makes possible the identification and quantification of the main chemical functions present in the sample [2,3]. The **Figure 21** represents the different energy levels of an isolated molecule subjected to electromagnetic radiation. In the case of IR spectroscopy (corresponding to the infrared medium in the area $4\,000\text{ cm}^{-1}$ - 400 cm^{-1}), we are interested in vibrational energy levels.

Beer-Lambert law (Eq. 1), makes possible to relate the absorbance at the frequency ν to the concentration of the absorbing chemical function:

$$A = \log\left(\frac{I_0}{I}\right) = \varepsilon \times L \times C \quad (\text{Eq. 1})$$

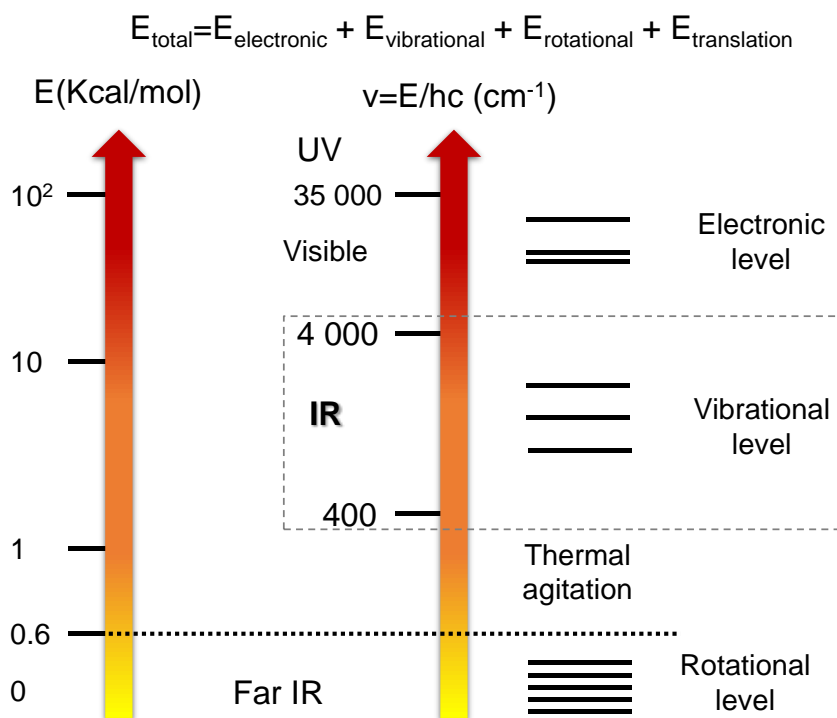


Figure 21. Energy levels diagram of an isolated molecule.

where A is the absorbance at the frequency ν , I_0 the intensity of the incident IR radiation, I the intensity of the transmitted IR radiation, ϵ the molar attenuation coefficient ($\text{mol}^{-1} \cdot \text{cm}^2$) associated with the chemical frequency function ν , L the thickness of the sample (cm), and C the concentration in ($\text{mol} \cdot \text{cm}^{-3}$).

The absorbance or transmission measurement can be performed using different types of equipment. Currently, Fourier transform spectrophotometers are the most widely used. They consist of a source generating the infrared radiation and of a detector for detecting radiation resulting from an optical system for selecting the path of IR radiation (**Figure 22**).

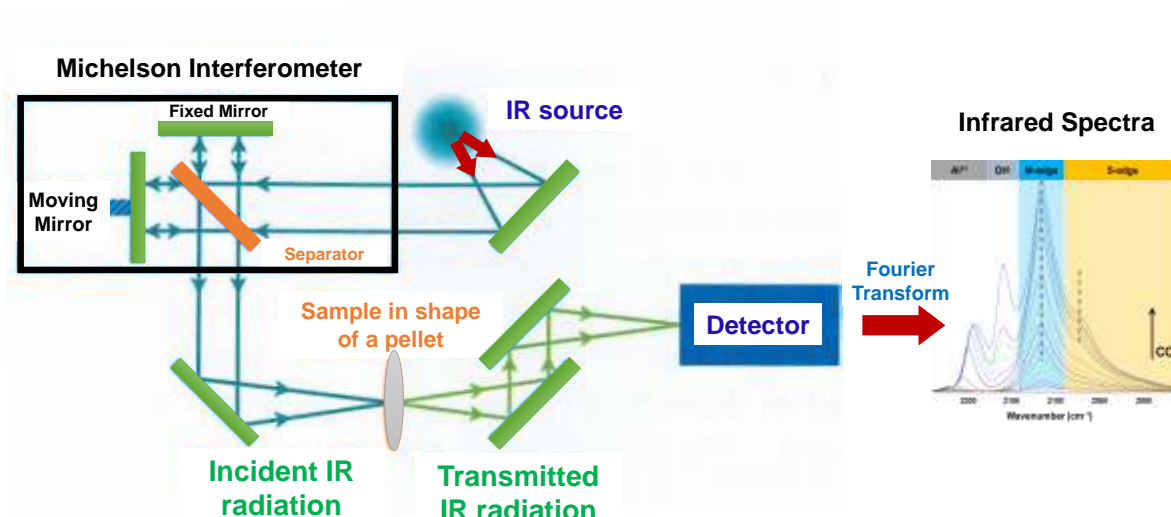


Figure 22. Scheme of the principle of functioning of an IR spectrometer.

A. The source

IR spectrometers generally have a polychromatic source. The operation of these sources is delicate because it is necessary to find a compromise between the energy of the source related to its temperature and its lifetime. The sources are usually made from refractory oxides or silicon carbide.

B. The detectors

The two more popular detectors for a FTIR spectrometer are the deuterated tryglycine sulfate (DTGS) and the Mercury cadmium telluride (MCT). Quantum detectors (PbS, MCT, etc.) are more sensitive and faster but require cooling at the liquid nitrogen temperature. In our study, we use a detector type MCT to obtain a better sensitivity during characterizations. In general the MCT detector is faster and more sensitive than the DTGS detector.

C. The optical principal of a Fourier transform IR spectrometer

Fourier transformer IR spectrometers use an optical system of the Michelson interferometer type. A semi-transparent separating blade and a mobile mirror allow the acquisition of an interferogram (electrical signal as a function of time). A mathematic treatment by Fourier transform then makes it possible to transform the information obtained in the space of time into information in the frequency space.

II.3.1. FTIR and probe molecules.

A powerful tool to obtain a detailed description of the catalyst surface properties is the use of probe molecules in combination with an investigative technique able to monitor with sufficient sensitivity the probe surface interaction [4,5]. One of the most widely used techniques that follows this approach, is mid-infrared spectroscopy ($4200\text{-}400\text{ cm}^{-1}$) using probe molecules. The method is indirect, in the sense that it monitors the surface through the perturbation inferred to the probe. The observables are the changes in vibrational frequency and intensity of the probe modes. The IR spectrum of an activated sample gives some direct information about the material. In most favorable cases, general conclusions can be drawn concerning the surface hydroxyl groups and some stable surface species. However the IR spectrum is “blind” with respect to the presence of coordinately unsaturated sites (CUS) ions, which are decisive for the catalytic properties. IR spectroscopy also gives rather poor information about the acidity of the surface hydroxyl groups which are of great importance for the surface properties. In addition, no discriminations between the core and surface can be drawn. These problems are solved by the use of probe molecules [2]. A probe molecule is a substance that interacts with the surface: the alteration of the spectra features as a result of adsorption can provide direct information about

the properties, location, and concentration and so on of the surface sites. The ideal probe molecule should meet the criteria listed in Table IV.

Table IV. Characteristics for selecting a probe molecule [2,6].

Qualities of a good probe molecule for FTIR	The functional group or the atom through which the molecule is bonded to the surface should be well known
	Adsorption complexes should be stable enough to allow characterization
	The probe molecule should occupy the same kind of sites during adsorption on different oxides and form complexes with similar structures.
	The probe molecules should have spectral parameters that are sensitive to the state of the sites on which they are adsorbed.
	The informative adsorption bands of the surface species should be in regions in which samples are transparent
	The attenuation coefficients of the informative band must be high
	The probe molecule should not cause any chemical modification of the surface
	The probe molecule should be small enough to avoid steric hindrance of the adsorption

II.3.2. Carbon monoxide as a probe molecule.

The most frequently used probe molecule is carbon monoxide (CO) due to its properties of being a clean (extra pure > 99 %) and small molecule, which leads to non-steric interactions and non-reactive adsorption [2]. The vibrational spectrum obtained is simple. Moreover, even if it depends on the nature of the bond with the surface, CO has a high molar attenuation coefficient (ϵ). Very interestingly, the $\nu(\text{C-O})$ stretching vibration is sensitive to the strength of the bond formed with the surface, and most oxide samples are transparent in the C-O stretching region. Therefore, CO is the most frequently used probe molecule

in IR spectroscopy. CO adsorption at room temperature is classically used to probe the oxidation and coordination states of metal ions through spectral behavior, stability and other characteristics of the carbonyl formed. Low-temperature CO adsorption (IR/CO) has applications for the determination of the acid strength of surface hydroxyl groups via the shift of the O-H stretching mode [2].

CO molecule has four filled bonding orbitals, $3\sigma_{n^2}$, $4\sigma_{s^2}$, $1\pi_x^2$, $1\pi_y^2$, and one occupied weakly anti-bonding orbital, $5\sigma_{n^2}$. In addition, there are three empty molecular orbitals, two $2\pi^*$ orbitals and one 6σ orbital. The highest occupied molecular orbital, HOMO, is the 5σ orbital, and the lowest unoccupied molecular orbital, LUMO, are the $2\pi^*$ orbitals. As both orbitals, 4σ (at the O atom) and 5σ (at the C atom) are occupied and oriented away from the molecule along the molecular axis, CO molecule can interact in coordination bonds as a weak Lewis base. The ability to donate electrons from the two orbitals is different and depends on the orbital energies: this is, the O atom of CO is a weaker Lewis basic center than the C atom because of the much lower orbital energy of the 4σ compared with the 5σ molecular orbitals.

The CO structure can be present as follows:



Where the structure on the right dominates. Then, CO interacts with metal ion by three different mechanisms:

1. Simple electrostatic interaction of the CO molecule with the field of the cation.
2. Formation of a σ bond with CO as an electron donor.

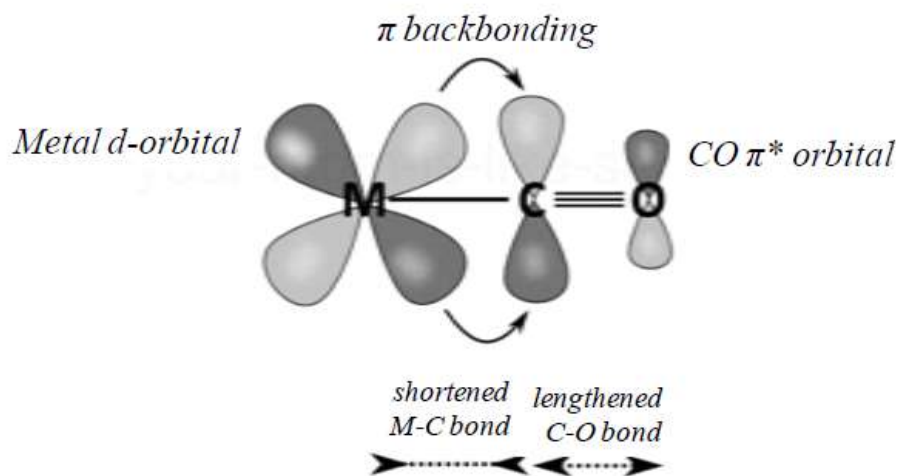
3. Formation of a π bond with CO as an electron acceptor (**Figure 23**).

Figure 23. Schematic representation of the orbital interactions in formation of σ and π bonds between CO and a metal ion.

CO adsorption strength depends strongly on the nature of the cations. Thus, some carbonyls are detected at low temperature only, whereas others are stable even at 670 K. Then, having a preliminary idea of the surface species, one can choose the experimental condition. Although CO stretching frequency is the most informative parameter, the determination of the stability of the various species can be decisive for the assignment of the bands [7]. For that, a helpful methodology (e.g. to calculate CO molar attenuation coefficient) is the successive adsorption of small doses of CO pressures up to saturation. This procedure provides information about the stabilities of the various species since the most energetic sites are the first to be occupied by CO molecule. For the characterization of sulfide catalysts supported on alumina, the low temperature adsorption of CO is used with such progressive introduction of small doses of CO.

II.3.3. IR spectroscopy: set up used for this thesis.

The low temperature IR setup (**Figure 24**) used in this work consist of the evacuation system, the IR In situ cell (**Figure 25**), the flow system and the spectrometer system. The evacuation system permits to reach ultra-high vacuum (10^{-5} Pa) in the IR cell, and the evacuation of the probe molecule and activation gases. The flow system allows introduction of activation gases with mass flow meter in very similar way as for the activation in catalytic set up. The outlet of the flow is connected with a NaOH solution bottle to avoid H_2S release. Using this cell, the sample can be treated at high temperature (up to 723 K), and characterized by the adsorption of probe molecule at 100 K. This cell allows the introduction of small calibrated doses of gas (1.628 cm^3). The IR cell has also a specific design to carry out the activation of the sample *in situ* with entrance of the gas flow below the oven and outlet at the top (**Figure 25**).

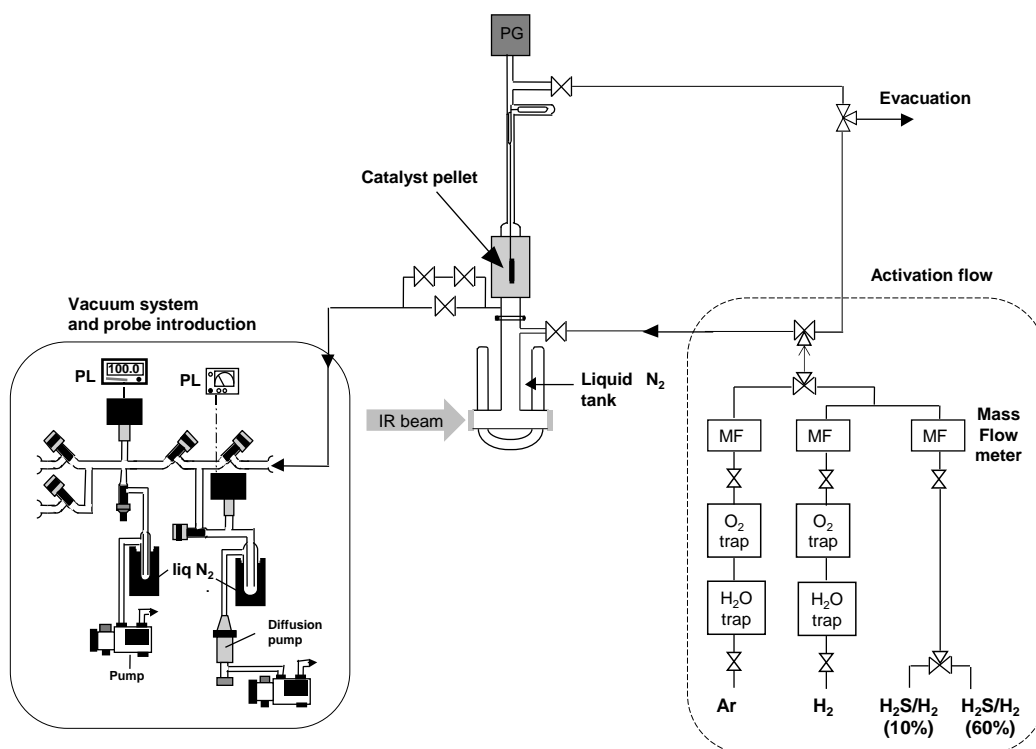


Figure 24. Low temperature CO adsorption IR set up.

The first step of the experiment consists in the sample preparation. Samples are grounded and pressed into a self-supporting pellet of ~10 mg and area of 2 cm² (precisely weighted). The pellet is introduced into the glass cell and is evacuated to 9.0×10⁻⁵ Pa to remove the air and physisorbed water. After that, the pellet is sulfided at 623 K or 673 K (heating rate of 3 K min⁻¹) under a flow of 30 ml·min⁻¹ 10 % H₂S/H₂ for 2h. Afterwards, the cell is flushed with Ar at 623 K during 15 min, and left under vacuum 1h at the sulfidation temperature, finally, the sample is cooled down to room temperature, still under vacuum. The final pressure in the IR cell after evacuation should reach 9.0×10⁻⁵ Pa. Followed by this, the pellet is cooled down by liquid nitrogen to 100 K for CO adsorption. The spectrometer is a Fourier Transform IR spectrometer from Nicolet, with a MCT (Mercury Cadmium Telluride) detector. The spectra are collected by 256 scans with a resolution of 4 cm⁻¹. CO adsorption at low temperature (100 K) is carried out introducing controlled CO pressure (gauge characteristics: range precision) measured in a standard volume called “small volume”, which is installed just before the entrance of the cell. This procedure allows to study the nature of CO/sites interaction, calculation of the molar attenuation coefficient from different species, and thus the quantification of adsorbed CO on different sites. The typical CO adsorption spectra on TMS/Al₂O₃ starts from small doses (known volume of 13.3 Pa of CO pressure) up to saturation using an equilibrium pressure in the cell of 133 Pa.

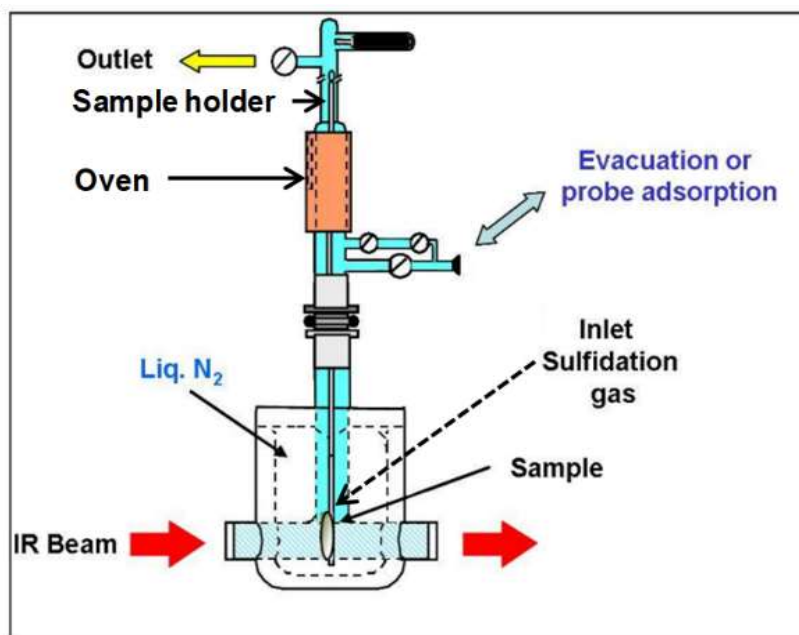


Figure 25. IR cell at low temperature

II.3.4. Spectra decomposition and treatment.

Before CO introduction, a spectrum of the sulfided sample (called reference spectrum) is always recorded at 100 K. Then, small calibrated doses of CO are introduced in the IR cell. Finally an equilibrium pressure of 133 Pa is established. A spectrum is taken after each CO introduction. All the CO spectra presented correspond to difference spectra i.e. spectrum after CO adsorption minus reference spectrum. The possibility of distinguishing the metal (Mo or W) located in M- and S-edge sites by IR/CO is a beneficial characteristic of this method, which allows a more precise study of sulfide catalysts. Until now, CO adsorption spectra were decomposed to distinguish the contributions of the support from the ones of the sulfide slabs. Particularly for the most studied system that is MoS₂, the spectra corresponding to the CO uptake on the sulfided catalysts present four main $\nu(\text{CO})$ bands at about 2186 cm⁻¹, 2156 cm⁻¹, 2110 cm⁻¹ and 2070 cm⁻¹, which are respectively attributed to CO adsorption

on the support (Al^{3+} and acidic OH groups), and on the M-edge and S-edge, for unpromoted MoS_2 (**Figure 26**). From a theoretical point of view, the IR spectrum of a gas can be decomposed using a Voigt type function (convolution of a Gaussian and a Lorentzian function). In the case of liquids or solids, the IR spectrum can be calculated as the sum of a Gaussian function and a Lorentzian function (pseudo Voigt function) [9]. Due to the computational expense of the convolution operation, the IR profile is often approximated using a pseudo-Voigt profile. Although CO is introduced as a gas, it is considered that once adsorbed, it is an integral part of the solid, and decompositions using pseudo Voigt functions are preferred. In our case, the spectrum of CO in interaction with the surface is decomposed using pseudo Voigt functions in the zone 2300 cm^{-1} - 1900 cm^{-1} which corresponds to the vibration domain of CO in interaction with the different surface sites of the sulfide catalyst.

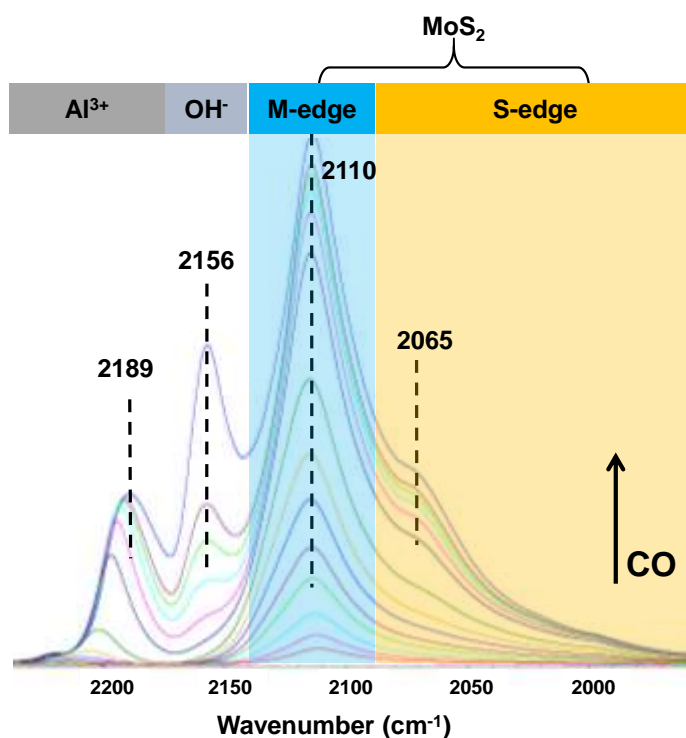


Figure 26. Typical CO adsorption spectra and band assignment of Mo/Al₂O₃ (12 %wt) at low temperature (increasing doses up to equilibrium pressure) [8].

The base line is corrected by a pseudo-convex approach. Then the spectrum is decomposed into several Voigt functions (**Figure 27**). For each band corresponding to the interaction of CO with the active phase of the catalyst the integrated area is calculated. It is then possible to follow the evolution of the integrated area of the band considered as a function of the quantity of CO introduced.

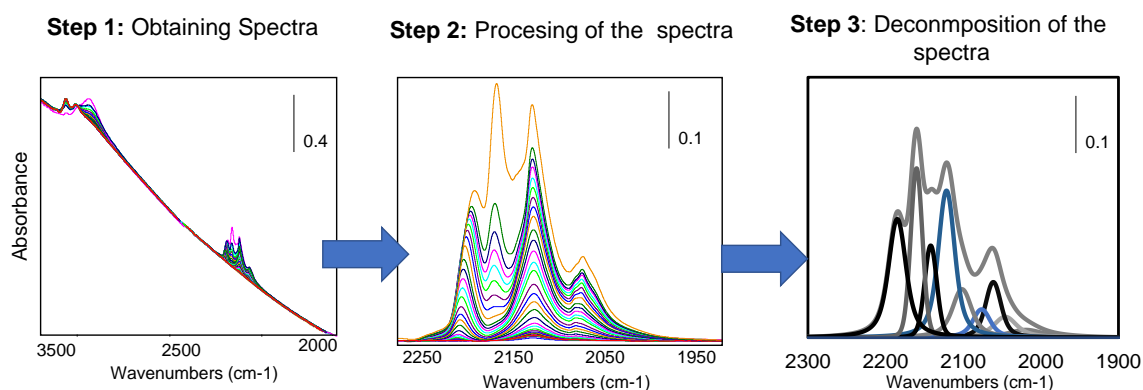


Figure 27. Steps of the treatment of IR spectra of CO adsorption on TMS/Al₂O₃.

The quantity of adsorbed CO is calculated from the law of ideal gas considering that all introduced CO is adsorbed (no residual pressure is measurable):

$$Q_{CO} = \frac{P \times V}{T \times R} \quad (\text{Eq. 2})$$

Where:

P= CO doses pressure (Pa)

V= standard volume (cm³)

T= atmospheric temperature (293 K)

R= ideal gases constant (cm³*Pa*K⁻¹*mol⁻¹)

II.4. Microscopy aspects.

The microscopy part of this Thesis was part of the project MIMOSA LABEX EMC3 in collaboration with Prof. Xavier Portier from the Centre de recherche sur les Ions, les Matériaux et la Photonique (CIMAP), located in Caen, France.

II.4.1. High-resolution Transmission Electron Microscopy (HRTEM).

All TEM images presented hereinafter have been taken using a double corrected JEOL ARM 200F cold FEG microscope operated at 200 kV. The image treatment was performed using the commercial software from GATAN (DIGITALMICROGRAPH) and Measurim software. The samples were sulfide *ex-situ* in a glass reactor over conventional sulfidation condition (30 ml·min⁻¹ of H₂S/H₂ 10% at 623 K (Mo and CoMo catalysts) and at 673 K (W and NiW catalysts) during 2 hours with a ramp at 3 K·min⁻¹). After sulfidation, the sample was manipulated in a dry box over inert flow (Argon, 100 ml·min⁻¹) to avoid as much as possible exposition of the sample with the atmosphere. Following, a small amount of powder samples was suspended in absolute ethanol and deposited in a 300 mesh copper grid with holey carbon film. The measure of slab length and stacking degree distributions of sulfide slabs were determined manually by measuring around 300 slabs per sample from HRTEM images. Slabs length and stacking degree distributions were obtained following the next equation:

$$M = \frac{\sum_i M_i N_i}{N} \quad (\text{Eq. 3})$$

Where M is an estimated quantity ($\langle L \rangle$: length, or $\langle S \rangle$: stacking), N_i in the number (frequency) of particles or slabs having the length or stacking within the discrete interval i (nm) or integer stacking i , and N total number of particles or slabs.

In all the microscopy measurements presented in this work, first the samples were analyzed in the transmission mode (TEM) followed by scanning mode (STEM).

II.4.2. HR-STEM HAADF as a tool for observing MS_2 morphology at atomic scale.

Scanning transmission electron microscopy (STEM) is based in scanning the region of interest with a focused electron beam collecting the scattered electrons using a detector. The main advantage of STEM over TEM is that, since in a STEM, a convergent beam in the form of a probe is scanning on the specimen, higher signal levels and better spatial resolution are available by detecting transmitted electrons [10] and the image contrast can be directly interpretable [11]. In STEM bright-field (STEM-BF), the bright field is a coherent signal that relies on phase contrast, it is therefore more sensitive to samples with lower atomic numbers, such as the carbon substrates of TEM grids. The STEM-BF signal is gained similar to conventional TEM images and is harder to interpret as the phase contrast means the signal is not directly proportional to atomic number or thickness. A STEM-BF image results from the interference of the direct beam with low-angle scattered electrons, this is, elastic and inelastic electrons. STEM-BF using an annular detector has shown promising results in imaging light elements. On the other hand, HAADF in STEM has attracted much interest. A high angular annular dark-field (HAADF) detector collects the

electron scattered at higher angles excluding the low-angle scattered electrons (e.g. the direct beam). The contrast in HAADF images is related to the chemical composition of the specimen, it is often termed as Z-contrast [12,13]. In comparison to all these imaging modes the high-angle annular dark field scanning transmission electron microscopy (HAADF STEM) or Z-contrast imaging provides a significant advantage since in this case it is possible to differentiate two elements from the difference related to their atomic number (intensity $I \propto \text{atomic number } Z^{1.7}$). Where Z is the atomic number of the considered element. The heavier the atoms, the brighter the contrast will be for the corresponding atomic image. For qualitative determination of atom nature and calculations of atomic column distances, HAADF-STEM imaging is widely used due to the simple interpretation. In combination with spectroscopic techniques such as energy-dispersive X-ray analysis (EDX) and electron energy loss spectroscopy (EELS) one can obtain single atom information combined with their corresponding chemical information [13]. With the advances in corrections of the spherical aberration, it is possible to reach the atomic resolution at the highest spatial resolution thanks to small probe sizes.

The imaging system comprises annular dark field and annular bright field (ADF/ABF) detectors collecting the transmitted electrons (**Figure 28**). Projectors are used to change the distance between the specimen and the detectors and thus the collection angle which is related to the camera length. Typically, an annular dark field (ADF) detector has detection range around 22 mrad and 100 mrad outside the illumination cone of the probe. Above 100 mrad it is called high angle annular dark field (HAADF). The annular bright field (ABF) has a

detection angle from around 11 mrad and 22 mrad and is within the illumination cone of the electron focused beam.

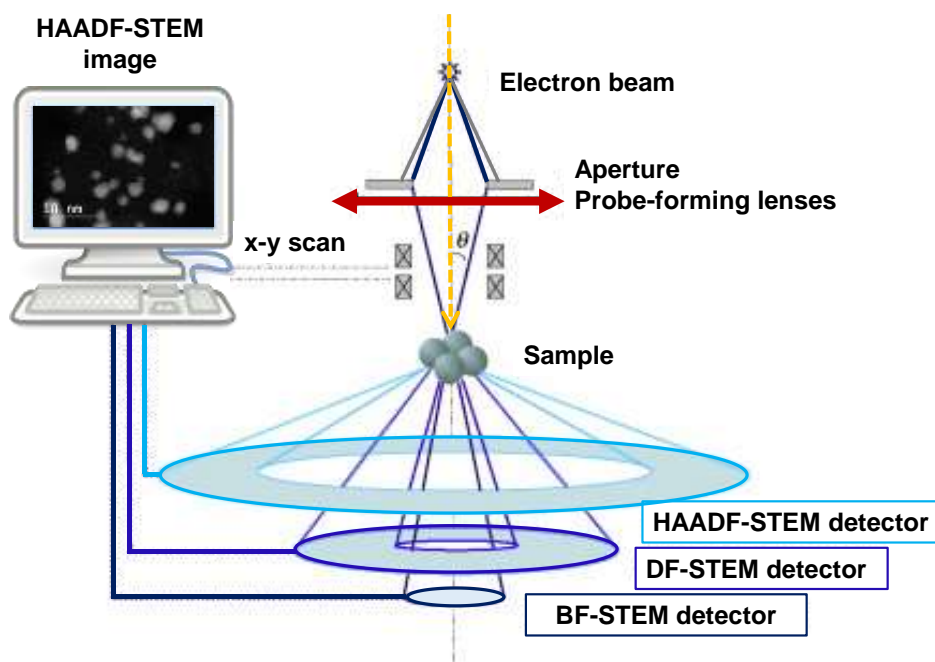


Figure 28. Representative example of the STEM system.

The scattered electrons in the range of an ADF detector are formed through inelastic diffusion and thus are incoherent. The use of a small camera length helps to further remove any residual diffraction contrast from Bragg reflections.

II.4.3. HR STEM-HAADF operation parameters.

HAADF images presented in this manuscript were obtained with acquisition time of an image of about 30 s with a resolution of 1024 pixels x 1024 pixels, (30 μ s of exposure time for each spot in the scanning mode). During this acquisition and despite exposure to the electron beam, the shapes of the particles remained unchanged, meaning that the slabs were quite stable under the electron beam. The possible effect of damage associated with the heating

effects caused by the incident beam in the TMS nanolayers is always a factor to consider. The advisable acceleration voltage is a low beam energy such as 80 kV. In our study, we did not observe significant changes during the acquisition of the images at 200 kV with a beam current value of about 12 μ A. Observations at 80 kV were also performed, but no significant difference in terms of slab stability was noticed. Therefore, it was concluded that the operation with an acceleration of 200 kV is compatible with our purpose of morphological analysis.

II.5. Density Functional Theory (DFT) calculations.

The nature and the location of the sites on which CO adsorb is still under debate and IR spectroscopy — as a single technique — is unlikely to provide an answer. The modeling of these nanocrystallites is one possible approach to get a better insight into the nature of the sites [14].

Computer simulations based on a quantum description of the interactions between electrons and between electrons and atomic nuclei have generated an increasingly important impact on the physics and chemistry of the solid state and on the science of materials, contributing to a deeper understanding, and also the possibility of significantly improving the design of materials for future technologies [15].

Since the 90s, a major advance has been seen in the development of methods for ab initio calculations of the properties of materials and for the simulations of processes in materials. The basis of this development has been established by the theory of functional density (DFT), which converts the intractable complexity of electron-electron interactions into many-electrons

systems into an effective one-electron potential, which is a particular function of the electron density [16,17].

II.5.1. The Vienna Ab Initio Simulation Package VASP — Basic Methodology.

The Vienna Ab initio Simulation Package (VASP) is a computer program for atomic scale materials modelling, e.g. electronic structure calculations and quantum-mechanical molecular dynamics, from first principles. VASP computes an approximate solution to the many-body Schrödinger equation, either within density functional theory (DFT), solving the Kohn-Sham equations, or within the Hartree-Fock (HF) approximation, solving the Roothaan equations. Hybrid functionals that mix the Hartree-Fock approach with density functional theory are implemented as well. Furthermore, Green's functions methods (GW quasiparticles, and ACFDT-RPA) and many-body perturbation theory (2nd-order Møller-Plesset) are available in VASP. In VASP, central quantities, like the one-electron orbitals, the electronic charge density, and the local potential are expressed in plane wave basis sets. The interactions between the electrons and ions are described using norm-conserving or ultrasoft pseudopotentials, or the projector-augmented-wave method. To determine the electronic groundstate, VASP makes use of efficient iterative matrix diagonalisation techniques, like the residual minimisation method with direct inversion of the iterative subspace (RMM-DIIS) or blocked Davidson algorithms. These are coupled to highly efficient Broyden and Pulay density mixing schemes to speed up the self-consistency cycle.

VASP is currently used by more than 1400 research groups in academia and industry worldwide on the basis of software licence agreements with the

University of Vienna. Ab initio calculations of the stable crystal structure and of phase transformations under increasing pressure and temperature are of course a very active field. Ab initio results are now available for almost all elements of the Periodic Table of the Elements and for a large number on inorganic compounds, with a few applications also to molecular crystals [15,18].

II.5.2. Computational techniques used for this work.

The density functional theory (DFT) calculations presented in this thesis were carried out in collaboration with Prof. Jean-Francois Paul from UCCS Lille, France.

The density functional theory (DFT) calculations were carried out with the Vienna Ab initio Simulation Package (VASP) software [15,19]. The energy is calculated using the non-local functional generalized gradient corrections (GGA) approximation as parameterized by Perdew et al. [16,17] The wave function is expanded in a plane wave basis set, and the electron–ion interactions are defined using the Projector Augmented Plane Wave (PAW) method [20]. In order to compute reliable adsorption energies, Van der Waals forces were considered in the calculations. The Perdew-Burke-Ernzerhof (PBE) functional was employed with 0.1 eV Gaussian smearing [21]. It has been shown that PBE gives good results in ionic systems if the van der Waals interactions are considered [22]. The solution of the Kohn–Sham equations was improved self-consistently until a difference lower than 10^{-5} eV was obtained between successive iterations. The atomic positions were optimized until the forces become less than $0.03 \text{ eV}\cdot\text{\AA}^{-1}$ Test calculations were done by varying cut-off energy from 300 to 500 eV and using the K-points mesh from $3 \times 1 \times 1$ to $3 \times 3 \times 3$ following Monkhorst–Pack [23] schemes to define calculation parameters.

From these evaluations, all the bulk and surface calculations were performed with a 450 eV cut-off energy, using a $3 \times 3 \times 1$ K-point mesh for all surface calculations. Using these parameters, the accuracy of the DFT calculation is expected to be better than 0.1 eV for the calculated adsorption energy.

II.6. Catalytic activity measurements: Thiophene HDS reaction.

Catalytic tests were performed to study the role of different active sites formation in HDS reaction. Thiophene HDS reaction is chosen as a rapid way to evaluate the catalytic performances of different samples. The thiophene HDS tests were carried out in a differential glass reactor (**Figure 29**). About 25 to 50 mg of catalysts (200–500 μm , precisely weighted) were first sulfided with 30 $\text{mL}\cdot\text{min}^{-1}$ 10% (v/v) $\text{H}_2\text{S}/\text{H}_2$ at 350 $^\circ\text{C}$ (Mo catalysts) or 400 $^\circ\text{C}$ (W catalysts) with a heat ramp of 3 $^\circ\text{C}\cdot\text{min}^{-1}$ for 2 h. Next, thiophene HDS test was carried out at 350 $^\circ\text{C}$ using a 90 $\text{mL}\cdot\text{min}^{-1}$ gas mixture consisting of 7.9% thiophene, 90.0% H_2 , and 2.1% H_2S . The concentrations of 1-butene, butane, cis-2-butene, trans-2-butene, tetrahydrothiophene (THT), and thiophene in the outlet gas were measured by a Varian 3900 chromatograph using a FID detector. In order to get a differential reactor, the conversion of thiophene is controlled below 10%. The specific rate (r_s , $\text{mol}\cdot\text{h}^{-1}\cdot\text{kg}^{-1}$) was calculated using the following equation:

$$r_s = \frac{x \times F}{m_{cat}} \quad (\text{Eq. 4})$$

Where x is thiophene conversion (%), F is molar flow rate of thiophene ($\text{mol}\cdot\text{h}^{-1}$), m_{cat} is the mass of the catalyst after sulfidation (initial mass corrected by weight loss as measured in IR experiment, kg).

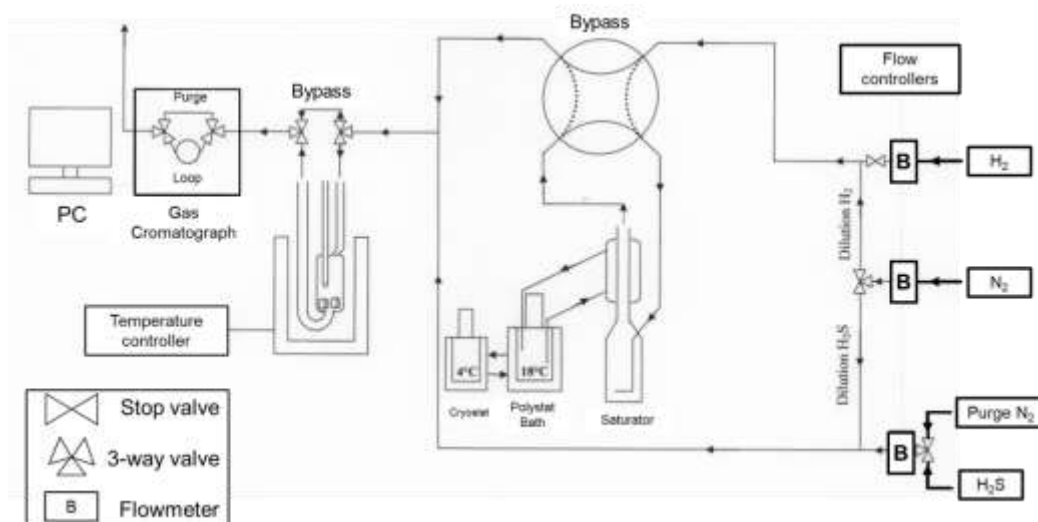


Figure 29. Thiophene test set up

II.7. Conclusions of the Experimental part.

The different analytical techniques used in this thesis project are complementary. They were chosen to finely characterize the active sites of supported sulfide catalysis. The following table summarizes the different information that can be obtained by their use.

Characterization Technique	Searched information
Nitrogen adsorption (BET)	Surface area, pore size, pore volume
Elemental analysis by Inductively Coupled Plasma (ICP)	Metal and sulfur content
CO/FTIR spectroscopy	Nature, surface sites concentration, type of edges (M-edge and/or S-edge)
High-resolution Transmission Electron Microscopy (HRTEM)	Average length and average stacking of the TMS slabs
High-angle annular dark field scanning Transmission Electron Microscopy (HR STEM-HAADF)	Atomic resolved 2D-morphology of the TMS slabs
DFT calculations	Modelling and location of nature and active sites

II.8. References

- [1] W. Suëtaka, *Surface infrared and raman spectroscopy: methods and applications*, 2013.
- [2] K.I. Hadjiivanov, G.N. Vayssilov, Characterization of oxide surfaces and zeolites by carbon monoxide as an IR probe molecule, *Adv. Catal.* 47 (2002) 307–511. doi:10.1016/S0360-0564(02)47008-3.
- [3] T. Kabe, A. Ishihara, Q. Zhang, Deep desulfurization of light oil. Part 2: hydrodesulfurization of dibenzothiophene, 4-methyldibenzothiophene and 4,6-dimethyldibenzothiophene, *Appl. Catal. A Gen.* 97 (1993) L1–L9.
- [4] G. Busca, Bases and Basic Materials in Chemical and Environmental Processes. Liquid versus Solid Basicity, *Chem. Rev.* 110 (2010) 2217–2249. doi:10.1021/cr9000989.
- [5] A. Vimont, F. Thibault-Starzyk, M. Daturi, Analysing and understanding the active site by IR spectroscopy, *Chem. Soc. Rev.* 39 (2010) 4928. doi:10.1039/b919543m.
- [6] A.A. Davydov, O.I. Goncharova, Use of IR spectroscopy in studies of catalysts based on molybdenum heteropoly compounds supported on oxides, *Russ. Chem. Rev.* 62 (1993) 105–120. doi:10.1070/rc1993v062n02abeh000008.
- [7] G. Pacchioni, G. Cogliandro, P.S. Bagus, Molecular orbital cluster model study of bonding and vibrations of CO adsorbed on MgO surface, *Int. J. Quantum Chem.* 42 (1992) 1115–1139. doi:10.1002/qua.560420504.
- [8] J. Chen, E. Dominguez Garcia, L. Oliviero, F. Maugé, How the CO molar extinction coefficient influences the quantification of active sites from CO adsorption followed by IR spectroscopy? A case study on MoS₂/Al₂O₃ catalysts prepared with citric acid, *J. Catal.* 332 (2015) 77–82. doi:10.1016/j.jcat.2015.09.005.
- [9] P.R. GRIFFITHS, J.A. de HASETH, Chapter I Theoretical Background, 2nd ed., Hoboken, New Jersey, 2007.
- [10] S.J. Pennycook, A.R. Lupini, M. Varela, A. Borisevich, Y. Peng, M.P. Oxley, K. Van Benthem, M.F. Chisholm, Scanning transmission electron microscopy for nanostructure characterization, in: *Scanning Microsc. Nanotechnol. Tech. Appl.*, Springer New York, 2007: pp. 152–191. doi:10.1007/978-0-387-39620-0_6.
- [11] R.A. Oliver, N.K. van der Laak, F.M. Ross, Structural Characterization of Quantum Dots, in: *Encycl. Mater. Sci. Technol.*, Elsevier, 2007: pp. 1–12. doi:10.1016/b978-008043152-9.02080-7.
- [12] L.D. Francis, J. Rivas, M. José-Yacamán, Understanding the structure of

- nanocatalysts with high resolution scanning/transmission electron microscopy, IOP Conf. Ser. Mater. Sci. Eng. 55 (2014). doi:10.1088/1757-899X/55/1/012005.
- [13] S.J. Nellist, P. D., & Pennycook, Direct Imaging of the Atomic Configuration of Ultradispersed Catalysts, *Science* (80-.). 274 (1996) 413–415. doi: 10.1126/science.274.5286.413%0AArticle.
- [14] A. Travert, C. Dujardin, F. Maugé, S. Cristol, J.F. Paul, E. Payen, D. Bougeard, Parallel between infrared characterisation and ab initio calculations of CO adsorption on sulphided Mo catalysts, *Catal. Today*. 70 (2001) 255–269.
- [15] J. HAFNER, Ab-Initio Simulations of Materials Using VASP: Density-Functional Theory and Beyond JÜRGEN, *J. Comput. Chem.* 29 (2008) 2044–2078. doi:10.1002/jcc.21057.
- [16] J.P. Perdew, Density-functional approximation for the correlation energy of the inhomogeneous electron gas, *Phys. Rev. B*. 33 (1986) 8822–8824.
- [17] J.P. Perdew, K. Burke, M. Ernzerhof, Generalized Gradient Approximation Made Simple, *Phys. Rev. Lett.* 77 (1996) 3865–3868.
- [18] G. Kresse, J. Hafner, Ab initio molecular dynamics for liquid metals, *Phys. Rev. B*. 47 (1993) 558–561.
- [19] G. Kresse, J. Furthmüller, Efficiency of ab-initio total energy calculations for metals and semiconductors using a plane-wave basis set, *Comput. Mater. Sci.* 6 (1996) 15–50.
- [20] G. Kresse, D. Joubert, From ultrasoft pseudopotentials to the projector augmented-wave method, *Phys. Rev. B Condens. Matter Mater. Phys.* 59 (1999) 1758–1775. doi:10.1103/PhysRevB.59.1758.
- [21] J.D. Pack, H.J. Monkhorst, Special points for Brillouin-zone integrations, *Phys. Rev. B Condens. Matter Mater. Phys.* 16 (1977) 1748. doi:10.1103/PhysRevB.16.1748.
- [22] H. Hijazi, L. Cantrel, J.-F.O. Paul, Reactivity of Silver Iodide (β -AgI) Surfaces: A Density Functional Theory Study, *J. Phys. Chem. C*. 122 (2018) 26401–26408. doi:10.1021/acs.jpcc.8b06931.
- [23] H.J. Monkhorst, J.D. Pack, Special points for Brillouin-zone integrations*, *Phys. Rev. B*. 13 (1976) 5188–5192. doi:10.1103/PhysRevB.13.5188.

CHAPTER III:

**Structure and quantification of edge sites of
WS₂/Al₂O₃ catalysts coupling IR/CO spectroscopy
and DFT calculations**

Content Chapter III: Structure and quantification of edge sites of WS₂/Al₂O₃ catalysts coupling IR/CO spectroscopy and DFT calculations

ABSTRACT	101
GRAPHICAL ABSTRACT:.....	102
KEYWORDS:.....	102
III.1. INTRODUCTION	102
III.2. EXPERIMENTAL SECTION	105
III.2.1. Catalyst preparation.	105
III.2.2. Low temperature CO adsorption followed by IR spectroscopy characterization (IR/CO).	106
III.2.3. Computational techniques.	107
III.2.3.1. Method description: computational parameters. ¡Error! Marcador no definido.	
III.2.3.2. Surface model description.	108
III.2.4. Determination of molar attenuation coefficients for CO adsorbed on M-edge and S-edge of site WS ₂ catalysts.	109
III.3. RESULTS AND DISCUSSION	111
III.3.1. Characterization by low-temperature IR spectroscopy of CO.	111
III.3.1.1. IR/CO of sulfided WS ₂ /Al ₂ O ₃ catalyst.	111
III.3.1.2. IR/CO of H ₂ -treated WS ₂ /Al ₂ O ₃	115
III.3.2. DFT calculations	117
III.3.2.1. Sulfur coverage and surfaces to study.	117
III.3.2.2. Calculation of CO adsorption.....	118
III.3.2.3. CO adsorption: Experiment vs Calculation	121
III.3.3. Influence of W loading on W- and S-edge bands.	123
III.3.4. Determination of molar attenuation coefficients for W- and S-edge bands.	125
III.3.5. The influence of W loading on WS ₂ slab morphology.	129
III.3.6. Comparison between W and Mo sulfide catalysts.....	130
III.4. CONCLUSIONS	132
III.5. REFERENCES	134

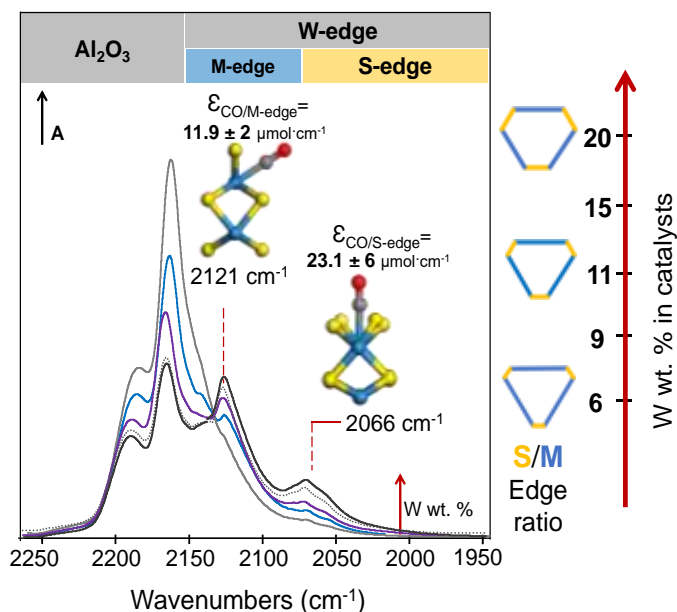
ABSTRACT

IR spectroscopy of CO adsorption (IR/CO) and Density Functional Theory (DFT) calculations on sulfide W/Al₂O₃ catalyst were investigated for a deep insight into the sulfide edge sites. Parallel between experimental and theoretical results allow to assign the $\nu(\text{CO})$ bands at 2121 and 2065 cm⁻¹ to CO adsorption on M- and S-edge sites of WS₂ phase, respectively.

Through a careful analysis of CO spectra on well-selected W catalysts, the molar attenuation coefficients for CO adsorbed on the two exposed edges could be determined. This allowed the morphology of WS₂ slabs to be calculated. This work shows that increasing the W loading (3-20 wt% W) changes the slab morphology from an almost pure triangle exhibiting mostly M-edge to a truncated hexagon.

On W as well as on Mo sulfide catalysts, IR spectroscopy and DFT calculation show that CO adsorption allows to account for M- and S-edge sites, and thus of the morphology of sulfide slabs. It was shown that increasing the W loading shifts the slab morphology from a triangle exposing predominantly M-edge towards a more hexagonal shape. For monolayer coverage of alumina, Mo and W sulfide slabs present similar shape i.e. truncated hexagon. However, edge sites of WS₂ slabs clearly exhibit greater stability under H₂ atmosphere than Mo sulfided ones.

Graphical abstract:



KEYWORDS: Hydrotreating catalyst, Tungsten disulfide (WS₂), CO adsorption, IR spectroscopy, density functional theory, morphology.

III.1. INTRODUCTION

Hydrotreating (HDT) of petroleum fractions is one of the central refining processes to produce clean fuels that meet current stringent ecological requirements. The present challenge is to meet the current requirements for ultra-low sulfur content in fuels by extracting from heavier oil deposits. Hydrodesulfurization (HDS) is a key process in refineries where transition metal disulfides (TMS) supported on gamma alumina (γ -Al₂O₃) are used for HDT processes. Among the different metals, Mo or W disulfides with Co or Ni metals as promoters have shown the most promising results in this field. The CoMo and NiMo/Al₂O₃ catalysts have been extensively studied, meanwhile NiW catalysts have remained less investigated [1]. The importance of NiW/Al₂O₃

sulfide catalysts is given by their excellent performance in hydrogenation reactions for deep HDS, providing a high potential for the conversion of alkyl-dibenzothiophenes (alkyl-DBTs). [2,3] HDS catalysts have been the subject of numerous characterization studies [4], and presently there is a general agreement that the sulfide phase MoS_2 (WS_2) presents a lamellar structure, formed by layers of MS_2 ($M=W, Mo$). The 2D morphology of these layers, their average stacking (~2 to 4) and their average size (~3 to 6 nm) depend on the sulfidation conditions, the metal loading among other parameters. Many correlations between the structure and the activity of these systems link the catalytic reaction to the sites along the edges of the individual layers MS_2 . At this location, the promoter atoms are also found in the so-called CoMoS type structures (NiMoS, CoWS and NiWS) [5]. The MS_2 slabs expose principally two types of edges: the metal terminated edge (M-edge) and the sulfur terminated edge (S-edge). Studies also indicate that M-edge and S-edge sites have different intrinsic activities in HDS reactions, S-edge being more active and keener for the promotion and the formation of the promoted phase [6].

An informative way to characterize sulfide sites on these catalysts is the low temperature CO adsorption followed by IR spectroscopy (IR/CO). In addition to the detection of the sulfide sites, this characterization offers the advantage of quantifying their concentration by means of the molar attenuation coefficient, and thus gives access to sulfide phase dispersion and intrinsic activity of the sulfide sites (ref). [7] It should be mentioned that several $\nu(CO)$ bands characterized the sulfide sites, even on unpromoted catalysts. IR spectroscopy as a unique technique can hardly provide an undeniable attribution of these CO bands to sulfide sites with specific structures. The continuous development of

modeling techniques as the Density Functional Theory (DFT) allows defining realistic surfaces models. The modeling of the stable sulfide surfaces according to the sulfide atmosphere is a powerful approach to obtain a description of the various CO adsorption sites [8,9]. Hence for MoS_2 , Travert et al. demonstrated that the coupling of techniques as IR/CO and DFT permitted to attribute the main $\nu(CO)$ bands to M-edge sites and to S-edge sites as well as to show that these sulfide sites can be modified by post-treatments with hydrogen [10,11]. Further, determination of the molar attenuation coefficients of $\nu(CO)$ bands characteristics of the M-edge and S-edge sites allowed quantification of these two edges and thus assessment of the morphology of MoS_2 slabs [12]. It was thus possible to demonstrate that the MoS_2 morphology (expressed by S_{edge}/M_{edge} ratio) varies with the preparation parameters (metal loading, chelating agent addition, support nature) [7,13–15] and the sulfidation conditions [13,16]. Recent observations of the sulfide catalysts by STEM HAADF confirmed the morphology of the MoS_2 slabs deduced from the spectroscopic analysis [17]. These knowledges allow a controlled design of the MoS_2 -based slabs from a slightly truncated to heavily truncated triangle sulfided slab morphology.

In comparison with Mo catalysts, W based ones are less documented in literature [18]. Although a considerable amount of research has been made on their activity, selectivity and in general catalytic properties of the W catalysts, an accurate description of the active sites is still lacking [13,19,20]. So far the available CO spectra representing W-based catalyst are rather limited, and no reports were established on the assignment of their specific IR/CO bands, neither on the quantification of these edge sites. Hence, this paper presents a

deep insight into the sulfided W/Al₂O₃ system characterized through IR spectroscopy and DFT calculation. We first perform the IR/CO adsorption experiments over W/Al₂O₃ catalyst, later the modeling of the WS₂ (1 0 0) stable surfaces and the calculation of the stretching frequencies of CO adsorbed on these surfaces. The nice parallel between experimental and theoretical results allows assigning the bands at 2121 and ~2066 cm⁻¹ to CO adsorbed on M- and S-edge sites, respectively. In a further step, the molar attenuation coefficient of these bands was successfully determined that allows accounting for the effect of W loading on the WS₂ slab morphology.

III.2. EXPERIMENTAL SECTION

III.2.1. Catalyst preparation.

The studied materials consisted in a series of unpromoted W/Al₂O₃ catalyst prepared by a one-step pore volume impregnation method with variable W loading (6, 9, 11, 16 and 20 W wt. %), 20 W wt. % corresponding to 3.3 atoms·nm⁻², e.g. a monolayer of W atoms. The catalysts were impregnated with an aqueous solutions of appropriate amounts of hydrated ammonium metatungstate ((NH₄)₆H₂W₁₂O₄₀·H₂O SIGMA-ALDRICH) on commercial γ-Al₂O₃ support (SASOL extrudates, specific surface area of 252 m²·g⁻¹ and pore volume of 0.82 ml·g⁻¹, precalcined in air flow at 723 K for 4 h. After impregnation, the materials were left for maturation at room temperature for 2 h and subsequently the complete catalyst series was thermally treated at 383 K for 16 h inside of a rotatory furnace under air 100 ml·min⁻¹ flow and a heating rate of 3 K·min⁻¹. Hereinafter, the W/Al₂O₃ catalysts are denoted as X_W/Al₂O₃ where X refers to the W wt. % loading in the catalysts.

III.2.2. Low temperature CO adsorption followed by IR spectroscopy characterization (IR/CO).

The WS₂ edge sites of these catalysts were characterized by low-temperature (~100 K) CO adsorption followed by IR spectroscopy (IR/CO). CO adsorption was performed at low temperature to avoid any reaction with the catalysts surface and to strengthen the interaction with the weakest adsorption sites of the catalyst surface. The oxide catalyst was grounded and pressed into self-supported wafer (ca. 10 mg, precisely weighted, for a 2.01 cm² disc) and placed into a quartz IR cell with CaF₂ windows. After *in situ* sulfidation under 10% H₂S/H₂ with a flow rate of 30 ml·min⁻¹ for 2 h at 673 K (sulfidation starting from room temperature with a heating rate of 3 K·min⁻¹), the cell was flushed with Ar for 10 min and evacuated down to $P < 1 \cdot 10^{-4}$ Pa maintaining the 673 K temperature during 1 h. Finally, the sample was cooled down to room temperature and further down to 100 K under vacuum. CO adsorption experiments were performed introducing small calibrated CO doses up to an equilibrium pressure of 133 Pa.

After the sulfidation following the previous procedure, pure hydrogen post-treatment was performed on the 20_W/Al₂O₃ catalyst. In such a case, the sulfide catalyst was *in situ* reduced under pure H₂ with a flow rate of 50 ml·min⁻¹ at 673 K for 2 h. After the aforementioned treatment, the sample was flushed under Ar flow for 10 minutes and the temperature was cooled down under high vacuum ($P = 9.7 \times 10^{-5}$ Pa residual pressure) to room temperature and then to 100 K to perform CO adsorption.

FTIR spectra were recorded with 256 scans and a resolution of 4 cm⁻¹ using Nicolet Nexus FTIR spectrometer equipped with a MCT detector (FTIR= Fourier Transform Infrared; MCT=Mercury-Cadmium-Tellurium). All spectra were normalized to a disc of 5 mg·cm⁻². The bands of the adsorbed CO species were obtained by subtracting the spectra recorded after CO adsorption minus before. All experiments were duplicated, with a maximum error of 5%. The band areas of the different $\nu(\text{CO})$ components of the WS₂ massif can be obtained by careful spectrum decomposition. In this work, the decomposition was done with Peakfit V4.12 software using the “Autofit peak III deconvolution Method”. Before the decomposition, second derivative of the spectra was performed to determine the number of bands. For the decomposition, the center and full width at half height (FWHH) of each band are allowed to vary in a small range ($\pm 3 \text{ cm}^{-1}$).

III.2.3. Computational techniques.

The theoretical part of this Thesis was carried out in collaboration with Prof. Jean-Francois Paul from the UCCS, Lille.

III.2.3.1. Method description: computational parameters.

The density functional theory (DFT) calculations were carried out with the Vienna Ab initio Simulation Package (VASP) software [21,22]. The energy is calculated using the non-local functional generalized gradient corrections (GGA) approximation as parameterized by Perdew et al. [23,24] The wave function is expanded in a plane wave basis set, and the electron–ion interactions are defined using the Projector Augmented Plane Wave (PAW) method [25]. In order to compute reliable adsorption energies, Van der Walls forces were considered in the calculations. The Perdew-Burke-Ernzerhof (PBE) functional

was employed with 0.1 eV Gaussian smearing [26]. It has been shown that PBE gives good results in ionic systems if the van der Waals interactions are considered [27]. The solution of the Kohn–Sham equations was improved self-consistently until a difference lower than 10^{-5} eV was obtained between successive iterations. The atomic positions were optimized until the forces become less than $0.03 \text{ eV}\cdot\text{\AA}^{-1}$. Test calculations were done by varying cut-off energy from 300 to 600 eV and using the K-points mesh from $3 \times 1 \times 1$ to $5 \times 3 \times 1$ following Monkhorst–Pack [28] schemes to define calculation parameters. From these evaluations, all the bulk and surface calculations were performed with a 550 eV cut-off energy, using a $3 \times 3 \times 1$ K-point mesh for all surface calculations. Using these parameters, the accuracy of the DFT calculation is expected to be better than 0.1 eV for the calculated adsorption energy.

III.2.3.2. Surface model description.

In the present work we have used a large supercell ($12.72 \times 12.50 \times 30 \text{ \AA}^3$) that allows a good description of the WS_2 surface dimensions (see **Figure 30**). This supercell model containing four rows in the x-direction, two layers along the y-direction, and five in the z-direction is appropriate for describing the structural and adsorption properties of the (1 0 0) WS_2 surface. A vacuum layer of 15 \AA is located above the WS_2 slab in the z direction in order to avoid interactions between slabs. The three upper W rows and the adsorbed molecules were allowed to relax during the geometry optimization, while the two lower ones were kept fixed at the bulk geometry. The CO vibration frequencies were calculated by numerical differentiation of the force matrix. The CO stretching vibrational mode being very weakly coupled with the vibration of the surface,

only the part of the matrix corresponding to the atoms closest to CO was considered in the diagonalization process of the hessian matrix.

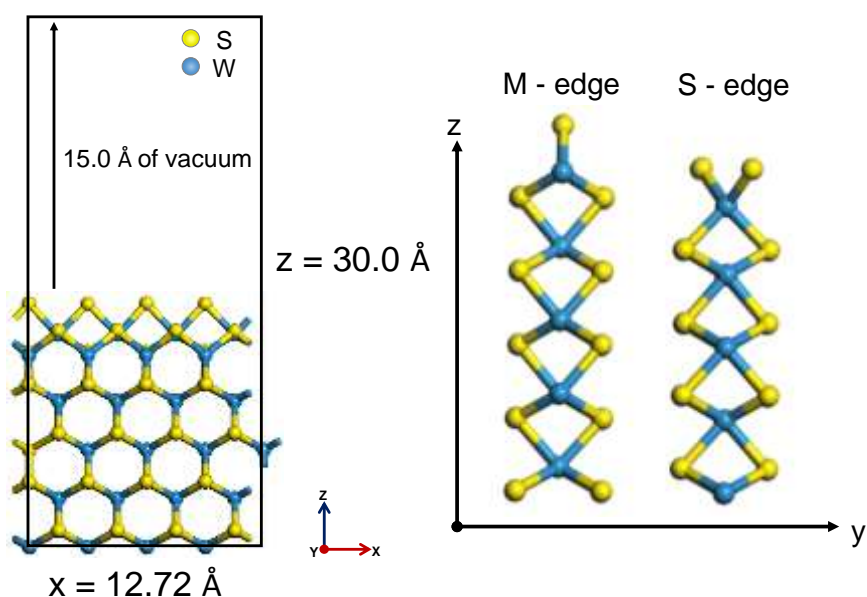


Figure 30. Representation of the supercell used for the calculations, showing the axes. On the left, cell showing the cut WS₂ (1 0 0) surface. Dark circles: W; light circles: S

III.2.4. Determination of molar attenuation coefficients for CO adsorbed on M-edge and S-edge of site WS₂ catalysts.

According to the adapted Beer-Lambert law (Eq. 1) to solid materials, the concentration of sites (n , $\mu\text{mol}\cdot\text{g}^{-1}$) on which CO is adsorbed can be calculated using the associated CO molar attenuation coefficient (ϵ , $\mu\text{mol}^{-1}\cdot\text{cm}$) and the area of $\nu(\text{CO})$ band (A , cm^{-1}) normalized to the surface (S , cm^2) and to the mass (m , g) of the catalyst wafer measured after sulfidation:

$$n = \frac{A \times S}{\epsilon \times m} \quad (\text{Eq. 1})$$

The typical CO adsorption experiments on WS₂/Al₂O₃ are performed by adding small CO doses, starting from 9.0x10⁻³ μmol up to saturation by equilibrium pressure 8.64 μmol (133 Pa). The ε values can be deduced from the slope of the linear relationship between the area of ν(CO) band (A_{CO}) and the amount of CO introduced onto the sample (n_{CO}). However, the determination of the amount of CO adsorbed on a given site can be very delicate, especially when the CO introduced interacts with several adsorbing sites.

In the present case, we had to determine the molar attenuation coefficient of two ν(CO) bands that can appear simultaneously. It has firstly required the selection of samples with a minimum number of adsorption sites types and the analysis of the spectra from the very first doses of CO when only these are adsorbed on the sites of interest. Thus, the molar attenuation coefficient (ε₁) could be determined using eq. (1).

For the spectra that present two contributions, the Beer Lambert law can be written as

$$n_{CO} = \frac{A_{CO1}S}{m\varepsilon_{CO1}} + \frac{A_{CO2}S}{m\varepsilon_{CO2}} \quad (\text{Eq. 2})$$

The molar attenuation coefficient of CO adsorbed on the second contribution (ε₂) can be determined as followed: after the determination of the area of the two contributions (A_{CO1}, A_{CO2}), the number of CO adsorbed on the site 1 (n_{CO1}) can be calculated from the previously determined ε_{CO1} value. Then, the number of CO adsorbed on the site 2 (n_{CO2}) is determined by subtracting from the total amount of CO introduced n_{CO}, the amount of CO adsorbed on site

1, n_{CO1} . Further, the ϵ_{CO2} value can be calculated from eq. (2). The same method was applied to the spectra obtained after introducing various small doses of CO onto the sulfided W/Al_2O_3 catalyst at 100 K.

For the calculation of the molar attenuation coefficients ϵ_{CO1} and ϵ_{CO2} , a series of oxidic W/Al_2O_3 catalyst with variable W loading (6-20 wt. %) was prepared. The heaviest W loaded material prepared in this synthesis corresponds to the concentration of a W monolayer on the alumina surface this is $3.3 W \text{ atoms}\cdot\text{nm}^{-2}$. The $\nu(\text{CO})$ band area of the components of CO adsorbed on WS_2 massif was obtained by careful spectrum decomposition using parameters described previously in Section 2.2.

III.3. RESULTS AND DISCUSSION

III.3.1. Characterization by low-temperature IR spectroscopy of CO.

III.3.1.1. IR/CO of sulfided WS_2/Al_2O_3 catalyst.

The IR spectra of CO adsorbed on sulfided 20_ W/Al_2O_3 catalyst are presented in **Figure 31**. Four main bands at 2185, 2160, 2121, and 2066 cm^{-1} were detected. The intensity of these bands increases with the amount of CO introduced. The higher wavenumber bands, namely 2185 and 2160 cm^{-1} , are attributed to coordination of CO on Lewis acid sites (Al^{3+}) of the alumina support and CO on hydrogen bonding with the support hydroxyl groups (OH), respectively [12,29,30]. Whereas the bands located at 2121 cm^{-1} and 2066 cm^{-1} are attributed to CO adsorbed on edge sites of the WS_2 slabs. At higher CO uptake appears a shoulder at 2141 cm^{-1} , corresponding to physisorbed CO. The two bands at 2121 cm^{-1} and 2066 cm^{-1} were observed since the very first introduced CO doses and were attributed to CO in interaction with

coordinatively unsaturated W sites (CUS) of low oxidation state [31]. Early work of *Duchet* [29] on W/Al₂O₃ catalysts already reported the presence of two bands at 2110 cm⁻¹ and 2060 cm⁻¹ on sulfided phase, called W₁ and W₂, respectively. On the other hand, *Crepeau* in his work on WS₂/ASA [32], reported the presence of W₁ and W₂ bands at 2127 cm⁻¹ and 2072 cm⁻¹. The difference in the wavenumber between that reported by *Duchet* on WS₂/Al₂O₃ and by *Crepeau* on WS₂/ASA shows that the bands characteristic of the WS₂ phase are also sensitive to the nature of the support.

The inset **Figure 32-A** that reports the spectra normalized to the most intense band, reveals that the band width located at 2121 cm⁻¹ (W₁) remains without alteration whatever the amount of CO introduced meanwhile the band at ~ 2066 cm⁻¹ shifts and widens. A closer inspection to the spectra at intermediate CO doses was carried out with the help of the second derivative function (**Figure 32-A**). This analysis points out that at least three components (2075, 2066 and 2051 cm⁻¹) can be distinguished in the W₂ band whereas the W₁ band only comprised one component at 2121 cm⁻¹. This analysis that specifies the maximum of the ν(CO) bands allows to carry out a proper decomposition of the CO spectra.

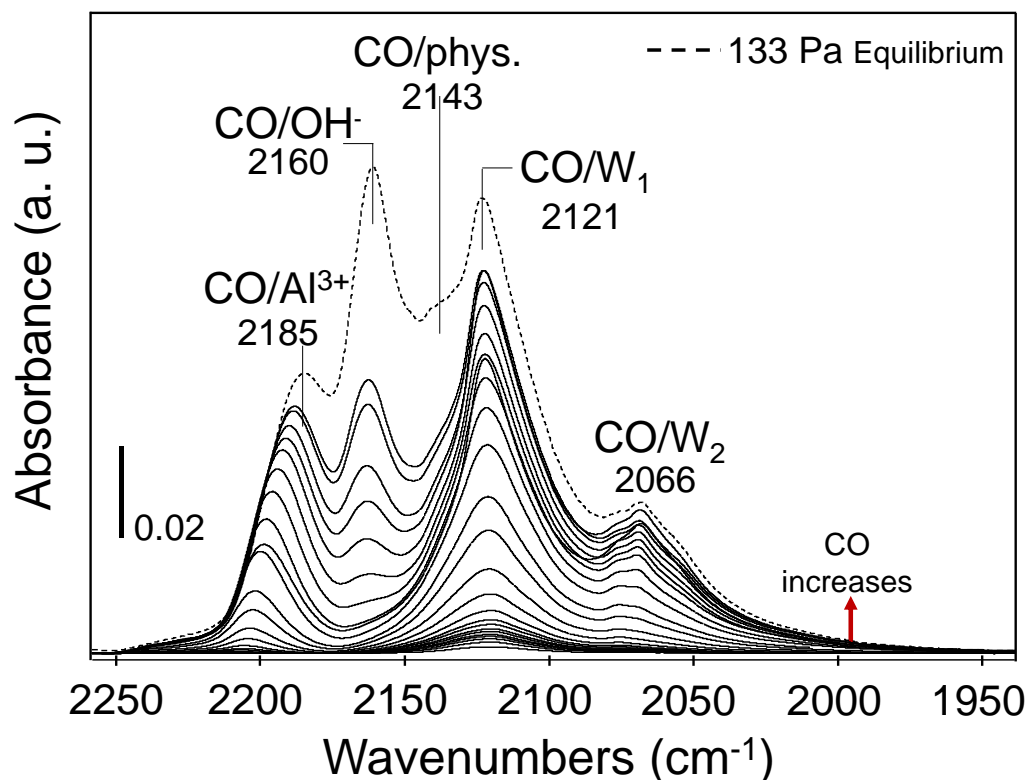


Figure 31. IR spectra of increasing CO doses (up to 133 Pa at equilibrium) adsorbed at 100 K on 20_W/ Al_2O_3 catalyst sulfided with 10% $\text{H}_2\text{S}/\text{H}_2$ at 673 K and 0.1 MPa.

As shown in **Figure 32-B**, on sulfided $\text{W}/\text{Al}_2\text{O}_3$ catalyst, the obtained IR spectrum was fitted with seven Voigt peaks. The three highest wavenumber peaks used to fit the $\nu(\text{CO})$ bands were ascribed to: CO coordinated to Lewis acid sites of the alumina support (Al^{3+}): 2186 cm^{-1} , CO in hydrogen bonding with the support.

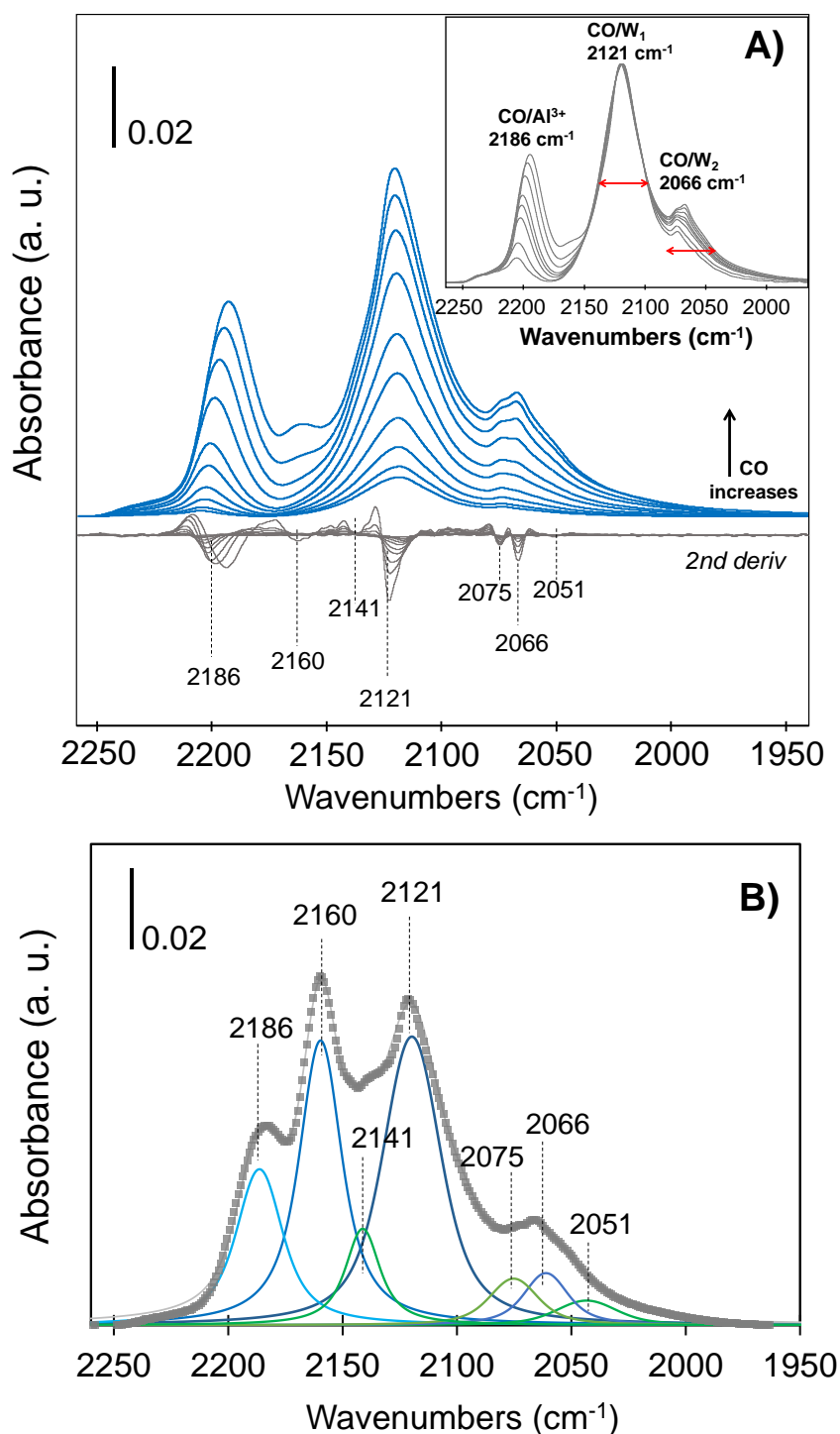


Figure 32. (A) IR spectra of intermediate CO doses adsorbed at 100 K on 20_W/ Al_2O_3 catalyst sulfided at 673 K, with their second derivatives ; (B) decomposition of the IR spectrum of CO adsorption ($P_{\text{CO}}=133$ Pa at equilibrium).

hydroxyl groups: 2160 cm^{-1} , and physisorbed CO molecules: 2140 cm^{-1} . Four peaks were generated in order to fit properly the $\nu(\text{CO})$ bands on WS_2 phase.

One peak was used to fit the $\nu(\text{CO})$ band on W₁-edge, which is located at 2121 cm⁻¹. Three peaks were employed to fit the $\nu(\text{CO})$ band on W₂-edge, which are located at 2075, 2066 and 2051 cm⁻¹. This confirms that W₁ band only comprised one single component whereas W₂ band comprised several components whose ratios change with CO doses.

III.3.1.2. IR/CO of H₂-treated WS₂/Al₂O₃.

As hydrogen is one of the reactants during the HDS process, its reactivity with HDS catalysts is of great importance [7,33]. Molecular hydrogen can be adsorbed dissociatively on WS₂ edges, leading to the creation of sulfur vacancies by removing sulfur in the form of H₂S and resulting in the WS₂ edges with lower sulfur coverage. The sulfur coverage at the edges of TMS nanoparticles depends on the H₂S/H₂ ratio. Thus, the ease for the creation of sulfur vacancies on the edge sites of the TMS catalyst can be evaluated by comparing the CO uptake before and after the H₂ treatment [34]. In order to investigate the effect of reductive treatment, the sulfided 20_W/Al₂O₃ catalyst was treated under pure H₂ flow for 2 h at 673 K at 1 atm pressure before being characterized by IR/CO. **Figure 33** shows that H₂ post-treatment leads to the creation of some supplementary Al³⁺ vacancies and hydroxyl groups (OH⁻), since it is possible to observe an increase of intensity of these bands (2160 and 2186 cm⁻¹). This can be explained by a possible breaking of Al–O–Al bridges during the H₂ post-treatment, leading to the creation of new Al³⁺ vacancies and hydroxyl groups. As observed in **Figure 33**, the H₂ post-treatment leads also to some increase of the $\nu(\text{CO})$ intensity in the region corresponding to W₂-edge (2000-2100 cm⁻¹), while the $\nu(\text{CO}/\text{W}_1\text{-edge})$ remained practically unchanged. These results indicate that vacancies creation occurs more easily on the W₂-

edge and only limited S atoms can be removed from the W₁ edge by H₂ treatment. An inspection in more detail of the three components associated with the W₂-edge reveals that they all increase with a same proportion (Inset **Figure 33**). Nevertheless, it should be underlined that intensity increases of the W₂ bands are small, suggesting that the edges of the sulfided WS₂ slabs are rather stable upon H₂-treatment.

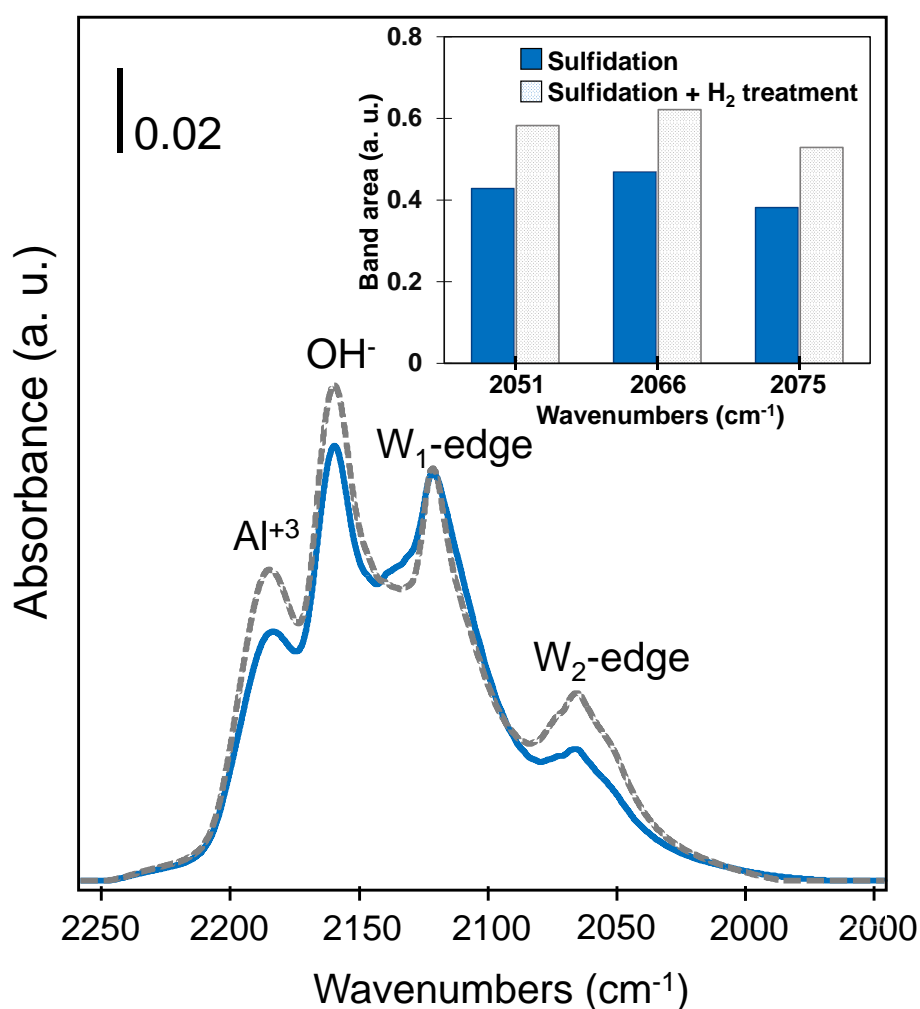


Figure 33. Effect of H₂ treatment at 623 K on CO adsorption (100 K, 133 Pa at equilibrium) on sulfided 20_W/Al₂O₃ catalyst. IR/CO spectrum obtained after sulfidation (continuous line) and after 2 h of H₂ treatment at 623 K (dashed line); Inset: Effect of the H₂ treatment on the area of the IR/CO bands of the three components of W₂ sites.

III.3.2. DFT calculations

III.3.2.1. Sulfur coverage and surfaces to study.

It has been shown that the number of sulfur atoms present at the edges of the slabs depends on the H₂/H₂S molar ratio. By observing the crystallographic structure of the WS₂ slabs, two types of edges are considered, namely, the metallic edge (M-edge) and the sulfur edge (S-edge). Two types of surfaces referring to sulfidation and reduction conditions were modeled for our purposes. Each surface is designated by the number of sulfur atoms exposed on each of the two edges: this is [S atoms_{M-edge} - S atoms_{S-edge}]. In sulfidation conditions ($10^{-4} < \text{H}_2/\text{H}_2\text{S} < 20$), the most stable surface corresponds to [4 - 8] (**Figure 34-A**). The coordination of both the W atoms of the S-edge and of the M-edge is six (VI). Under this configuration, each W atom in the M-edge is bridged to 2 S atoms in the plane above the surface of the W atoms, while each W atom in the S-edge is bridged to 4 S atoms in the plane above the surface of the W atoms. The coordination of the W atoms on both edges being (VI), it means that there is no more unsaturated sites (CUS) on the edges of the slab. The second surface studied is stable under reductive conditions, (hydrogen rich atmosphere: $\text{H}_2/\text{H}_2\text{S} > 20$), and is labeled [4 - 4] (**Figure 34-B**). The coordination numbers of W atoms is 6 on the M-edge (W_{6c}) and is 4 (W_{4c}) on the S-edge. The terminal S atoms are in bridging position between two W atoms on both edges, the W-S distances are similar to the distances in the crystal (2.40 Å). Considering only coordination numbers, we can suppose that CO adsorption on the S-edge will be favored in a reductive environment. Here, the coordination of the W atoms of the S-edge decreases from VI to IV when

increasing the H₂/H₂S ratio, while no change was observed in the geometry of the M-edge.

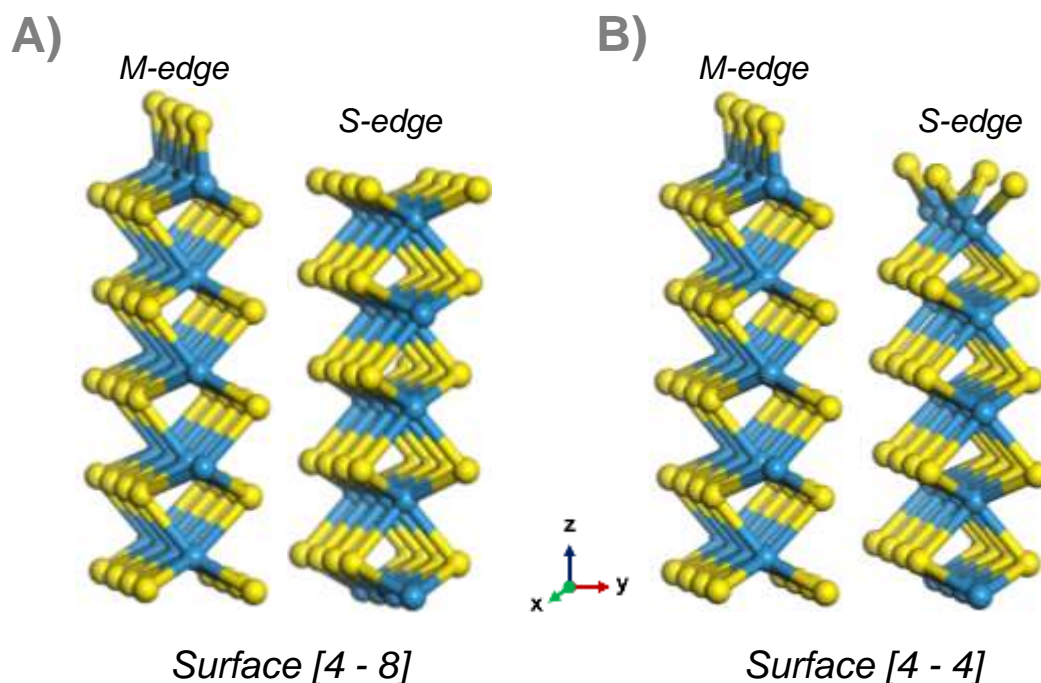


Figure 34. Depiction of the thermodynamically WS₂ stable surfaces according to the H₂S/H₂ partial pressures: (A) surface [4-8], stable surface when the $10^{-4} < H_2/H_2S < 20$; (B) surface [4 - 4], stable surface when $H_2/H_2S > 20$.

III.3.2.2. Calculation of CO adsorption

The treatments to which the catalysts were subjected before the adsorption of CO were carried out to correspond to two of the three stable surfaces of the WS₂ edges. The stable zone corresponding to the sulfidation procedure under pure H₂S was not considered in our case since it is less frequently used at industrial level. All computed adsorption energies and vibrational frequencies of CO on [4 - 8] and [4 - 4] surfaces for both edges are reported in **Table V**.

On the M-edge either in sulfiding [4 - x], or in reducing conditions [4 - x], CO adsorption can take place with an adsorption energy ranging between -0.63 to -0.70 eV, depending on the exact geometry of the M-edge. The geometry of the

W surface is subject to Peierls distortion, but this does not lead to any effect on the $\nu(\text{CO})$ frequency that is 2025 cm⁻¹.

Table V. Calculated parameters of CO adsorbed on M-edge (W) and S-edge (S) of WS₂.

Edge	Conditions	Surface	W coordination	E ads (eV)	$\nu(\text{CO})$ (cm ⁻¹)	D _{W-C} (Å)	D _{C-O} (Å)
M-	sulfidation	[4-x]	6	-0.63 to -0.70	2025	2.11	1.15
M-	reductive	[4-x]	6	-0.63 to -0.70	2025	2.11	1.15
S-	sulfidation	[x-8]	6	-0.90	2010	2.09	1.16
S-	reductive	[x-4]	4	-0.83 ; 1.04	1949 ; 1959	2.09	1.16

Figure 35 represents the optimized geometry of the structure of the M-edge where the CO interacts with a single W atom. In **Figure 35-A** the optimized distances are depicted while in **Figure 35-B** the coordination of the tungsten on the M-edge is shown. In sulfiding condition, the stable surface of the S-edge is [x – 8], a top CO adsorption on W_{6c} is also possible with adsorption energy of -0.90 eV. In this configuration, the CO molecule is almost perpendicular to the surface and the $\nu(\text{CO})$ wavenumber is now calculated at 2010 cm⁻¹. In conditions corresponding to high hydrogen amount, the stable surface is the [x – 4]. 4 S atoms are removed, creating CUS sites (W_{4c} atoms) on the S-edge. The S atoms on the S-edge form a zigzag chain that is flexible.

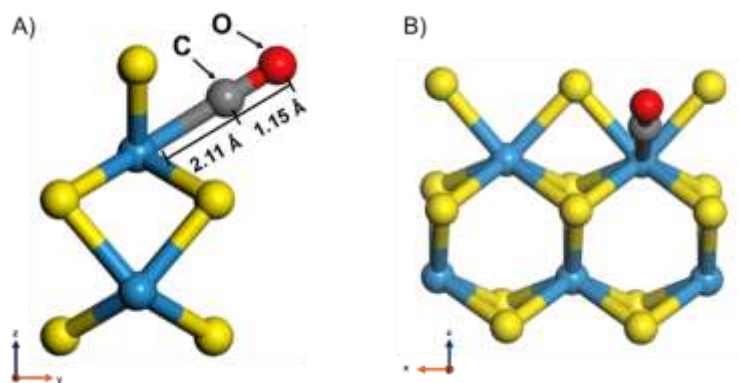


Figure 35. Optimized configuration for one CO molecule adsorbed on the M-edge [4-x] of WS₂ surface. A) Front view of the optimized distances between the W atom and the CO molecule. B) Side view of the M-edge showing the W coordination.

On the most stable geometry, the adsorption energy is -1.04 eV and the associated wavenumber is 1959 cm⁻¹. The displacement of a sulfur atom from one side of the W plane to the other one reduced the stability of the S-edge, the adsorption energy is then -0.83 eV. In this configuration, the CO stretching wavenumber is computed at 1949 cm⁻¹. Thus there is a difference around 70 cm⁻¹ between CO adsorbed on the S-edge and on the M-edge. Due to the multiple configurations on the S-edge, a broadening of the $\nu(\text{CO})$ band on S-edge is expected. A representation of the most stable structure is given in **Figure 36**. The CO molecule is adsorbed on the S-edge perpendicular to the surface (**Figure 36-A**).

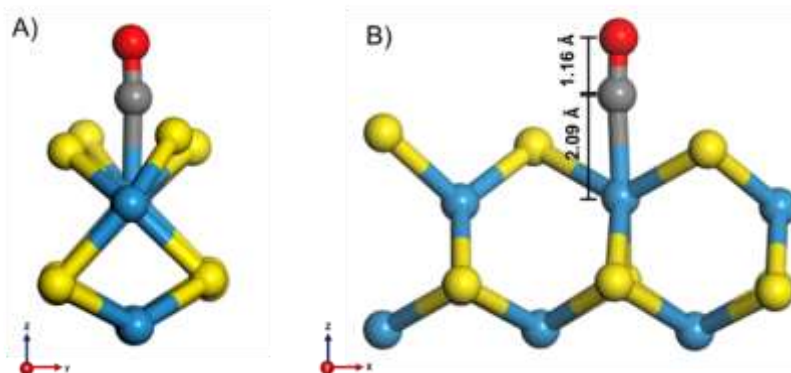


Figure 36. Optimized configuration for one CO molecule adsorbed on the S-edge [x-4] of WS_2 surface. A) Front view of the optimized distances between the W atom and the CO molecule. B) Side view of the S-edge showing the W coordination.

III.3.2.3. CO adsorption: Experiment vs Calculation

Experimental spectra present two main $\nu(\text{CO})$ bands (W_1 , W_2) separated by $\sim 55 \text{ cm}^{-1}$. Their intensity ratio varies significantly with the conditions of treatment and preparation (**Figure 33 and 37**) indicating that they are characteristics of two distinct sites of the sulfided slabs. In parallel, DFT calculations shows that CO adsorption on M-edge and on S-edge of WS_2 surface give rise to $\nu(\text{CO})$ bands separated by $\sim 70 \text{ cm}^{-1}$. This allows us to propose assigning the high wavenumber band (W_1 , 2121 cm^{-1}) to CO adsorbed on M-edge and the low wavenumber band (W_2 , 2066 cm^{-1}) to CO adsorbed on S-edge. It should be mentioned that, as for DFT calculation, the differences of wavenumber are more reliable than the value of wavenumbers since no scaling factor nor anharmonic correction have been taken into account. It has to be remarked that DFT calculation indicates that, on S-edge, CO frequencies should be different in sulfiding and reducing conditions (**Table V**). From the calculated wavenumber in sulfiding conditions (2110 cm^{-1}), one should expect the detection of a band in the low wavenumber side of that at 2121 cm^{-1} . Spectral analysis even for the

first CO doses of sulfided catalysts excluded the formation of this species. However, it has to be recalled that the experimental sulfidation comprised a H_2S/H_2 treatment at 673 K that is followed by a flush under Ar and evacuation at 673 K until reaching $P 1.10^{-4}$ Pa. It was shown that these final steps lead to the elimination of some sulfur atoms from the sulfide phase surface. Thus after this sulfidation procedure, the sulfide slab edges are not completely saturated in sulfur whereas calculations are based on a completely saturated S-edge [x , 8] (Table 1). As the sulfiding conditions, the model used for DFT calculation is not completely representative of the experimental system, explaining the discrepancy between prediction and experiments. By contrast, very good agreement appears for reductive conditions. Note that, in our early paper on Mo sulfide catalyst [10], discrepancies between calculation and experiment also appear for sulfiding conditions. No CO adsorption on M-edge of MoS_2 slab was predicted whereas a band at 2110 cm^{-1} was observed after sulfidation as after H_2 treatment. It should be underlined that, on sulfide Mo as on W catalyst, results of experiments and calculations at low H_2S/H_2 ratio nicely agree [10].

Other interesting parallel between experiment and calculation on W system appear. First, the experimental spectra (**Figure 32** A and B) point out that the W_1 band at 2121 cm^{-1} correspond to one single species and DFT calculation reports that there is one single geometry for CO adsorption on M-edge. Second, experiments show that the W_2 component comprised several bands ($2075, 2066, 2051\text{ cm}^{-1}$) and calculation shows for the CO adsorption on the S-edge that numerous geometries and orientations of the S atoms are stable, giving rise to more than one type of possible adsorption of CO at this edge. Moreover,

despite the existence of different types of geometry, the variation of the calculated wavenumber from one band to another is relatively small (10 cm⁻¹).

Another feature to mention is that reductive treatment leads to very limited change of W₁ band intensity whereas W₂ band increases more markedly (Figure 4). This is in good agreement with trends reported by calculation that indicates greater change in W coordination on S-edge than on M-edge between sulfiding and reductive conditions (Table V). The nice agreement between experimental and calculated features supports the assignment of the band at 2121 cm⁻¹ to CO adsorption on M-edge (CO_{M-edge}) and that at ~2066 cm⁻¹ to CO adsorption on S-edge (CO_{S-edge}).

III.3.3. Influence of W loading on W- and S-edge bands.

A series of W/Al₂O₃ catalysts, in which the W coverage was increased from 0.85 to 3.3 atoms·nm⁻² (i.e. from 6 to 20 wt% W), has been analyzed by IR/CO from small CO doses up to 133 Pa at equilibrium. **Figure 37** compares the spectra obtained at 113 Pa CO at equilibrium of the different W-catalysts, while **Figure 38** reports the spectra for the first doses of CO introduced.

As a general manner, bands similar as those reported on W₂₀/Al₂O₃ catalyst (**Figure 31**) are observed although with intensity and ratio that depends on the W amount and on the alumina coverage. At the lowest metal loading (6 wt. %) and under 133 Pa of CO, ν(CO) bands in the 2130-2000 cm⁻¹ region are almost undetectable (**Figure 37**). This is partly due to the high intensity of the ν(CO) bands associated with the support, which overshadow the signal corresponding to the sulfided sites. However, when observing the spectra of the first doses of CO introduced (**Figure 38**), a band centered at 2118 cm⁻¹ with a small shoulder at 2075 cm⁻¹ can be detected. These are respectively assigned

to CO adsorbed on M-edge (CO_{M-edge}) and S-edge sites CO_{S-edge} . As the W concentration increases, the $\nu(CO)$ bands associated to WS_2 phase gain intensity and are better defined (**Figure 37**). In addition to the well-visible band CO_{M-edge} band, now centered at 2121 cm^{-1} , the CO_{S-edge} band begins to appear at 2066 cm^{-1} . The intensity of CO_{S-edge} band increases with the W loading in the catalyst. On the other hand, the intensity of the $\nu(CO)$ bands associated to the support (Al^{3+} Lewis acid sites and OH^- groups of Al_2O_3) decrease as a result of a more covered surface of the alumina support by WS_2 , which agrees with the increase of the W loading.

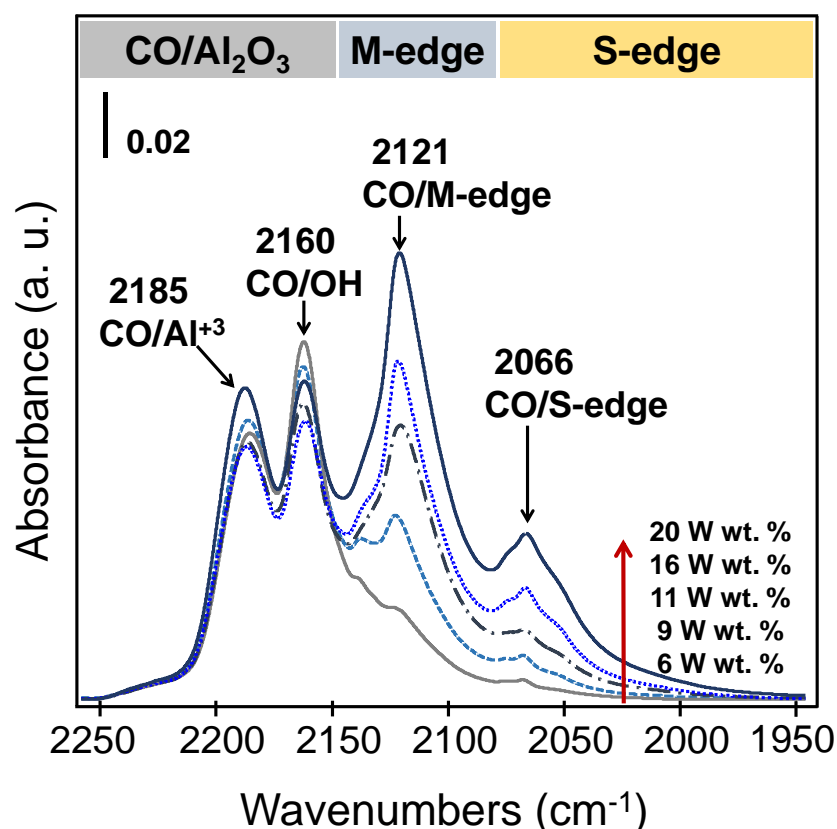


Figure 37. IR spectra of CO adsorption (133 Pa CO at equilibrium, 100 K) on WS_2/Al_2O_3 prepared with different W loading. The WS_2/Al_2O_3 catalysts were obtained by sulfidation at 673 K and 0.1 MPa with 10% H_2S/H_2 .

III.3.4. Determination of molar attenuation coefficients for W- and S-edge bands.

In previous works of our group on MoS₂-based catalysts [35], distinct molar attenuation coefficient values were obtained for CO adsorbed on either M-edge ($\epsilon_{\text{CO/M-edge}}$) or S-edge ($\epsilon_{\text{CO/S-edge}}$) (Table VI). These values allowed the quantification of MoS₂ sites of each edges and thus calculation of the S-/M-edge ratio that defines the morphology of the MoS₂ slabs [14]. Recent work on sulfided Mo/Al₂O₃ catalysts prepared with and without citric acid showed a good agreement between sulfided slab shape determined from IR/CO, and that observed on transmission electron microscope by HAADF-STEM [17]. This gave a proof by image of the morphological changes of the catalyst according to the preparation modes, and also underlined that IR/CO method allows to reach a representative average picture of the sulfided slab shapes. Thus, the determination of the morphology of the WS₂ particles requires the measurement of the molar attenuation coefficients of the $\nu(\text{CO})$ bands characteristics of M-edge and S-edge. In the literature, no ϵ_{CO} values for M-edge and S-edge are reported for any of the species formed in the WS₂ or NiWS catalysts. A close inspection of the spectra obtained for the first doses of CO introduced shows that, at low W loading, only one $\nu(\text{CO})$ band characteristic of M-edge sites appears (Figure 9 A-C). However, spectra obtained on 6_W/Al₂O₃ present signals associated to CO adsorbed on alumina Lewis acid sites from the first CO doses. This is in agreement with the very limited support coverage by W phase (0.85 atoms·nm⁻²), but this prevent using the spectra obtained on the catalyst with the lowest W amount to calculate $\epsilon_{\text{CO/M-edge}}$ sites. However, when the W amount is somehow greater as for 9_W/Al₂O₃ and 12_W/Al₂O₃, the relationship between the variation of the band area of CO adsorbed on M-edge

and the number of CO introduced can be used to calculate the $\epsilon_{\text{CO/M-edge}}$. As shown on **Figure 39**, close $\epsilon_{\text{CO/M-edge}}$ values were obtained for these two catalysts i.e. $11.4 \pm 2 \mu\text{mol}\cdot\text{cm}^{-1}$ for 9_W/Al₂O₃ and $12.2 \pm 2 \mu\text{mol}\cdot\text{cm}^{-1}$ for 12_W/Al₂O₃. At higher W loading (**Figure 38** D-E) i.e. for 16_W/Al₂O₃ and 20_W/Al₂O₃, two $\nu(\text{CO})$ bands are detected even for low CO doses. They correspond to CO interaction with the M-edge site (2121 cm^{-1}) and the S-edge site (2072 cm^{-1}). With the molar attenuation coefficient of CO adsorbed on M-edge ($\epsilon_{\text{CO/M-edge}}$) already determined, the amount of CO adsorbed specifically on S-edge sites can be calculated from the band area of these sites and using the methodology described in section 3.5. Hence, a relationship between the variation of the band area of CO adsorbed on S-edge and the number of CO adsorbed on S-edge sites (calculated from the total number of CO introduced in the cell minus the number of CO adsorbed on M-edge sites) was used to calculate the attenuation coefficient of CO adsorbed on S-edge ($\epsilon_{\text{CO/S-edge}}$). The slope of this relationship is the $\epsilon_{\text{CO/S-edge}}$.

$$\left[\frac{n_T}{S} - \frac{A_{M\text{-edge}}}{\epsilon_{M\text{-edge}}} \right] \epsilon_{M\text{-edge}} = A_{S\text{-edge}} \quad (3)$$

Note that a CO band specific of Lewis acid sites appears from the third CO doses, but the signal being low, it has been neglected in the $\epsilon_{\text{CO/M-edge}}$ calculations. **Figure 39** shows that close $\epsilon_{\text{CO/S-edge}}$ values are obtained for these two catalysts i.e. $22.9 \pm 6 \mu\text{mol}\cdot\text{cm}^{-1}$ for 16_W/Al₂O₃ and $23.4 \pm 6 \mu\text{mol}\cdot\text{cm}^{-1}$ for 20_W/Al₂O₃. Thus, the average molar attenuation coefficients $\epsilon_{\text{CO/M-edge}}$ and $\epsilon_{\text{CO/S-edge}}$ for sulfided W/Al₂O₃ catalysts are $11.9 \pm 2 \mu\text{mol}\cdot\text{cm}^{-1}$ and 23.1 ± 6

μmol·cm⁻¹ respectively. Note that in all the calculations (**Figure 39**) an adequate fit and line tendency were obtained.

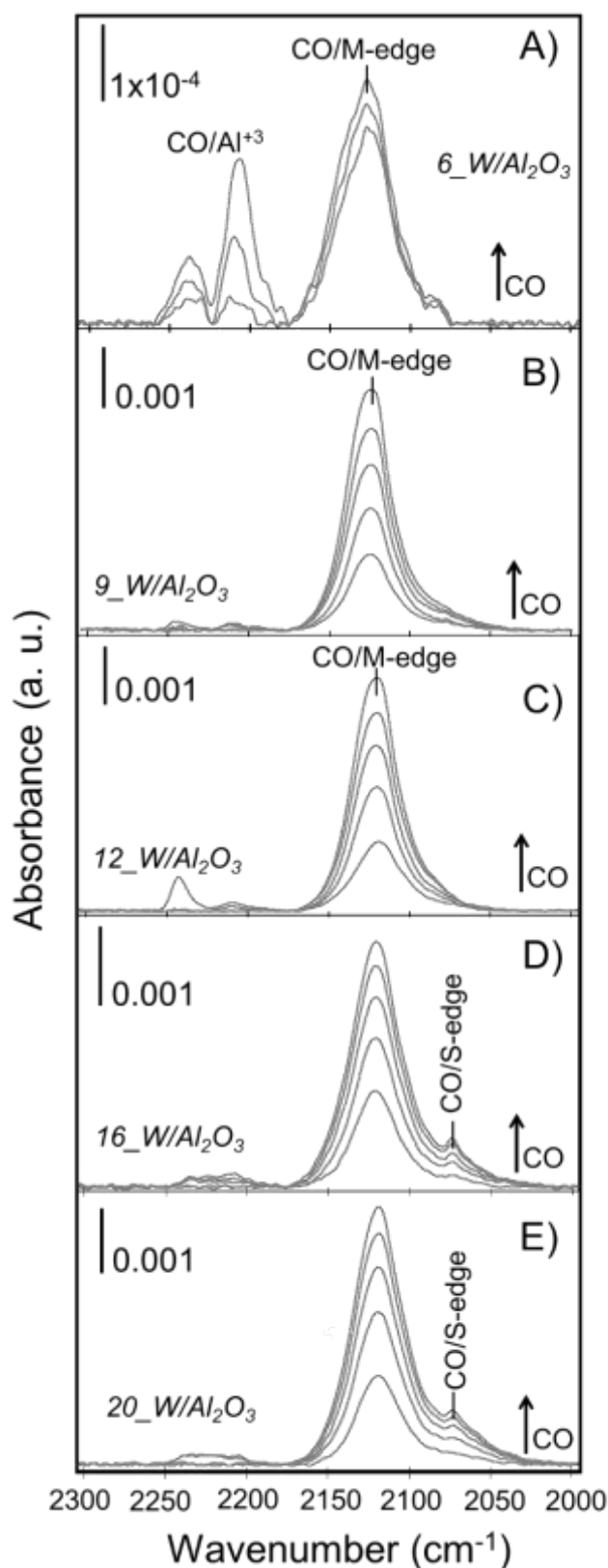


Figure 38. IR spectra of the first CO doses adsorbed ($T = 100$ K) on sulfided W/Al_2O_3 at different metal loadings. Intermediate W concentrations results on CO adsorption only on the metallic edge. (first doses: 0.001, 0.002, 0.003, and 0.004 $\mu\text{mol CO}\cdot\text{mg}^{-1}$ sulfided catalyst).

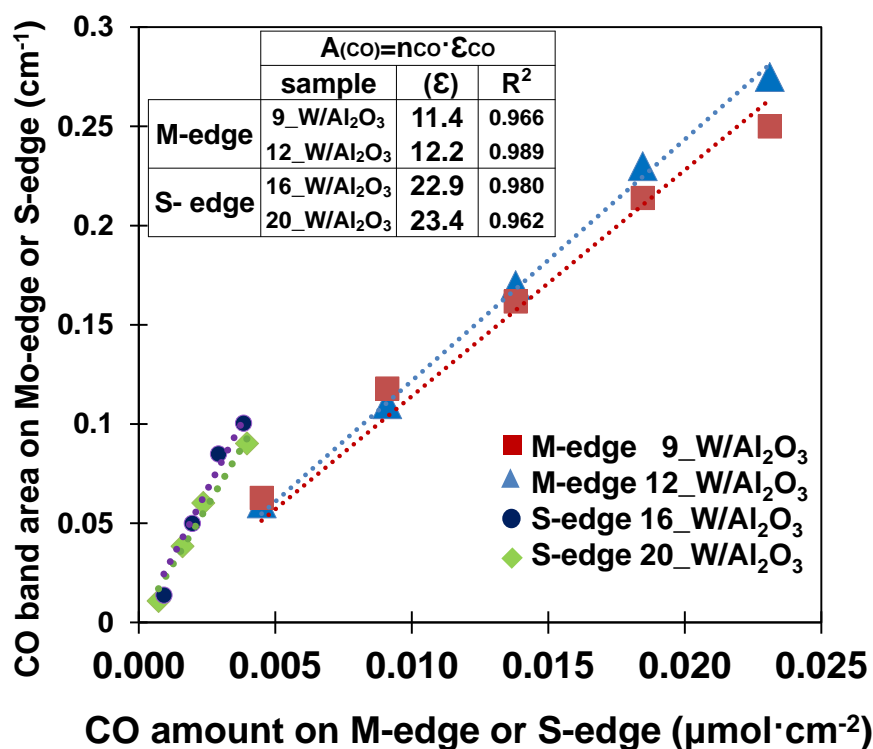


Figure 39. Determination of the molar attenuation coefficients (ϵ) of CO adsorbed on WS₂. The spectra for ϵ determination are reported in **Figure 9**. The ϵ values are the slope of the linear relationship between the area of $\nu(\text{CO})$ band and the amount of CO introduced onto a cm² of the sample.

III.3.5. The influence of W loading on WS₂ slab morphology.

As observed in **Figure 37**, the increase of metal loading has an effect not only on the intensity of the bands associated to the M- and S- edges, but also on their ratio. From the molar attenuation coefficients for both edge sites, the S-edge/M-edge ratio can be calculated for the various W catalysts (**Figure 40**). The value of the ratio suffers a steady increase along with the W loading and shows that the morphology of the WS₂ slabs changes from slightly truncated triangles exposing mainly the M-edge (S-edge/M-edge = 0.17) to a more heavily truncated triangle exposing more S-edge (S-edge/M-edge = 0.32). Similar effect of metal loading has been earlier reported for MoS₂/Al₂O₃ catalysts [13].

In Mo system, this phenomenon was associated to a change in the sulfide phase - support interactions with metal loading. This, since the MS_2 phase interacts with Al_2O_3 support by the M–O–Al linkages that are located at the edges of the slabs instead of at the core slab sites [13,36]. Similarly, the concentration of the W–O–Al linkages will decrease with increasing WS_2 size. It is observed that the WS_2 slabs on WS_2/Al_2O_3 catalysts exposed more S-edge with increasing the W loading. All these results suggest that the WS_2 – Al_2O_3 interactions decrease with increasing W loading.

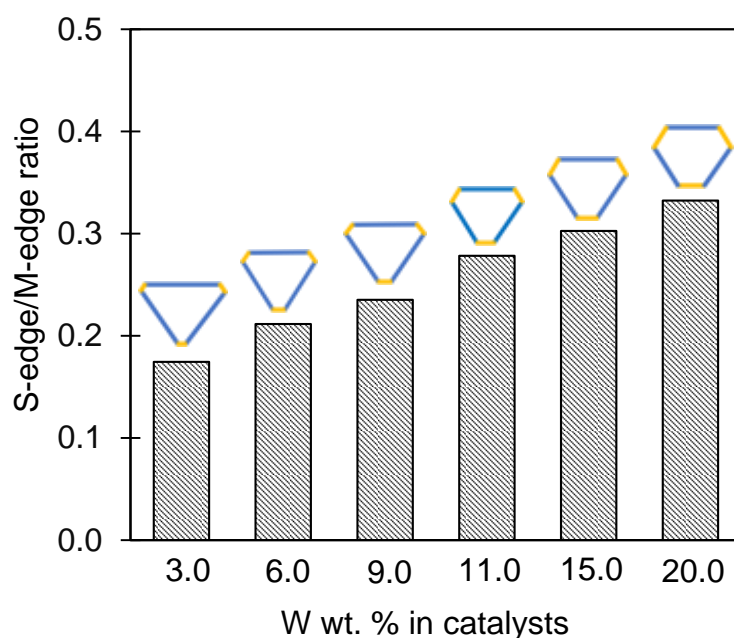


Figure 40. The ratios of S-edge/M-edge and corresponding morphologies of WS_2 slabs as function of W loading of WS_2/Al_2O_3 catalysts.

III.3.6. Comparison between W and Mo sulfide catalysts.

As summarized in **Table VI**, many similarities appear for CO adsorption on W and Mo sulfide catalysts.

For sulfide W as well as for sulfide Mo catalysts, CO adsorbed on sulfide slabs gives rise to 2 IR bands separated by about 50 cm^{-1} that allows distinguishing

M-edge (CO_{M-edge}) and S-edge (CO_{S-edge}). On both systems, the frequencies of CO_{M-edge} appear at greater frequency than the CO_{S-edge} . This is in agreement with the calculated Mo and W coordination that is greater on M-edge (M_{6C}) than on S-edge (M_{4C}) (Table 1, Ref. [10]). In agreement with their higher frequencies, molar attenuation coefficient (ϵ) for CO_{S-edge} is greater than for CO_{M-edge} . From these values, the morphology of the TMS slabs could be calculated. For alumina supported catalysts with metal amount corresponding to monolayer coverage, sulfided slabs with very close morphology i.e. highly truncated hexagonal (S-/M- ratio = 0.30-0.32) are formed on alumina supported Mo and W catalysts.

In both systems, an accurate analysis shows that CO adsorbed on S-edge is characterized by a broad band consisting of several $\nu(CO)$ components. The three bands (2065, 2045 and 2020 cm^{-1}) characterizing CO adsorption on S-edge of Mo/Al_2O_3 have been associated to different CO coverages [10,11,35,37]. Whereas the three components (2075, 2066 and 2051 cm^{-1}) detected on S-edge of W/Al_2O_3 have been associated to various orientations of the edge sulfur atoms giving rise to more than one $\nu(CO)$ band. By contrast, M-edge sites present a more homogeneous geometry. For W catalyst, only one component is detected whatever the H_2S/H_2 ratio whereas for Mo/Al_2O_3 system, a band is detected at 2110 cm^{-1} after sulfidation while a second one develops under reductive atmosphere (2098 cm^{-1}) [10,35].

A noticeable difference between the Mo and W systems is their difference of stability toward reductive treatment. When submitted to H_2 -post-treatment, the stability of the edge sites of sulfide W catalyst is remarkable (only S-edge site amount increases by 16%). By contrast, on Mo system, the CO uptake

increases of about 55% both on M- and S-edges. This great sulfur depletion of MoS₂ edge is in agreement with the appearance of a new band (2098 cm⁻¹) after reductive treatment whereas no frequency shift are observed on W catalysts. Hence, sulfided slabs of Mo and W alumina supported catalysts present similar morphologies but different stability regarding H₂ treatment.

Table VI. Comparison of experimental $\nu(\text{CO})$ frequencies and molar attenuation coefficients of CO on M- and S-edge, as well as MS₂ slab morphology for (9 %) Mo/Al₂O₃ and (20 %) W/Al₂O₃ catalysts sulfided under H₂S/H₂* or post –treated under H₂ at 473K atmosphere.

Catalyst	Edge type	Sulfidation		H ₂ post-treatment vs sulfidation
		$\nu(\text{CO})$ frequency (cm ⁻¹)	Epsilon, ϵ_{CO} ($\mu\text{mol}\cdot\text{cm}^{-1}$)	CO band area enhancement
Mo	M-edge	2110	20.0 ± 3	+60%
	S-edge	2065	35.0 ± 9	+54%
	Slab morphology	Truncated hexagon Ratio S/M = 0.30		
W	M-edge	2121	11.9 ± 2	~0%
	S-edge	2066	23.1 ± 6	+16%
	Slab morphology	Truncated hexagon Ratio S/M = 0.32		

* Values corresponding to a metal monolayer on the alumina surface.
Sulfidation conditions: Mo/Al₂O₃ Ts = 423 K, 2h : W/Al₂O₃ Ts = 473 K, 2h.

III.4. Conclusions

In the present work, carbon monoxide adsorption on alumina-supported sulfided W catalysts was studied by means of IR spectroscopy pairing with DFT calculations. The parallel between experimental and calculated data allowed us

to attribute, for the first time, the two $\nu(\text{CO})$ bands observed at 2121 cm⁻¹ and about 2066 cm⁻¹ to CO adsorbed on the M-edge and S-edge sites of the WS₂ slabs, respectively.

The integrated molar attenuation coefficients of CO associated with the M- and S-edge sites were successfully determined, allowing determination of the WS₂ morphology. Increasing the W loading (3-20 wt% W) allows going from an almost pure triangle exhibiting mostly M-edge to a truncated hexagon.

Parallel between experiments and DFT calculation of CO adsorption on W and Mo sulfide catalysts provides evidence for many similarities between the two systems. On both TMS, CO adsorption give rise to two main $\nu(\text{CO})$ bands separated by about 50 cm⁻¹ that allowed to discriminate M-edge and S-edge sites. For M loading corresponding to monolayer coverage of alumina, Mo and W sulfide slab present a similar shape i.e. truncated hexagon. However, edge sites of WS₂ slabs clearly exhibit greater stability under H₂ atmosphere than Mo sulfided ones.

III.5. REFERENCES

- (1) Kabe, T.; Ishihara, A.; Zhang, Q. Deep Desulfurization of Light Oil. Part 2: Hydrodesulfurization of Dibenzothiophene, 4-Methyldibenzothiophene and 4,6-Dimethyldibenzothiophene. *Appl. Catal. A Gen.* **1993**, *97*, L1–L9.
- (2) Santolalla-Vargas, C. E.; Suarez Toriello, V. A.; De los Reyes, J. A.; Cromwell, D. K.; Pawelec, B.; Fierro, J. L. G. Effects of PH and Chelating Agent on the NiWS Phase Formation in NiW/ γ -Al₂O₃ HDS Catalysts. *Mater. Chem. Phys.* **2015**, *166*, 105–115. <https://doi.org/10.1016/j.matchemphys.2015.09.033>.
- (3) Suárez-Toriello, V. A.; Santolalla-Vargas, C. E.; De Los Reyes, J. A.; Vázquez-Zavala, A.; Vrinat, M.; Geantet, C. Influence of the Solution PH in Impregnation with Citric Acid and Activity of NiW/Al₂O₃ Catalysts. *Journal Mol. Catal. A, Chem.* **2015**, *404–405*, 36–46. <https://doi.org/10.1016/j.molcata.2015.04.005>.
- (4) Brorson, M.; Carlsson, A.; Topsøe, H. The Morphology of MoS₂, WS₂, Co-Mo-S, Ni-Mo-S and Ni-W-S Nanoclusters in Hydrodesulfurization Catalysts Revealed by HAADF-STEM. *Catal. Today* **2007**, *123* (1–4), 31–36. <https://doi.org/10.1016/j.cattod.2007.01.073>.
- (5) Topsøe, H., Clausen, B. S., & Massoth, F. E. *Catalysis Science and Technology*; Anderson, John R., M. B., Ed.; Springer: Berlin, 1996. https://doi.org/doi.org/10.1007/978-3-642-61040-0_1.
- (6) Okamoto, Y.; Hioka, K.; Arakawa, K.; Fujikawa, T.; Ebihara, T.; Kubota, T. Effect of Sulfidation Atmosphere on the Hydrodesulfurization Activity of SiO₂-Supported Co-Mo Sulfide Catalysts: Local Structure and Intrinsic Activity of the Active Sites. *J. Catal.* **2009**, *268* (1), 49–59. <https://doi.org/10.1016/j.jcat.2009.08.017>.
- (7) Chen, J.; Maugé, F.; Fallah, J. El; Oliviero, L. IR Spectroscopy Evidence of MoS₂ Morphology Change by Citric Acid Addition on MoS₂/Al₂O₃ Catalysts – A Step Forward to Differentiate the Reactivity of M-Edge and S-Edge. *J. Catal.* **2014**, *320* (320), 170–179. <https://doi.org/10.1016/j.jcat.2014.10.005>.
- (8) Khalil, I.; Jabraoui, H.; Maurin, G.; Lebègue, S.; Badawi, M.; Thomas, K.; Maugé, F. Selective Capture of Phenol from Biofuel Using Protonated Faujasite Zeolites with Different Si/Al Ratios. *J. Phys. Chem. C* **2018**, *122* (46), 26419–26429. <https://doi.org/10.1021/acs.jpcc.8b07875>.
- (9) Jabraoui, H.; Khalil, I.; Lebègue, S.; Badawi, M. Ab Initio Screening of Cation-Exchanged Zeolites for Biofuel Purification. *Mol. Syst. Des. Eng.* **2019**, *4* (4), 882–892. <https://doi.org/10.1039/c9me00015a>.
- (10) Travert, A.; Dujardin, C.; Maugé, F.; Cristol, S.; Paul, J. F.; Payen, E.; Bougeard, D. Parallel between Infrared Characterisation and Ab Initio Calculations of CO

- Adsorption on Sulphided Mo Catalysts. *Catal. Today* **2001**, *70*, 255–269.
- (11) Travert, A.; Dujardin, C.; Maugé, F.; Veilly, E.; Cristol, S.; Paul, J.-F.; Payen, E. CO Adsorption on CoMo and NiMo Sulfide Catalysts: A Combined IR and DFT Study. *Phys. Chem. B* **2006**, *110*, 1261–1270. <https://doi.org/10.1021/jp0536549>.
- (12) Maugé, F.; Lavalley, J. C. FT-IR Study of CO Adsorption on Sulfided Mo/Al₂O₃ Unpromoted or Promoted by Metal Carbonyls: Titration of Sites. *J. Catal.* **1992**, *137*, 69–76. [https://doi.org/10.1016/0021-9517\(92\)90139-9](https://doi.org/10.1016/0021-9517(92)90139-9).
- (13) Chen, J.; Oliviero, L.; Portier, X.; Maugé, F. On the Morphology of MoS₂ Slabs on MoS₂/Al₂O₃ Catalysts: The Influence of Mo Loading. *RSC Adv.* **2015**, *5* (99), 81038–81044. <https://doi.org/10.1039/C5RA14768A>.
- (14) Chen, J.; Dominguez Garcia, E.; Oliviero, E.; Oliviero, L.; Maugé, F. Effect of High Pressure Sulfidation on the Morphology and Reactivity of MoS₂ Slabs on MoS₂/Al₂O₃ Catalyst Prepared with Citric Acid. *J. Catal.* **2016**, *339*, 153–162. <https://doi.org/10.1016/j.jcat.2016.04.010>.
- (15) Dominguez Garcia, E.; Chen, J.; Oliviero, E.; Oliviero, L.; Maugé, F. New Insight into the Support Effect on HDS Catalysts: Evidence for the Role of Mo-Support Interaction on the MoS₂ Slab Morphology. **2020**. <https://doi.org/10.1016/j.apcatb.2019.117975>.
- (16) Vrinat, M.; Breyse, M.; Geantet, C.; Ramirez, J.; Massoth, A. Effect of MoS₂ Morphology on the HDS Activity of Hydrotreating Catalysts; 1994; Vol. 26.
- (17) Zavala-sanchez, L.; Portier, X.; Maugé, F.; Oliviero, L. High Resolution STEM-HAADF Microscopy on γ - Al₂O₃ Supported MoS₂ Catalyst – Proof by Image of the Changes in Dispersion and Morphology of the Slabs with Addition of Citric Acid. *Nanotechnology* **2019**, No. Xxx, 1–10.
- (18) Hensen, E. J. M.; Van Der Meer, Y.; Van Veen, J. A. R.; Niemantsverdriet, J. W. Insight into the Formation of the Active Phases in Supported NiW Hydrotreating Catalysts. *Appl. Catal. A Gen.* **2007**, *322*, 16–32. <https://doi.org/10.1016/j.apcata.2007.01.003>.
- (19) Alphazan, T.; Bonduelle-Skrzypczak, A.; Legens, C.; Gay, A. S.; Boudene, Z.; Girleanu, M.; Ersen, O.; Copéret, C.; Raybaud, P. Highly Active Nonpromoted Hydrotreating Catalysts through the Controlled Growth of a Supported Hexagonal WS₂ phase. *ACS Catal.* **2014**, *4* (12), 4320–4331. <https://doi.org/10.1021/cs501311m>.
- (20) Chen, J.; Dominguez Garcia, E.; Oliviero, L.; Maugé, F. How the CO Molar Extinction Coefficient Influences the Quantification of Active Sites from CO Adsorption Followed by IR Spectroscopy? A Case Study on MoS₂/Al₂O₃

- Catalysts Prepared with Citric Acid. *J. Catal.* **2015**, 332, 77–82. <https://doi.org/10.1016/j.jcat.2015.09.005>.
- (21) Hafner, J.; Ab-Initio Simulations of Materials Using VASP: Density-Functional Theory and Beyond. *J. Comput. Chem.* **2008**, 29 (13), 2044–2078. <https://doi.org/10.1002/jcc.21057>.
- (22) Kresse, G.; Furthmüller, J. Efficiency of Ab-Initio Total Energy Calculations for Metals and Semiconductors Using a Plane-Wave Basis Set. *Comput. Mater. Sci.* **1996**, 6, 15–50.
- (23) Perdew, J. P. Density-Functional Approximation for the Correlation Energy of the Inhomogeneous Electron Gas. *Phys. Rev. B* **1986**, 33 (12), 8822–8824.
- (24) Perdew, J. P.; Burke, K.; Ernzerhof, M. Generalized Gradient Approximation Made Simple. *Phys. Rev. Lett.* **1996**, 77 (18), 3865–3868.
- (25) Kresse, G.; Joubert, D. From ultrasoft pseudopotentials to the projector augmented-wave method. *Phys. Rev. B Condens. Matter Mater. Phys.* **1999**, 59 (3), 1758–1775. <https://doi.org/10.1103/PhysRevB.59.1758>.
- (26) Pack, J. D.; Monkhorst, H. J. Special Points for Brillouin-Zone Integrations. *Phys. Rev. B Condens. Matter Mater. Phys.* **1977**, 16, 1748. <https://doi.org/10.1103/PhysRevB.16.1748>.
- (27) Hijazi, H.; Cantrel, L.; Paul, J.-F. O. Reactivity of Silver Iodide (β -AgI) Surfaces: A Density Functional Theory Study. *J. Phys. Chem. C* **2018**, 122 (46), 26401–26408. <https://doi.org/10.1021/acs.jpcc.8b06931>.
- (28) Monkhorst, H. J.; Pack, J. D. Special Points for Brillouin-Zone Integrations*. *Phys. Rev. B* **1976**, 13 (12), 5188–5192. <https://doi.org/10.1103/PhysRevB.13.5188>.
- (29) Duchet, J. C., Lavalley, J. C., Housni, S., Ouafi, D., Bachelier, J., Lakhdar, M., ... & Cornet, D. Carbon Monoxide and Oxygen Chemisorption and Functionalities of Sulphided Ni-W/Al₂O₃ Hydrotreating Catalysts. *Catal. Today* **1988**, 4 (1), 71–96. [https://doi.org/10.1016/0920-5861\(88\)87047-0](https://doi.org/10.1016/0920-5861(88)87047-0).
- (30) Muller, B.; Van Langeveld, A. D.; Moulijn, J. A.; Knozinger, H. Characterization of Sulfided Mo/Al₂O₃ Catalysts by Temperature-Programmed Reduction and Low-Temperature Fourier Transform Infrared Spectroscopy of Adsorbed Carbon Monoxide. *J. Phys. Chem.* **1993**, 97, 9028–9033. <https://doi.org/10.1021/j100137a031>.
- (31) Ouafi, D.; Mauge, F.; Bonelle, J. P. Nature and Structure of Tungsten Surface Species Present on NiO-WO₃/Al₂O₃ Hydrotreating Catalysts. *Catal. Today* **1988**, No. 4, 23–37.
- (32) Crépeau, G. Caractérisation de l'acidité de Catalyseurs d'hydrocraquage

- Amorphes Sulfures., University of Caen, 2002.
- (33) Travert, A.; Nakamura, H.; Van Santen, R. A.; Cristol, S.; Paul, J.-F. O.; Payen, E. Hydrogen Activation on Mo-Based Sulfide Catalysts, a Periodic DFT Study. **2002**. <https://doi.org/10.1021/ja011634o>.
- (34) Cristol, S.; Paul, J. F.; Payen, E.; Bougeard, D.; Clémendot, S.; Hutschka, F. Theoretical Study of the MoS₂ (100) Surface: A Chemical Potential Analysis of Sulfur and Hydrogen Coverage. 2. Effect of the Total Pressure on Surface Stability. **2002**. <https://doi.org/10.1021/jp0134603>.
- (35) Chen, J.; Labruyere, V.; Maugé, F.; Quoineaud, A. A.; Hugon, A.; Oliviero, L. IR Spectroscopic Evidence for MoS₂ Morphology Change with Sulfidation Temperature on MoS₂/Al₂O₃ Catalyst. *J. Phys. Chem. C* **2014**, *118* (51), 30039–30044. <https://doi.org/10.1021/jp510470g>.
- (36) Costa, D.; Arrouvel, C.; Breysse, M.; Toulhoat, H.; Raybaud, P. Edge Wetting Effects of γ -Al₂O₃ and Anatase-TiO₂ Supports by MoS₂ and CoMoS Active Phases: A DFT Study. *J. Catal.* **2007**, *246*, 325–343. <https://doi.org/10.1016/j.jcat.2006.12.007>.
- (37) Dujardin, C.; Lélias, M. A.; Van Gestel, J.; Travert, A.; Duchet, J. C.; Maugé, F. Towards the Characterization of Active Phase of (Co)Mo Sulfide Catalysts under Reaction Conditions-Parallel between IR Spectroscopy, HDS and HDN Tests. **2007**. <https://doi.org/10.1016/j.apcata.2007.01.010>.

Chapter IV:

High Resolution STEM-HAADF microscopy on γ - Al_2O_3 supported MoS_2 catalysts – Proof by image of the changes in dispersion and morphology of the slabs with addition of citric acid

Content Chapter IV: HR STEM-HAADF microscopy on γ -Al₂O₃ supported MoS₂ catalysts.

ABSTRACT	141
IV.1. INTRODUCTION	141
IV.2. EXPERIMENTAL PROCEDURES	148
IV.2.1. Catalyst preparation	148
IV.2.2. HRTEM and High-resolution Scanning Transmission Electron Microscopy - High Angular Annular Dark Field (HR STEM-HAADF).	149
IV.2.3. Two-Dimensional (2D) quantitative morphology analysis from HAADF-TEM images.	150
IV.2.3.1 Particle dispersion analysis	151
IV.2.3.2 S-edge/M-edge ratio calculation	152
IV.2.4. IR spectroscopy of CO adsorption (IR/CO)	153
IV.3. RESULTS AND DISCUSSION	154
IV.3.1. Length and stacking degree determined by HRTEM analysis	154
IV.3.2. Dispersion calculated from HR HAADF-STEM images.	155
IV.3.3. MoS ₂ slab morphology (shape) and S-edge/M-edge ratio.....	157
IV.3.4. Morphology based on IR/CO of MoS ₂ /Al ₂ O ₃ catalysts prepared with citric acid.....	160
IV.4. CONCLUSION	161
IV.5. REFERENCES	163

ABSTRACT

Atomic-scale images of MoS₂ slabs supported on γ -Al₂O₃ were obtained by High Resolution Scanning Transmission Electron Microscopy equipped with High Angular Annular Dark Field detector (HR STEM-HAADF). These observations, obtained for sulfide catalysts prepared without or with citric acid as chelating agent, evidenced variations in morphology (shape) and size of the MoS₂ nanoslabs, as detected indirectly by the adsorption of CO followed by Infrared spectroscopy. Quantitative dispersion values and a morphology index (S-edge/M-edge ratio) were determined from the slabs observed. In this way, HR STEM-HAADF underlines that the addition of citric acid to Mo catalysts decreases the size of the particles and modifies the shape of the MoS₂ nanoslabs from slightly truncated triangles to particles with a higher ratio of S-edge/M-edge. These findings are of great significance since tailoring the morphology of the slabs is a way to increase their catalytic activity and selectivity. Furthermore, this work demonstrated that the IR/CO method is a relevant approach to describe MoS₂ morphology of supported catalysts used in hydrotreatment processes for clean fuel production.

KEYWORDS: HR STEM-HAADF, IR spectroscopy, MoS₂, morphology, citric acid

IV.1 INTRODUCTION

In order to face with the severe environmental legislations as well as the decrease of light oil resources, heavy crude oils have to be refined into ultra-low sulfur content transportation fuel. Co (or Ni)-promoted Transition Metal Sulfides (TMS) supported catalysts have been the most important hydrodesulfurization (HDS) catalysts in petroleum refineries for many years. To meet the very

restrictive regulation demands, a challenge is to develop catalysts with improved activity and controlled selectivity. Hence, there is a strong concern in the implementation of characterization methods able to account for the local structures of the active sites of industrial catalysts as well as their role in the HDS reaction. Indeed, atomic-scale structural information of catalysts prepared under the same conditions as those used industrially can lead to a more rational design of catalysts for industrial applications. Conventional HDS catalysts consist of a bimetallic (CoMo, NiMo) sulfide phase supported on alumina. The sulfide phase is presented as nanoparticles with lamellar structure. High Resolution Transmission Electron Microscopy (HRTEM) observations account for dimensional parameters of these nanoslabs and report values of average stacking (~2 to 4) and average length (~3 to 6 nm) that depend on the sulfidation conditions [135,136]. Since several decades, the most accepted structure model of the catalytic active sites on sulfided CoMo/Al₂O₃ catalysts is the one proposed by Topsøe *et al.* [125,137]. The very well-known MoS₂ structure establishes that the TMS slab presents, in its crystallographic (0001) plane (2D perspective), two types of edges: the Mo-terminated edge (M-edge) and the sulfur-terminated edge (S-edge). It is important to mention that only those atoms found at the edges participate in the HDS reaction, thus, dispersion (D) is a common parameter of interest in catalysis by sulfides that gives the proportion of edge atoms from the total atom number. Moreover, it has been found that M-edge and S-edge have different intrinsic catalytic activity, being the S-edge more active than the M-edge [49]. Theoretical calculations [34] as well as Scanning Tunneling Microscopy (STM) of TMS [3] confirmed the presence of these two edges on model MoS₂ phase and reported that metal

promoters (Co or Ni) have different affinities towards M-edge and S-edge, being the S-edge more favored for the promotion. These results suggest that the morphology of MoS₂ slabs, in particular the type and quantity of the edges exposed, has significant influence in the selectivity and activity, and in the overall performance of the catalyst. On silica supported MoS₂ catalysts, Okamoto *et al.* showed by X-ray absorption spectroscopy techniques that the local edge structures of the MoS₂ slabs affect the Co-anchoring. This study also indicates that M-edge and S-edge sites have different intrinsic activities in HDS reactions, S-edge being more active and more favorable for the promotion and the formation of CoMoS phase [86]. Thus, these previous studies performed on model catalysts report that morphology of MoS₂ slabs, in particular the type and amount of the edges exposed, has a significant influence on both the CoMoS site concentration and their intrinsic activity. As a proven technique, the adsorption of CO at low temperature followed by infrared spectroscopy (IR/CO) has been used intensively to probe the edges of MoS₂ slabs in HDS catalysts for several decades. It has been observed by IR/CO that there are two different CO adsorption bands located at ~ 2110 and ~ 2070 cm⁻¹ on MoS₂ edges [8–10]. Chen *et al.* reported on an advance towards industrial catalysts by showing IR/CO can discriminate between M-edge and S-edge sites of alumina-supported MoS₂ phase. These results were based on a parallel study between Density Functional Theory (DFT) calculations and variations in position and intensity of IR bands of CO adsorbed on MoS₂/Al₂O₃ sulfided at various temperatures. The two $\nu(\text{CO})$ distinguished contributions, one at 2115 cm⁻¹ ascribed to CO in interaction with M-edge sites and one at 2065 cm⁻¹ ascribed to CO in interaction with S-edge sites. Since the molar extinction coefficients for

each contribution were determined, the IR/CO technique allowed to inform on the amount on Mo sites on M- and S-edges of sulfided Mo/Al₂O₃, and thus, accounted for the shape of the MoS₂ nanoslabs. This way, IR demonstrated to be a reliable technique to recognize the morphology of the particles as well as the quantification of active sites exposed by the slab giving access to the site dispersion and then to intrinsic activity. It has been also shown that MoS₂ morphology is strongly influenced by the sulfide phase - support interactions [11]. On MoS₂/Al₂O₃, the addition of an organic additive or a chelating agent during the impregnation stage can alter these interactions [8,12]. Thereby, chelating agent addition can change MoS₂ slab morphology of Mo catalyst deposited on industrially used support such as γ -Al₂O₃. However, direct information regarding the morphology of the MoS₂ prepared in presence of citric acid remains scarce. Since this information is obtained by IR/CO characterization i. e., by an indirect method, the question that arises now is: how to obtain a direct observation of these morphological changes? The morphology of TMS slabs deposited on an industrial support such as γ -alumina is usually characterized by HRTEM [38–41]. HRTEM observations provide an insight on general parameters such as the length, stacking of the slabs and defects such as bending or dislocations. When it comes to the morphological study, one of the obstacles is that TEM images undergo contrast perturbation due to the support, particularly when this one is such a strong insulator like alumina. To achieve the observation, the orientation of the MoS₂ slabs in relation to the direction of the incident electron beam is a determining factor. Only MoS₂ slabs that are oriented perpendicular to the [0001] axis are observable by means of HRTEM. This is explained because along these

directions, parallel to the slabs, the atomic density is quite high, therefore the resulting contrast in the image is easily visible. Whereas for the top view images of the MoS₂ slabs (along the [0001] crystallographic direction) the contrast is very low because the electron beam is crossing only one atomic layer (in the case of one slab). Moreover, although the HRTEM technique allows the observation of metallic particles of subnanometric dimensions, when these particles are immersed in an irregular matrix such as γ -Al₂O₃, their location is complex. Easily, particles of such minimal dimensions can be unnoticed and be confused as part of the support (γ -Al₂O₃). For this reason, it is necessary to process the images in order to modify the intensities for a possible interpretation and detection of the slabs.

Some advances in HRTEM technique have allowed to obtain images of MoS₂ nanoparticles along the [0001] direction of unsupported films and TMS with conductive supports with single-atom sensitivity. For instance, Kisielowski *et al.* reported imaging of greater than 10 nm length MoS₂ particles along the [0001] direction with resolved information about the shape and structure of the nanocatalysts [138]. In spite of the fact that catalysts were prepared in an industrial style, they were synthesized on a non-industrial support (graphitic powder). The selection of the support for preparing catalysts plays a major role, since each support has its own characteristics and presents different interactions with the active phase. These different interactions between the active sites and the support translate into changes in morphology, size and activity among others. Furthermore, carbon supports are conductive and this allows a better observation of the slabs by means of the HRTEM mode. Nevertheless, this is unattainable with the catalysts supported on alumina.

Some researchers have explored chemical attack treatments in an attempt to separate the TMS particles from the support. A method used to overcome the contrast disturbance from the alumina support is to dissolve the support by HF etching [139]. Nevertheless, for CoMoS catalysts, this leads to strong alterations. Indeed, it was found that the dissolution of the support by HF solution led to a partial destruction of the active phase with loss of cobalt and a rearrangement of the MoS₂ particles [140].

Experiments of scanning tunneling microscopy (STM) at atomic resolution, provided an overview of the effect of sulfo-reductive atmospheres, sulfidation agents, promoter atoms, and type of support in the equilibrium morphology of single-layer MoS₂ [3,47,141]. However, majority of these results are not quite scalable to the commercial catalysts because the preparation and characterization conditions are significantly different from the standard ones used in operation conditions. For instance, in the reported STM studies MoS₂ nanoparticles were supported on Au. Indeed, the sample preparation requires conditions of ultra-high vacuum (UHV) and an oriented substrate like Au (111) or carbon. However, this tailored particle growth on a conductive substrate presents strong differences compared with a commercial catalyst, where the active sites are dispersed in an insulator and multi-faceted surface support like amorphous silica-alumina (ASA) or γ -Al₂O₃.

Advances in electron microscopy have opened new routes to address the atomic-scale structure of catalytic materials [57,142]. Compared to classical image modes, bright-field (BF) and dark-field (DF), High Resolution Scanning Transmission Electron Microscopy in High-Angle Annular Dark Field mode (HR STEM-HAADF) or Z-contrast image mode offers a significant advantage.

Indeed, it facilitates the distinction of the elements according to their atomic number (Z), since the contrast is directly proportional to $Z^{1.7}$, even for objects of a single atomic plane [57]. HR STEM-HAADF mode is suitable for the study of small nanoparticles made of heavy elements, especially if they are deposited on a support composed of lightweight elements, such as industrial alumina. Recently, Alphazan *et al.* [19,68] reported on highly active W-based catalysts prepared through controlled surface chemistry whose enhanced activities are explained by the 2D hexagonal-like morphology of WS₂ particles. These differences in morphology induce a change in the distribution of M-edge and S-edge sites around the crystallites, affecting the catalytic activity of WS₂. W catalysts have been chosen because this metal provides better contrast with Al₂O₃ compared to Mo due to the difference in atomic number. Nevertheless, to obtain better crystallized and dispersed slabs, the sulfidation was performed at higher temperature ($T_s = 600^\circ\text{C}$) than the usual operating one, and the selected metal coverage was considerably lower than the commonly used. When the metal load decreases, the overlapping of many particles is limited, which improves the quality of the observation. In addition, a higher sulfidation temperature results in more crystalline structures with higher stability under the electron beam. Thus, these modifications can lead to morphological changes, i.e. S-edge/M-edge ratio of the sulfided slabs can be modified compared to that of catalysts prepared in a standard manner [6,143]. Therefore, a gap arises between catalytic activity and morphology studies.

Hence, the aim of the present work is to obtain a direct characterization of the slab morphology of Al₂O₃ supported MoS₂ catalysts prepared in exactly the same conditions of synthesis and sulfidation than the ones for the catalytic

application. With this objective, a parallel study by means of HR STEM-HAADF (*direct approach*) and IR/CO spectroscopy method (*indirect approach*) is carried out on Mo catalysts prepared without or with citric acid. Modification of the slab parameters (length, stacking, and shape) according to the preparation conditions is analyzed via HR STEM-HAADF observations and compared with HRTEM and IR/CO results. The coherence between the results from these different approaches validates the indirect characterization of the MoS₂ slab by IR/CO method. Thus, the study is a proof by image of the IR spectroscopic results that gives new insight into the characterization of active sites of TMS catalyst.

IV.2. Experimental procedures

IV.2.1. Catalyst preparation

Two Mo/Al₂O₃ catalysts, without and with citric acid (CA), were prepared by a one-step pore volume impregnation method (figure 1).

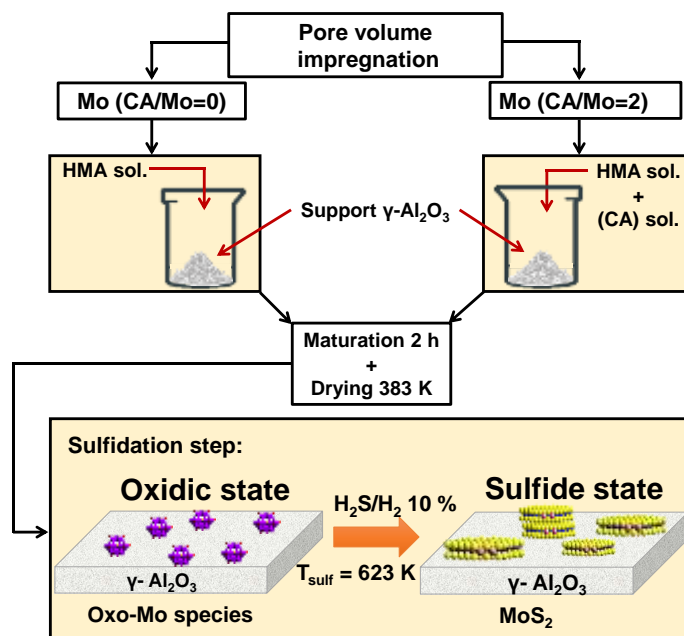


Figure 1. Scheme of preparation of sulfide conventional Mo catalysts for HDS.

The aqueous impregnation solutions were prepared by dissolving a fixed amount of ammonium heptamolybdate tetrahydrate ((NH₄)₆Mo₇O₂₄·4H₂O MERCK) in order to reach 3 Mo atoms.nm⁻² of Al₂O₃ support. CA was incorporated at this stage by dissolving the required amount of citric acid (C₆H₈O₇·H₂O PROLABO) to obtain a CA/Mo = 2. Afterwards, the solution was added to the pretreated γ - Al₂O₃ support (SASOL, specific surface area of 252 m².g⁻¹ and pore volume of 0.84 mL.g⁻¹, precalcined in air at 723 K for 2 h), strongly shaken and left for maturation during 2 h. Finally, the catalysts were dried at 383 K for 16 h. Note that these catalysts were not calcined in order to keep the chelating agent if present in its initial form. Hereinafter, the Mo/Al₂O₃ catalysts are denoted Mo(CA/Mo = x)/Al₂O₃. X refers to the molar ratio of CA to Mo. x = 0 or 2.0.

IV.2.2. HRTEM and High-resolution Scanning Transmission Electron Microscopy - High Angular Annular Dark Field (HR STEM-HAADF).

All TEM images presented hereinafter have been taken using a double corrected JEOL ARM 200F cold FEG microscope operated at 200 kV. First, slab length and stacking degree distributions of sulfide slabs were determined manually by measuring around 200 slabs per sample from HRTEM images. The image treatment was performed using the commercial software from GATAN (DIGITALMICROGRAPH). The nanostructure and morphology of the MoS₂ slabs were analyzed by high resolution scanning transmission electron microscopy (HR STEM) using a high angle annular dark field (HAADF) detector. The catalyst precursors were firstly sulfided at 623 K (heating rate of 3 K min⁻¹) and 0.1 MPa for 2 h under a 30 mL min⁻¹ flow of 10% H₂S/H₂. Then, to limit detrimental exposure to air, the sulfided catalysts were unloaded from the

sulfidation reactor under argon flow and poured into absolute ethanol. A few drops of the suspension of catalyst were put on a 300 mesh copper grid with holey carbon film. All the images presented in this manuscript were acquired in HAADF mode and the acquisition of an image lasted about 30 s with a resolution of 1024 pixels x 1024 pixels, (30 μ s of exposure time for each spot in the scanning mode). During this acquisition and despite exposure to the electron beam, the shapes of the particles remained unchanged, meaning that the slabs were quite stable under the electron beam. The possible effect of damage associated with the heating effects caused by the incident beam in the MoS₂ nanolayers is always a factor to consider. The advisable acceleration voltage is a low beam energy such as 80 kV. In our study, we did not observe significant changes during the acquisition of the images at 200 kV with a beam current value of about 12 μ A. Observations at 80 kV were also performed, but no significant difference in terms of slab stability was noticed. Therefore, it was concluded that the operation with an acceleration of 200 kV is compatible with our purpose of morphological analysis.

IV.2.3. Two-Dimensional (2D) quantitative morphology analysis from HAADF-TEM images.

In a previous work, Baubet *et al.* reported a reliable methodology for quantification of the morphology from HR HAADF-STEM images [62]. Two methods were compared. The first one consists of the determination of the S-edge/M-edge ratio through the measurement of the lengths of the regular shaped particle. For the second one, a 2D shape morphology index was determined by analysis of the slabs whatever its shape taking into account ten parameters. The results obtained for catalysts sulfided under different

conditions were comparable with both methods and were consistent with what was predicted by DFT calculations. In this work, following a similar approach, a sample of a dozen observable isolated particles for both Mo(CA/Mo=0)/Al₂O₃ and Mo(CA/Mo=2)/Al₂O₃ samples was taken through contrast optimization in our images, to obtain statistical information about the morphology of the MoS₂ slabs. In these regular slabs, a contour was drawn by a simple shape model with straight edges and the corresponding edge lengths were measured, as well as the area of the particle with the help of the Mesurim Pro software. The limited number of particles is explained by the difficulty to observe isolated specimens with faceted edges in these realistic samples.

For assigning M-edge and S-edge, we rely on DFT calculations that predicted that M-edge is energetically more stable than S-edge in a wide range of sulfur chemical potential and, therefore, that the morphology of MoS₂ is truncated triangle terminated by mainly M-edge under typical sulfidation and HDS conditions [54].

IV.2.3.1. Particle dispersion analysis

Considering that for each slab, the dispersion is the ratio of edge atoms per total atoms, the calculated dispersion (D) values were obtained through the measurement of slab area and perimeter with the following equation:

$$D = \frac{\text{atoms at the edge}}{\text{total number of atoms per slab}} = \frac{P/d - N_c}{A/d^2} \quad (1)$$

Where:

D = dispersion

P = particle perimeter (nm)

d = atomic diameter Mo (nm)

N_c = number of corner atoms in the corner

A = particle area (nm²)

IV.2.3.2. S-edge/M-edge ratio calculation

According to DFT calculations and STM observations, the morphologies of MoS₂ 2D are influenced by parameters as temperature, sulfo-reducing conditions and by the presence of a promoter [51]. In previous works, it has been determined that for typical sulfidation and reaction conditions ($T = \sim 623$ K and low H₂S/ H₂ partial pressure ratio), the shape of the MoS₂ particles must exhibit mainly Mo edges [54]. Atom resolved STM experiments of MoS₂ supported on Au (111) also sustain these considerations to measure the distribution of both edges [4,144]. Given that the morphology of these slabs is well in accordance with the prediction of DFT, we consider them to be nanoparticles in "equilibrium". Therefore, we rely on the aforementioned considerations to assign the chemical nature of the edge. Indeed, for the sulfidation process that we used, the particles must exhibit a majority of M-edge. Hence, for all the slabs observed, the largest edge is assigned to the M-edge and then we consider alternation of S- and M-edges. For each particle, all edges were measured carefully. Considering the largest edge length being an M-edge (L_M) and taking into account the intercalation between M-edge and S-edge, the S-edge/M-edge ratio is calculated by the following equation (2):

$$S - edge / M - edge \text{ Ratio} = \frac{L_{S_1} + \dots + L_{S_N}}{L_{M_1} + \dots + L_{M_N}} \quad (2)$$

With L_{S_i} and L_{M_i} , the lengths of each S-edge and M-edge respectively.

IV.2.4. IR spectroscopy of CO adsorption (IR/CO)

The MoS₂ edge sites of these catalysts were in-situ characterized by low-temperature CO adsorption followed by IR spectroscopy. The oxidic catalyst was grounded and pressed into a self-supported wafer (10 mg for a disc of 2.01 cm²) and positioned into a quartz IR cell with CaF₂ windows. Prior to the adsorption experiments, the sample was sulfided in situ in the IR cell. For this purpose, the catalysts were sulfided in a gas mixture containing 10% H₂S/H₂ (30 ml.min⁻¹) at 623 K for two hours with a heating rate of 3 K.min⁻¹. After sulfidation, the cell was flushed with Ar and evacuated down to $P < 1 \cdot 10^{-4}$ Pa until the catalyst reached room temperature. Then, CO adsorption was performed at low temperature (~100 K) to avoid any reaction with the catalysts surface. Small calibrated doses of CO were introduced into the IR cell until equilibrium pressure of 133 Pa. After each CO introduction, FTIR spectra were recorded with 256 scans and a resolution of 4 cm⁻¹ using Nicolet Nexus FT-IR spectrometer equipped with a MCT Detector. The quantification of each edge sites present in the series of catalysts was obtained after the spectral decomposition performed in Peakfit V4.12 using "Autofit peak III-deconvolution". In the spectral decomposition, the values of the center and the full width at half maximum (FWHM) correspond to those previously reported on [6]. The used CO molar extinction coefficients are 20 ± 3 (M-edge) and 35 ± 9 (S-edge) cm \cdot μ mol⁻¹ as determined in SI of [6].

IV.3. Results and discussion

IV.3.1 Length and stacking degree determined by HRTEM analysis

In **figure 2**, representative images (A-B) and distributions of length and stacking (C-D) of the sulfide slabs obtained for $\text{Mo}(\text{CA}/\text{Mo}=0)/\text{Al}_2\text{O}_3$ and $\text{Mo}(\text{CA}/\text{Mo}=2)/\text{Al}_2\text{O}_3$ catalysts are presented. A careful process of measuring the length of the slabs present in each sample was carried out. The addition of citric acid leads to a decrease of the average slab length from 2.90 ± 0.12 nm to 1.70 ± 0.10 nm. Also an increase of the average stacking number (1.80 ± 0.04 to 2.20 ± 0.05) is noticed.

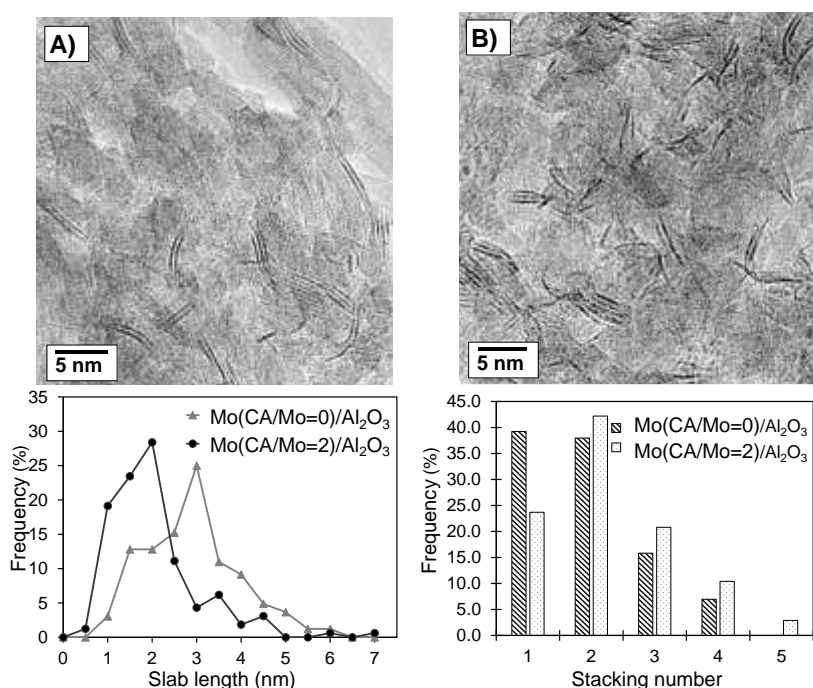


Figure 2. TEM analysis: images of $\text{Mo}(\text{CA}/\text{Mo}=0)/\text{Al}_2\text{O}_3$ (A) and $\text{Mo}(\text{CA}/\text{Mo}=2)/\text{Al}_2\text{O}_3$ (B), slab length distribution (C) and stacking number distribution (D).

While the presence of particles stacked in two or more slabs is significant in both samples, the amount of the rather small monolayer slabs observed in the $\text{Mo}(\text{CA}/\text{Mo}=2)/\text{Al}_2\text{O}_3$ sample was much higher than in the $\text{Mo}(\text{CA}/\text{Mo}=0)/\text{Al}_2\text{O}_3$ sample. Such results are in accordance with previously reported results and

ascribed to the reduced interaction between the MoS₂ slabs and the support due to the addition of citric acid [49].

IV.3.2. Dispersion calculated from HR HAADF-STEM images.

In **figure 3** (A and C) the HR STEM-HAADF micrographs representative of Mo(CA/Mo=0)/Al₂O₃ and Mo(CA/Mo=2)/Al₂O₃ are shown respectively. Observed particles are characterized by a good contrast and thus the acquisition mode is adequate to reveal the 2D morphology of slabs in industrial-grade alumina support. Indeed, planar MoS₂ slabs are displayed with atomic resolution of the Mo atoms (bright dots) present in the slabs.

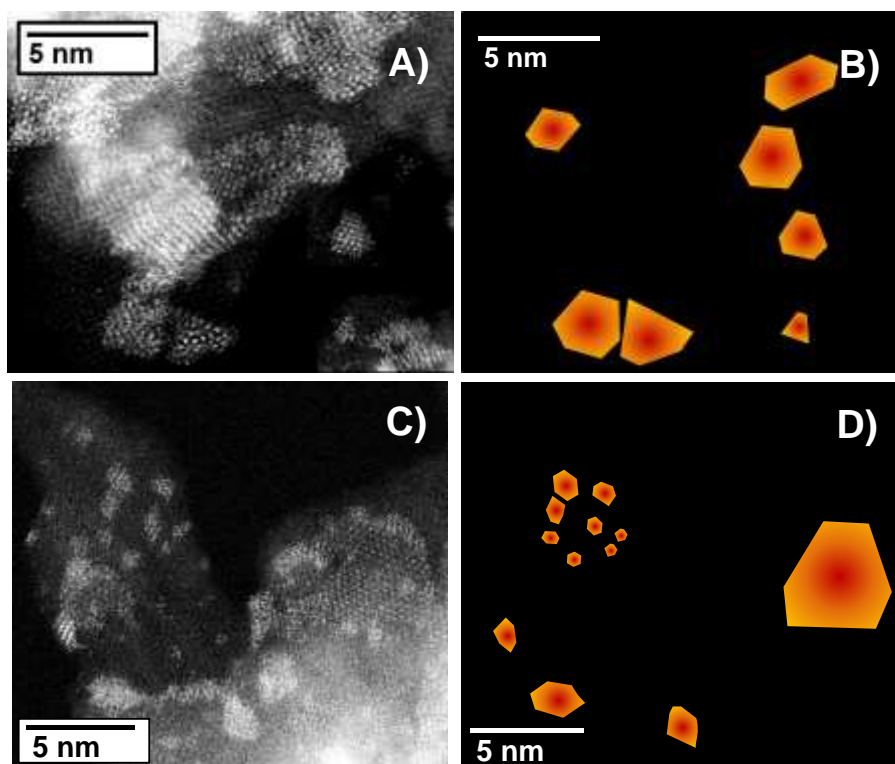


Figure 3. Processing of HR STEM-HAADF micrographs of MoS₂ particles of Mo(CA/Mo=0)/Al₂O₃ (A and B) and Mo(CA/Mo=2)/Al₂O₃ (C and D). In figures B and D, the contour of selected contrasted particles is shown.

These HR HAADF-STEM observations reveal differences in slab growth between the two samples analyzed. Indeed, the general topology of

Mo(CA/Mo=0)/Al₂O₃ is characterized by MoS₂ slabs grown in the form of plates and by a contrast variation among the slabs (figure 3 (A)).

It is also noticeable that some of the slabs in Mo(CA/Mo = 2)/Al₂O₃ are much smaller than the ones observed in Mo(CA/Mo = 0)/Al₂O₃ sample. In both samples, brighter areas can be attributed to an increase in the density of Mo that is related to the agglomeration of stacked slabs present. However, according to **figure 3 (C)**, the particles whose length is less than 1 nm, are appreciated with an intensity of homogeneous brightness, which suggests that they are particles of thickness of a single atomic layer (not stacked). In **figure 3 (B and D)**, the contour of the more isolated slabs in both samples is presented. By optimization and variation of contrast by region, a dozen slabs per sample were drawn in order to carry out a statistical analysis of their length and dispersion (eq. (1)). Note that the longest length observed in the 2D particles images was taken into account for determining the length of the MoS₂ slabs. Results are gathered in Table I and **figure 4 and 6**. In accordance with the results obtained from HRTEM, HR STEM HAADF study reveals that the addition of citric acid promotes the reduction of MoS₂ particle size. However, for both samples the value obtained by the HR STEM HAADF study is lower than the one obtained by the HRTEM study, underlying that the smallest particles can be hard to distinguish in HRTEM. Moreover, the latter approach is less accurate since the slab length measurements are done from the projection of the slabs which is not necessarily the longest distance of the slabs. Additionally, the distribution in length obtained by both studies is also different: more homogeneous lengths are observed in HR STEM HAADF than in HRTEM. Finally, the fact that the 2D morphology of the slabs is revealed by the HR

STEM HAADF study allows calculating realistic dispersion values for each particle. The average value of dispersion is then significantly increased with the addition of citric acid: from 0.42 ± 0.06 for the $\text{Mo}(\text{CA}/\text{Mo}=0)/\text{Al}_2\text{O}_3$ sample to 0.60 ± 0.05 for the $\text{Mo}(\text{CA}/\text{Mo}=2)/\text{Al}_2\text{O}_3$ sample.

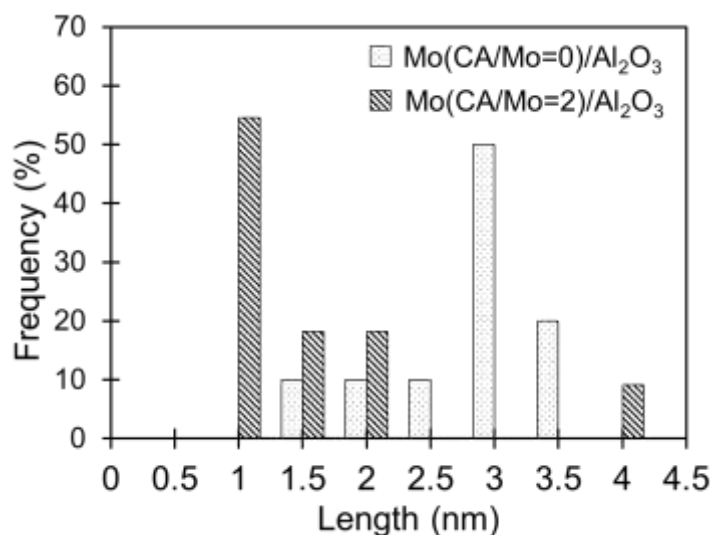


Figure 4. Histogram of the measured length of the particles observed in HR HAADF-STEM.

IV.3.3. MoS_2 slab morphology (shape) and S-edge/M-edge ratio

As shown in images at greater magnification in **figures 5(A-C)**, the MoS_2 particles in $\text{Mo}(\text{CA}/\text{Mo}=0)/\text{Al}_2\text{O}_3$ have a geometry, whose shape resembles a triangle with slightly truncated edges. Accurate observation of picture of **figure 5(B)** shows a particle with this shape superimposed on a larger one, leading to a different projected pattern. Inset of **figure 5(B)** shows a Fast Fourier Transform (FFT) of a single region of the slab in the image, and the as expected six-fold symmetry of the Mo atoms arrangement is clearly evidenced. Furthermore, when analyzing filtered images (inset in **figure 5(C)** as an example), it was determined that the interatomic distance between the atoms of Mo is ~ 0.31 nm corresponding to that of the Mo atoms in a MoS_2 crystal (0.317

nm). In general, the particles observed for $\text{Mo}(\text{CA}/\text{Mo}=2)/\text{Al}_2\text{O}_3$ displayed different morphologies than the ones for $\text{Mo}(\text{CA}/\text{Mo}=0)/\text{Al}_2\text{O}_3$. It is noticeable that after CA addition each slab presents more uniform edge lengths, as seen in **figure 5(A'-C')**. In order to rationalize these morphology observations, calculation of the S-edge/M- edge ratio for a dozen observed particles has been performed.

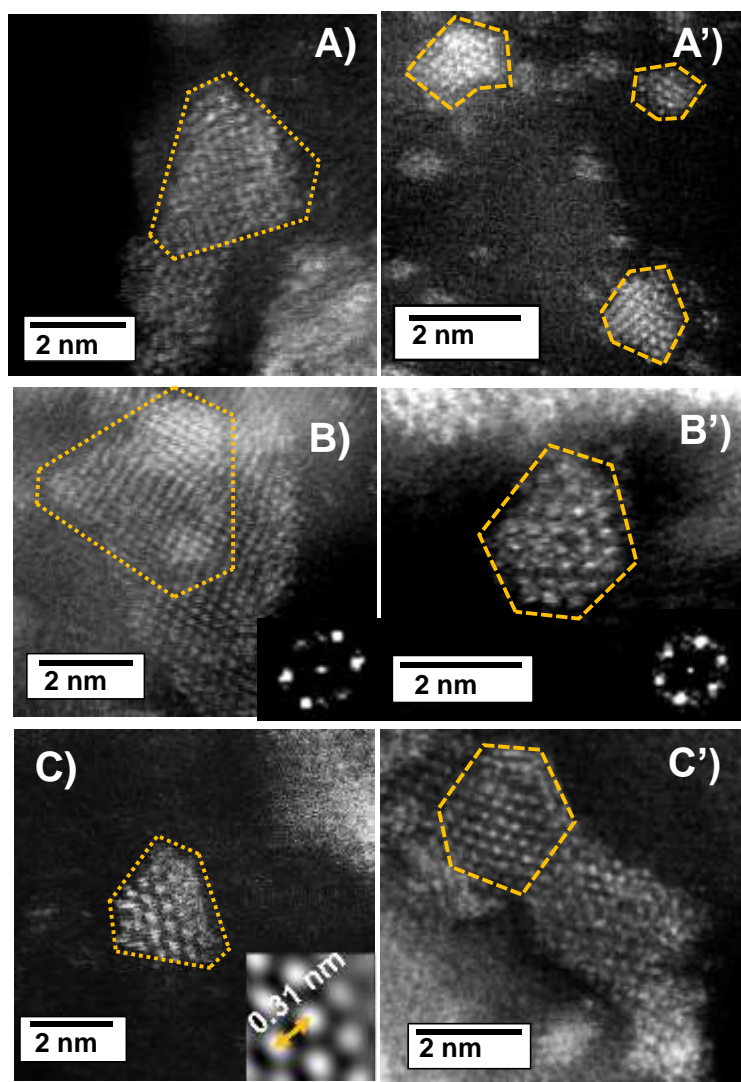


Figure 5. HR STEM-HAADF micrographs of MoS_2 particles of $\text{Mo}(\text{CA}/\text{Mo}=0)/\text{Al}_2\text{O}_3$ and $\text{Mo}(\text{CA}/\text{Mo}=2)/\text{Al}_2\text{O}_3$ of different zones. Inset *B* and *B'* FFT of a single slab and inset *C* zoom on the filtered image.

Since HR HAADF-STEM analysis does not allow one to identify the type of edge exposed by the nanoparticles, as done in ref. [62], the longest length was ascribed to M-edge since this is the most stable edge at the sulfidation conditions we used [6]. The S-edge/M-edge ratio from HR HAADF-STEM were then calculated following eq. (2): the distribution in S-edge/M-edge ratio is reported in figure 6 and the average value is 0.39 ± 0.07 for Mo(CA/Mo=0)/Al₂O₃ and 0.78 ± 0.05 for Mo(CA/Mo=2)/Al₂O₃ (Table I).

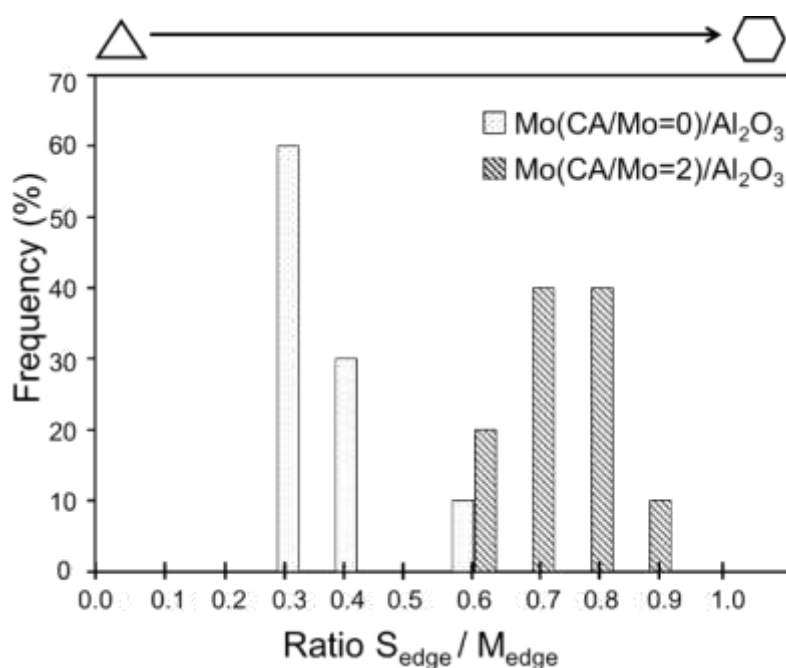


Figure 6. Histogram of the S-edge/M-edge ratio based on the measured edge lengths for Mo(CA/Mo=0)/Al₂O₃ and Mo(CA/Mo=2)/Al₂O₃.

The significant increase in average S-edge/M-edge ratio value and the clear difference in distribution pattern agree with the more isotropic character of the slabs for the catalyst prepared with citric acid as previously observed.

Table I. Parameters calculated from the HR STEM-HAADF images for both catalyst.

Parameters	Catalyst	
	Mo(CA/Mo=0)	Mo(CA/Mo=2)
Average length (nm)	2.60 ± 0.40	1.40 ± 0.60
Ratio S _{-edge} /M _{-edge}	0.39 ± 0.07	0.78 ± 0.05
Dispersion	0.42 ± 0.06	0.60 ± 0.05

IV.3.4. Morphology based on IR/CO of MoS₂/Al₂O₃ catalysts prepared with citric acid

IR/CO spectroscopy has revealed that several parameters during the preparation and sulfidation stage can modify the morphology of MoS₂ slabs of supported catalysts [6,49,94,128]. For example, and for the present study, the addition of citric acid promotes the growth of S-edge (IR/CO band at 2065 cm⁻¹), while it inhibits that of M-edge (IR/CO band at 2115 cm⁻¹) (figure 7). From these variations, it is expected that the morphology of MoS₂ slabs is progressively modified from a slightly truncated triangle with predominant M-edge to a more hexagonal shape with closer amount of M-edge and S-edge, as the quantity of citric acid present in the preparation stage is increased. Our HR STEM-HAADF images and deduced results reveal indeed a change in morphology from one sample to another with the addition of citric acid. However, HR STEM-HAADF images also show that not only model forms (triangle and hexagon) are present. Indeed, the obtained images mainly evidenced particles changing from slightly truncated to more-faceted shapes, but the same trend is observed, i.e. the S-edge/M-edge ratio increases with citric acid addition. Another important point is that the increase in dispersion (i.e. decrease in slab length) deduced from the HR STEM-HAADF study is also in accordance with the global increase in edge sites concentration obtained by the IR/CO method.

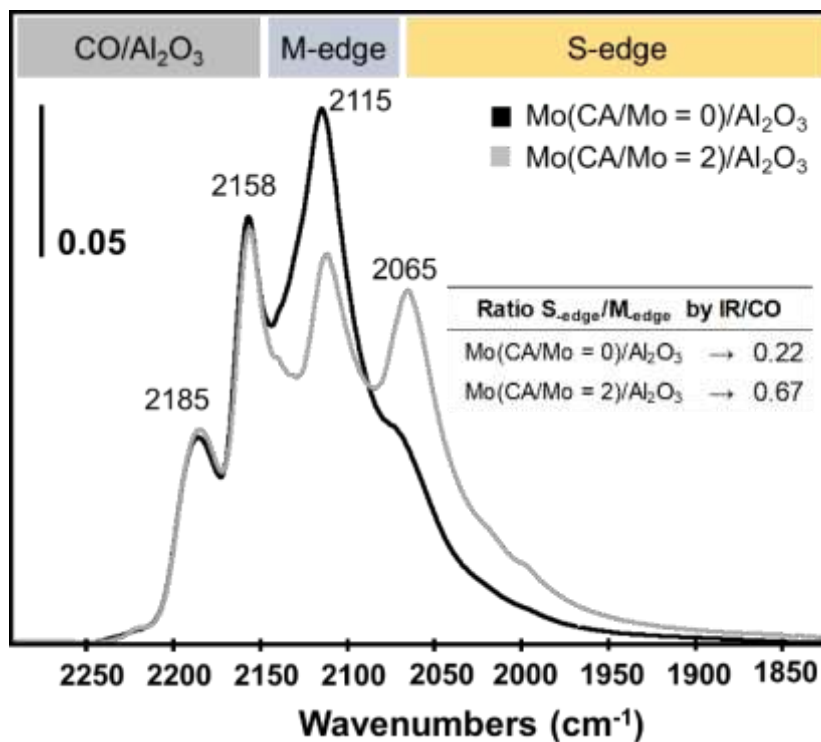


Figure 7. IR spectra of CO adsorption on sulfided Mo(CA/Mo=0 or 2)/Al₂O₃ catalysts.

IV.4. CONCLUSION

One guideline of this work was to characterize catalysts prepared in conditions close to the ones used for applications and not specifically chosen to meet the requirements of these advanced techniques of characterization. This has made very delicate the observation of the shape of sulfide slabs by electron microscopy. However, atomic-scale images of γ -Al₂O₃ supported Mo nanoparticles were obtained by HR STEM-HAADF for sulfide catalysts prepared without and with citric acid. HR STEM-HAADF observations and subsequent exploitation highlighted that the addition of citric acid during the preparation step of Mo catalysts changes the shape of the MoS₂ nanoslabs. Indeed, the S-edge/M-edge ratio obtained by HR STEM-HAADF study is significantly increased by addition of citric acid as it was previously obtained by the IR/CO

method. Moreover, the study shows that HR STEM-HAADF allows more easily to distinguish the smallest slabs (< 2 nm) from the oxide support. So, this HR STEM-HAADF study is a proof by image of the results obtained by the IR/CO method. The direct observations validate the variation of morphology of MoS₂ nanoslabs detected indirectly by the IR/CO method thus consolidating also the $\nu(\text{CO}/\text{Mo})$ band attribution to CO interacting on the two different edges. Such morphology change is of great importance to the catalytic performance, as it has been reported that M-edge and S-edge present different reactivity in hydrodesulfurization (HDS) reactions. As a consequence, this study strengthens the importance of coupling techniques like microscopy that allows a direct observation of the shape of a group of sulfided slabs and IR spectroscopy that allows an indirect detection of the shape but of a large number of sulfided slabs. The coupling of characterization techniques, allows a detailed understanding of the influence of the chelating agent on the final structure of the catalyst. This enables tailoring the morphology of the active phase particles, which is a way to modulate the catalytic activity and selectivity. The present study paves the way for further investigations on promoted catalysts comparable to the ones used in the HDS industry.

IV.5. REFERENCES

- [1] Marien Bremmer G, Van Haandel L, Hensen E J M, Frenken J W M and Kooyman P J 2019 The effect of oxidation and resulfidation on (Ni/Co)MoS₂ hydrodesulfurisation catalysts *Appl. Catal. B Environ.* **243** 145–50
- [2] Toledo-Antonio J A, Cortes-Jacome M A, Escobar-Aguilar J, Angeles-Chavez C, Navarrete-Bolá J and López-Salinas E 2017 Upgrading HDS activity of MoS₂ catalysts by chelating thioglycolic acid to MoO_x supported on alumina *Appl. Catal. B Environ.* **213** 106–17
- [3] Topsøe H and Clausen B S 1984 Importance of Co-Mo-S Type Structures in Hydrodesulfurization *Catal. Rev. Sci. Eng.* **26** 395–420
- [4] Brorson M, Carlsson A and Topsøe H 2007 The morphology of MoS₂, WS₂, Co-Mo-S, Ni-Mo-S and Ni-W-S nanoclusters in hydrodesulfurization catalysts revealed by HAADF-STEM *Catal. Today* **123** 31–6
- [5] Chen J, Maugé F, Fallah J El and Oliviero L 2014 IR spectroscopy evidence of MoS₂ morphology change by citric acid addition on MoS₂/Al₂O₃ catalysts – A step forward to differentiate the reactivity of M-edge and S-edge *J. Catal.* **320** 170–9
- [6] Byskov L S, Nørskov J K, Clausen B S and Topsøe H 2000 Edge termination of MoS₂ and CoMoS catalyst particles *Catal. Letters* **64** 95–9
- [7] Lauritsen J V., Helveg S, Lægsgaard E, Stensgaard I, Clausen B S, Topsøe H and Besenbacher F 2001 Atomic-scale structure of Co-Mo-S nanoclusters in hydrotreating catalysts *J. Catal.* **197** 1–5
- [8] Okamoto Y, Hioka K, Arakawa K, Fujikawa T, Ebihara T and Kubota T 2009 Effect of sulfidation atmosphere on the hydrodesulfurization activity of SiO₂-supported Co-Mo sulfide catalysts: Local structure and intrinsic activity of the active sites *J. Catal.* **268** 49–59
- [9] Vradman L, Landau M V, Herskowitz M, Ezersky V, Talianker M, Nikitenko S, Koltypin Y and Gedanken A 2003 High loading of short WS₂ slabs inside SBA-15: promotion with nickel and performance in hydrodesulfurization and hydrogenation *J. Catal.* **213** 163–75
- [10] Huang Z D, Bensch W, Kienle L, Fuentes S, Alonso G and Ornelas C 2009 SBA-15 as support for Ni-MoS₂ HDS catalysts derived from sulfur-containing molybdenum and nickel complexes in the reaction of HDS of DBT: An all sulfide route *Catal. Letters* **127** 132–42
- [11] Nava R, Ortega R A, Alonso G, Ornelas C, Pawelec B and Fierro J L G 2007 CoMo/Ti-SBA-15 catalysts for dibenzothiophene desulfurization *Catal. Today*

127 70–84

- [12] Dimitrov L, Palcheva R, Spojakina A and Jiratova K 2011 Synthesis and characterization of W-SBA-15 and W-HMS as supports for HDS *J. porous Mater.* **18** 425–34
- [13] Kisielowski C, Ramasse Q M, Hansen L P, Brorson M, Carlsson A, Molenbroek A M, Topsøe H and Helveg S 2010 Imaging MoS₂ nanocatalysts with single-atom sensitivity *Angew. Chemie - Int. Ed.* **49** 2708–10
- [14] Li Y, Li A, Li F, Liu D, Chai Y and Liu C 2014 Application of HF etching in a HRTEM study of supported MoS₂ catalysts *J. Catal.* **317** 240–52
- [15] Berhault G, De La Rosa M P, Mehta A, Ya M J and Chianelli R R 2008 The single-layered morphology of supported MoS₂-based catalysts-The role of the cobalt promoter and its effects in the hydrodesulfurization of dibenzothiophene *Appl. Catal. A Gen.* **345** 80–8
- [16] Walton A S, Lauritsen J V, Topsøe H and Besenbacher F 2013 MoS₂ nanoparticle morphologies in hydrodesulfurization catalysis studied by scanning tunneling microscopy *J. Catal.* **308** 306–18
- [17] Besenbacher F, Brorson M, Clausen B S, Helveg S, Hinnemann B, Kibsgaard J, Lauritsen J V., Moses P G, Nørskov J K and Topsøe H 2008 Recent STM, DFT and HAADF-STEM studies of sulfide-based hydrotreating catalysts: Insight into mechanistic, structural and particle size effects *Catal. Today* **130** 86–96
- [18] Nellist, P. D., & Pennycook S J 1996 Direct Imaging of the Atomic Configuration of Ultradispersed Catalysts *Science (80-.)*. **274** 413–5
- [19] Hillyard S and Silcox J 1995 Detector geometry, thermal diffuse scattering and strain effects in ADF STEM imaging *Ultramicroscopy* **58** 6–17
- [20] Alphazan T, Bonduelle-Skrzypczak A, Legens C, Gay A S, Boudene Z, Girleanu M, Ersen O, Copéret C and Raybaud P 2014 Highly active nonpromoted hydrotreating catalysts through the controlled growth of a supported hexagonal WS₂ phase *ACS Catal.* **4** 4320–31
- [21] Alphazan T, Bonduelle-Skrzypczak A, Legens C, Boudene Z, Taleb A L, Gay A S, Ersen O, Copéret C and Raybaud P 2016 Improved promoter effect in NiWS catalysts through a molecular approach and an optimized Ni edge decoration *J. Catal.* **340** 60–5
- [22] Chen J, Oliviero L, Portier X and Maugé F 2015 On the morphology of MoS₂ slabs on MoS₂/Al₂O₃ catalysts: the influence of Mo loading *RSC* **5** 81038–44
- [23] Chen J, Labruyere V, Maugé F, Quoineaud A A, Hugon A and Oliviero L 2014 IR Spectroscopic Evidence for MoS₂ Morphology Change with Sulfidation Temperature on MoS₂/Al₂O₃ Catalyst *J. Phys. Chem. C* **118** 30039–44

- [24] Baubet B, Girleanu M, Gay A S, Taleb A L, Moreaud M, Wahl F, Delattre V, Devers E, Hugon A, Ersen O, Afanasiev P and Raybaud P 2016 Quantitative Two-Dimensional (2D) Morphology-Selectivity Relationship of CoMoS Nanolayers: A Combined High-Resolution High-Angle Annular Dark Field Scanning Transmission Electron Microscopy (HR HAADF-STEM) and Density Functional Theory (DFT) Study *ACS Catal.* **6** 1081–92
- [25] Schweiger H, Raybaud P, Kresse G, and Toulhoat H 2002 Shape and Edge Sites Modifications of MoS₂ Catalytic Nanoparticles Induced by Working Conditions: A Theoretical Study *J. Catal.* **207** 76–87
- [26] Krebs E, Silvi B and Raybaud P 2008 Mixed sites and promoter segregation: A DFT study of the manifestation of Le Chatelier's principle for the Co(Ni)MoS active phase in reaction conditions *Catal. Today* **130** 160–9
- [27] Lauritsen J V, Kibsgaard J, Olesen G H, Moses P G, Hinnemann B, Helveg S, Nørskov J K, Clausen B S, Topsøe H, Laegsgaard E and Besenbacher F 2007 Location and coordination of promoter atoms in Co-and Ni-promoted MoS₂-based hydrotreating catalysts *J. Catal.* **249** 220–33
- [28] Kibsgaard J, Tuxen A, Knudsen K G, Brorson M, Topsøe H, Laegsgaard E, Lauritsen J V and Besenbacher F Comparative atomic-scale analysis of promotional effects by late 3d-transition metals in MoS₂ hydrotreating catalysts *J. Catal.* **272** 195–203
- [29] Chen J, Dominguez Garcia E, Oliviero E, Oliviero L and Maugé F 2016 Effect of high pressure sulfidation on the morphology and reactivity of MoS₂ slabs on MoS₂/Al₂O₃ catalyst prepared with citric acid *J. Catal.* **339** 153–62
- [30] Chen J, Oliviero L, Portier X and Maugé F 2015 On the morphology of MoS₂ slabs on MoS₂/Al₂O₃ catalysts: the influence of Mo loading *RSC Adv.* **5** 81038–44

High-resolution STEM-HAADF microscopy on a γ -Al₂O₃ supported MoS₂ catalyst—proof of the changes in dispersion and morphology of the slabs with the addition of citric acid

Luz Zavala-Sanchez¹ , Xavier Portier², Françoise Mauge¹ and Laetitia Oliviero¹ 

¹Normandie Université, ENSICAEN, UNICAEN, CNRS, LCS, 14000 Caen, France

²Centre de recherche sur les Ions, les Matériaux et la Photonique, CEA, UMR CNRS 6252, Normandie Université, ENSICAEN, UNICAEN, CNRS, 6, bd du Maréchal Juin, 14050 Caen, France

E-mail: laetitia.oliviero@ensicaen.fr

Received 16 May 2019, revised 20 August 2019

Accepted for publication 26 September 2019

Published 21 October 2019



CrossMark

Abstract

Atomic-scale images of MoS₂ slabs supported on γ -Al₂O₃ were obtained by high-resolution scanning transmission electron microscopy equipped with a high angular annular dark field detector (HR STEM-HAADF). These observations, obtained for sulfide catalysts prepared with or without citric acid as a chelating agent, evidenced variations in morphology (shape) and size of the MoS₂ nanoslabs, as detected indirectly by the adsorption of CO followed by infrared spectroscopy. Quantitative dispersion values and a morphology index (S-edge/M-edge ratio) were determined from the slabs observed. In this way, HR STEM-HAADF underlines that the addition of citric acid to Mo catalysts decreases the size of the particles and modifies the shape of the MoS₂ nanoslabs from slightly truncated triangles to particles with a higher ratio of S-edge/M-edge. These findings are of great significance since tailoring the morphology of the slabs is a way to increase their catalytic activity and selectivity. Furthermore, this work demonstrated that the IR/CO method is a relevant approach to describe the MoS₂ morphology of supported catalysts used in hydrotreatment processes for clean fuel production.

Keywords: HR STEM-HAADF, IR spectroscopy, MoS₂, morphology, citric acid

(Some figures may appear in colour only in the online journal)

CHAPTER V:

**Promoter location on NiW/Al₂O₃ catalysts
by parallel between IR/CO spectroscopy
and High Resolution STEM-HAADF
microscopy.**

Content Chapter V: Promoter location on NiW/Al₂O₃ catalysts by parallel between IR/CO spectroscopy and High Resolution STEM-HAADF microscopy

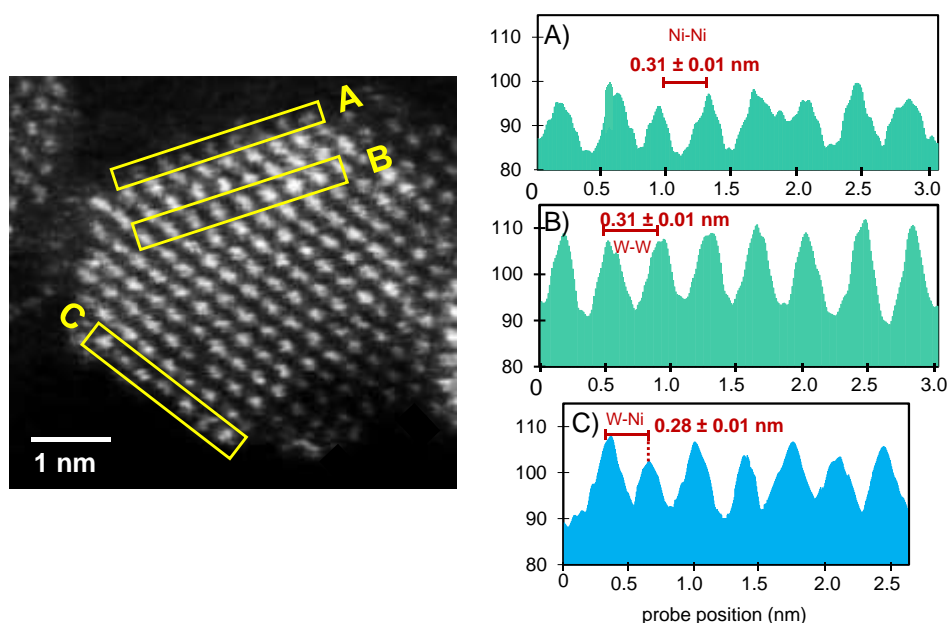
ABSTRACT:	171
Graphical Abstract.....	172
V.1. INTRODUCTION	172
V.2. EXPERIMENTAL SECTION	176
V.2.1. Catalysts preparation.....	176
V.2.2. Composition and textural properties	177
V.2.2.1. Chemical analysis by Inductively Coupled Plasma	177
V.2.2.2. Nitrogen physisorption analysis	177
V.2.3. Thiophene hydrodesulfurization test.	178
V.2.4. Low temperature CO adsorption followed by IR spectroscopy	179
V.2.5. Microscopy study by HRTEM and HR STEM-HAADF	180
V.3. RESULTS AND DISCUSSIONS	181
V.3.1. Elemental analysis.....	181
V.3.2. Textural properties.....	182
V.3.3. Thiophene HDS activity	183
V.3.3.1. Effect of sulfidation temperature	183
V.3.3.2. Effect of the citric acid amount.....	185
V.3.4. IR spectroscopy of sulfided NiW/Al ₂ O ₃ catalysts	186
V.3.5. Electron microscopy by HRTEM and STEM HAADF	195
V.4. CONCLUSIONS	201
V.5. REFERENCES	203

ABSTRACT:

In this work, the effect of citric acid (CA) on the structure and activity of Ni promoted WS₂ particles supported on γ -Al₂O₃ were investigated by HRTEM (High Resolution Transmission Electron Microscopy), HR STEM-HAADF (High Resolution Scanning Transmission Electron Microscopy equipped with High Angular Annular Dark Field detector), CO adsorption followed by IR (infrared) spectroscopy and thiophene HDS (hydrodesulfurization) test.

It is shown that citric acid addition increases the thiophene HDS activity. This can be directly related to the augmentation of NiWS sites as detected by IR. HRTEM underlines that the addition of CA to NiW catalysts decreases the average size of the particles. This is confirmed by HR STEM-HAADF that even evidence the presence of nanoclusters on NiW catalysts prepared with citric acid. Contrast and interatomic distances were analyzed on the atomic-scale images obtained by HR STEM-HAADF. These measurements allow identifying the nature of the core and edge atoms of the sulfided particles. The metal atoms of particle core are only W ones whereas the edges of the particles could be either fully promoted with detection of only Ni, or partially promoted with detection of both Ni and W. Hence, local and global analysis of the NiW samples are in good agreement to account for more NiWS sites by CA addition.

Graphical Abstract



KEYWORDS:

HR STEM-HAADF, NiWS, Citric acid, CO adsorption, IR spectroscopy, contrast variations, HDS, promoter location, sulfide nanoparticle morphology.

V.1. INTRODUCTION

Nowadays, it is fundamental to direct the efforts in the field of hydrodesulfurization (HDS) science towards highly active and sustainable catalysts. The demand for petroleum products that are more ecological and have lower sulfur content is growing due to the environmental and health problems caused by SO_x emissions. The industrial HDS process uses Co (or Ni)-promoted Transition Metal Sulfides (TMS) supported catalysts. The bimetallic sulfide phase, commonly called CoMoS, NiMoS or NiWS phase, corresponds to a nanolayer of Mo(W)S₂ decorated by the promoter at its edges [1]. For years, the outstanding catalytic properties of NiW-based catalysts have

attracted great attention due to its good performance in hydrogenation (HYD) and hydrodenitrogenation (HDN) reactions, especially in severe working conditions [2,3]. The strong hydrogenation function of WS₂ is also beneficial in hydrocracking (HCK) [4]. In addition, NiW/Al₂O₃ sulfide catalysts have a high potential for the conversion of heavy fractions [5]. With the incoming emphasis on the production of ultra-low sulfur transport fuels in particular from heavy feedstocks, there is renovated interest in going deep insight into the structure of such NiW/Al₂O₃ sulfide catalysts [6]. The MoS₂ based catalysts including those promoted by Co and Ni, have been extensively investigated at atomic level through surface science study of model catalysts as well as through theoretical and experimental studies of industrial-like catalysts. By contrast, the WS₂ phase and its promoted counterparts are poorly understood at the atomic level [4]. Even though NiWS catalysts provide an improvement in the catalytic activity in aromatic hydrogenation, its use is not as widely extended as CoMoS system. Often several difficulties arise that limit the use of NiW/Al₂O₃ catalysts such as (i) the difficulty to reach a high level of sulfidation of the NiW phase due to strong metals-support interaction and (ii) the unsuitable formation of the active mixed phase of NiWS, catalyst compared to the Mo-based catalysts [7,8]. The lower concentration of NiWS in the catalysts is associated with the differences of sulfidation temperature of the metal supported species, which caused a premature sulfidation of the Ni and a subsequent segregation of the phases of Ni and W-sulfides [8]. One strategy to overcome this challenge is the use of chelating agents during the preparation stage of the NiW phase. Indeed, organic chelating agents have been successfully used to prepare highly active Mo-based HDS catalysts with increased promotion degree [9–12]. Chelating

agents simplify the procedure of catalyst preparation since they are usually applied in a one-step co-impregnation procedure. Chelating agents favor the formation of strong complexes during the preparation and lead to a weakening of the metal-support interaction, all these features limit the separated sulfidation of the metal and promoter [13]. Among the various organic additives used, addition of citric acid (CA) has been well documented as an effective method to prepare a highly active bimetallic catalysts for HDS reactions [7,14,15]. The impact of CA addition on the structure of the active phase has been investigated for both Mo (Chapter IV of this thesis) and W based catalysts [16–22]. However, for W-based catalysts, no clear evidence of the effect of the additive in the sulfide phase structure has been already presented.

As a proven technique, low-temperature CO adsorption followed by infrared spectroscopy (IR/CO) has been used to characterize sulfide catalysts since several decades. It is now well established that IR/CO spectra of unpromoted Mo-based catalysts present two different CO adsorption bands [23], which are located at ~2110 and ~2070 cm⁻¹ that accounts for Mo sites on M-edge and S-edge sites of MoS₂ slabs. Quantification of the sites of these two edges allowed to account for the morphology of the MoS₂ slabs (S-edge/M-edge ratio). These results are in agreement with morphologies observed by STEM-HAADF for the same catalysts [24]. In addition, very recently through a parallel between IR/CO experiments and DFT calculations, it was possible to point out that the two IR/CO bands at 2126 and 2066 cm⁻¹ observed on sulfide W/Al₂O₃ catalysts also reflect the M-edge and S-edge sites of WS₂ slabs (chapter III of this thesis) [25]. In general, IR/CO is particularly effective for the characterization of surface sites of the sulfide catalysts, since it enables to characterize both the acidity of the

support, the amount and the nature of the edge site of the sulfide sites as well as the sulfide slab geometry [26].

The observations by high resolution transmission electron microscopy (HRTEM) provide morphological information of the supported TMS slabs [27–30]. When it comes to the sulfide slab shape observation, one of the obstacles is that HRTEM images suffer from contrast disturbances due to the support, particularly when this is an insulator as strong as alumina. Only slabs parallel to the electron beam can be observed. In contrast, in the high angle annular dark-field scanning transmission electron microscopy (STEM-HAADF), images are formed by collecting electrons scattered at high angles by a dark field annular detector, whereby the intensities of the images depend on the atomic number of the elements. HR STEM-HAADF or Z-contrast image mode offers a significant advantage. Indeed, it facilitates the distinction of the elements according to their atomic number (Z), since the contrast is directly proportional to $Z^{1.7}$, even for objects of a single atomic plane [31]. This mode is adequate for the study of small nanoparticles formed by heavy elements, especially if they are deposited on a light-weighted support such as industrial alumina. Despite experimental evidence of differences in activity, NiWS catalysts are mostly assumed to behave similar to the much more studied HDS CoMoS catalyst. Lately, STEM-HAADF has been successfully applied to investigate the shapes of WS₂. Recently, Alphazan *et al.* [32,33] reported on highly active W-based catalysts that their enhanced activities are explained by the 2D-hexagonal morphology of WS₂ particles. Nevertheless, a matter of question continues to be: what about the morphology of promoted-W catalysts prepared with chelating agents as citric acid? And more challenging, what about the location of the promoter? And

finally, how the promoter decoration pattern is specifically in industrial-type catalysts?

In this work we report the effect of citric acid (CA) as a chelating agent on activity and structure of NiW supported catalysts. This work aims to explain the beneficial role of the citric acid at a molecular level. The formation of NiWS sites during catalyst sulfidation was *in situ* followed by CO adsorption. The improved thiophene HDS activity on NiW catalysts prepared with CA can be related to the enhanced amount of NiWS sites as evidenced by CO adsorption followed by IR spectroscopy. The consequent modifications of the use of CA on the morphology parameters such as average length, stacking and shape of the nanoparticles are analyzed by HR STEM-HAADF.

V.2. EXPERIMENTAL SECTION

V.2.1. Catalysts preparation

The series of NiW catalysts studied, which are denoted as NiW/(CA/M=x)/Al₂O₃, where x refers to the molar ratio of CA/M, (M= Ni + W), were prepared by a one-step pore volume impregnation method. Hereafter, x refers to the molar ratio of CA/M (M = Ni + W) (x = 0, 0.5, 1.0, and 2.0). The aqueous impregnation solutions, were prepared by dissolving variable amounts of citric acid (C₆H₈O₇·H₂O) and fixed amounts of ammonium metatungstate (NH₄)₆H₂W₁₂O₄₀·xH₂O (Aldrich) and nickel (II) nitrate hexahydrate (Ni(NO₃)₂·6H₂O) (Aldrich) in deionized water at room temperature. The NiW(CA/M=x) solutions were added to the Al₂O₃ support (SASOL, specific surface area: 252 m²·g⁻¹; pore volume: 0.84 mL·g⁻¹) followed by a maturation stage of 2h at room temperature. To maintain the citric acid in its initial form up to the sulfidation stage, the catalysts were only dried for 16 h at 383 K without

further calcination. All catalysts samples were prepared with a constant amount of W and Ni (20 % wt. W and 2 %wt. Ni content). For all the NiW(CA/M=x)/Al₂O₃ catalysts, the content of W was fixed with 3.3 W atoms·nm⁻², and the Ni/(Ni + W) ratio was equal to 0.3.

V.2.2. Composition and textural properties

V.2.2.1. Chemical analysis by Inductively Coupled Plasma

The elemental contents of Ni, W, and S in sulfide catalysts were determined by ICP method. Oxide catalysts were sulfided ex-situ in a glass reactor under 10% H₂S/H₂ (30 mL·min⁻¹) flow. Catalysts were sulfided at 673K with a rate of 3 K·min⁻¹ during 2h. After, the temperature was cooled down to room temperature under ultra-pure N₂ flow (30 ml·min⁻¹). The catalyst inside the reactor was introduced in a dry glove box under Ar flow, to avoid air contact. Afterwards, inside of the dry glove box, 50 mg of sample was dissolved in hydrofluoric acid, aqua regia, boric acid, and water with a total volume of 100 ml. Tungsten and sulfur amount present in the catalysts were quantified by an inductively coupled plasma atomic emission spectrometry (ICP-AES) using a PerkinElmer Optima 330DV ICP instrument.

V.2.2.2. Nitrogen physisorption analysis

Nitrogen adsorption/desorption isotherms of oxide and sulfide catalysts were measured at -196 °C using Micrometrics Model ASAP 2020 volumetric adsorption analyzer. Oxide samples were sulfided ex-situ in a glass reactor at 673 K (heating rate of 3 K min⁻¹) under 30 ml·min⁻¹ of 10% H₂S/H₂ for 2 h. After that, the reactor was flushed by Ar at 623 K and cooled down to room temperature. Then, the catalysts were degassed at 523 K under vacuum for 12 h prior to analysis. Specific surface areas were determined from the BET

equation. The total volume was calculated from the volume adsorbed at $P/P^0 = 0.95$. Pore size distributions of solids were estimated by Barrett-Joyner-Halenda (BJH) method.

V.2.3. Thiophene hydrodesulfurization test.

The thiophene hydrodesulfurization (HDS) test was carried out with a differential glass reactor. Since the catalytic bed is very thin, it can be considered that the specific velocity corresponds to the initial velocity. Sulfidation procedure before thiophene HDS test, was performed at different temperatures (573-773 K) with a heating rate of 3 K min⁻¹ and 0.1 MPa for 2 h under a 30 mL min⁻¹ flow of 10% H₂S/H₂. Then, thiophene HDS test was carried out at 623 K and 0.1 MPa with around (but precisely weighted) 25 mg of sulfided catalyst. Next, thiophene HDS test was carried out at 350 °C using a 90 mL·min⁻¹ gas mixture consisting of 7.9% thiophene, 90.0% H₂, and 2.1% H₂S. The 90 mL·min⁻¹ gas mixture consisted of 7.9% thiophene, 90.0% H₂, and 2.1% H₂S. During 16 h reaction, the outlet gas was analyzed by a Varian 3900 chromatograph equipped with flame ionization (FID) detector. In order to maintain a differential reactor, the thiophene conversion is controlled below 10%. The reaction rate (r_s) (mol·h⁻¹·kg⁻¹) was calculated using the formula as follows:

$$r_s = \frac{x \times F}{m_{cat}}$$

Where x is thiophene conversion (%), F is molar flow rate of thiophene (mol·h⁻¹), m_{cat} is the mass of the catalyst after sulfidation, respectively. The initial catalyst mass was corrected by precisely weighting the catalyst after catalytic test.

V.2.4. Low temperature CO adsorption followed by IR spectroscopy

The series of catalysts were *in situ* characterized by low-temperature (~100 K) CO adsorption followed by IR spectroscopy (IR/CO). CO adsorption is performed at low temperature to avoid any reaction with the catalyst surface. The oxidic catalyst was grounded and pressed into a self-supported wafer (~ 10 mg – precisely weighted, for a disc of 2.01 cm²) and positioned into a quartz IR cell with CaF₂ windows. Before to the adsorption experiments, the sample was sulfided *in situ* in the IR cell. For this, the catalysts was sulfided with a gas mixture containing 10% H₂S/H₂ (30 ml.min⁻¹) at 673 K (sulfiding flow starting from room temperature) for two hours with a heating rate of 3 K.min⁻¹. After sulfidation, the cell was flushed with Ar and evacuated down to P < 10⁻⁴ Pa until the catalyst reached room temperature. CO adsorption at low temperature (100 K) was carried out introducing controlled CO pressure measured in a standard volume called small volume. These small calibrated doses of CO were introduced into the IR cell until equilibrium pressure of 133 Pa was reached. After each CO introduction, FTIR spectra were recorded with 256 scans and a resolution of 4 cm⁻¹ using Nicolet Nexus FTIR spectrometer equipped with a MCT detector (FTIR = Fourier Transform Infrared; MCT=Mercury-Cadmium-Tellurium). All spectra were normalized to a disc of 5 mg·cm⁻². The bands of the adsorbed CO species were obtained by subtracting the spectra recorded after and before CO introduction. The spectra were decomposed with Peakfit V4.12 using "Autofit peak III-deconvolution" and considering Voigt functions. For all the spectra, the second derivative function was used to ensure the good position of the bands in the spectral decomposition. For the decomposition of all

spectra, the center and full width at half height (FWHH) of each peak are allowed to vary in a small range ($\pm 3 \text{ cm}^{-1}$).

V.2.5. Microscopy study by HRTEM and HR STEM-HAADF

For microscopy observations, the oxide catalysts were sulfided at 673 K (heating rate of 3 K min^{-1}) and 0.1 MPa for 2 h under a 30 mL min^{-1} flow of 10% H₂S/H₂. Then, to limit detrimental exposure to air, the sulfided catalysts were unloaded from the sulfidation reactor under argon flow and poured into absolute ethanol. A few drops of the suspension of catalyst were put on a 300 mesh copper grid with holey carbon film. The images of sulfided catalysts presented in this work have been taken using a double corrected JEOL ARM 200F cold FEG microscope operated at 200 kV. First, length and stacking degree distributions of sulfide slabs were determined manually by measuring at least 300 slabs per sample from HRTEM images. The image treatment was performed using the commercial software from GATAN (DIGITALMICROGRAPH) and free Mesurim software. The average length (\bar{L}) and (\bar{N}) were calculated according to the following distribution modes given by the equations (1) and (2):

$$\bar{L} = \frac{\sum_{i=1}^n n_i L_i}{\sum_{i=1}^n n_i} \quad (1)$$

Where is (\bar{L}) the average length, n_i is the number (frequency) of slabs having the length within the discrete interval i (nm), and n total number of particles or slabs. The number of slabs per stacked particle was determined to obtain the average stacking degree (\bar{N}):

$$\bar{N} = \frac{\sum_{i=1}^n n_i N_i}{\sum_{i=1}^n n} \quad (2)$$

Where n_i is the number of slabs in N_i layers and n total number of particles or slabs.

The nanostructure and morphology of the NiWS slabs were analyzed by high resolution scanning transmission electron microscopy (HR STEM) using a high angle annular dark field (HAADF) detector. All the images presented in this manuscript were acquired in HAADF mode. The acquisition of one image lasted about 30 s with a resolution of 1024 pixels x 1024 pixels, (30 μ s of exposure time for each spot in the scanning mode). During this acquisition and despite exposure to the electron beam, the shapes of the particles remained unchanged, meaning that the slabs were quite stable under the electron beam.

V.3. RESULTS AND DISCUSSIONS

V.3.1. Elemental analysis

Elemental analysis was performed after the sulfidation stage of the catalysts in order to verify the sulfidation degree of the NiW catalysts (**Table VII**). All the catalysts presented sufficient sulfur to form WS₂, that is, the molar concentration of sulfur is about twice that of tungsten. It is also observable that the S/W ratio increases with citric acid amount. Thus, this is an indication that the presence of citric acid may favor the sulfidation of W.

Table VII. Elemental analysis of NiW catalysts before and after sulfidation at 673K.

Sulfide catalyst	% wt.W	% wt. Ni	Ni/(W+Ni) *	S/(W+Ni) *
NiW(CA/M=0)/Al ₂ O ₃	21	12	0.4	1.7
NiW(CA/M=0.5)/Al ₂ O ₃	22	11	0.3	1.9
NiW(CA/M=1)/Al ₂ O ₃	21	10	0.3	2.0
NiW(CA/M=2)/Al ₂ O ₃	20	10	0.3	2.2

* Atomic ratio

V.3.2. Textural properties.

The nitrogen adsorption-desorption isotherms for both the dried (oxidic) and sulfided NiW/Al₂O₃ catalysts correspond to a type IV isotherm according to IUPAC classification with a H1 hysteresis loop, characteristic for mesoporous materials [34]. **Table VIII** presents the effect of sulfidation on the specific surface area and pore diameter of the catalysts prepared with and without citric acid. It is appreciated that as the concentration of the citric acid in the impregnation solution increases, the oxide catalyst suffers from a decrease in its surface area, possibly due to the blockage of the pores of the alumina by citric acid molecules. However, when carrying out the sulfidation process, it is observed how the catalysts progressively recover their surface area. This is a consequence of the low decomposition temperature (~448 K) of the citric acid relative to the sulfidation temperature (T_s=673 K). If we consider the surface area (252 m²/g) and pore size diameter of the pure γ -alumina carrier (12.5 nm), it is observed that the textural properties are almost maintained at the final stage of the catalyst with just a small decrease in surface area and pore size that is more marked when the amount of CA increases. This is likely related to

the rising of the amount of carbonaceous deposits formed by CA on the catalyst.

Table VIII. Textural properties of NiW catalysts before and after sulfidation at 673K.

Catalyst	SBET (m ² ·g ⁻¹)		Pore diameter (nm)	
	dried	sulfided	dried	sulfided
NiW(CA/M=0)/Al ₂ O ₃	193	224	10.6	11.9
NiW(CA/M=0.5)/Al ₂ O ₃	160	221	10.9	11.7
NiW(CA/M=1)/Al ₂ O ₃	107	212	10.5	11.4
NiW(CA/M=2)/Al ₂ O ₃	89	207	9.7	11.1

V.3.3. Thiophene HDS activity

V.3.3.1. Effect of sulfidation temperature

It is generally reported that W-based catalysts present a greater difficulty for the sulfidation process than the Mo-based ones. This translates into, that compared to Mo-based catalysts, higher activation temperatures as well as longer sulfidation times are required. It should be noted that nowadays there is no established protocol or a widely accepted process regarding the optimal sulfidation parameters to use for W-based catalysts. In order to guarantee an optimal sulfidation procedure for the series of samples studied in this work, we carried out catalysts activation varying the sulfidation temperature in a range of 573K to 723 K with 50 K intervals. To follow the sulfidation procedure impact, thiophene HDS performances were tested for all these catalysts sulfided in different conditions (**Figure 41**).

For NiW(CA/Mo=0)/Al₂O₃, its HDS reaction rate increases with the sulfidation temperature, it exhibits the lowest HDS rate compared to catalyst prepared with CA. Moreover, in addition to being the catalyst with the lowest

catalytic activity, it is also the only catalyst that shows an increase in reaction rate after sulfidation at 673 K.

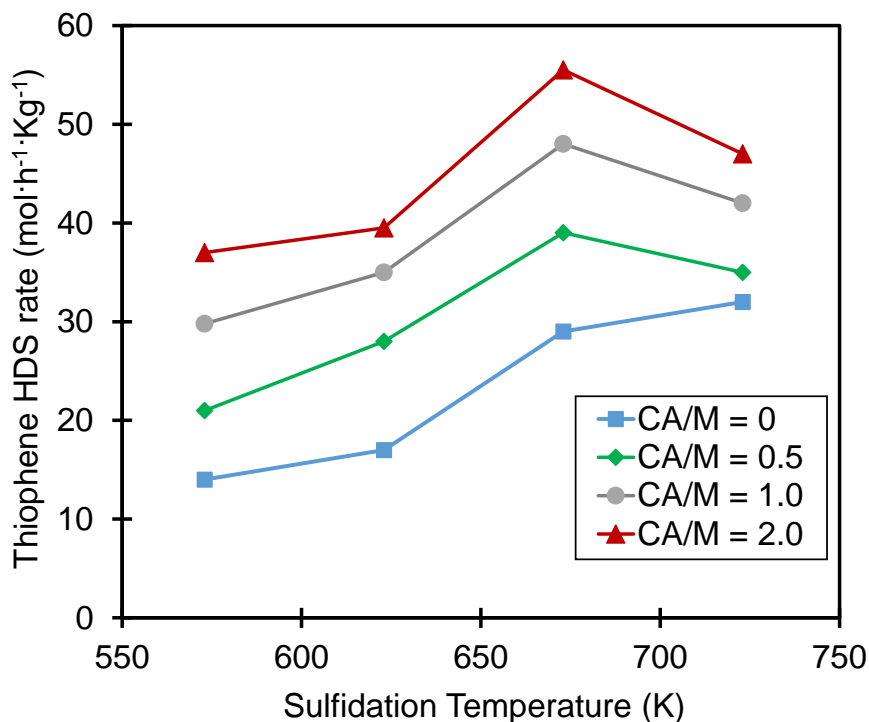


Figure 41. Effect of sulfidation temperature of NiW(CA/M=x)/Al₂O₃ catalysts on the thiophene HDS activity.

This indicated that the catalyst is not completely activated even at this high temperature. This is in agreement with the expected difficulty of sulfidation reported for W based catalysts.

As a general trend, the addition of citric acid increased the catalytic activity as observed for the NiW(CA/Mo= x)/Al₂O₃ with x=0.5,1.0 and 2. It is noticeable that even a small concentration of CA leads to a clear beneficial effect. Moreover, the catalytic tests showed that an increase in the CA content accelerates the rate of reaction at any of the sulfidation temperatures. For the three samples prepared with CA, the sulfidation temperature at which the highest reaction rate is obtained is found to be 673 K. If the catalysts are sulfided at higher temperature (T_s=723 K), a decrease in activity is observed.

This may be linked to an agglomeration of the sulfided particles. This detrimental effect of high T_s is not observed with the catalyst prepared without CA. This can be explained by an improvement of the sulfidation degree at lower sulfidation temperature that counterbalanced the active phase sintering effect, and also, this can be related to a stronger anchorage of the sulfided phase on the support in absence of CA that limits the sintering.

The beneficial effect of the addition of CA in the catalysts can be explained by the fact that, by adding citric acid, an increase in the amount of Ni-AC complexes that will interact with tungsten is promoted, which makes it possible to form more NiWS active sites. This assumption will be explored by low temperature CO adsorption followed by IR spectroscopy.

V.3.3.2. Effect of the citric acid amount.

The influence of citric acid amount on the thiophene HDS activity of the sulfided NiW(CA/M=x)/Al₂O₃ is presented in **Figure 42**. The catalytic activity was compared to the counter partner CoMo/Al₂O₃, it is observed that the NiW series present enhanced activity and that the rate of increase of HDS velocity is similar for both systems. NiW(CA/M = 0)/Al₂O₃ catalyst exhibits the lowest HDS rate, and a general trend of increasing activity with the addition of citric acid is observed. The thiophene HDS rate gradually increases from 29 mol·h⁻¹·kg⁻¹ on NiW(CA/M=0)/Al₂O₃ to 56 mol·h⁻¹·kg⁻¹ on NiW(CA/M=2)/Al₂O₃. As already reported, the addition of citric acid in NiWS catalysts increases the catalytic activity [7].

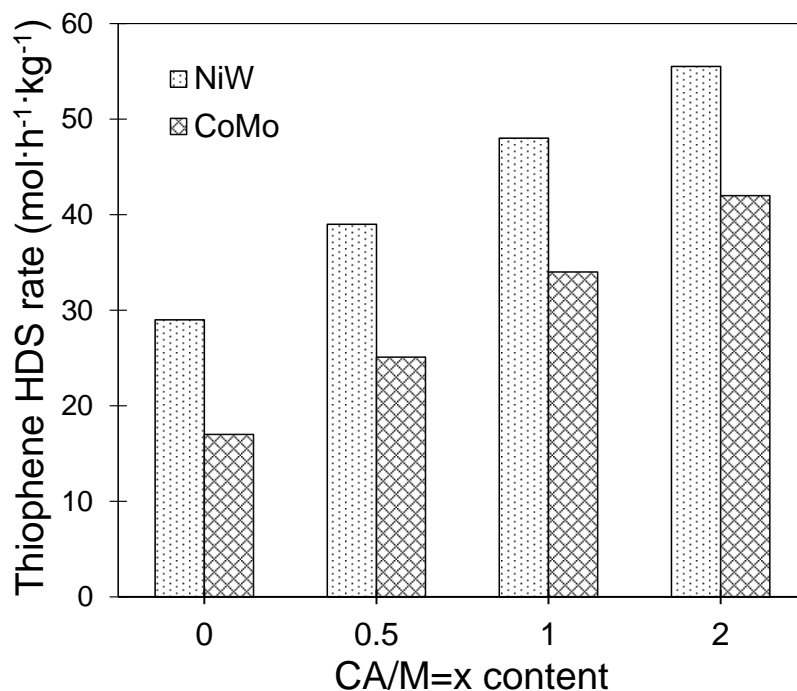


Figure 42. Effect CA addition on thiophene HDS activity of sulfided NiW(CA/M=x)/Al₂O₃ catalysts sulfided at 673 K and CoMo(CA/M=x)/Al₂O₃ catalysts sulfided at 623 K.

V.3.4. IR spectroscopy of sulfided NiW/Al₂O₃ catalysts

Figure 43 shows the IR spectra of adsorption of 133 Pa of CO (Tads ~100 K) on sulfided NiW(CA/M=x)/Al₂O₃ catalysts prepared with different CA amounts. It has to be noted that the sulfidation of the NiW catalysts causes a marked decrease in the transmission of IR radiation. Globally, transmission is low due to the high metal loading present in the catalysts (23% wt. metal).

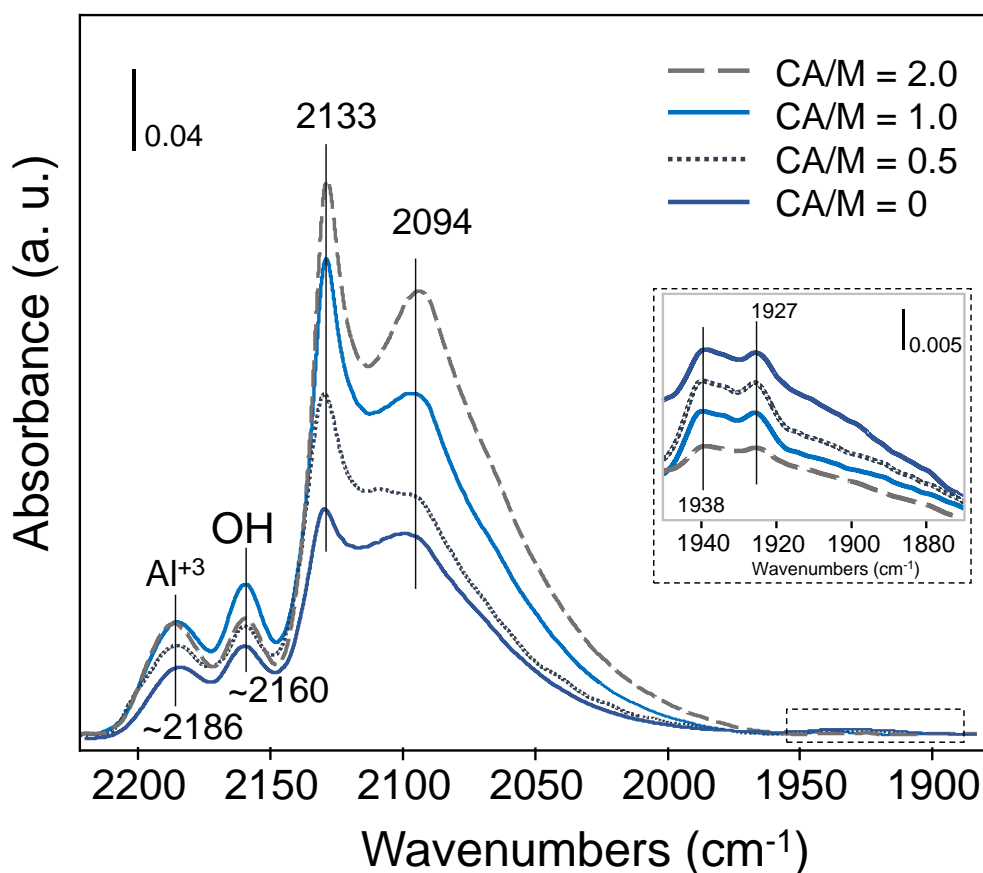


Figure 43. IR spectra of CO adsorption (133 Pa CO at equilibrium, $T_{\text{ads}}=100\text{K}$) on NiW(CA/M=x)/Al₂O₃ catalysts sulfided at 673K. The inset zooms on the low wavenumber bands.

Four main $\nu(\text{CO})$ bands at ~ 2186 , ~ 2160 , 2133 and 2094 cm^{-1} are observed on these catalysts. The higher wavenumber bands are assigned to CO adsorption on Lewis acid sites and acidic OH groups of the Al₂O₃ support. The two bands at lower wavenumber are ascribed to CO adsorbed on the sulfide phase. The addition of CA increases the intensity ratio I_{2133}/I_{2094} . As confirmed by the inset of **Figure 43** spectra also shows the presence of weak bands in the 1950 - 1900 cm^{-1} region, ascribed to metallic Ni.

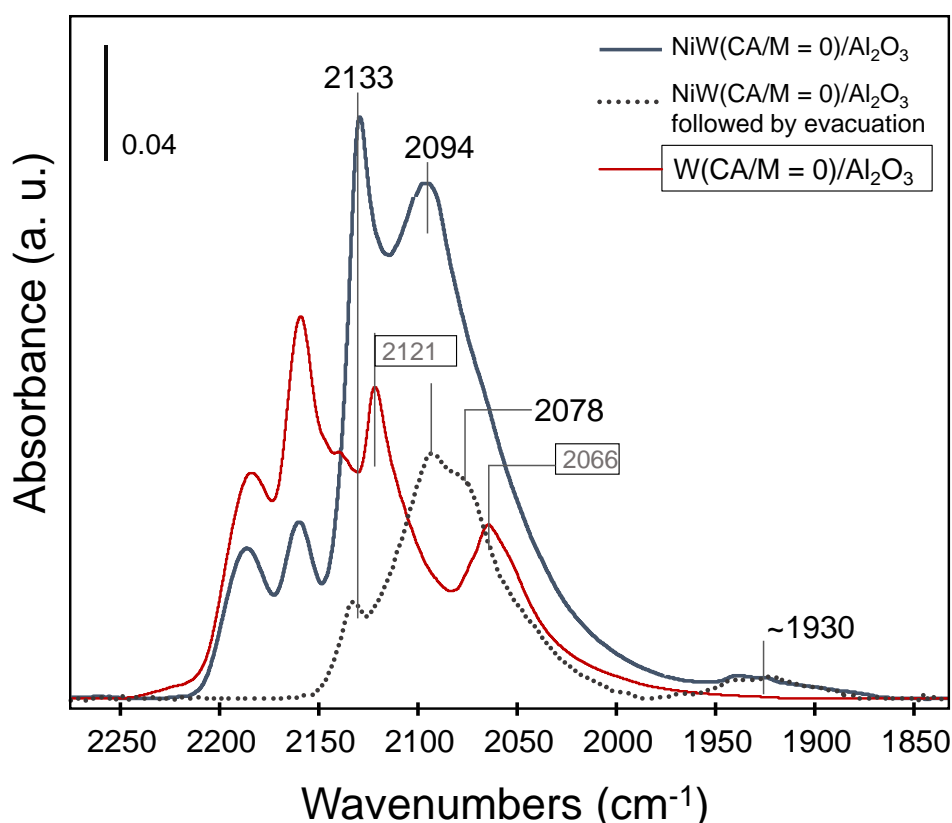


Figure 44. IR spectra of CO adsorbed on sulfided NiW(CA/M=0)/Al₂O₃ and W(CA/M=0)/Al₂O₃. Continuous lines: spectra taken at 100K in presence of P_{equil} = 133 Pa CO. Dotted line: spectra taken after evacuation of CO at room temperature until reaching P < 10⁻⁴ Pa.

Figure 44 compares spectra taken on NiW(CA/M=0)/Al₂O₃ and W(CA/M=0)/Al₂O₃ catalysts at different CO coverages, i.e., at full coverage (equilibrium 133 Pa) and after evacuation at 298K. On W/Al₂O₃, two main bands at 2121 cm⁻¹ and 2066 cm⁻¹ characterize the sulfide phase. After evacuation at 298K, no more CO adsorbed on sulfide sites is detected. As shown in a recent paper, these bands are respectively associated to CO adsorbed on M-edge and S-edge of the WS₂ slabs [25]. This confirms that the CO adsorption on the unpromoted W sites is weak.

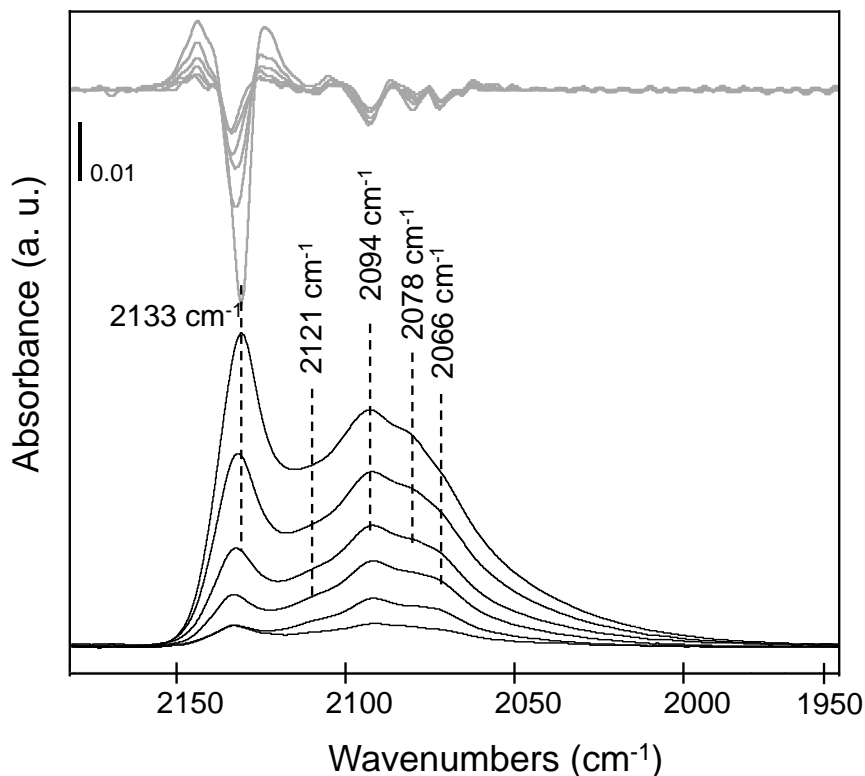


Figure 45. IR spectra of first CO doses (0.002 to 0.012 $\mu\text{mol CO}\cdot\text{mg}^{-1}$) adsorbed at 100 K on NiW(CA/M=0)/Al₂O₃ sulfided at 673 K. Each spectrum is presented with its second derivative function (lighter curves).

Conversely, on NiW(CA/M=0)/Al₂O₃ catalyst, the main bands observed at 2133 and 2094 cm^{-1} remain after evacuation at 298K with decreased intensity. The evacuation also puts in evidence the presence of a new component at 2078 cm^{-1} . As observed on **Figure 43**, the presence of low wavenumber bands at $\sim 1930 \text{ cm}^{-1}$ is also noted on **Figure 44**.

A more accurate view can be obtained by analyzing the spectra for the first doses of CO introduced on NiW catalyst without CA (**Figure 45**). **Figure 45** also presents the corresponding second derivatives calculated in order to specify the position of the various bands. The presence of the bands ascribed to non-promoted sites is also highlighted by this way. In conclusion, it can be

considered that CO adsorbed on the sulfided phase of NiW catalysts with and without CA gives rise to at least five bands at 2133, 2121, 2094, 2078 and 2066 cm⁻¹.

Next we focus on the assignment of these five contributions. As mentioned before, comparison between spectra obtained on NiW and W catalysts, allows assigning the two bands at 2121 and 2066 cm⁻¹ to the CO adsorbed on unpromoted W sites, located respectively on M-edge and S-edge. The question now concerns the assignment of the bands at 2133, 2094 and 2075 cm⁻¹. These wavenumbers are very close to those reported on NiW catalysts by Zuo [35] and Duchet [36]. The poor spectral quality of the spectra presented in the early work of Duchet [36] makes difficult specifying if these bands are characteristics of promoted or unpromoted W sites. Nevertheless, this work shows that increasing the temperature of gas phase sulfidation in the range 673-873 K preferentially enhances the intensity of the band at ~2090 cm⁻¹ [36]. Later, Zuo *et al.* studied the influence of the catalysts composition : increasing the Ni/W ratio (0.17 to 0.41) increases the CO uptake with development of the three bands [35]. Thus, these bands were ascribed to NiWS sites. It was also reported that the wavenumber of CO band at ~2096 cm⁻¹ is very close to that observed on Ni sulfide catalyst (2098 cm⁻¹). Moreover, this band presents a specific behavior upon H₂ treatment of sulfided NiW catalysts. Indeed, it markedly increases whereas the two others bands at 2127 and 2079 cm⁻¹ tends to disappear. Zuo *et al* proposed that the three bands characterized interaction between Ni and W but in a different way : the band at ~2096 cm⁻¹ is ascribed to Ni particles perturbed by WS_x phase whereas the bands at 2127 and 2079 cm⁻¹ would characterize NiWS sites with different environments.

This interpretation can be refined considering previous assignments based on DFT calculation of CO adsorbed on Ni-promoted system [37]. Thus, these bands could correspond to NiWS sites but with different degrees of promotion (partially and totally). Hence, the bands at 2094 and 2078 cm⁻¹ would correspond to CO adsorbed on partially promoted sites whereas the band at 2131 cm⁻¹ would correspond to CO adsorbed on totally promoted NiW sites. This is also in agreement with the electron transfer on NiWS that should be from Ni to W. Thus compared to unpromoted WS₂ sites (2121 cm⁻¹), $\nu(\text{CO})$ wavenumbers on partially promoted sites are detected at lower frequencies (2094 and 2078 cm⁻¹). On totally promoted sites, CO only interacts with Ni atoms. Compared to pure NiS_x sites (2098 cm⁻¹), the CO frequency is indeed at greater value (2131 cm⁻¹). Such rather high CO wavenumber was also reported for promoted sites of NiMo catalysts (2120 cm⁻¹) [37].

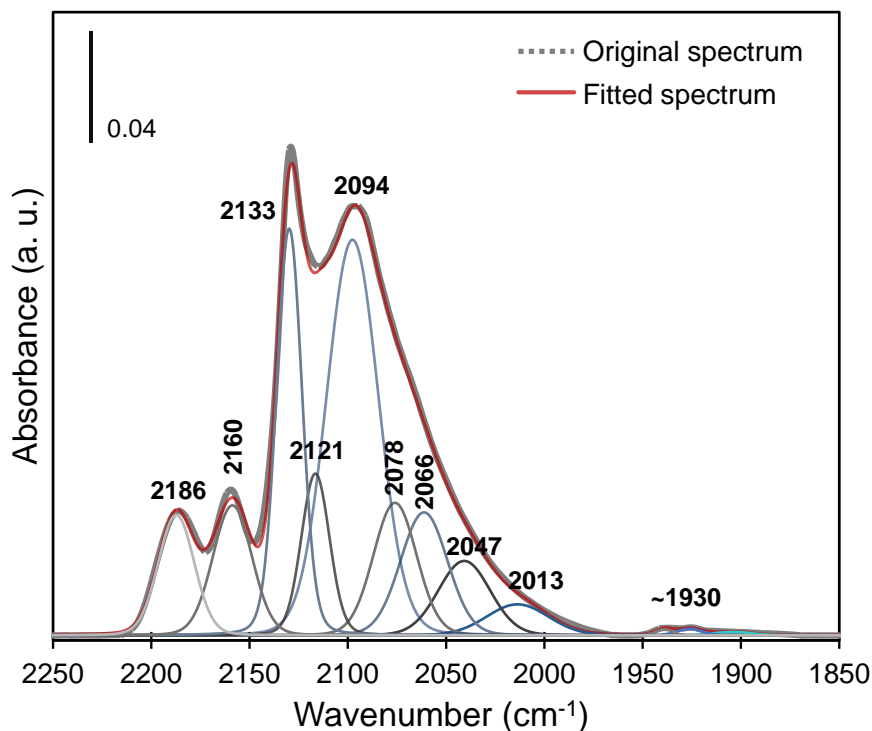


Figure 46. Decomposition of the IR spectrum of CO adsorption (PCO=133 Pa at equilibrium, T=100 K) on NiW(CA)/Al₂O₃ catalyst sulfided at 673 K with Peakfit V4.12.

Table IX. Assignment of main $\nu(\text{CO})$ bands on NiW(CA)/Al₂O₃ catalysts and parameters used to fit the IR spectral bands.

Band assignment	$\nu(\text{CO})$ band experimental (cm ⁻¹)	FWHH (cm ⁻¹)	Reference
Lewis Acid sites Al ³⁺	2186 ± 2	22 ± 3	
Acidic Al-OH	2160 ± 3	23 ± 3	
Ni totally promoted edges	2133 ± 2	20 ± 3	[78,160]
Unpromoted M-edge	2121 ± 3	20 ± 3	[157]
Partially promoted Ni M-edge I	2094 ± 3	30 ± 3	
Partially promoted Ni M-edge II	2078 ± 3	25 ± 3	Detected with 2 nd derivative
Unpromoted S-edge	2066 ± 3	28 ± 3	[157]
Metallic Ni	1927 ± 8	20 ± 3	[107]

all peaks are Voigt Amp G/L

Hence, CO spectra can account for partially and totally promoted NiWS sites (**Table III**). Going further in the assignment of promoted sites to M-and S-edge

would require complementary experiments. As for the low wavenumber and small contribution at $\sim 1927\text{ cm}^{-1}$, it is ascribed to metallic Ni in accordance to reference [26].

Figure 47 shows the influence of CA amount on the total area of the massive ascribed to CO in interaction with the sulfide sites. To go further, these spectra were decomposed as shown on **Figure 46** and using the parameters mentioned in **Table VIII**. An increase of the three $\nu(\text{CO})$ bands (2133 , 2094 and 2078 cm^{-1}) specific of NiWS sites is reported in **Figure 47**. These three NiWS bands increase in a very similar proportion with CA addition. In parallel and as expected, the intensity of the bands specific of unpromoted W sites (2121 and 2066 cm^{-1}) decreases, however slightly, with CA addition. They are detected whatever the CA amount is, indicating that, even for the highest CA amount i.e., for the catalyst that presents the greatest amount of NiWS, some edges of WS₂ slabs stays unpromoted. **Figure 47** also points out a nice parallel between the increase of $\nu(\text{CO})$ bands characteristic of NiWS sites and the augmentation of HDS activity.

Parallel between IR characterization and activity tests shows that the increase of HDS activity on catalyst prepared with CA can be related to the enhanced formation of NiWS sites. This work shows that the increase of HDS activity on catalyst prepared with CA can be related to the enhanced formation of NiWS phase. These results can be compared with previous work, indeed, it has been shown that citric acid coordinates the Ni atoms, which prevents the formation of insoluble Ni species of the type $[\text{Ni}(\text{OH})_2(\text{H}_2\text{O})_4]$ in the impregnating

solution and promotes the formation of soluble Ni-AC complexes.

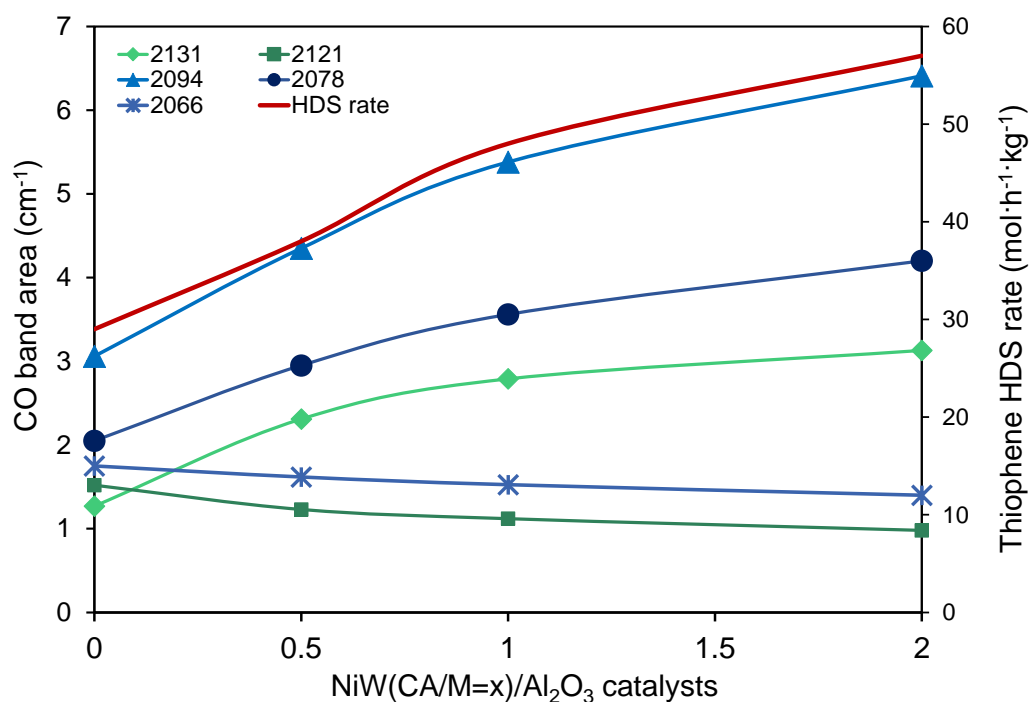


Figure 47. Effect of citric acid addition on the areas of different bands of the sulfided NiW (CA/M=x)/Al₂O₃ catalysts obtained by CO/IR. In this graphic the HDS thiophene rate divided by a factor of ten is presented to evidence the parallel growth of certain bands along with the catalytic activity.

The majority species in an acidic pH medium would be under the forms [Ni(HCit)(Cit) (H₂O)₄]³⁻ and [Ni(Cit)₂(H₂O)₄]⁴⁻. These ionic species will interact with the support and form AlO-Ni-AC complexes. [7,15]. All these features are beneficial for NiWS phase formation. In addition, as shown on Mo-based catalysts [39] CA likely decreases the sulfide phase-support interaction. This will make tungsten more available and allows WS₂ sulfidation at lower temperature avoiding early nickel sulfidation. Thus, this feature should also favored NiWS formation. Moreover as shown previously changing the W-support interaction also could affect the morphology of the sulfide phase.

V.3.5. Electron microscopy by HRTEM and STEM HAADF

Electron microscopy of NiW(CA/M=0)/Al₂O₃ and NiW(CA/M=2)/Al₂O₃ was performed by HRTEM and in HR-STEM HAADF. The objective is to account for change of sulfide phase morphology i.e. slab size and stacking, shape of the sulfide slabs, as well as to try to get information on the nature of the sulfide slab edges. **Figure 48**, shows representative HRTEM images of NiW(CA/M = 0)/Al₂O₃ and NiW(CA/M = 2)/Al₂O₃ catalysts. The distributions of length and stacking of the sulfide slabs were obtained after a careful analysis of more than 300 slabs. It should be mentioned that in this work, we are able to reliably account for slabs of about 1 nm. These could be obtained by adjusting the local contrast of each zone analyzed of the high resolution pictures of outstanding quality. It was observed that the addition of citric acid does not lead to a significant decrease of the average slab length (3.11 ± 0.14 nm to 2.95 ± 0.14 nm).

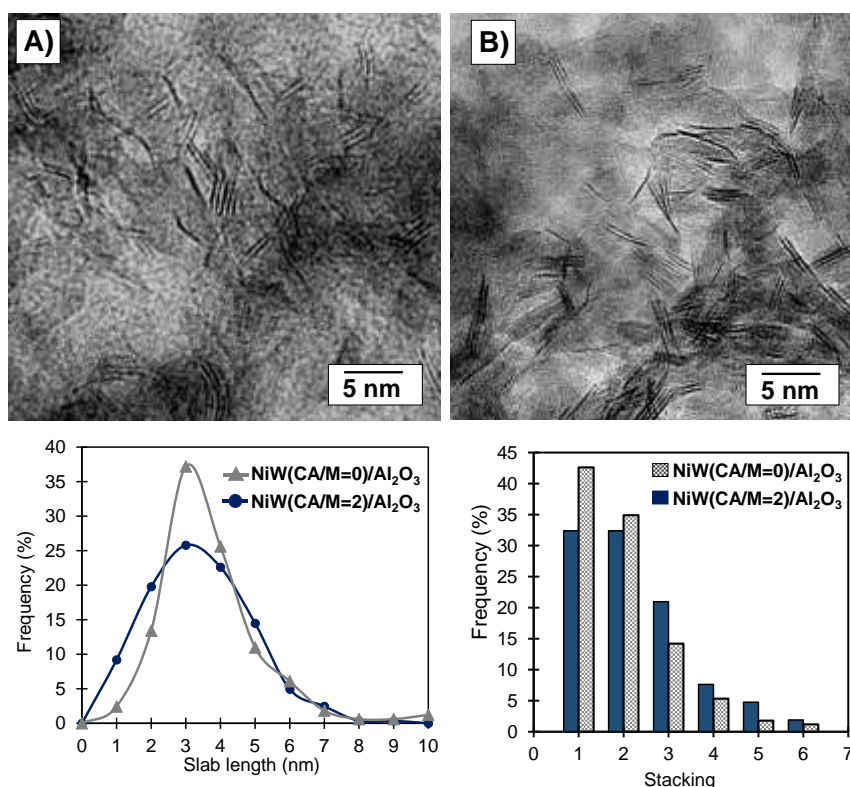


Figure 48. HRTEM images of NiW(CA/M=0)/Al₂O₃ (A) and NiW(CA/M=2)/Al₂O₃ (B), with their slab length distribution and stacking number distribution.

But, this graph also shows that CA significantly increases the number of very small slabs of about 1 nm. Similarly, the average stacking degree is not significantly different between the samples (from 2.0 ± 0.1 to 2.3 ± 0.2 when citric acid is added). Although the distribution is varied, in particular, the presence of some very small-sized monolayer slabs is detected mainly for NiW(CA/M=2)/Al₂O₃. These could be obtained by adjusting the local contrast of each zone analyzed of the high resolution pictures of outstanding quality.

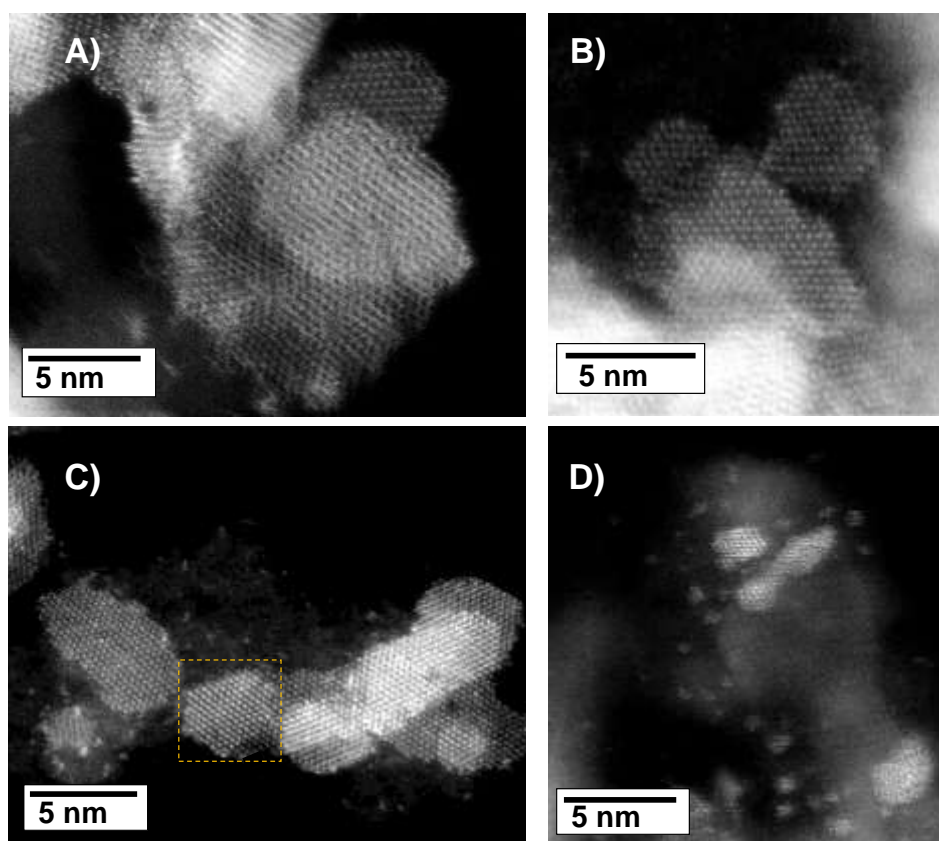


Figure 49. HR STEM-HAADF micrographs of NiWS particles of NiW(CA/M=0)/Al₂O₃ (A and B) and NiW(CA/M=2)/Al₂O₃ (C and D).

To get information about the shape of the sulfided particles and their local composition, STEM-HAADF analysis was performed on NiW catalysts prepared without or with CA (**Figure 49**). It has to be mentioned that, compared to HRTEM, only a limited number of zones of the image are exploitable by STEM-HAADF. Indeed, due to the high metal loading, it is difficult to get the isolated sulfided slabs that are required for obtaining atomic scale observations. Nevertheless, some differences appear between the catalysts prepared without (**Figure 49A and B**) and with CA (**Figure 49C and D**). First, regarding the particles greater than 1 nm, no clear difference in their morphology could be evidenced, they all appear as hexagonal shaped more or less rounded. However, the most remarkable features is the detection of tiny particles of less

than one nanometer as well of agglomerates of few atoms on NiW(CA/M = 2)/Al₂O₃ sample (**Figure 49C** and **D**). Such small particles could not be observed on catalyst prepared without CA (**Figure 49A** and **B**). This is in accordance with the previous results obtained by HRTEM.

The next question was how to get the nature of the atoms observed on the HR-STEM HAADF images, and particularly the nature of the edge atoms. EELS or EDX analysis were carried out but due to the very low signal (CPS), the results were not conclusive regarding the promoter localization. Among the difficulties one has to quote the very limited amount of matter of the each analyzed zone and the high insulator properties of the support. Nevertheless, thanks to the contrast sensitivity of the HAADF technique it is possible to measure the variations in contrast intensity between Ni and W atom. Indeed, they present strong differences in their Z number, contrast in HAADF mode being sensitive to the $Z^{1.7}$, a good contrast between these two atoms is expected ($Z^{1.7}(W) / Z^{1.7}(N) = 5.22$). This technique can thus be used to study metal atom distribution within monolayer catalysts [40,41]. By this way it should be possible to obtain a profile of intensity from a line of atoms located in different regions of the slab.

To perform such analysis, a special attention was taken to analyze non-overlapping particles with monolayer stacking, in addition, image of these isolated slabs should present an excellent resolution. As a matter of fact, the images of the particles answering to these criteria are scarce. A detailed inspection of the particle presented in **Figure 50** reveals variations in the contrast of the atoms as differences between contrasts of the atoms located in the edges and in the bulk.

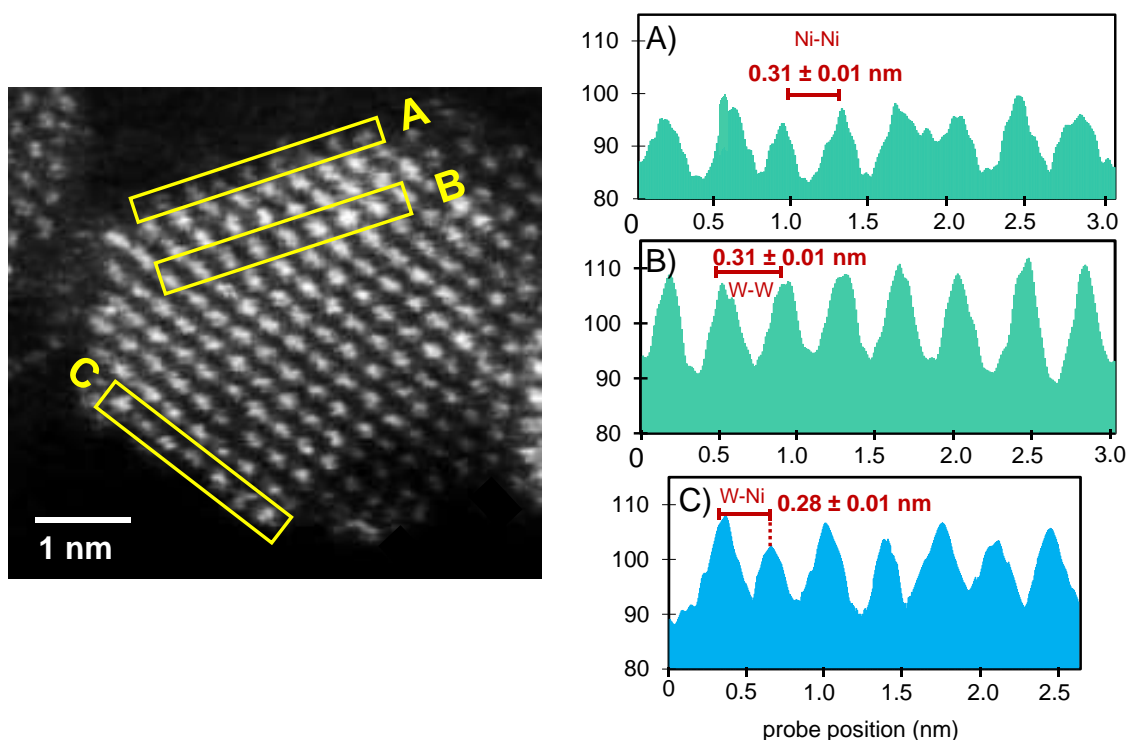


Figure 50. Variations of contrast and interatomic distances at different zones of a sulfided slab of NiW (CA/Mo=2)/Al₂O₃ (particle with right with dotted frame in Figure 9C).

It was assumed that due to the visible atomic arrangement that this particle presented, a single slab was being observed. Stacking of slabs would lead to a more complex pattern due to the expected shift of the slabs. Therefore, the variations in the contrast of the STEM HAADF images cannot be explained as a function of thickness changes since no overlapping planes are detected in the slab.

Thus, this variations in contrast can be attributed to variations in location of W and Ni atoms. As shown in **Figure 50**, the atoms located in the bulk (region B), present a homogeneous brightness while the atoms at the edges present in general a less intense contrast (regions A and C). The measurement of the interatomic distances in the region B shows distances between the atoms of

0.311±0.010 nm. This is in good agreement with the distances obtained by EXAFS for W-W atoms (0.316 nm) in WS₂/Al₂O₃ [42].

In the region (A), majority of the atoms of the edges are less bright compared to the bulk (W) atoms of the region B. This suggests the presence of Ni atoms at this sulfided edge. Interatomic distances measured at this edge reaches 0.317 ± 0.010 nm. From the atomic model reported by Girleanu *et al.* [43], the Ni-Ni distances were found to have a value of 0.32 nm, i.e., slightly greater than the one measured in the core of the particle. This is in good agreement with the value measured between the atoms of the region A. Thus, the interatomic distance as well as the low contrast of the atoms located at region A, allow to assert the presence of only Ni atoms at this edge.

In the region C, atoms present different contrasts one from each other, this feature suggests different natures of the atoms at this edge. Interatomic distances measured at this edge reaches 0.280 ± 0.010 nm i.e., a lower value than that measured in the core of the particles and on edge A. The DFT calculations of Girleanu *et al.* determined Ni-W distances in the range 0.274–0.285 nm [43]. Thus, the good agreement with what is measured in region C as well as the change of contrasts of the atoms located allow to conclude to the presence of both Ni and W atoms at the edge C. Analysis of contrast and distance at core and edge of a sulfide particle in another zone was also performed (**Figure 51**). As for the atoms located in the core of the particle, their contrast stays constant and the interatomic distances oscillate around 0.311 nm. At the periphery of this particle, one can see one atom next to brighter one whose interatomic distance is 0.281 nm. By their side, there are three less

bright atoms (with the lowest contrast at the edge), that exhibit an interatomic distance of around 0.317 nm.

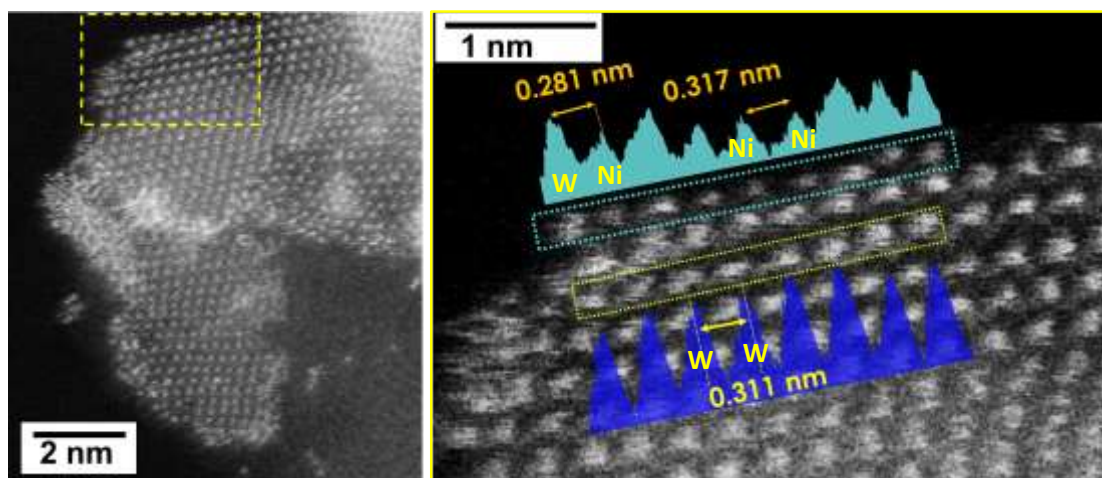


Figure 51. HR HAADF-STEM image of sulfided NiW(CA/M=2)/Al₂O₃ catalyst. Inset of the figure shows the contrast variations and characteristic distances observed in the atoms located in the periphery and in the bulk of the slab.

This indicates the coexistence of Ni and W atoms at the sulfide slab edge. Similar analysis of the several sulfide particles by STEM-HAADF shows that, as expected, only W atoms are present in the core of the particles whereas the edges can expose either exclusively Ni atoms or Ni and W atoms within various configurations. Presence of totally promoted edges and partially promoted edges are highlighted by STEM-HAADF in accordance with IR assignments.

V.4. CONCLUSIONS

The aim of this study was to obtain an atomic level analysis of the structure of the active sites of Ni promoted WS₂ particles supported on γ -Al₂O₃ prepared with and without citric acid.

Thiophene hydrodesulfurization test shows that citric acid addition during the preparation stage markedly increases the catalytic activity. Parallel with IR/CO indicates that this is a consequence of the increased formation of NiWS sites in presence of citric acid. A careful analysis of the IR/CO spectra at various CO coverages was performed. First it shows that unpromoted sites characterized by a bands at 2121 cm⁻¹ (W on M-edge) and 2066 cm⁻¹ (W on S-edge) are still detected whatever the amount of citric acid. Second it points out that the NiWS sites give rise to three bands. Parallel with previous works allowed to assign the 2094 and 2077 cm⁻¹ bands to partially promoted sites and the band at 2131 cm⁻¹ to totally promoted sites.

HRTEM shows that citric acid addition favors the formation of very small particles of about 1 nm. HR STEM HAADF images confirm this and, even provides evidence for the formation of clusters of few atoms. Moreover, by analyzing contrast and interatomic distances on atomic scale images of sulfide particles obtained by HR STEM HAADF, it was possible to identify the nature of the core and edge atoms of the particles. The metal atoms of particle core are only W ones whereas the edges of the particles could be either fully promoted with detection of only Ni atoms, or partially promoted with detection of both Ni and W atoms. Hence, local and global analysis of NiW slabs are in good agreement to account for more fully promoted and partially promoted NiW sites by CA addition.

V.5. REFERENCES

- [1] S. Topsøe, H., Clausen, B. S., Candia, R., Wivel, C., & Mørup, In Situ Mössbauer Emission Spectroscopy Studies of Unsupported and Supported Sulfided Co-Mo Hydrodesulfurization Catalysts: Evidence for and Nature of a Co-Mo-S Phase, *J. Catal.* 68 (1981) 433–452. doi:10.1016/0021-9517(81)90114-7.
- [2] P.P. Minaev, P.A. Nikulshin, M.S. Kulikova, A.A. Pimerzin, V.M. Kogan, NiWS/Al₂O₃ hydrotreating catalysts prepared with 12-tungstophosphoric heteropolyacid and nickel citrate: Effect of Ni/W ratio, "Applied Catal. A, Gen. 505 (2015) 456–466. doi:10.1016/j.apcata.2015.05.012.
- [3] A. Stanislaus, A. Marafi, M.S. Rana, Recent advances in the science and technology of ultra low sulfur diesel (ULSD) production, *Catal. Today.* 153 (2010) 1–68. doi:10.1016/j.cattod.2010.05.011.
- [4] H.G. Füchtbauer, A.K. Tuxen, P.G. Moses, H. Topsøe, F. Besenbacher, J. V Lauritsen, Morphology and atomic-scale structure of single-layer WS₂ nanoclusters, *Phys. Chem. Chem. Phys.* 15 (2013) 15971. doi:10.1039/c3cp51758f.
- [5] B.H. Cooper, B.B.L. Donnis, Aromatic saturation of distillates: an overview, *Appl. Catal. A Gen.* 137 (1996) 203–223.
- [6] A. Carlsson, M. Brorson, H. Topsøe, Morphology of WS₂ nanoclusters in WS₂/C hydrodesulfurization catalysts revealed by high-angle annular dark-field scanning transmission electron microscopy (HAADF-STEM) imaging, *J. Catal.* 227 (2004) 530–536. doi:10.1016/j.jcat.2004.08.031.
- [7] V.A. Suárez-Toriello, C.E. Santolalla-Vargas, J.A. De Los Reyes, A. Vázquez-Zavala, M. Vrinat, C. Geantet, Influence of the solution pH in impregnation with citric acid and activity of NiW/Al₂O₃ catalysts, "Journal Mol. Catal. A, Chem. 404–405 (2015) 36–46. doi:10.1016/j.molcata.2015.04.005.
- [8] M. Breyse, M. Cattenoti, T. Decamp, R. Fretyl, C. Gachet, M. Lacroix, C. Leclercq, L. de Mourgues, J.L. Portefaix, M. Vrinat, M. Houari, J. Grimblot, S. Kasztelan, J. Pierre BONNELLE, J. Bachelier, J. Claude DUCHET, influence of sulfidation conditions on the properties of NiW/Al₂O₃ hydrotreating catalysts, *Catal. Today.* 4 (1988) 39–55.
- [9] H. Li, M. Li, Y. Chu, F. Liu, H. Nie, Essential role of citric acid in preparation of efficient NiW/Al₂O₃ HDS catalysts, *Appl. Catal. A Gen.* 403 (2011) 75–82. doi:10.1016/j.apcata.2011.06.015.
- [10] Y. Yoshimura, T. Sato, H. Shimada, N. Matsubayashi, M. Imamura, A. Nishijima, M. Higo, S. Yoshitomi, Preparation of nickel-tungstate catalysts by a novel impregnation method, *Catal. Today.* 29 (1996) 221–228.

- [11] M.A. Lérias, E. Le Guludec, L. Mariey, J. van Gestel, A. Travert, L. Oliviero, F. Maugé, Effect of EDTA addition on the structure and activity of the active phase of cobalt–molybdenum sulfide hydrotreatment catalysts, *Catal. Today*. 150 (2010) 179–185. doi:10.1016/J.CATTOD.2009.07.107.
- [12] M.A. Lérias, J. van Gestel, F. Maugé, J.A.R. van Veen, Effect of NTA addition on the formation, structure and activity of the active phase of cobalt–molybdenum sulfide hydrotreating catalysts, *Catal. Today*. 130 (2008) 109–116. doi:10.1016/J.CATTOD.2007.07.018.
- [13] D. Valencia, T. Klimova, Kinetic study of NiMo/SBA-15 catalysts prepared with citric acid in hydrodesulfurization of dibenzothiophene, *CATCOM*. 21 (2012) 77–81. doi:10.1016/j.catcom.2012.02.003.
- [14] T. Fujikawa, Highly Active HDS Catalyst for Producing Ultra-low Sulfur Diesel Fuels, *Top. Catal.* 52 (2009) 872–879. doi:10.1007/s11244-009-9228-y.
- [15] C.E. Santolalla-Vargas, V.A. Suarez Toriello, J.A. De los Reyes, D.K. Cromwell, B. Pawelec, J.L.G. Fierro, Effects of pH and chelating agent on the NiWS phase formation in NiW/γ-Al₂O₃ HDS catalysts, *Mater. Chem. Phys.* 166 (2015) 105–115. doi:10.1016/j.matchemphys.2015.09.033.
- [16] J. Chen, F. Maugé, J. El Fallah, L. Oliviero, IR spectroscopy evidence of MoS₂ morphology change by citric acid addition on MoS₂/Al₂O₃ catalysts – A step forward to differentiate the reactivity of M-edge and S-edge, *J. Catal.* 320 (2014) 170–179. doi:10.1016/j.jcat.2014.10.005.
- [17] J. Chen, J. Mi, K. Li, X. Wang, E. Dominguez Garcia, Y. Cao, L. Jiang, L. Oliviero, F. Oise, Role of Citric Acid in Preparing Highly Active CoMo/Al₂O₃ Catalyst: From Aqueous Impregnation Solution to Active Site Formation, *Ind. Eng. Chem. Res.* 56 (2017) 14172–14181. doi:10.1021/acs.iecr.7b02877.
- [18] J. Chen, E. Dominguez Garcia, L. Oliviero, F. Maugé, How the CO molar extinction coefficient influences the quantification of active sites from CO adsorption followed by IR spectroscopy? A case study on MoS₂/Al₂O₃ catalysts prepared with citric acid, *J. Catal.* 332 (2015) 77–82. doi:10.1016/j.jcat.2015.09.005.
- [19] E.D. Garcia, Effet du support sur la morphologie et l'activité des catalyseurs d'hydrodésulfuration, Université de Caen, 2017.
- [20] L. Zavala-sanchez, X. Portier, F. Maugé, L. Oliviero, High Resolution STEM-HAADF microscopy on γ - Al₂O₃ supported MoS₂ catalyst – Proof by image of the changes in dispersion and morphology of the slabs with addition of citric acid, *Nanotechnology*. (2019) 1–10.

- [21] J. Chen, E. Dominguez Garcia, E. Oliviero, L. Oliviero, F. Maugé, Effect of high pressure sulfidation on the morphology and reactivity of MoS₂ slabs on MoS₂/Al₂O₃ catalyst prepared with citric acid, *J. Catal.* 339 (2016) 153–162. doi:10.1016/j.jcat.2016.04.010.
- [22] L. Van Haandel, G.M. Bremmer, E.J.M. Hensen, T. Weber, Influence of sulfiding agent and pressure on structure and performance of CoMo/Al₂O₃ hydrodesulfurization catalysts, (2016). doi:10.1016/j.jcat.2016.07.009.
- [23] D. Bachelier, J., Tilliette, N. J., Cornac, M., Duchet, J. C., Lavalley, J. C., & Cornet, SULFIDED CoMo/Al₂O₃ CATALYSTS: CARBON MONOXIDE CHEMISORPTION AND SURFACE STRUCTURES, *Bull. Des Sociétés Chim. Belges.* 93 (1984) 743–750.
- [24] L. Zavala-Sanchez, X. Portier, F. Maugé, L. Oliviero, High Resolution STEM-HAADF microscopy on γ -Al₂O₃ supported MoS₂ catalyst-Proof by image of the changes in dispersion and morphology of the slabs with addition of citric acid., *Nanotechnology.* (2019). doi:10.1088/1361-6528/ab483c.
- [25] L. Zavala-sanchez, I. Khalil, L. Oliviero, J. Paul, Structural sites investigation and quantification of WS₂/Al₂O₃ catalysts: coupling between IR/CO and DFT calculations for a deep insight into edge sites, *Chem Cat Chem.* (2019) 1–36.
- [26] K.I. Hadjiivanov, G.N. Vayssilov, Characterization of oxide surfaces and zeolites by carbon monoxide as an IR probe molecule, *Adv. Catal.* 47 (2002) 307–511. doi:10.1016/S0360-0564(02)47008-3.
- [27] L. Vradman, M. V Landau, M. Herskowitz, V. Ezersky, M. Talianker, S. Nikitenko, Y. Kolytyn, A. Gedanken, High loading of short WS₂ slabs inside SBA-15: promotion with nickel and performance in hydrodesulfurization and hydrogenation, *J. Catal.* 213 (2003) 163–175. doi:S0021-9517(02)00012 -X.
- [28] Z.D. Huang, W. Bensch, L. Kienle, S. Fuentes, G. Alonso, C. Ornelas, SBA-15 as support for Ni-MoS₂HDS catalysts derived from sulfur-containing molybdenum and nickel complexes in the reaction of HDS of DBT: An all sulfide route, *Catal. Letters.* 127 (2009) 132–142. doi:10.1007/s10562-008-9656-5.
- [29] R. Nava, R.A. Ortega, G. Alonso, C. Ornelas, B. Pawelec, J.L.G. Fierro, CoMo/Ti-SBA-15 catalysts for dibenzothiophene desulfurization, *Catal. Today.* 127 (2007) 70–84. doi:10.1016/J.CATTOD.2007.02.034.
- [30] L. Dimitrov, R. Palcheva, A. Spojakina, K. Jiratova, Synthesis and characterization of W-SBA-15 and W-HMS as supports for HDS, *J. Porous Mater.* 18 (2011) 425–434. doi:10.1007/s10934-010-9394-0.

- [31] S.J. Nellist, P. D., & Pennycook, Direct Imaging of the Atomic Configuration of Ultradispersed Catalysts, *Science* (80-.). 274 (1996) 413–415. doi:10.1126/science.274.5286.413%0AArticle.
- [32] T. Alphazan, A. Bonduelle-Skrzypczak, L. Legens, A.-S. Gay, Z. Boudene, M. Girleanu, O. Ersen, C. Cope, P. Raybaud, Highly Active Nonpromoted Hydrotreating Catalysts through the Controlled Growth of a Supported Hexagonal WS₂ Phase, *ACS Catal.* 4 (2014) 42. doi:10.1021/cs501311m.
- [33] T. Alphazan, A. Bonduelle-Skrzypczak, C. Legens, Z. Boudene, A.-L. Taleb, A.-S. Gay, O. Ersen, C. Copéret, P. Raybaud, Improved promoter effect in NiWS catalysts through a molecular approach and an optimized Ni edge decoration, *J. Catal.* 340 (2016) 60–65. doi:10.1016/j.jcat.2016.05.004.
- [34] K. Sing, D. Everett, R. Haul, L. Moscou, R. Pierotti, J. Rouquerol, T. Siemieniowska, reporting physisorption data for gas/solid systems with Special Reference to the Determination of Surface Area and Porosity, *Pure Appl. Chem.* 57 (1985) 603–619.
- [35] D. Zuo, M. Vrinat, H. Nie, F. Maugé, Y. Shi, M. Lacroix, D. Li, The formation of the active phases in sulfided NiW/Al₂O₃ catalysts and their evolution during post-reduction treatment, *Catal. Today.* 93–95 (2004) 751–760. doi:10.1016/j.cattod.2004.06.078.
- [36] D. Duchet, J. C., Lavalley, J. C., Housni, S., Ouafi, D., Bachelier, J., Lakhdar, M., ... & Cornet, Carbon monoxide and oxygen chemisorption and functionalities of sulphided Ni-W/Al₂O₃ hydrotreating catalysts, *Catal. Today.* 4 (1988) 71–96. doi:10.1016/0920-5861(88)87047-0.
- [37] A. Travert, C. Dujardin, F. Maugé, E. Veilly, S. Cristol, J.-F. Paul, E. Payen, CO Adsorption on CoMo and NiMo Sulfide Catalysts: A Combined IR and DFT Study, *Phys. Chem. B.* 110 (2006) 1261–1270. doi:10.1021/jp0536549.
- [38] F. Mauge, J.C. Duchet, J.C. Lavalley, S. Houssenbay, E. Payen, J. Grimblot, S. Kasxtelan, The sulphided state of nickel molybdenum catalysts supported on zirconia and aluminates, *Catal. Today.* (1991) 561–577. doi:10.1016/0920-5861(91)80039-C.
- [39] E. Dominguez Garcia, J. Chen, E. Oliviero, L. Oliviero, F. Maugé, New insight into the support effect on HDS catalysts: evidence for the role of Mo-support interaction on the MoS₂ slab morphology, *Appl. Catal. B Environ.* 260 (2020) 117975. doi:10.1016/j.apcatb.2019.117975.
- [40] M. Nikulshina, A. Mozhaev, C. Lancelot, M. Marinova, P. Blanchard, E. Payen, C. Lamonier, P. Nikulshin, MoW synergetic effect supported by HAADF for alumina based catalysts prepared from mixed SiMo_nW_{12-n} heteropolyacids, (2017). doi:10.1016/j.apcatb.2017.11.049.

- [41] M. Nikulshina, A. Mozhaev, C. Lancelot, P. Blanchard, M. Marinova, C. Lamonier, P. Nikulshin, Enhancing the hydrodesulfurization of 4,6-dimethyldibenzothiophene through the use of mixed MoWS₂ phase evidenced by HAADF, *Catal. Today*. 329 (2019) 24–34. doi:10.1016/j.cattod.2018.11.051.
- [42] C. Thomazeau, C. Geantet, M. Lacroix, M. Danot, V. Harle, EXAFS Characterization of New Active Phases for Catalytic Hydrotreatment: Two Cations Disulfide Layers in the Mo_xW_(1-x)S₂ Lamellar Solid Solution, *Oil Gas Sci. Technol. IFP*. 60 (2005) 781–790.
- [43] M. Girleanu, T. Alphazan, Z. Boudene, A. Bonduelle-Skrzypczak, C. Legens, A.S. Gay, C. Copéret, O. Ersen, P. Raybaud, Magnifying the morphology change induced by a nickel promoter in tungsten(IV) sulfide industrial hydrocracking catalyst: A HAADF-STEM and DFT study, *ChemCatChem*. 6 (2014) 1594–1598. doi:10.1002/cctc.201402115.

Chapter VI:

Evidence of modifications in growth of CoMoS particles by the addition of Citric Acid as chelating agent: A High resolution HAADF-STEM microscopy study.

Content Chapter VI: Evidence of modifications in growth of CoMoS particles by the addition of Citric Acid as chelating agent: A High resolution STEM-HAADF microscopy study

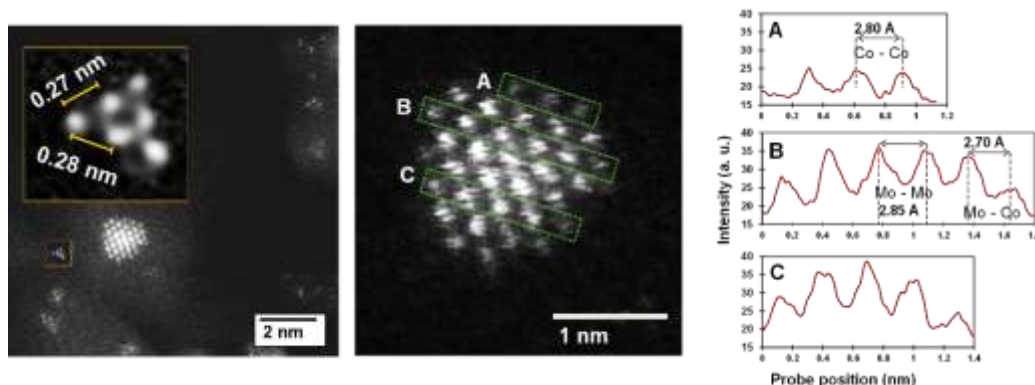
ABSTRACT	211
Graphical Abstract:.....	212
VI.1. INTRODUCTION	212
VI.2. EXPERIMENTAL SECTION	215
VI.2.1 Catalyst preparation.....	215
VI.2.2 Thiophene Hydrodesulfurization (HDS) Test.	216
VI.2.3 Low-Temperature CO Adsorption Followed by IR Characterization (IR/CO).....	216
VI.2.4 HRTEM and High-resolution Scanning Transmission Electron Microscopy - High Angular Annular Dark Field (HR STEM-HAADF).....	217
VI.3. RESULTS AND DISCUSSION	219
VI.3.1. IR/CO Characterizations of Sulfided CoMo(CA/M =0 and 2)/Al ₂ O ₃ Catalysts.	219
VI.3.2 Length and stacking degree determined by HRTEM analysis	220
VI.3.3 Effect of citric acid addition in the 2D-morphology of CoMo(CA/M=x)/Al ₂ O ₃	221
VI.3.4 Observation of used CoMo/Al ₂ O ₃ catalyst.	224
VI.3.5. Promoter location in CoMo(CA/M=2)/Al ₂ O ₃ catalyst.....	227
VI.4. CONCLUSION	230
VI.5. REFERENCES	231

ABSTRACT

In this work, we present atomic-scale images of Co promoted MoS₂ slabs supported on γ -Al₂O₃ obtained by High Resolution Scanning Transmission Electron Microscopy equipped with High Angular Annular Dark Field detector (HR STEM-HAADF). These images allow to study the effect of citric acid (CA) addition during preparation in the slab length and its stability during thiophene hydrodesulfurization (HDS) reaction. Thus, the observations, obtained for sulfide catalysts prepared without or with citric acid as chelating agent, evidenced strong decrease in size of the CoMoS nano-slabs as detected indirectly by the adsorption of CO followed by Infrared spectroscopy. Quantitative dispersion values were calculated from the images taking into account the true shape of the particles instead of the classical hexagonal shape hypothesis. Since STEM-HAADF facilitates the distinction of the elements according to their atomic number, the location of Co in the planar slabs was revealed by contrast variations and detected in the periphery of the nano-slab. The assignment of the nature of the observed atoms is confirmed by the variation of interatomic distance. Such observations allow to have a better understanding of the effect of chelating agent addition in promoted MoS₂ samples in order to explain their catalytic activity.

KEYWORDS: HR STEM-HAADF, CoMoS, Citric acid, CO adsorption, IR spectroscopy, Sulfide nanoparticles morphology, promoter location, used catalyst.

Graphical Abstract:



VI.1. INTRODUCTION

The increasing demand for low sulfur fuels puts pressure on the development of more active catalysts for production of clean transportation fuels. However, current petroleum deposits have higher sulfur concentration [1] and, strict fuel regulations are being established in both developed and developing countries [2]. To meet environmental standards, the oil industry is producing ultra-low sulfur diesel fuel (ULSD), a cleaner fuel containing a maximum of 10 parts per million (ppm) of sulfur. This level is likely to be decreased further by environmental legislation in the following years. Hydrodesulfurization (HDS) catalysts are mainly based on supported transition-metal disulfides (TMS) [3]. The TMS active phase is usually composed of molybdenum (Mo) or tungsten (W), promoted by cobalt (Co) or nickel (Ni). Although the non-promoted MoS₂ (WS₂) catalysts do not present high catalytic activity, a very significant increase in activity can be achieved by adding Co or Ni [4]. Then it is formed a bimetallic sulfide phase, typically called the CoMoS, NiMoS, or NiWS phase, whose structure corresponds to a two-dimensional (2D) nanolayer of Mo(W)S₂ decorated by the promoter at its edges [5]. These particles are often supported

on high specific surface area carriers such as γ -alumina (γ -Al₂O₃). The sulfide phase presents a lamellar structure, formed by layers of MS₂ (M = W, Mo). It is widely accepted that the promoter atoms occupy the edges of the MoS₂ nanoparticles, as described in the so-called CoMoS model [6–8]. Co-promoted MoS₂ nanostructured catalysts are traditionally used for hydrotreatment reactions. CoMo catalysts are some of the most used catalyst used for reaching ULSD levels. They have been the subject of investigation of numerous studies to determine their structure and to identify their active sites. Active sites in sulfided CoMoS catalysts are associated to the nano-slabs exposed edges, i.e. M-edge and S-edge. Low-temperature CO adsorption followed by infrared spectroscopy (IR/CO) is a technique that gives access to the site dispersion and then to their intrinsic activity. It has been intensively used to probe the edges sites of MoS₂ slabs on MoS₂/Al₂O₃ catalysts. Previous results of our group [9–11], have demonstrated that the S-edge is more active than the M-edge and also more keen to be promoted, thus the increase of S-edge/M-edge ratio derives into an increase of HDS activity. In this way, CoMoS slabs morphology can be expected to be related to the catalytic activity. The characterization of the concentration of these sites and the distinction of the promoted sites on the two different edges exposed by the MoS₂ slabs is essential to explain in fine their activity and their selectivity as well as the role of the parameters of preparation of these catalysts (effect of support, conditions for the preparation of the initial oxide phase, sulfurization conditions among others).

Recent advances in high-resolution scanning transmission electron microscopy (STEM) imaging have opened up the possibility of studying two-dimensional materials with atomic-level resolution and sensitivity. In addition to

conventional TEM-based modes, a very useful alternative to characterize materials at a sub-nanometer scale is HR STEM-HAADF. In this STEM mode, the annular detector collects high angle scattered electrons and the intensity of the image depends on the atomic number within the sample and is approximately proportional to $Z^{1.7-2}$ [12,13]. Due to its high sensitivity to heavy metal atoms (such as Mo, W and even Co and Ni), a STEM-HAADF analysis is the best alternative to evaluate parameters such as slab shape and structural characteristics.

Improving the dispersion degree of active metals is another crucial idea to enhance the activity of sulfided catalysts. Various methods have been developed to prepare well-dispersed catalysts. The addition of chelating agents have a special and efficient role in increasing the dispersion degree of Co(Ni)–Mo–S active phases [14–16] by interacting with the precursor ions and the support surface. However, the effect of the addition of citric acid in the preparation of promoted catalysts is always somewhat controversial since both increase [17] and decrease [18] in dispersion have been reported. Moreover, while in the non-promoted catalysts the variation of morphology with the addition of citric acid was indirectly observed by IR/CO method, i. e. the S-edge/M-edge ratio was closer to one after CA addition, for the promoted systems this is not still conclusive. In particular, a better distinction of the nature of the promoted sites by IR/CO is required. But, the results of catalytic activity as well as those of IR spectroscopy obtained on non-promoted and promoted samples, whether synthesized with or without citric acid, have a certain consistency, such as a considerable increase in catalytic activity and in total site concentration with citric acid addition.

In this work, the aim is to observe by direct image characterization of the slab morphology of sulfided Al₂O₃ supported CoMo catalysts prepared at the same conditions of synthesis and sulfidation that the ones for the catalytic application. The aim is a parallel study of the effect of citric acid by means of HR STEM-HAADF and IR/CO spectroscopy methods.

VI.2. EXPERIMENTAL SECTION

VI.2.1 Catalyst preparation

CoMo/Al₂O₃ catalysts, without and with citric acid (CA), were prepared by a one-step pore volume impregnation method. The aqueous impregnation solutions were prepared by dissolving a fixed amount of ammonium heptamolybdate tetrahydrate ((NH₄)₆Mo₇O₂₄·4H₂O MERCK) and cobalt (II) nitrate hexahydrate (Co(NO₃)₂·6H₂O Alfa Aesar) in deionized water at room temperature. Citric Acid (CA) was incorporated at this stage by dissolving the required amount (C₆H₈O₇·H₂O PROLABO) to obtain a CA/(M) = 0 or 2, (M=Mo+Co). Afterwards, the solution was added to the pretreated γ-Al₂O₃ support (SASOL, specific surface area of 252 m².g⁻¹ and pore volume of 0.84 mL.g⁻¹, precalcined in air at 723 K for 2 h), strongly shaken and left for maturation during 2 h. Finally, the catalysts were dried at 383 K for 16 h. Note that these catalysts were not calcined in order to keep the chelating agent if present in its initial form. Hereinafter, the CoMo/Al₂O₃ catalysts are denoted CoMo(CA/M=x)/Al₂O₃. X refers to the molar ratio of CA to Mo. x = 0 or 2.0. For these two CoMo(CA/M=x)/Al₂O₃ catalysts, the content of Mo was fixed to 3.2 Mo atoms per nm², and the Co/(Co + Mo) ratio was equal to 0.3.

VI.2.2 Thiophene Hydrodesulfurization (HDS) Test.

The CoMo(CA/M=2)/Al₂O₃ catalysts were then tested in thiophene hydrodesulfurization (HDS) reaction. A mass of 100 mg of catalysts (20–40 meshes, precisely weighted) was first sulfided with 30 mL·min⁻¹ 10% (v/v) H₂S/H₂ at 623 K (3 K·min⁻¹) for 2 h. Then, the catalytic activity of thiophene HDS was tested at 623 K using a 90 mL·min⁻¹ gas mixture consisting of 7.9% thiophene, 90.0% H₂, and 2.1% H₂S. The sample was left under these conditions during 72 h.

VI.2.3 Low-Temperature CO Adsorption Followed by IR Characterization (IR/CO).

The CoMoS edge sites of these catalysts were in-situ characterized by low-temperature CO adsorption followed by IR spectroscopy. First, the dried catalyst was grounded and pressed into a self-supported wafer (~10 mg for a disc of 2.01 cm²) precisely weighted and positioned into a quartz IR cell with CaF₂ windows. Prior to the adsorption experiments, the sample was sulfided in situ in the IR cell. For this, the catalysts were sulfided in a gas mixture containing 10% H₂S/H₂ (30 mL·min⁻¹) at 623 K for two hours with a heating rate of 3 K·min⁻¹. After sulfidation, the cell was flushed with Ar and evacuated up to P < 1·10⁻⁴ Pa until the catalyst reached room temperature. Then, CO adsorption was performed at low temperature (~100 K) to avoid any reaction with the catalysts surface. Small calibrated doses of CO were introduced into the IR cell until equilibrium pressure of 133 Pa. After each CO introduction, FTIR spectra were recorded with 256 scans and a resolution of 4 cm⁻¹ using Nicolet Nexus FT-IR spectrometer equipped with a MCT Detector.

VI.2.4 HRTEM and High-resolution Scanning Transmission Electron Microscopy - High Angular Annular Dark Field (HR STEM-HAADF).

All presented TEM images were taken using a double corrected JEOL ARM 200F cold FEG microscope operated at 200 kV. First, slab length and stacking degree distributions of sulfide slabs were determined manually by measuring around 300 slabs per sample from HRTEM images. The image treatment was performed using the commercial software from GATAN (DIGITALMICROGRAPH). The nanostructure and morphology of the MoS₂ slabs were analyzed by high resolution scanning transmission electron microscopy (HR STEM) using a high angle annular dark field (HAADF) detector. The catalyst precursors were firstly sulfided at 623 K (heating rate of 3 K min⁻¹) and 0.1 MPa for 2 h under a 30 mL·min⁻¹ flow of 10% H₂S/H₂. Then, to limit detrimental exposure to air, the sulfided catalysts were unloaded from the sulfidation reactor under argon flow and deposited into absolute ethanol. A few drops of the suspension of catalyst were put on a 300 mesh copper grid with holey carbon film. The STEM images presented in this manuscript were acquired in HAADF mode and the acquisition of an image lasted about 30 s with a resolution of 1024 pixels x 1024 pixels, (30 μs of exposure time for each spot in the scanning mode). The possible damage associated with the heating effects caused by the incident beam in the nanolayers is always a factor to check. In this study, it was not observed significant changes of particles morphology during the acquisition of the images at 200 kV with a beam current value of about 12 μA. Observations at 80 kV were also performed, but no significant differences in terms of slab stability were noticed. Therefore, it was

concluded that the operation with an acceleration of 200 kV is compatible with our purpose of morphological analysis.

In this work, following a similar approach than in our recent work [18], quantitative analysis of the images obtained in HAADF mode were performed in order to obtain statistical information about the morphology of the Co promoted MoS₂ slabs. On sulfided CoMo(CA/M=0)/Al₂O₃, sulfided CoMo(CA/M=2)/Al₂O₃ and used CoMo(CA/M=2)/Al₂O₃ (i.e. after 72h thiophene HDS reaction), a set of 20 isolated particles could be selected through contrast optimization of the images. In these isolated specimens, the outline of the shape was drawn and the corresponding particle lengths were measured, as well as the area of the particle with the help of the *Mesurim Pro* software. The limited number of particles analyzed by HAADF compared to HRTEM is explained by the difficulty to observe isolated specimens with faceted edges in these realistic samples. This is associated to the high metal loading present in this type of catalysts. Considering that for each slab, the dispersion is the ratio of edge atoms per total atoms, the calculated dispersion (D) values were obtained through the measurement of slab area and perimeter with the following equation (1):

$$D = \frac{\text{atoms at the edge}}{\text{total number of atoms per slab}} = \frac{P/d - N_c}{A/d^2} \quad (1)$$

Where:

D = dispersion

P = particle perimeter (nm)

d = atomic diameter Mo (nm)

N_c = number of corner atoms in the slab

A = particle area (nm²)

Calculating a numerical value of dispersion will reflect in a more straightforward way the effect of citric acid in the morphology of the studied catalysts than only observation.

VI.3. Results and discussion

VI.3.1. IR/CO Characterizations of Sulfided CoMo(CA/M =0 and 2)/Al₂O₃ Catalysts.

Low-temperature CO adsorption followed by in situ IR spectroscopy (IR/CO) allows distinguishing non-promoted (MoS₂) sites and promoted (CoMoS) sites [17,19,20] on the supported CoMo catalyst. **Figure 52** reports the IR/CO spectra obtained on the CoMo(CA/M=x)/Al₂O₃ catalysts. The two bands at around 2189 and 2156 cm⁻¹ are ascribed respectively to CO interaction with Lewis acid sites and hydroxyl groups of the Al₂O₃ support.

The strong band at around 2072 cm⁻¹ is attributed to the CO adsorption on Co-promoted MoS₂ edges (the so-called CoMoS sites), while the small shoulder at 2115 cm⁻¹ is attributed to CO adsorption on unpromoted MoS₂ sites [11,17]. In addition, in CoMo(CA/M =x)/Al₂O₃ sample, a second band in the promoted massive is observed at 2060 cm⁻¹, assigned by Dominguez *et al.* [21] to partially promoted S-edge. It was observed that the CO adsorption bands at 2072 cm⁻¹ and 2060 cm⁻¹ increase with the addition of citric acid, demonstrating that citric acid favors strongly the formation of CoMoS sites.

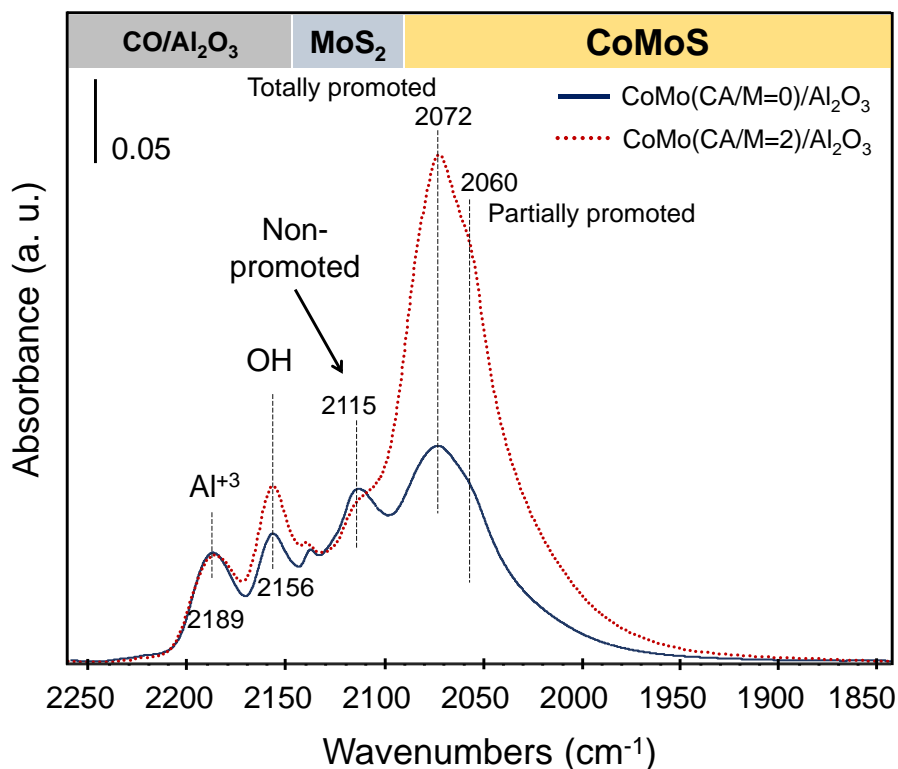


Figure 52. IR spectra of CO adsorption ($-173\text{ }^{\circ}\text{C}$ and 133 Pa CO at equilibrium) on $\text{CoMo}(\text{CA}/\text{M}=0)/\text{Al}_2\text{O}_3$ and $\text{CoMo}(\text{CA}/\text{M}=2)/\text{Al}_2\text{O}_3$ catalysts sulfided with 10% (v/v) $\text{H}_2\text{S}/\text{H}_2$ at atmospheric pressure and $350\text{ }^{\circ}\text{C}$ for 2 h.

This effect on promoted edge site concentration has previously been reported with other chelating agents such as ethylene diaminetetraacetic acid (EDTA) [22] and nitrilo triacetic acid (NTA) [23,24].

VI.3.2 Length and stacking degree determined by HRTEM analysis

A careful process of measuring the length of the slabs present in each sample was carried out modifying the contrast to be sure of seeing smallest particles. The addition of citric acid leads to a decrease of the average slab length from $2.90 \pm 0.12\text{ nm}$ to $1.70 \pm 0.10\text{ nm}$. The distribution in length is given in **Figure 53**.

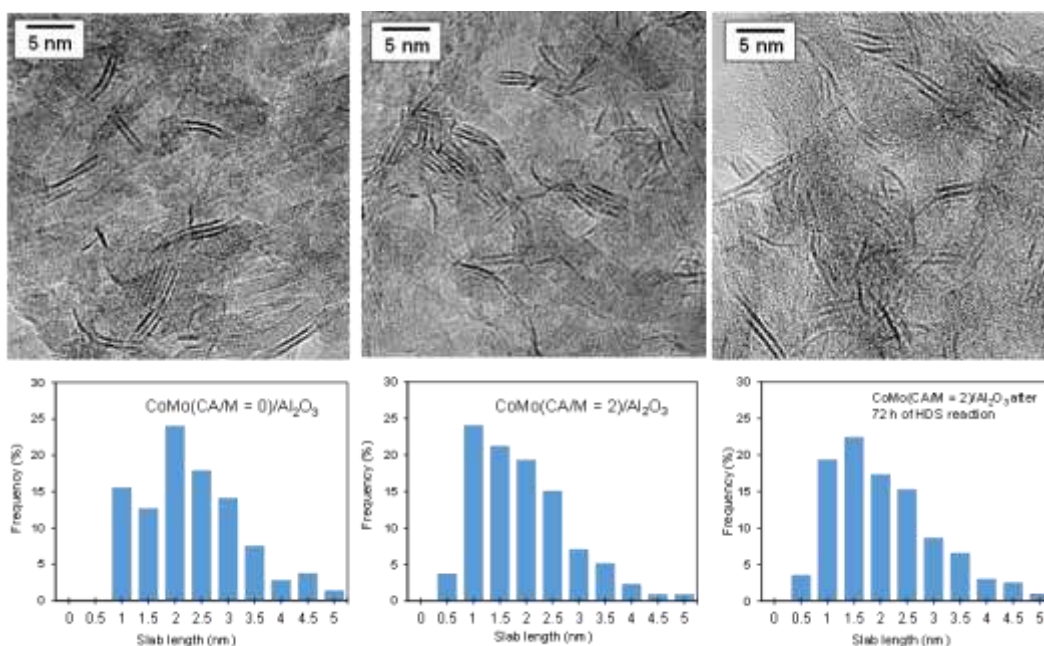


Figure 53. HRTEM analysis of slab length distribution: images of CoMo(CA/M=0)/Al₂O₃, CoMo(CA/M=2)/Al₂O₃ and CoMo(CA/M=2)/Al₂O₃ after 72 h of thiophene reaction.

Also an increase of the average stacking number (1.80 ± 0.04 to 2.20 ± 0.05) is noticed. The presence of particles stacked in two or more slabs is significant in both samples, but the amount of the rather small monolayer slabs observed in the CoMo(CA/M=2)/Al₂O₃ sample was much higher than in the CoMo(CA/M=0)/Al₂O₃ sample. Such results are in accordance with previously reported results on Mo catalysts and ascribed to the reduced interaction between the (Co)MoS slabs and the support due to the addition of citric acid [17].

VI.3.3 Effect of citric acid addition in the 2D-morphology of CoMo(CA/M=x)/Al₂O₃

Figure 54 presents the HR STEM-HAADF micrographs of sulfided CoMo(CA/M=0)/Al₂O₃ (**Figure 54 A-C**) and CoMo(CA/M=2)/Al₂O₃ (**Figure 54 D-F**) respectively. As expected for the HAADF mode, the observed particles have a good quality contrast and, therefore, the acquisition parameters used are suitable for revealing the 2D morphology of the slabs in these industrial grade catalysts. On a large field of view, sample CoMo(CA/M=0)/Al₂O₃ consists of CoMoS slabs that are distributed over the alumina support in the form of plates. Higher contrast in some zones of both sets of images are attributed to an increase of metal density. This is observed more in sample CoMo(CA/M=0)/Al₂O₃ and is related to agglomerated or stacked slabs. On the other hand, striking changes are observed for the sample that was prepared in presence of citric acid. The particles observed in the CoMo(CA/M=2)/Al₂O₃ sample are characterized by their relatively small size compared to the ones observed in CoMo(CA/M=0)/Al₂O₃, and in many occasions, what resembles groups of a few atoms and even individual atoms dispersed all over the support are observed. The zoom-in in **Figure 54-E**), puts in evidence a particle with dispersion of 1 i.e. whose all the atoms of the slab are exposed. Their interatomic distances, that are of the order of 2.7 Å, are in good agreement with the ones expected for Mo-Mo interatomic distances of MoS₂ disulfide [4,25]. Recently, we reported a similar observation for non-promoted MoS₂ prepared as well with and without citric acid as a chelating agent.

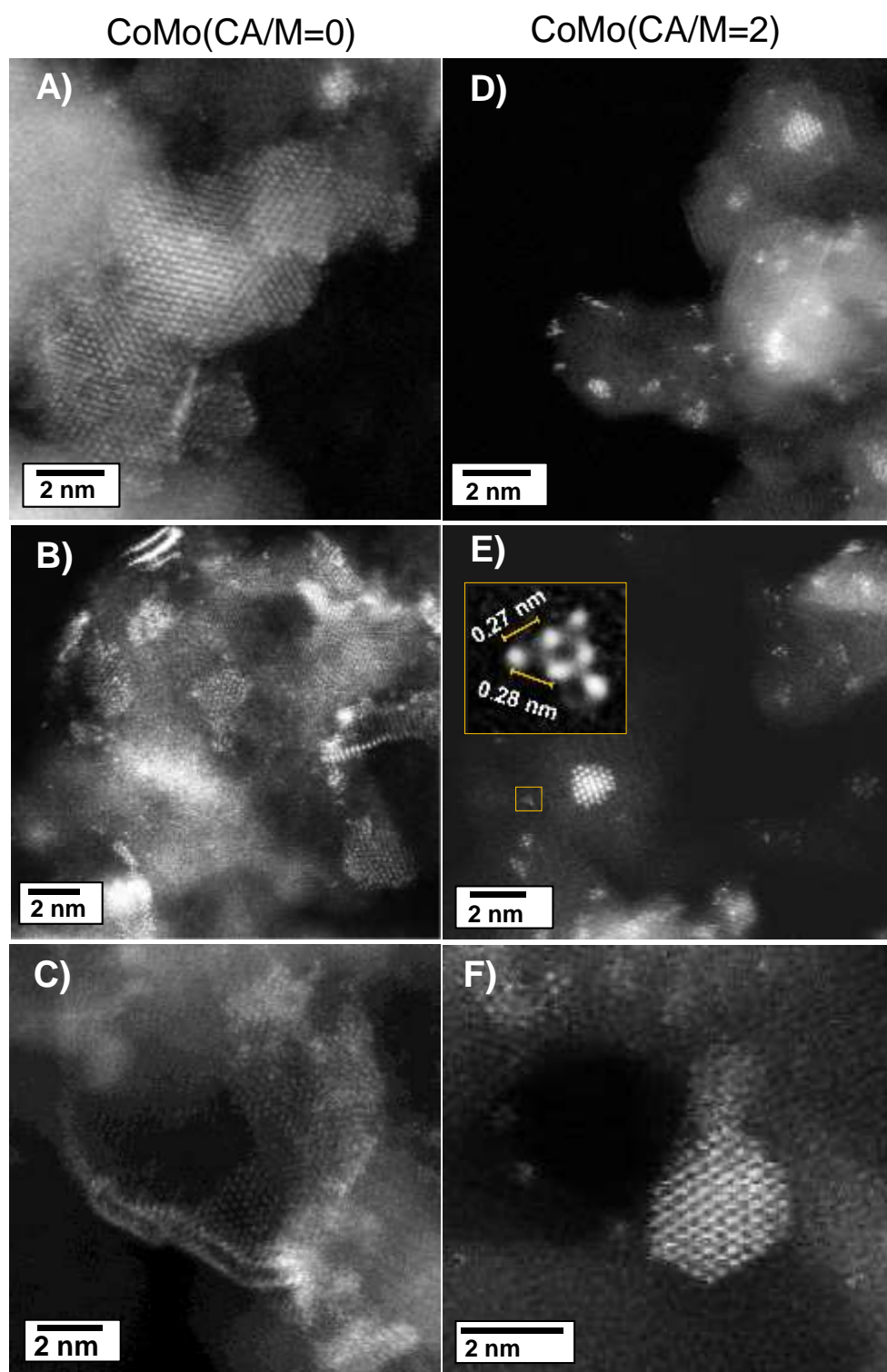


Figure 54. HR STEM-HAADF micrographs of CoMoS particles of CoMo(CA/M=0)/Al₂O₃ (A-C) and CoMo(CA/M=2)/Al₂O₃ (D-F) of different zones. Inset E: zoom of particle with dispersion degree of 1.0.

To better understand the improvement of the dispersion degree measurements of the length and perimeter were carried out in each one of the samples, and using the **Eq. 1**, it was found that the addition of citric acid decreases the average length from 2.60 ± 0.5 to 1.40 ± 0.5 nm. The calculated particle dispersion (D) value passes from 48% for CoMo (CA/M=0)/Al₂O₃ to 80% for CoMo (CA/M=2)/Al₂O₃. **Table 1** gathers together the measured and calculated parameters for each of the analyzed samples. Since the catalytic HDS reaction activity is ascribed to the coordinatively unsaturated sites (CUS) of the slabs, located in the edges of the slab, an increase of dispersion is therefore associated to an increase in activity.

VI.3.4 Observation of used CoMo/Al₂O₃ catalyst.

Very often TMS catalysts are analyzed after the sulfidation stage, nevertheless, sometimes the fact that during the catalytic reaction stage the catalyst is contacted with hydrogen and also with H₂S is overlooked. One question that arises is the nature and stability of the very small agglomerates observed in the sulfided CoMo (CA/M=2)/Al₂O₃ catalyst. If we take into account that during the catalytic reaction the catalyst is in contact with H₂ and with H₂S present as a by-product, could there be a subsequent transformation or reorganization of such agglomerates? To answer this, a sample was analyzed after being subjected for 72 hours of HDS test in order to know if the nanoslabs undergo any alteration. Thus, this analysis is one way to observe their stability against prolonged reaction conditions.

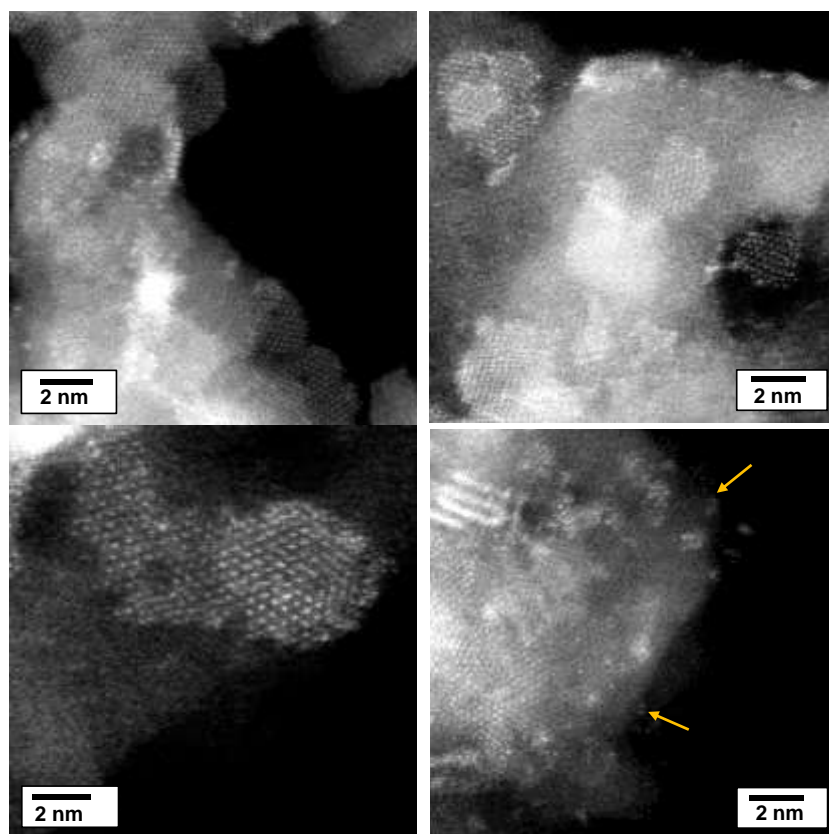


Figure 55. HR STEM-HAADF micrographs of CoMoS particles of CoMo(CA/M=2)/Al₂O₃ after 72 h of thiophene HDS reaction at 623K. The arrows indicate that the few atoms agglomerates observed in CoMo(CA/M=2)/Al₂O₃ after sulfidation are still present.

The HAADF images of **Figure 55** reveal that no radical change in the shape of the slabs occurs upon HDS reaction. The agglomerates of a few atoms previously observed in the freshly sulfided CoMo(CA/M=2)/Al₂O₃ catalyst are still observed in the used catalyst. Indeed, one can see the outline of some isolated particles. These results suggest that the subnanometric particles have a good stability under reaction conditions.

Figure 56 allows the comparison of the three promoted samples, sulfided CoMo(CA/M=0)/Al₂O₃, sulfided CoMo(CA/M=2)/Al₂O₃ and used CoMo(CA/M=2)/Al₂O₃ after thiophene HDS reaction in terms of length

distribution after processed STEM-HAADF images. Complementary, **Table I** give the values of average length and stacking obtained by HRTEM for the three samples and the average length and dispersion obtained by STEM-HAADF for the three samples. Comparison between these values confirm the stability of the CoMo(CA/M=2) catalyst under reaction conditions.

Table X. Parameters calculated from the HRTEM and HR STEM-HAADF images for the γ -Al₂O₃ supported Catalyst.

Mode	Parameters	CoMo(CA/M=0)	CoMo(CA/M=2)	CoMo(CA/M=2) after 72 h HDS reaction
TEM	Average length (nm)	2.90 ± 0.12	1.70 ± 0.10	1.94 ± 0.2
	Stacking	1.80 ± 0.04	2.20 ± 0.05	2.26 ± 0.05
HAADF	Average length (nm)	2.60 ± 0.50	1.40 ± 0.50	1.60 ± 0.50
	Dispersion (measured)	0.48 ± 0.08	0.80 ± 0.08	0.70 ± 0.08

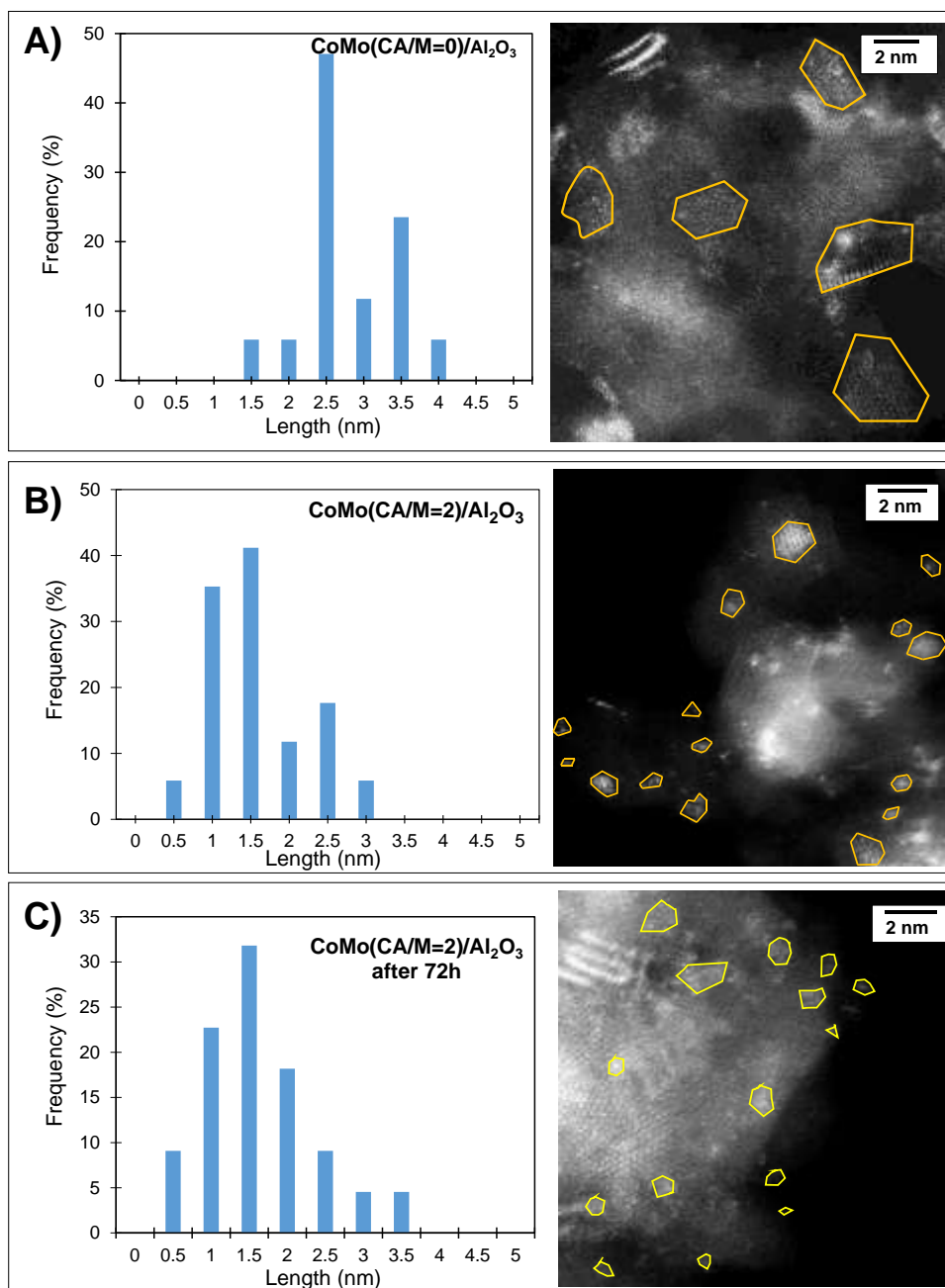


Figure 56. Distribution of the measured length and STEM-HAADF images of the particles of CoMo(CA/M=0)/Al₂O₃, CoMo(CA/M=2)/Al₂O₃ and CoMo(CA/M=2)/Al₂O₃ after thiophene HDS reaction (72h).

VI.3.5. Promoter location in CoMo(CA/M=2)/Al₂O₃ catalyst

A close inspection of the contrast in some of the particles observed in a HAADF image revealed interesting facts. First, atoms located in the periphery of the

particle present a different contrast in comparison to the ones located in the inner part of the particle. This is a suggestion of where the promoter is located.

It has to be mentioned that one of the restrictive factors for obtaining chemical information of the slabs is related to the limiting amount of matter. In many cases these nanoparticles are formed only by one or a few atomic planes and the necessary exposure time per pixel for recording a chemical map by EELS or EDX with correct signal/noise ratio, has to be much longer than for the STEM-HAADF image acquisition. Therefore, after a long exposures, the slabs are easily damaged. Furthermore, if we consider the added difficulty of the charge effect of the insulator alumina carrier, achieving this analysis becomes an extremely hard task. One way to overcome these problems, is to take advantages of the HAADF mode by analyzing the contrast variation associated to the atomic number [26,27]. For this, it is necessary to select a well-defined and isolated particle or edge and then, to process intensity profiles of an atomic row. **Figure 57** shows three intensity profiles obtained for a CoMo(CA/M=2)/Al₂O₃ nanoslab. We are assuming that due to the clearly visible atomic arrangement that this particle presents, we are talking about a single slab. Stacking of slabs would lead to a more complex pattern due to the expected shift of the slabs. The bar profile drawn along the less bright atomic row (A) revealed homogeneous brightness intensity and interatomic distances of ~2.80 Å. Next, this same bar profile was applied to a lower row of atoms (B). Starting from right to left, it was detected that the atoms at the beginning and at the end of the row present less intensity than the ones in the inner part. When the interatomic distances were measured, it was found that the distance

between the penultimate and the last atom of the row, corresponds to 2.70 Å, while the interatomic distance of the brightest atoms is greater, corresponding to 2.85 Å. Similar behavior was detected on the row of atoms (C). This variation in distance was explained by Deepak *et al.* in terms of the substitution of Co in the Mo lattice, occupying the Mo sites in the periphery of the particle. It is important to mention that in their work, the contrast analysis was carried out along a row of the bright atomic columns [28]. Instead, we present an atom by atom contrast measurement.

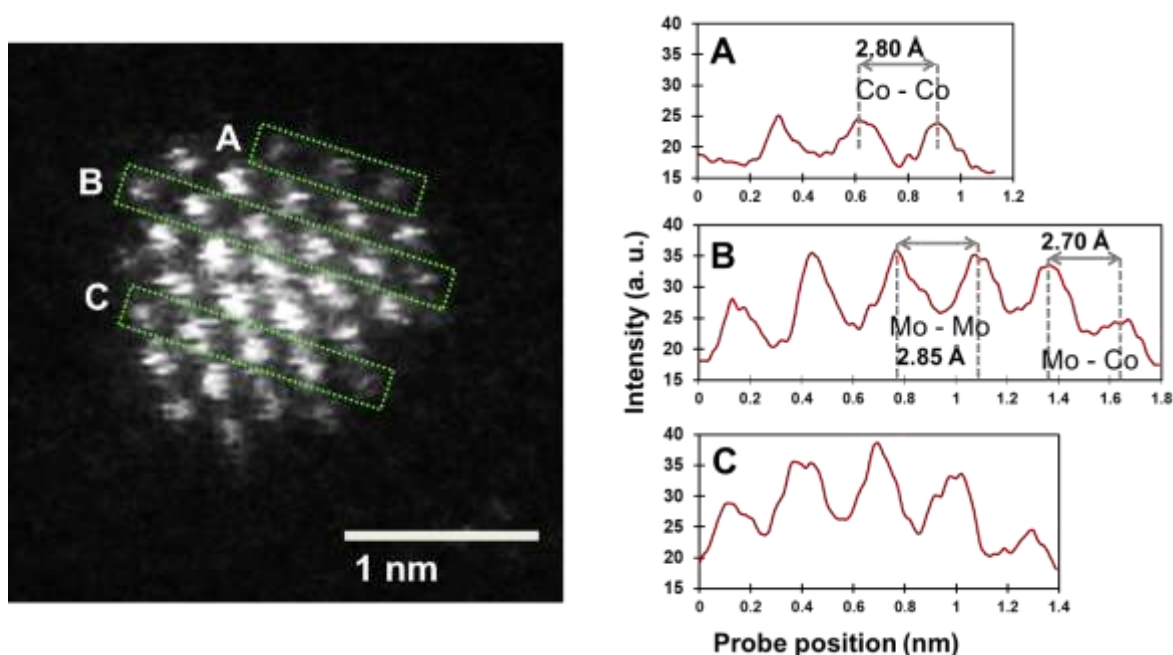


Figure 57. STEM-HAADF image of sulfided CoMo(CA/M=2)/Al₂O₃ with the corresponding intensity profiles measured at different regions of the slab. The spacing between the Co-Co, Mo-Mo and Co-Mo was revealed by this profile.

The variations on the HAADF contrast cannot be explained on the basis of thickness changes since no overlapping planes are observed in this particular slab, we are still able to see the interatomic spacing while in a stacked particle

this would not be observable, due to the superposition of the slabs. Thus the contributions are originated from compositional variations, revealed by the difference in atomic number (Z) that exists among molybdenum (atomic number = 42) and cobalt (atomic number = 27).

VI.4. CONCLUSION

STEM-HAADF unequivocally demonstrates that adding citric acid in the preparation of CoMo catalysts significantly reduces the size of CoMoS nanoslabs. HR STEM-HAADF highlighted that the addition of citric acid changes shape and size of the nanoslabs. Since there is a greater amount of particles in the catalyst prepared with AC compared to the preparation without AC, there is a greater amount of exposed sides. This result goes hand in hand with the infrared spectra results observed, where the band associated with the active CoMoS sites increases considerably. Numerous agglomerates formed by a few atoms (clusters) with a high degree of dispersion are detected in the sulfide sample CoMo(CA/M=2)/Al₂O₃. These clusters are proved to be stable after being subjected to a thiophene HDS reaction for 72 hours in the same way as the nanometric ones. This demonstrates that the catalysts retain their integrity during the catalytic reaction process and therefore that analyzing the catalyst after sulfurization is equivalent to analyzing the catalyst under HDS operational conditions. Edge contrast differences indicate the location of the promoter at the periphery of the particle in accordance with the decoration model.

VI.5. REFERENCES

- [1] Sulfur production report by the United States Geological Survey, No Title, Minerals.Usgs.Gov. (2017).
- [2] EIA, Annual Energy Outlook 2019 with projections to 2050, USA, 2019. www.eia.gov/aeo.
- [3] T. Alphazan, A. Bonduelle-Skrzypczak, L. Legens, A.-S. Gay, Z. Boudene, M. Girleanu, O. Ersen, C. Cope, P. Raybaud, Highly Active Nonpromoted Hydrotreating Catalysts through the Controlled Growth of a Supported Hexagonal WS₂ Phase, *ACS Catal.* 4 (2014) 42. doi:10.1021/cs501311m.
- [4] F.L. Deepak, R. Esparza, B. Borges, X. Lopez-Lozano, M. Jose-Yacaman, Direct Imaging and Identification of Individual Dopant Atoms in MoS₂ and WS₂ Catalysts by Aberration Corrected Scanning Transmission Electron Microscopy, *ACS Catal.* 1 (2011) 537–543. doi:10.1021/cs100141p.
- [5] F.E. Topsøe, H., Clausen, B. S., & Massoth, *Catalysis Science and Technology*, Springer, Berlin, 1996. doi:doi.org/10.1007/978-3-642-61040-0_1.
- [6] F. Besenbacher, M. Brorson, B.S. Clausen, S. Helveg, B. Hinnemann, J. Kibsgaard, J. V. Lauritsen, P.G. Moses, J.K. Nørskov, H. Topsøe, Recent STM, DFT and HAADF-STEM studies of sulfide-based hydrotreating catalysts: Insight into mechanistic, structural and particle size effects, *Catal. Today.* 130 (2008) 86–96. doi:10.1016/j.cattod.2007.08.009.
- [7] H. Topsøe, B.S. Clausen, Importance of Co-Mo- S Type Structures in Hydrodesulfurization, *Catal. Rev. Sci. Eng.* 26 (1984) 395–420. doi:10.1080/01614948408064719.
- [8] S. Topsøe, H., Clausen, B. S., Candia, R., Wivel, C., & Mørup, In Situ Mössbauer Emission Spectroscopy Studies of Unsupported and Supported Sulfided Co-Mo Hydrodesulfurization Catalysts: Evidence for and Nature of a Co-Mo-S Phase, *J. Catal.* 68 (1981) 433–452. doi:10.1016/0021-9517(81)90114-7.
- [9] J. Chen, F. Maugé, J. El Fallah, L. Oliviero, IR spectroscopy evidence of MoS₂ morphology change by citric acid addition on MoS₂/Al₂O₃ catalysts – A step forward to differentiate the reactivity of M-edge and S-edge, *J. Catal.* 320 (2014) 170–179. doi:10.1016/j.jcat.2014.10.005.
- [10] J. Chen, L. Oliviero, X. Portier, F. Maugé, On the morphology of MoS₂ slabs on MoS₂/Al₂O₃ catalysts: the influence of Mo loading, *RSC Adv.* 5 (2015) 81038–81044. doi:10.1039/C5RA14768A.

- [11] A. Travert, C. Dujardin, F. Maugé, S. Cristol, J.F. Paul, E. Payen, D. Bougeard, Parallel between infrared characterisation and ab initio calculations of CO adsorption on sulphided Mo catalysts, *Catal. Today*. 70 (2001) 255–269.
- [12] M. Girleanu, S. Lopes Silva, D. Ihiwakrim, A. Chaumonnot, A. Bonduelle-Skrzypczak, F. Lefebvre, V. Dufaud, A.S. Gay, O. Ersen, HAADF-STEM high-resolution study of nanometric MoS₂ inside mesoporous SBA-15, *Microporous Mesoporous Mater.* 217 (2015) 190–195. doi:10.1016/j.micromeso.2015.06.021.
- [13] S.J. Nellist, P. D., & Pennycook, Direct Imaging of the Atomic Configuration of Ultradispersed Catalysts, *Science* (80-). 274 (1996) 413–415. doi:10.1126/science.274.5286.413%0AArticle.
- [14] K. Al-Dalama, A. Stanislaus, A Comparative Study of the Influence of Chelating Agents on the Hydrodesulfurization (HDS) Activity of Alumina and Silica-Alumina-Supported CoMo Catalysts, *Energy and Fuels*. 20 (2006) 1777–1783. doi:10.1021/ef060125a.
- [15] R. Cattaneo, T. Shido, R. Prins, The Relationship between the Structure of NiMo/SiO₂ Catalyst Precursors Prepared in the Presence of Chelating Ligands and the Hydrodesulfurization Activity of the Final Sulfided Catalysts, *J. Catal.* 185 (1999) 199–212. doi:10.1006/JCAT.1999.2492.
- [16] S. Badoga, K.C. Mouli, K.K. Soni, A.K. Dalai, J. Adjaye, Beneficial influence of EDTA on the structure and catalytic properties of sulfided NiMo/SBA-15 catalysts for hydrotreating of light gas oil, *Appl. Catal. B Environ.* 125 (2012) 67–84. doi:10.1016/j.apcatb.2012.05.015.
- [17] J. Chen, J. Mi, K. Li, X. Wang, E. Dominguez Garcia, Y. Cao, L. Jiang, L. Oliviero, F. Oise, Role of Citric Acid in Preparing Highly Active CoMo/Al₂O₃ Catalyst: From Aqueous Impregnation Solution to Active Site Formation, *Ind. Eng. Chem. Res.* 56 (2017) 14172–14181. doi:10.1021/acs.iecr.7b02877.
- [18] L. Zavala-sanchez, X. Portier, F. Maugé, L. Oliviero, High Resolution STEM-HAADF microscopy on γ -Al₂O₃ supported MoS₂ catalyst – Proof by image of the changes in dispersion and morphology of the slabs with addition of citric acid, *Nanotechnology*. (2019) 1–10.
- [19] A. Travert, C. Dujardin, F. Maugé, E. Veilly, S. Cristol, J.-F. Paul, E. Payen, CO Adsorption on CoMo and NiMo Sulfide Catalysts: A Combined IR and DFT Study, *Phys. Chem. B*. 110 (2006) 1261–1270. doi:10.1021/jp0536549.
- [20] F. Maugé, J.C. Lavalley, FT-IR Study of CO Adsorption on Sulfided Mo/ Al₂O₃ Unpromoted or Promoted by Metal Carbonyls: Titration of Sites, *J. Catal.* 137

- (1992) 69–76. doi:10.1016/0021-9517(92)90139-9.
- [21] E.D. Garcia, Effet du support sur la morphologie et l'activité des catalyseurs d'hydrodésulfuration, Université de Caen, 2017.
- [22] M.A. Lélías, E. Le Guludec, L. Mariey, J. van Gestel, A. Travert, L. Oliviero, F. Maugé, Effect of EDTA addition on the structure and activity of the active phase of cobalt–molybdenum sulfide hydrotreatment catalysts, *Catal. Today*. 150 (2010) 179–185. doi:10.1016/J.CATTOD.2009.07.107.
- [23] M.A. Lélías, J. van Gestel, F. Maugé, J.A.R. van Veen, Effect of NTA addition on the formation, structure and activity of the active phase of cobalt–molybdenum sulfide hydrotreating catalysts, *Catal. Today*. 130 (2008) 109–116. doi:10.1016/J.CATTOD.2007.07.018.
- [24] M.A. Lélías, P.J. Kooyman, L. Mariey, L. Oliviero, A. Travert, J. Van Gestel, J.A.R. Van Veen, F. Maugé, Effect of NTA addition on the structure and activity of the active phase of cobalt-molybdenum sulfide hydrotreating catalysts, (2009). doi:10.1016/j.jcat.2009.07.006.
- [25] B. Baubet, M. Girleanu, A.S. Gay, A.L. Taleb, M. Moreaud, F. Wahl, V. Delattre, E. Devers, A. Hugon, O. Ersen, P. Afanasiev, P. Raybaud, Quantitative Two-Dimensional (2D) Morphology-Selectivity Relationship of CoMoS Nanolayers: A Combined High-Resolution High-Angle Annular Dark Field Scanning Transmission Electron Microscopy (HR HAADF-STEM) and Density Functional Theory (DFT) Study, *ACS Catal.* 6 (2016) 1081–1092. doi:10.1021/acscatal.5b02628.
- [26] M. Nikulshina, A. Mozhaev, C. Lancelot, P. Blanchard, M. Marinova, C. Lamonier, P. Nikulshin, Enhancing the hydrodesulfurization of 4,6-dimethyldibenzothiophene through the use of mixed MoWS₂ phase evidenced by HAADF, (2018). doi:10.1016/j.cattod.2018.11.051.
- [27] M. Nikulshina, A. Mozhaev, C. Lancelot, M. Marinova, P. Blanchard, E. Payen, C. Lamonier, P. Nikulshin, MoW synergetic effect supported by HAADF for alumina based catalysts prepared from mixed SiMo_nW_{12-n} heteropolyacids, *Appl. Catal. B Environ.* 224 (2018) 951–959. doi:10.1016/j.apcatb.2017.11.049.
- [28] F.L. Deepak, R. Esparza, B. Borges, X. Lopez-Lozano, M. Jose-Yacaman, Direct Imaging and Identification of Individual Dopant Atoms in MoS₂ and WS₂ Catalysts by Aberration Corrected Scanning Transmission Electron Microscopy, *ACS Catal.* 1 (2011) 537–543. doi:10.1021/cs100141p.

Chapter VII:
**General Conclusion and
Perspectives**

VII.1. General Conclusion

In order to develop more efficient catalysts, a fundamental approach should include cutting edge characterization techniques. The aim of this doctoral project was to improve the understanding at atomic and molecular level of the parameters that modify the morphology of transition metal disulfide (TMS) nanoslabs supported on alumina.

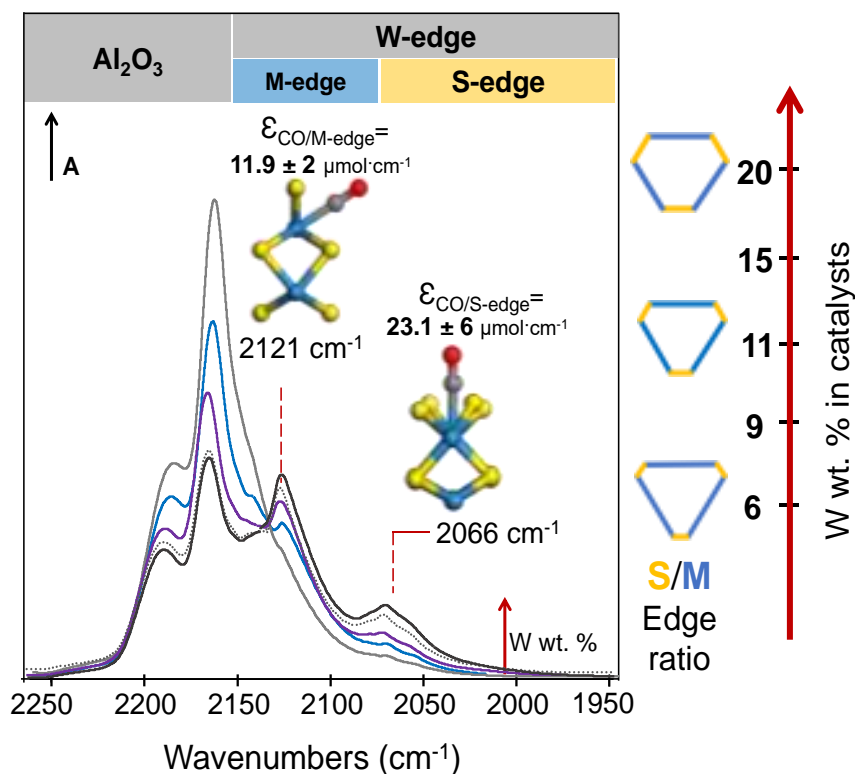
By using cutting edge characterization techniques, special efforts were made to understand the factors that affect the sulfide phase morphology and to show the consequences of the morphological changes on the catalytic activity. Therefore, it was studied in parallel in situ low temperature CO adsorption followed by IR spectroscopy (CO/IR) with advanced characterization techniques as Density Functional theory (DFT) calculations and High Resolution Scanning Transmission Electron Microscopy in the High Angular Annular Dark Field mode (HR STEM HAADF). Hence, the nature of the active phase was investigated, especially the slab morphology in the unpromoted (Mo and W) systems and the location of the promoter in the promoted in (CoMo and NiW) systems.

We have learned that HR STEM HAADF allows a direct observation of the shape of few sulfided slabs while IR/CO gives an indirect detection of the shape of a large number of sulfided slabs.

In all the experiments presented in this manuscript, the characterization techniques were carried out respecting exactly the same conditions of synthesis and sulfidation than the ones for the catalytic application. The main highlights of this work are listed below.

1) Structure and quantification of edge sites of WS₂/Al₂O₃ catalysts coupling IR/CO spectroscopy and DFT calculations

Carbon monoxide adsorption on alumina-supported sulfided W catalysts was studied by means of IR spectroscopy pairing with DFT calculations. The parallel between experimental and calculated data allowed us to attribute, for the first time, the two $\nu(\text{CO})$ bands observed at 2121 cm⁻¹ and about 2066 cm⁻¹ to CO adsorbed on the M-edge and S-edge sites of the WS₂ slabs, respectively.



The integrated molar attenuation coefficients of CO associated with the M- and S-edge sites were successfully determined, allowing determination of the WS₂ morphology. Increasing the W loading (3-20 wt% W) allows going from an almost pure triangle exhibiting mostly M-edge to a truncated hexagon.

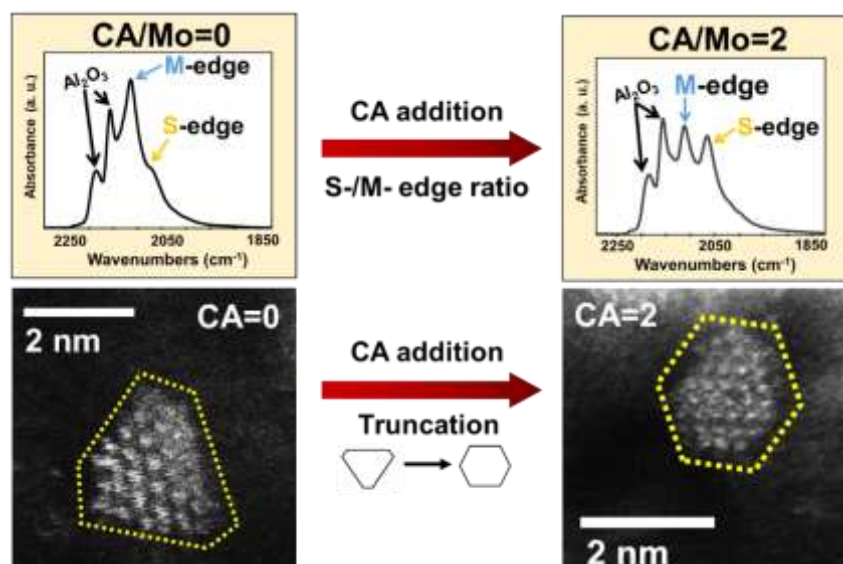
A parallel between the experiments and DFT calculation of CO adsorption on W and Mo sulfide catalysts provides evidence of many similarities between the two

systems. On both TMS, CO adsorption gives rise to two main $\nu(\text{CO})$ bands separated by about 50 cm^{-1} that allowed to discriminate M-edge and S-edge sites. For M load corresponding to a monolayer coverage on alumina, Mo and W sulfide slabs present a similar shape, this is, a truncated hexagon.

2) High Resolution STEM-HAADF microscopy on $\gamma\text{-Al}_2\text{O}_3$ supported MoS_2 catalyst – Proof by image of the changes in dispersion and morphology of the slabs with addition of citric acid.

One guideline of this work was to characterize catalysts prepared in conditions close to those used for applications and not specifically chosen to meet the requirements of these advanced characterization techniques. This has made the observation of the shape of sulfide slabs by electron microscopy very delicate. However, atomic-scale images of $\gamma\text{-Al}_2\text{O}_3$ supported Mo nanoparticles were obtained by HR STEM-HAADF for sulfide catalysts prepared without and with citric acid. HR STEM-HAADF observations and subsequent exploitation highlighted that the addition of citric acid during the preparation step of Mo catalysts changes the shape of the MoS_2 nanoslabs. Indeed, the S-edge/M-edge ratio obtained by HR STEM-HAADF study increased significantly with addition of citric acid as previously determined by the IR/CO method. Moreover, the study shows that HR STEM-HAADF makes it easier to distinguish the smallest slabs ($< 2 \text{ nm}$) from the oxide support. So, this HR STEM-HAADF study is a proof by image of the results obtained by the IR/CO method. The direct observations validate the variation of morphology of MoS_2 nanoslabs detected indirectly by the IR/CO method thus consolidating also the $\nu(\text{CO}/\text{Mo})$ band attribution to CO interacting on the two different edges. Such morphology

change is of great importance to the catalytic performance, as it has been reported that M-edge and S-edge present different reactivity in hydrodesulfurization (HDS) reactions.



As a consequence, this study strengthens the importance of coupling techniques like microscopy that allows a direct observation of the shape of a group of sulfided slabs and IR spectroscopy that allows an indirect detection of the shape but of a large number of sulfided slabs.

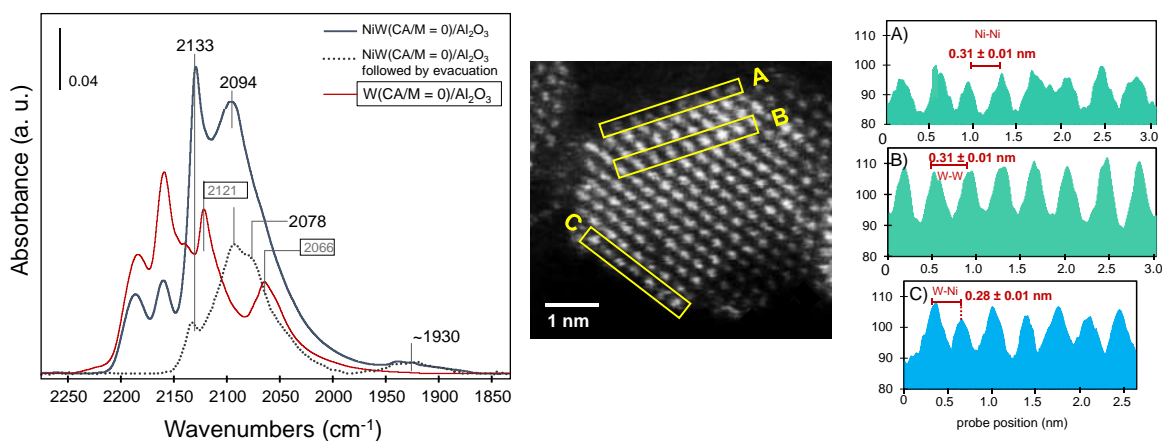
The present study opens the way for further investigations on promoted catalysts comparable to the ones used in the HDS industry.

3) Morphology and promoter location in NiW and CoMo catalysts: parallel between IR/CO spectroscopy and HR STEM-HAADF microscopy.

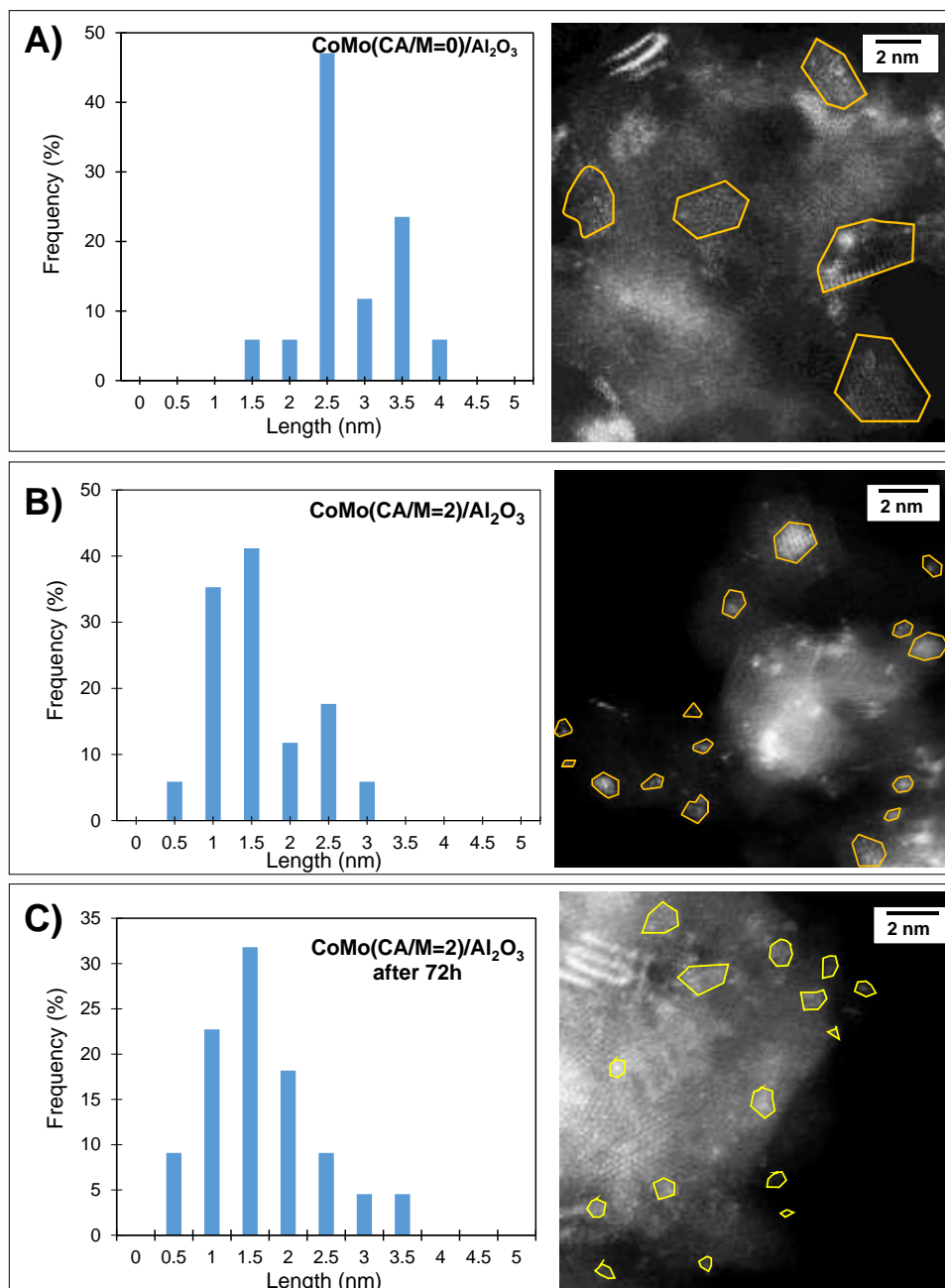
The effect of citric acid (CA) in the morphology of Ni promoted WS₂ and Co promoted MoS₂ particles supported on γ -Al₂O₃ was investigated. Atomic-scale images of sulfide slabs supported on γ -Al₂O₃ were obtained by HR STEM-HAADF. The aim of this study was to obtain an atomic level analysis of the

structure of the active sites of Ni promoted WS_2 particles supported on $\gamma-Al_2O_3$ prepared with citric acid. For both systems, thiophene HDS test shows that citric acid addition markedly increases the catalytic activity. Parallel with IR/CO indicates that this is a consequence of the increased formation of NiWS or CoMoS sites in presence of citric acid.

A careful analysis of the IR/CO spectra of NiW catalysts showed that the NiWS sites give rise to three bands that can be assigned to partially promoted (2094 and 2078 cm^{-1}) and to totally promoted NiWS sites (2133 cm^{-1}).



High resolution microscopy showed that citric acid addition favors the formation of very small particles of about 1 nm and even smaller in freshly sulfided NiW and CoMo catalysts. Analysis of a used CoMo(CA/M=2) catalyst after 72 h of thiophene HDS test proved the dispersion to be stable after such test. In this case, this demonstrates that the catalysts maintain their integrity during the catalytic reaction process and, therefore, analyzing the catalyst after sulfidation is equivalent to analyzing the catalyst under HDS operating conditions.



Moreover, by analyzing contrast and measurement of interatomic distances on HR STEM HAADF images of sulfide particles, it was possible to identify the nature of the core and edge atoms of the W- and Mo-based particles. On both systems, it appears the edges of the particles could be either fully promoted with detection of only Ni or Co, or partially promoted with detection of both Ni

and W, or Co and Mo atoms. This is in accordance with the IR spectroscopy that account for both the presence of totally and partially promoted edges.

STEM-HAADF unequivocally demonstrates that adding citric acid in the preparation of NiW and CoMo catalysts significantly reduces the size of the nano-slabs. This result goes hand in hand with the infrared spectra results observed, where the band associated with the active NiWS and CoMoS sites increases considerably.

4) Atomic scale characterization of sulfide slab sites through IR/CO, DFT and HR STEM-HAADF

The results of this PhD reveal the singularities and the strong complementarities of IR/CO, DFT and HR STEM-HAADF.

IR/CO spectroscopy can explain the nature of sulfide edge sites. Indeed, $\nu(\text{CO})$ bands allow discriminating unpromoted sites on M- and on S-edges, from promoted sites. This work even points out that partially and completely promoted can be distinguished by CO/IR. It should be mentioned that DFT can be very helpful for establishing the band assignments. From determination of molar attenuation coefficients of the $\nu(\text{CO})$ bands (that is often not straightforward to measure), quantification of the sulfide sites can be obtained. Hence, the amount of M- and on S-edges of unpromoted catalysts can be calculated and thus, the sulfide slab morphology. It appears that CA addition change the slab morphology from truncated triangle to a hexagon. It should be noted that the IR/CO technique gives global information on the sulfide slabs of the catalysts.

As for HR STEM-HAADF, it provides atomic scale images of the sulfided particles and even evidences the presence of small groups (clusters) of few atoms. The shape of the slab, the dispersion of the slab, as well as their heterogeneity could be observed. Through the analysis of contrast and interatomic distances measurements, HR STEM HAADF can provide information of the nature of the atoms. Thus, this work reports, for the first time, the nature of the atoms at the edges of the TMS slabs for representative sulfide catalysts (alumina supported catalyst with standard amount of metal and sulfided in classical conditions). HR STEM HAADF allows visualizing completely promoted edges as well as partially promoted edges for CoMo and NiW systems. However, obtaining such information required the analysis of images of very high quality of isolated and monolayer slabs, and such images are scarce! Thus the interrogation of the representativeness of these results is still open.

Hence by coupling the data issued from IR/CO (indirect and global analysis) and from electron microscopy (direct and local analysis) is indeed a good way to validate the conclusions.

VII.2. Particular perspectives for the work.

Regarding the results that were addressed throughout this manuscript, further validation of the IR assignment of the observed $\nu(\text{CO})$ bands for sulfided NiW supported on alumina catalysts is required. This could be achieved by another spectral treatment called 2D Infrared Inverse Spectroscopy (2D-IRIS) [1]. This method takes in consideration the different CO absorption energies. In particular, 2D-IRIS could allow to confirm the assignment of the differently promoted edges (totally and partially promoted edges). This method has been successfully used for sulfided CoMo [2] and has the potential to further validate the assignment proposed in this work.

Another interesting aspect is to study the WS_2 surface when the promotion by Ni take place. This can be done with the application of theoretical – and most especially of ab-initio calculations. These types of studies have the potential to show what the most favorable configuration is and could show as well the most stable promoter degree on the edges. The comparison between the theoretical results and the available experimental data could be a way to establish the validity of the theoretical models of the active site.

STEM-HAADF results for CoMoS catalyst prepared with chelating agent and after hydrodesulfurization (HDS) reaction were presented. Nevertheless, a comparative regarding what happened to the catalysts spectroscopically speaking is necessary. For this, IR spectroscopy analysis of the catalysts after reaction is necessary. In situ Infrared spectroscopy of the catalysts after hydrodesulfurization reaction are the next step for this project. Carrying out experiments in operando will fill the gap existing as well. However, there are

very few techniques that allow the characterization operando of sulfide materials.

There are significantly fewer studies on characterization and processing of NiW used catalysts than used CoMo and NiMo catalysts. Another potential aspect to research on NiW catalysts is the regeneration procedure of the used catalyst. Since the NiW system has demonstrated having different behavior at the moment of activation and during the catalytic reaction, several questions were raised and remained to be answered. For example, are the NiW active sites more stable than CoMo sites when submitted to HDS and reductive conditions? And, would the deactivation rate be higher or lower than with CoMo catalysts? Chelating agents enhance the catalytic activity in a great manner, in particular by decreasing the size of the sulfide particles but will this catalysts prepared this way deactivate faster or less faster than the ones that were not prepared with the citric acid? The three typical causes of deactivation of hydroprocessing catalysts are coke formation, sintering and contamination [3].

VII.2. General Perspectives for supported transition metal disulfides (TMS) in catalysis.

The increasing consumption of fossil fuel has triggered the global energy crisis and global warming. In order to address these problems, developing clean energy and new energy storage technologies that are environmentally friendly and inexpensive is urgently necessary. Exploring a renewable and sustainable alternative to fossil fuel has become an important research area. Hydrogen has been considered as a clean energy resource that can be easily stored and used without producing any greenhouse gases. Platinum is currently the best-known

catalyst for the hydrogen evolution reaction (HER) but the scarcity and high cost of platinum limits its widespread technological use.

Transition metal disulfides (TMS) constitute an important class of materials whose abundance of catalytically active edge sites and layered crystal structure make them promising for fabrication of novel energy storage devices and applications in (HER) and environmental remediation [4,5]. Recent discoveries have proved the usefulness of these sulfide materials in HER, by electrocatalysis [6] or in photocatalysis [7], thus new perspectives are opening. Among TMS, MoS₂ and WS₂ attracted considerable attention because they show a wide range of electronic, optical, mechanical chemical and thermal properties. Although many efforts have been devoted to enhancing the catalytic activity in HER and photocatalysis, the in-depth understanding of mechanisms is still limited. Few preliminary reports have studied the effect of slab morphology on the photocatalytic activity [8]. Recently, Maheu et al. [9] has studied in depth TMS deposited on anatase titania (MS_x/TiO₂) composites and demonstrated that metal sulfides have versatile and highly tunable properties. Another perspective for the field is to understand better electronic structure, phase transitions, and electrochemical properties of the molybdenum and tungsten disulfide. This will provide more control at the preparation stage.

In conclusion, the unique properties of TMS-based catalysts and their good performance in different applications suggest them to be promising earth-abundant catalysts useful in HER production.

VII.3. REFERENCES

- [1] P. Stelmachowski, S. Sirotin, P. Bazin, F. Maugé, A. Travert, Speciation of adsorbed CO₂ on metal oxides by a new 2-dimensional approach: 2D infrared inversion spectroscopy (2D IRIS), *Phys. Chem. Chem. Phys.* 15 (2013) 9335. doi:10.1039/c3cp51146d.
- [2] E.D. Garcia, Effet du support sur la morphologie et l'activité des catalyseurs d'hydrodésulfuration, Université de Caen, 2017.
- [3] P. Dufresne, Hydroprocessing catalysts regeneration and recycling, (2007). doi:10.1016/j.apcata.2007.01.013.
- [4] T.F. Jaramillo, K.P. Jørgensen, J. Bonde, J.H. Nielsen, S. Horch, I. Chorkendorff, Identification of active edge sites for electrochemical H₂ evolution from MoS₂ nanocatalysts, *Science* (80-.). 317 (2007) 100–102. doi:10.1126/science.1141483.
- [5] J. Kibsgaard, T.F. Jaramillo, F. Besenbacher, Building an appropriate active-site motif into a hydrogen-evolution catalyst with thiomolybdate [Mo₃S₁₃]²⁻ clusters, *Nat. Chem.* 6 (2014) 248–253. doi:10.1038/nchem.1853.
- [6] B. Hinnemann, P.G. Moses, J. Bonde, K.P. Jørgensen, J.H. Nielsen, S. Horch, I. Chorkendorff, J.K. Nørskov, Biomimetic hydrogen evolution: MoS₂ nanoparticles as catalyst for hydrogen evolution, *J. Am. Chem. Soc.* 127 (2005) 5308–5309. doi:10.1021/ja0504690.
- [7] Z. Li, X. Meng, Z. Zhang, Recent development on MoS₂-based photocatalysis: A review, *J. Photochem. Photobiol. C Photochem. Rev.* 35 (2018) 39–55. doi:10.1016/j.jphotochemrev.2017.12.002.
- [8] K. Hong Hu, X. Guo Hu, Y. Fu Xu, X. Zhi Pan, The effect of morphology and size on the photocatalytic properties of MoS₂, (n.d.). doi:10.1007/s11144-010-0173-3.
- [9] C. Maheu, E. Puzenat, C. Geantet, L. Cardenas, P. Afanasiev, Titania-Supported transition metals sulfides as photocatalysts for hydrogen production from propan-2-ol and methanol, (2019). doi:10.1016/j.ijhydene.2019.05.080.

RÉSUMÉ EN FRANÇAIS

A. Introduction générale

Pour faire face aux législations environnementales plus sévères et à la diminution des ressources en pétrole léger, les pétroles bruts lourds doivent être raffinés pour devenir un carburant de transport à très faible teneur en soufre. L'utilisation d'une telle quantité d'huile entraîne des problèmes environnementaux cruciaux en raison de la présence de quantités considérables de soufre, d'azote et d'impuretés métalliques. L'impact négatif sur l'environnement causé par la combustion de combustibles fossiles est une préoccupation majeure au niveau mondial. Outre l'augmentation de la température mondiale due aux émissions de CO₂, les émissions de particules et de gaz toxiques tels que les NO_x et les SO_x ont également des conséquences dramatiques sur la qualité de l'air, la santé humaine et la préservation de l'environnement. Par conséquent, dans la plupart des pays, les gouvernements appliquent ou adoptent des réglementations plus drastiques, telles que les réglementations relatives à la quantité de soufre contenue dans les carburants de transport terrestre.

Des réglementations sur la quantité de soufre dans les carburants des transports maritimes sont également mises en œuvre. Pour répondre aux exigences très strictes de la réglementation, le défi consiste à développer des

catalyseurs ayant une activité améliorée et une sélectivité contrôlée pour les produits souhaités, ainsi qu'une résistance accrue aux poisons catalytiques.

Les processus d'hydrotraitement (HDT), tels que l'hydrodésulfuration (HDS), l'hydrodénitrogénéation (HDN), l'hydrodésoxygénation (HDO) et l'hydrodémétallisation (HDM), constituent le processus principal d'élimination du soufre, de l'azote, de l'oxygène et des métaux. Dans ces procédés catalytiques, on utilise des catalyseurs dont la phase active est une phase mixte sulfure de métal de transition (TMS) préparée à partir de molybdène (Mo) ou de tungstène (W), promu par du cobalt (Co) ou du nickel (Ni). Parmi ces catalyseurs, il est reconnu que les phases mixtes NiWS sont plus actives que les phases NiMoS et CoMoS dans l'hydrogénation de composés aromatiques. Ils sont aussi actifs que les phases NiMoS en hydrodésazotation et plus efficaces que les phases CoMoS. Néanmoins, la sulfuration limitée de W par rapport à Mo amène les fabricants à préférer les catalyseurs à base de Mo. Toutefois, étant donné que le pétrole brut tend à devenir de plus en plus lourd, ce qui signifie que les molécules contenant des hétéroatomes sont de plus en plus grosses et donc plus réfractaires, il existe un intérêt accru pour les catalyseurs NiW. En effet, leur potentiel d'hydrogénation élevé est une caractéristique recherchée pour réaliser des HDS profondes de carburants diesel. Il est donc primordial de mieux comprendre la nature des phases actives et le rôle du promoteur dans les catalyseurs à base de NiW. Cependant, les propriétés chimiques et morphologiques distinctes des catalyseurs à base de tungstène sont mal comprises par rapport au niveau actuel d'informations disponibles pour les catalyseurs à base de molybdène. Basée sur la riche compréhension de la relation entre structure et activité, la conception de catalyseurs HDS à structure

et fonctionnalités contrôlées est en train de devenir une tendance [1]. Pour améliorer les performances des catalyseurs HDS, plusieurs méthodes sont envisagées. Il convient de mentionner l'utilisation d'agents chélatants pendant l'étape de préparation, l'optimisation de la pression et de la température de sulfuration et de la charge en métal. L'effet positif de l'addition d'agent chélatant sur les performances catalytiques est bien documenté. Néanmoins, l'origine de cet effet positif fait encore l'objet d'un débat. Par conséquent, la mise en œuvre de méthodes de caractérisation capables de prendre en compte les structures locales des sites actifs de catalyseurs industriels ainsi que leur rôle dans la réaction de HDS suscite de vives préoccupations.

La caractérisation de la concentration de ces sites et la distinction des sites promus sur les deux bords différents exposés par les feuillets de MoS₂ sont essentielles pour expliquer en détail leur activité et leur sélectivité ainsi que le rôle des paramètres de préparation de ces catalyseurs (effet du support, conditions de préparation de la phase initiale d'oxyde, conditions de sulfuration). Cependant, il existe peu de méthodes pour obtenir cette information. Par spectroscopie photoélectronique à rayons X (XPS), il est possible d'obtenir la concentration globale dans les sites CoMoS mais sans distinction de leur position sur l'un ou l'autre des bords du feuillet. En microscopie à effet tunnel (STM), le groupe de Lauritsen *et al.* [2–4] a pu observer la morphologie des feuillets et distinguer les deux bords ainsi que leur promotion, mais les catalyseurs étudiés sont des catalyseurs modèles, différents dans leur composition et ses conditions de préparation de ceux utilisés industriellement. La caractérisation des catalyseurs sulfurés et métalliques par adsorption de CO à basse température puis par spectroscopie

infrarouge (IR/CO) permet de quantifier la concentration en sites actifs et donne ainsi accès à la dispersion des sites puis à leur activité intrinsèque [5]. Ainsi, IR/CO a été utilisé de manière intensive pour sonder les sites de bord des feuillets de MoS₂ sur des catalyseurs MoS₂/Al₂O₃. Il a été observé qu'il existe deux bandes d'adsorption de CO différentes lorsque le CO interagit avec les bords de MoS₂. En combinant des spectres infrarouges expérimentaux et des calculs DFT, il a été établi que ces bandes correspondent à une adsorption de CO sur les sites du bord M et du bord S des feuillets de MoS₂. En outre, une évaluation quantitative des concentrations sur les sites du bord M et du bord S sur les catalyseurs MoS₂/Al₂O₃ peut être obtenue après détermination du coefficient d'extinction molaire intégré du CO adsorbé sur chaque bord [6]. Cette approche quantitative via le rapport bord-S/bord-M a fourni une démonstration expérimentale de la modification de la morphologie de catalyseurs industriels, c'est-à-dire préparée par le procédé d'imprégnation conventionnel et supporté sur des oxydes. Cette méthode de caractérisation ouvre une voie prometteuse pour rationaliser la conception de catalyseurs de HDT plus actifs et sélectifs. Cependant, cela reste une technique indirecte et doit être comparé à l'observation directe de nanofeuillets. Celui-ci peut être obtenu grâce à la microscopie HR STEM-HAADF. Pour les éléments ayant un numéro atomique supérieur (Z), plus d'électrons sont dispersés à des angles plus élevés en raison d'interactions électrostatiques plus importantes entre le noyau et le faisceau d'électrons. De ce fait, le détecteur HAADF détecte un plus grand signal issu des atomes avec un Z plus élevé, les faisant apparaître plus lumineux dans l'image résultante. Cette forte dépendance vis-à-vis de Z (avec un contraste proportionnel à Z^{1.7}) fait de HAADF un moyen utile pour identifier

dans des petites zones un élément à Z élevé dans une matrice de matériau à Z inférieur. Dans cette optique, l'application du STEM HAADF en recherche en catalyse hétérogène est en vis pour développer, car la détermination de la taille des particules métalliques et de leur distribution est extrêmement importante. La présente thèse de doctorat vise à obtenir un aperçu moléculaire approfondi de la phase sulfure des catalyseurs HDT et HDS. Dans ce travail, un effort particulier a été fait pour comprendre les facteurs qui affectent la morphologie de la phase sulfure et les conséquences des changements morphologiques sur l'activité catalytique. Ainsi, nous étudions la nature de la phase active, en particulier la morphologie du feuillet dans les systèmes Mo, CoMo, W, NiW promus et non promus dans des systèmes à base d'alumine. Dans ce but, nous avons mis en œuvre en parallèle la spectroscopie IR avec des techniques de caractérisation de pointe, telles que les calculs DFT et STEM HAADF pour étudier la morphologie des catalyseurs sulfurés sur support Al_2O_3 préparés dans les mêmes conditions de synthèse et de sulfuration que celles utilisées pour l'application catalytique.

L'étude présentée dans ce manuscrit est divisée en six parties principales: Dans la première partie, nous présentons une étude bibliographique axée sur les catalyseurs sulfurés et sur l'état de la technique en matière de caractérisation de leur phase active. La deuxième partie est consacrée à la description des modes de préparation de tous les matériaux catalytiques et présente également les techniques analytiques. Le troisième chapitre est consacré au couplage entre les calculs IR/CO et DFT pour déterminer les sites actifs dans les catalyseurs $\text{W}/\text{Al}_2\text{O}_3$ en se concentrant sur la distinction du bord M et du bord S de ces catalyseurs. Dans le quatrième chapitre, nous

présentons une étude du parallèle entre IR/CO et HAADF-STEM comme preuve des variations morphologiques dues à l'ajout d'acide citrique sur un catalyseur Mo/Al₂O₃. Le cinquième chapitre décrit l'effet de l'acide citrique sur les catalyseurs NiW/Al₂O₃. En particulier, le couplage des études HAADF-STEM et IR / CO a permis de discriminer les bords promus. Enfin, dans le sixième chapitre, les résultats HAADF-STEM sur les catalyseurs sulfurés CoMo/Al₂O₃ avant et après la réaction thiophène HDS sont présentés. Nous terminons ce manuscrit par une conclusion générale et les perspectives envisagées pour la suite de ce travail.

B. Conclusion générale

Afin de développer des catalyseurs plus efficaces, une approche fondamentale devrait inclure des techniques de caractérisation de pointe. L'objectif de ce projet de doctorat était d'améliorer la compréhension à l'échelle atomique et moléculaire des paramètres qui modifient la morphologie des nano feuillets de TMS (bisulfure de métal de transition) supportés sur alumine.

En utilisant des techniques de caractérisation de pointe, des efforts particuliers ont été déployés pour comprendre les facteurs qui affectent la morphologie de la phase sulfure et pour montrer les conséquences des changements morphologiques sur l'activité catalytique. Par conséquent, l'adsorption de CO à basse température in situ, suivie d'une spectroscopie IR (CO/IR) a été étudié en parallèle avec des techniques de caractérisation avancées telles que les calculs de théorie de la densité fonctionnelle (DFT) et la microscopie électronique à balayage haute résolution en mode champ

annulaire angulaire élevé (HR STEM HAADF). Par conséquent, la nature de la phase active a été étudiée, en particulier la morphologie de la dalle dans les systèmes non promus (Mo et W) et la localisation du promoteur dans les systèmes promus (CoMo et NiW).

Dans toutes les expériences présentées dans ce manuscrit, les techniques de caractérisation ont été réalisées en respectant exactement les mêmes conditions de synthèse et de sulfuration que celles utilisées pour les applications catalytiques.

Références

[1] S. Eijsbouts, On the flexibility of the active phase in hydrotreating catalysts, *Appl. Catal. A Gen.* 158 (1997) 53–92.

[2] F. Lauritsen, J. V., Nyberg, M., Vang, R. T., Bollinger, M. V., Clausen, B. S., Topsøe, H., ... & Besenbacher, Chemistry of one-dimensional metallic edge states in MoS₂ nanoclusters., *Nanotechnology.* 14 (2003) 385.

[3] J. V. Lauritsen, S. Helveg, E. Lægsgaard, I. Stensgaard, B.S. Clausen, H. Topsøe, F. Besenbacher, Atomic-scale structure of Co-Mo-S nanoclusters in hydrotreating catalysts, *J. Catal.* 197 (2001) 1–5. doi:10.1006/jcat.2000.3088.

[4] J. V Lauritsen, J. Kibsgaard, G.H. Olesen, P.G. Moses, B. Hinnemann, S. Helveg, J.K. Nørskov, B.S. Clausen, H. Topsøe, E. Laegsgaard, F. Besenbacher, Location and coordination of promoter atoms in Co-and Ni-promoted MoS₂-based hydrotreating catalysts, *J. Catal.* 249 (2007) 220–233. doi:10.1016/j.jcat.2007.04.013.

[5] J. Chen, E. Dominguez Garcia, L. Oliviero, F. Maugé, How the CO molar extinction coefficient influences the quantification of active sites from CO adsorption followed by IR spectroscopy? A case study on MoS₂/Al₂O₃ catalysts prepared with citric acid, *J. Catal.* 332 (2015) 77–82. doi:10.1016/j.jcat.2015.09.005.

Titre : Catalyseurs à base de disulfure de métal de transition pour l'HDS ultra-profond: Etude par spectroscopie IR et microscopie électronique haute résolution pour une connaissance à l'échelle atomique de la structure des sites actifs.

RESUME:

Ce travail de thèse a permis d'obtenir une caractérisation à l'échelle atomique des feuillets (Co)MoS₂ et (Ni)WS₂ de catalyseurs d'hydrotraitement supportés sur alumine et de déterminer l'impact d'un additif organique, l'acide citrique (CA). Dans cette étude des techniques avancées ont été mises en œuvre telles la caractérisation par adsorption de CO à basse température suivie par spectroscopie IR (IR/CO), des calculs DFT et des observations par microscopie électronique haute résolution en mode transmission et par STEM HAADF.

Sur les catalyseurs non promu à base de W et de Mo, l'adsorption de CO permet de discriminer les sites des bords M- et des bords S- des feuillets de TMS. La détermination des coefficients d'extinction molaire des bandes liées au CO adsorbé permet de déduire la morphologie des feuillets. L'HR STEM HAADF confirme que l'addition de CA modifie la morphologie des feuillets TMS d'un triangle tronqué à une forme hexagonal.

Sur les catalyseurs promus NiW et CoMo, la microscopie électronique montre que l'addition de CA diminue la taille des feuillets de TMS et conduit aussi à la création de petits clusters (<1 nm). L'analyse de particules isolées par HR STEM HAADF permet d'identifier la nature des atomes du bord du feuillet de TMS. Ainsi la microscopie et l'IR/CO mettent en évidence que au sein d'un même feuillet sulfure peuvent coexister des bords totalement promus, et partiellement promus.

MOTS-CLÉS: HR STEM-HAADF, spectroscopie IR, calcul DFT, MoS₂, WS₂, CoMoS, NiWS, acide citrique, hydrotraitement

Title: Supported transition metal disulfide catalysts for ultra-deep HDS: Coupling of IR spectroscopy and high resolution electron microscopy for a deeper insight into active sites.

ABSTRACT:

This work was focused on obtaining an atomic scale characterization of the (Co)MoS₂ and (Ni)WS₂ slabs of hydrotreating catalysts supported on alumina and to determine the impact of citric acid (CA) addition. In this study, advanced techniques were implemented such as low temperature CO adsorption followed by IR spectroscopy (IR/CO), DFT calculations and high resolution electron microscopy observations in transmission mode and by STEM HAADF.

On the non-promoted W and Mo catalysts, CO adsorption makes it possible to discriminate between the sites of the M- and S- edges of the TMS slabs. The determination of the molar extinction coefficients of the adsorbed CO bands allows the morphology of the slabs to be deduced. HR STEM HAADF confirms that the addition of CA modifies the morphology of the TMS slabs from a truncated triangle to a hexagonal shape.

On the promoted NiW and CoMo catalysts, electron microscopy shows that the addition of CA decreases the size of the TMS slabs and also leads to the creation of very small clusters (<1 nm). The analysis of isolated particles by HR STEM HAADF allows identifying the nature of the atoms on the edge of the TMS slabs. Thus microscopy and IR/CO show that within the same sulfide slabs, can coexist edges that are fully promoted and partially promoted.

KEYWORDS: HR STEM-HAADF, IR spectroscopy, DFT calculations, MoS₂, WS₂, CoMoS, NiWS, citric acid, hydrotreatment
